University of Plymouth

PEARL **https://pearl.plymouth.ac.uk**

04 University of Plymouth Research Theses 01 Research Theses Main Collection

2017

Excitotoxic Injury Mechanisms in Central White Matter

Doyle, Sean P.

http://hdl.handle.net/10026.1/9586

http://dx.doi.org/10.24382/734
University of Plymouth

All content in PEARL is protected by copyright law. Author manuscripts are made available in accordance with publisher policies. Please cite only the published version using the details provided on the item record or document. In the absence of an open licence (e.g. Creative Commons), permissions for further reuse of content should be sought from the publisher or author.

RESEARCH DEGREES WITH PLYMOUTH UNIVERSITY

Excitotoxic Injury Mechanisms in Central White Matter

By

Seán P. Doyle

A thesis submitted to Plymouth University

in partial fulfilment for the degree of

Doctor of Philosophy

Peninsula School of Medicine and Dentistry,

Plymouth University

April 2017

Copyright Statement:

This copy of the thesis has been supplied on condition that anyone who consults it is understood to recognise that its copyright rests with its author and that no quotation from the thesis and no information derived from it may be published without the author's prior consent.

Abstract:

Excitotoxic Injury Mechanisms in Central White Matter

Seán P. Doyle

Myelinated axons are crucial for rapid information transmission within the central nervous system (CNS). Myelin injury is a common feature of white matter (WM) pathology in a number of disease states, including ischemic stroke. Myelin disruption can lead to a complete failure in saltatory action potential conduction, resulting in devastating neurological deficits. However, the fundamental mechanism of ischemic myelin injury is controversial. Glutamate-mediated excitotoxicity is now recognised as a crucial event in the development of ischemic WM pathology. This thesis investigates the potential mechanisms of glutamate release in central WM and examines the hypothesis that NMDA receptor over-activation mediates ischemic myelin damage. Using glutamate biosensor microelectrodes and FM-dye imaging, I show that axonal depolarisation in the adult corpus callosum evokes rapid vesicular docking in axons, capable of elevating extracellular glutamate concentration. My findings show that vesicular fusion occurs under the myelin sheath in myelinated axons, which supports the existence of a novel synapse between the axon and overlaying myelin. Simulation of ischemia triggered an early and robust rise in optic nerve extracellular glutamate levels. Unexpectedly, a significant component of ischemic glutamate release also originated from axonal vesicular fusion. Together, these findings show that the axon-myelin synapse represents a significant site of excitotoxic injury during ischemia. Resolving prior conflicting results, I show that NMDA receptor antagonists prevent myelin degradation and improve functional recovery when applied for sufficient time to penetrate the sheath. Finally, I identify a fluorescent myelin stain (QNZ-46) which is a negative allosteric modulator of NR2C/D-containing NMDA receptors. QNZ-46 selectively accumulates in myelinated WM regions of the CNS following systemic administration, and is retained following wash-out. As a result, QNZ-46 provides persistent protection during ischemia by preserving myelin structure and improving functional recovery.

Author's Declaration:

At no time during the registration for the degree of Doctor of Philosophy has the author been registered for any other University award without prior agreement of the Graduate Sub-Committee.

Work submitted for this research degree at the Plymouth University has not formed part of any other degree either at Plymouth University or at another establishment.

This study was financed with the aid of a studentship from Plymouth University.

I declare that the work contained in this thesis is original research carried out during the registration for this degree under the supervision of Prof. Robert Fern at Plymouth University. All work was carried out at Plymouth University with the exception of experiments requiring the use of two-photon microscopy, which were performed at the Department of Physiology and Biochemistry, University of Malta, under the supervision of Prof. Mario Valentino. All of the work in this thesis was carried out by Seán P. Doyle, with the exception of PLP-GFAP/fluromyelin dual-imaging (Fig. 5.21) which was performed by Dr. Daniel Bloch Hansen, who also provided assistance with QNZ-46 imaging (Chapter 5).

Word count (excluding bibliography): 63,394

Signed…….

Date …….

Acknowledgements:

First and foremost, I would like express my sincere appreciation and thanks to my supervisor, Prof. Robert Fern, who has been an exceptional mentor throughout the duration of this project. His continuous guidance and support has been invaluable.

I would also like to thank the members of my lab group; Dr. Angelo Da Rosa, Dr. Daniel Bloch Hansen and Sarah Ellwood, who were always willing to help. I would like to thank Mr. Waldemar Woznica for his assistance with I.P. injections. In addition, I would also like to give specific thanks to our collaborators at the University of Malta, particularly Prof. Mario Valentino, Robert Zammit and Dr. Christian Zammit, for their assistance during my stay. Their help and generosity made my time in Malta a real pleasure.

Personal and special thanks to my parents and brother, Luke, for their unconditional support and encouragement throughout the years. Last but not least, a very special thank you to my partner, Corí, for always being there.

Table of Contents

List of Figures:

List of Tables:

List of Abbreviations:

$[Glut]_e$= extracellular glutamate concentration

$[ion]_e$= extracellular concentration of an ion

$[ion]_i$= intracellular concentration of an ion

3α5βHS= preg*n*anolone hemisuccinate

5-HT= serotonin

aCSF= artificial cerebrospinal fluid

AIS= axon initial segment

AMPA= α-amino-3-hydroxy-5-methyl-4-isoxazolepropionic acid

AP= action potential

AQP= aquaporin

ATP= adenosine triphosphate

ATT= aminotransferase

Baf-a1= bafilomycin-a1

BAPTA-AM= N,N'-[1,2-ethanediylbis(oxy-2,1-phenylene)]bis[N-[2-[(acetyloxy)methoxy]-2-oxoethyl]]-, bis[(acetyloxy)methyl] ester

BBB= blood brain barrier

BDNF= brain-derived neurotrophic factor

BoNT= botulinum toxin

CAP= compound action potential

CBF= cerebral blood flow

CBX= carbenoxolone

CC= corpus callosum

CHD= congenital heart disease

CIQ= (3-Chlorophenyl) [3,4-dihydro-6,7-dimethoxy-1-[(4-methoxyphenoxy)methyl]-2(1*H*)-isoquinolinyl]methanone

CNQX= 6-cyano-7-nitroquinoxaline-2,3-dione

CNS= central nervous system

CP= cerebral palsy

DMSO= dimethyl sulfoxide

E= embryonic day

EAAC-1= excitatory amino acid carrier 1

EAAT= excitatory amino acid transporter

ECS= extracellular space

EGTA= ethylene glycol-bis(β-aminoethyl ether)-N,N,N',N'-tetraacetic acid

E_{ion}= equilibrium potential for an ion

EPSC= excitatory post-synaptic currents

EPSP= excitatory post-synaptic potential

ER= endoplasmic reticulum

ETC= electron transport chain

FDA= food and drug administration

FM4-64= dye*N*-(3-triethylammoniumpropyl)-4-(6-(4-(diethylamino)phenyl)hexatrienyl) pyridinium dibromide

GABA= γ-aminobutyric acid

GDH= glutamate dehydrogenase

GDP= guanine diphosphate

GFAP= glial fibrillary acidic protein

GFP= green fluorescent protein

GLAST= glutamate-aspartate transporter

GLT-1= glial-type glutamate transporter

GLU-= glutamate biosensor

GLUT-1= glutamate transporter 1

GM= grey matter

GS= glutamine synthase

GTP= guanine triphosphate

HEPES= 2-[4-(2-hydroxyethyl)piperazin-1-yl]ethanesulfonic acid

HPLC= high performance liquid chromatography

I.P.= intraperitoneal

i= current

IC_{50}= half maximal inhibitory concentration

ICH= immunohistochemistry

Ig= immunoglobulin

iGluR= ionotropic glutamate receptor

IP_3= inositol-1,4,5-triphosphate

Ka= kainate

kDa= kilodalton

KGDH= α-ketoglutarate dehydrogenase

K_v= K^+ channel

MAG= myelin-associated glycoprotein

MBP= myelin basic protein

MCAO= middle cerebral artery occlusion

MCT= monocarboxylate transporters

ME= malic enzyme

mGluR= metabotropic glutamate receptor

MK801= (5*S*,10*R*)-(+)-5-Methyl-10,11-dihydro-5*H*-dibenzo[*a*,*d*]cyclohepten-5,10-imine maleate

MON= mouse optic nerve

mOsm= milliosmoles

Na_v= Na^+ Channel

NBQX= 2,3-Dioxo-6-nitro-1,2,3,4-tetrahydrobenzo[*f*]quinoxaline-7-sulfonamide

NCX= sodium-calcium exchanger

NF= neurofilament

NKCC= Na-K-Cl- co-transporter

NMDA= N-methyl-D-aspartate

NMDG= N-methyl-d-glucamine

NO= nitric oxide

NPPB= 5-Nitro-2-(3-phenylpropylamino)benzoic acid

NRG= neuregulin

OGD= oxygen-glucose deprivation

ON= optic nerve

OPC= oligodendrocyte precursor cell

P= postnatal day

PBGST= PBS/goat serum/triton mixture

PBS= phosphate buffered saline

PC= pyruvate carboxylase

PDGFα= platelet-derived growth factor *α*

PDH= pyruvate dehydrogenase

PFA= paraformaldehyde

PGE_2= prostaglandin E_2

PH= pregnanolone hemisuccinate

PLP= proteolipid protein

PNS= peripheral nervous system

Pt= platinum

PTP= permeability transition pore

PVL= periventricular leukomalacia

PWMI= periventricular white matter injury

QNZ-46= 4-[6-Methoxy-2-[(1E)-2-(3-nitrophenyl)ethenyl]-4-oxo-3(4H)quinazolinyl]benzoic acid

RB= rose bengal

ROI= region of interest

RON= rat optic nerve

ROS= reactive oxygen species

RyR= ryanodine receptors

SAS= sulfasalazine

SAT= sodium-coupled amino acid transporters

SCaMPER= sphingolipid Ca^{2+} release-mediating protein of the ER

SD= sprague dawley

SEM= standard error of the mean

SN1= system N transporter 1

TBOA= DL-*threo*-β-Benzyloxyaspartic acid

TCA= tricarboxylic acid

tDCS= direct current stimulation

TMA= transcranial magnetic stimulation

t-PA= tissue-plasminogen activator

TPM= two-photon microscopy

TRC= Toronto Research Chemicals

TRP= Transient Receptor Potential

TTX= tetrodotoxin

VGCC= voltage-gated Ca^{2+}-channels

VGKC= voltage-gated K^+ channel

VGLUT= vesicular glutamate transports

VGNC= voltage-gated Na^+ channel

V_m= membrane potential

VRAC= volume regulated anion channel

WHO= World Health Organisation

WM= white matter

YFP= yellow fluorescent protein

$\Delta\psi_m$= mitochondrial membrane potential

Chapter 1:

Introduction

1.1: White Matter

The mammalian central nervous system (CNS) is divided into two distinct regions; grey matter (GM) and white matter (WM). GM regions, such as the neocortex, are primarily populated by neuronal cell bodies, dendrites and glial cells. Conventional neuronal synapses are abundant in discrete regions of GM and therefore, it plays an essential role in information processing, learning and memory (Bakiri, Burzomato et al. 2009). WM consists of a collection of compact axonal bundles and supporting glia. WM tracts form the connections between distinct GM regions and are essentially responsible for information transmission within the CNS, relaying electrical signals between different neuronal networks. They are typically grouped together in a source-destination dependant manner, forming groups of association, commissural and projection fibres. These connect cortical areas within the same hemisphere, between hemispheres and to the brainstem/spinal cord, respectively (Wakana, Jiang et al. 2004). Although topographically segregated, there are no distinct barriers separating the two regions (Goldberg and Ransom 2003). In fact, WM tracts are known to run within subcortical GM regions such as the basal ganglia and thalamus (Filley 2012). Interestingly, WM occupies approximately 50% of the adult brain by volume and is estimated to consume between 30 and 43.8% of the brain's total energy supply at rest (Filley 1998, Zhang and Sejnowski 2000, Matute 2011, Harris and Attwell 2012).

1.1.1: The Axon

Information transmission along WM tracts is accomplished by axons. Axons are long cylindrical processes extending from the axon hillock of neuronal cell bodies and projecting to distant target regions. They occupy approximately 44% of the available space in human WM (Beiu, Madappuram et al. 2011). Neurofilaments and microtubules are the major structural components of the axonal cytoskeleton, running parallel along the longitudinal axis to maintain a cylindrical shape. Microtubule tracks also play an important role in intra-axonal transport. Anterograde and retrograde axonal transport is essential for the supply of newly synthesised proteins and lipids to the distant synapse, and the clearance of misfolded or

damaged proteins, respectively (Chevalier-Larsen and Holzbaur 2006). While organelles such as mitochondria and smooth endoplasmic reticulum (ER) are present throughout the axon, they generally contain fewer organelles than neuronal cell bodies, lacking both Golgi apparatus and rough ER (Waxman and Kocsis 1995). The axon is surrounded by the axonal membrane, or axolemma, which is structurally similar to the plasma membrane found at the cell body (Waxman and Kocsis 1995). The function of the axon is to propagate an electrical impulse known as the action potential (AP).

1.1.1.1: Resting Membrane Potential

In quiescent axons, the resting membrane potential (V_m) is approximately -65mV due to an unequal distribution of charged ions across the axolemma (Waxman and Kocsis 1995). The resting V_m is largely maintained by the activity of the Na^+/K^+-ATPase, an energy-dependant ion pump, responsible for maintaining a gradient of positively charged Na^+ and K^+ ions across the axolemma (Wright 2004, Filley 2012). The Na^+/K^+-ATPase extrudes intracellular Na^+ ($[Na^+]_i$) in exchange for extracellular K^+ ($[K^+]_e$) in a 3:2 ratio. Thus, it maintains a low axoplasmic concentration of Na^+ and a high concentration of $[K^+]_i$.

The negative resting V_m is a consequence of a surplus of negatively charged intracellular ions, relative to the extracellular side of the axolemma (Wright 2004). At rest, the axolemma is slightly permeable to K^+ ions (through K2P-channels (Renigunta, Schlichthorl et al. 2015)), leading to a net efflux of positively charged K^+ ions which drives the resting V_m closer to equilibrium potential for K^+ (E_K, approximately -90mV). The equilibrium potential for an ion (E_{ion}) is the theoretical membrane potential where there is no net flow of the ion across the membrane, assuming the membrane is selectively permeable to this ion. For the case of K^+, it is where the movement of K^+ ions down their concentration gradient out of the cell (diffusional force) is equal to the movement of positively charged K^+ ions into the more negatively charged intracellular domain (electrical force) (Barnett and Larkman 2007). The theoretical E_{ion} can be calculated using the Nernst equation;

$$E_{ion} = RT/z_{ion}F \ln [ion]_o/[ion]_I,$$

where R=gas constant, T=temperature in °K, F=Faraday constant and Z= valence of the ion. Reviewed by (Barnett and Larkman 2007).

However, the resting V_m does not reside at E_k as the axonal membrane is also slightly permeable to other ions such as Ca^{2+}, Cl^- and Na^+. Depolarising inward currents from either Ca^{2+} or Na^+ will contribute to the less negative resting V_m of -65mV. The resting V_m can be calculated using the Goldman-Hodgkin-Katz equation based on the relative membrane permeability for Na^+, K^+ and Cl^- ions (Goldman 1943, Hodgkin et al. 1952).

1.1.1.2: The Action Potential (AP)

Neurons are excitable cells and their capacity to relay rapid signals along the axon cylinder is accomplished via the propagation of APs. An AP is characterised by the rapid depolarisation and subsequent repolarisation of the axonal V_m. This rapid change of V_m is based on the flow of ionic current across the axolemma (Wright 2004, Filley 2012).

When a neuron receives sufficient stimulation to depolarise the resting V_m by ~20mV (threshold value), it leads to the initiation of an AP. If the initial stimulus does not cause the V_m to surpass this threshold value, an AP will not pursue. This is referred to as an 'all-or-nothing' event. Single synaptic events are typically incapable of pushing the V_m to its threshold. However, either spatial or temporal summation of synaptic inputs may be sufficient (Stuart, Spruston et al. 1997). Once the threshold is surpassed, it leads to the opening of voltage-gated Na^+ channels (VGNCs), allowing an influx of depolarising Na^+ ions, driving the V_m close to E_{Na} (+60mV). This is referred to as the rising or depolarising phase of an AP.

However, this depolarisation does not quite reach E_{Na} due to a combination of rapid inactivation of VGNCs (preventing further Na^+ influx) and the delayed activation of voltage-gated K^+ channels (VGKCs). Compared to VGNCs, the gating of VGKCs requires a much larger depolarisation (Barnett and Larkman 2007). As VGKCs open, the subsequent efflux of K^+ ions repolarises the membrane potential back towards resting V_m. Similar to their delayed activation, VGKCs are also slow to inactivate, leading to an after-hyperpolarisation where the membrane potential will temporarily overshoot to approximately -80mV (see Fig. 1.1) (Barnett and Larkman 2007).

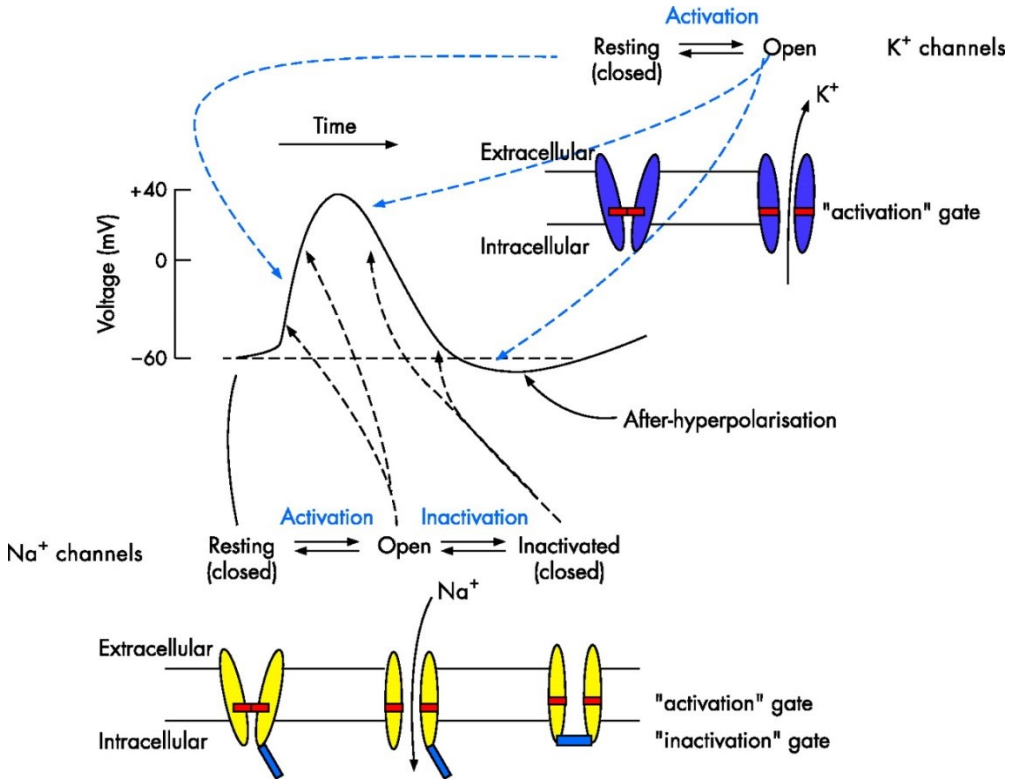

Fig. 1.1: The action potential.

A schematic representation of the different phases of an action potential. Taken from (Barnett and Larkman 2007).

AP propagation along an axon is unidirectional. Depolarisation of the axolemma will depolarise adjacent regions of axolemma typically travelling away from the neuronal cell body towards the end terminal or synapse (Barnett and Larkman 2007). Once an AP occurs, the membrane experiences a 'refractory period' which prevents an AP returning back towards the neuronal cell body. Na^+ channel inactivation prevents any further Na^+ influx and thus ensures that only Na^+ channels ahead of the AP will activate. In addition, the K^+ channel mediated after-hyperpolarisation also increases the input stimulus required to reach threshold (Barnett and Larkman 2007). By the time Na^+ have returned to their resting state and when resting V_m has been restored, the AP will have travelled along the axon and so any further AP generation will require another stimulus.

1.1.1.3: Mode of Action Potential conduction and Myelin Sheath

The mode of AP conduction is dependent on presence of a myelin sheath, an ensheathing lipid layer which insulates the axon cylinder. During the first half of gestation, all central axons lack myelin sheath. While many axons are myelinated during development, a significant population remain unmyelinated in the mature CNS. AP conduction in unmyelinated axons travels progressively along the axon in a wave-like manner (Fig. 1.2). Unmyelinated AP conduction is facilitated by the expression of a low density of $Na_v1.2$ Na^+ channels ($2/\mu m^2$), evenly distributed along the axolemma (Waxman, Black et al. 1989). This mode of conduction is relatively slow due to the high capacitance of unmyelinated axons (Waxman, Black et al. 1989). The bare axolemma is exposed to the extracellular space and therefore, separates charged ions on either side of the membrane. However, the axolemma itself is relatively thin, which leads to an accumulation of charged ions along the membrane. This stored electrical charge is referred to as capacitance, which hinders AP conduction, reducing AP conductance velocity. As a result, AP propagation in unmyelinated axons is typically slow and continuous.

In the mature CNS, many central axons are ensheathed by multiple insulating wraps of myelin sheath. Myelin has a very high proportion of lipid and has a water content of about 40% *in situ*. While cell membranes typically have a higher ratio of protein to lipid, myelin on the other hand, has a dry weight of approximately 70% lipid. Cholesterol and cerebrosides are the most abundant lipids found in myelin, respectively accounting for 40% and 20% of total myelin lipid content (Quarles, Macklin et al. 2006, Filley 2012). Myelin also expresses a variety of structural proteins responsible for compacting its various layers, including myelin-associated glycoprotein (MAG), proteolipid protein (PLP) and myelin basic protein (MBP) (Filley 2012). The ensheathing myelin layer is separated from the axolemma by a narrow region known as the periaxonal space (approximately 20nm). Each subsequent wrap of myelin is separated by very thin spaces of cytoplasm, typically measuring 4-5nm wide (Blaurock 1981). Myelin thickness is defined by the number of myelin wraps around an axon and their compactness (Velumian and Samoilova 2014). It is quantified by a *g-ratio*, which is the ratio of the axon diameter to the diameter of the axon plus the myelin sheath. Generally speaking, it is directly proportional to axon size, with larger axons having thicker myelin (Waxman and Sims 1984). Myelin is typically thinner on central axons when compared those in the peripheral nervous

system (PNS). For example, the typical g-ratio of mature PNS axons is 0.6, while the CNS has a typical g-ratio of 0.75 (Waxman and Sims 1984). For several mammalian species, as brain size increases, the fraction of axons which are myelinated also increase (Wang, Shultz et al. 2008). Similarly, the overall percentage volume of WM in the brain also increases with size (Beiu, Madappuram et al. 2011).

Myelination typically begins late in the final trimester during human foetal development and continues well into adulthood. It is carried out by oligodendrocytes in the CNS (or Schwann cells in the PNS). Prior to the onset of myelination, many axons undergo a programme of radial expansion in preparation for contact with oligodendrocyte processes (Alix, Zammit et al. 2012). Increasing axonal diameter decreases internal resistance, which in itself increases AP conduction velocity. Myelination is carried out in segments along the axon, covering ~99% of the axon cylinder, starting less than 100µm away from the neuronal cell body and continuing right up to the synaptic terminal (Stys 2005, Back 2014, Velumian and Samoilova 2014). However, in the optic nerve axon, myelin typically begins millimetres from the retinal ganglion cells in order to prevent light scattering which would occur if myelin was present (Doyle, Simon et al. 2008, Velumian and Samoilova 2014). The unmyelinated region between the axon hillock and the beginning of myelin is termed the axon initial segment (AIS) and is characterised by a high density of voltage-gated channels (Kole and Stuart 2012). The segments of myelin sheath are separated by a narrow gap, known as the node of Ranvier, which expose the axolemma to the extracellular space (approximately 1µm wide). Directly adjacent the node is the paranodal domain which contains a tight axo-myelin junction (paranodal junction) and has a high expression of adhesion proteins such as contactin and Caspr (Rios, Melendez-Vasquez et al. 2000). The distance between each node is proportional to the diameter of the axon (Waxman and Sims 1984). The wraps of insulating myelin between each node of Ranvier increase electrical resistance and decrease capacitance. High electrical resistance prevents the loss of current across the axolemma and thus, promotes AP movement along the axon. Capacitance is inversely proportional to the thickness of the membrane separating two conductors. So by increasing the thickness of the membrane (with myelin), it also lowers the capacitance by increasing the distance between the two conductors. This decreases the stored charge on either side of the axolemma. Therefore, the increased

resistance and decrease in capacitance provided by myelin facilitates the rapid and passive conduction of an AP to the next node.

During myelination, the expression of $Na_v1.2$ Na^+ channels along the unmyelinated axolemma is replaced by clusters of $Na_v1.6$ Na^+ channels which form at the node of Ranvier. The high density of $Na_v1.6$ channels restricts inward Na^+ currents to less than 1% of the axon surface (Waxman, Craner et al. 2004, Nave 2010). For this reason, myelinated APs propagate via saltatory or 'jumping' conduction between nodes (Fig. 1.2). While saltatory conduction is much faster, it is also much more energy efficient when compared to unmyelinated axons (Stys 2011). The restoration of ionic gradients (by Na^+/K^+-ATPase, also found at the node) is restricted to small areas along the axon, dramatically reducing the energy demand (Nave 2010). Unlike Na^+ channels, K^+ channels are typically dispersed within the juxtaparanodal region of the axon, concealed underneath the myelin sheath (Doyle, Simon et al. 2008, Baltan, Carmichael et al. 2014). This restricts the involvement K^+ channels during AP conduction, seen with the lack of an after-hyperpolarisation in myelinated axons. The K^+ channels under myelin are known to contain $K_v1.1$ and $K_v1.2$ subunits (Velumian and Samoilova 2014).

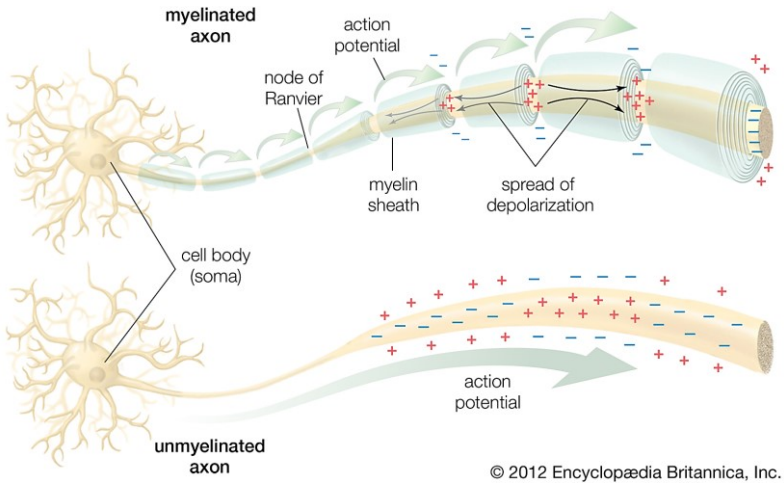

Fig. 1.2: **Action potential conduction.**

Schematic representation of AP conduction in myelinated and unmyelinated axons. Myelinated AP propagation is via saltatory conduction, where the AP 'jumps' between the node of Ranvier. In contrast, unmyelinated AP conduction is continuous as it propagates along the entire axolemma. Taken from '*Encyclopaedia Britannica Online- Node of Ranvier*'.

1.1.2: Glial Cells

Aside from axons, WM contains a number of glial cells including fibrous astrocytes, oligodendrocytes, NG2 glia and microglia (Goldberg and Ransom 2003). Axons are highly dependent on a close interaction with these glial cells, which actually outnumber the amount of neurons in the mammalian CNS. The word *glia* originates from the Greek word for 'glue' as they were initially considered to act as a scaffold for supporting neurons. However, it is now well known that they play a much more important role within the CNS (Nave 2010). The intimate interaction between axons and their neighbouring glial cells is essential for the survival, integrity and normal functioning WM tracts.

1.1.2.1: Oligodendrocytes

The term oligodendrocyte originates from the Greek words for few (*oligo*), branches (*dendro*) and cell (*cyte*) and was initially introduced by Pio Del Rio-Hortega in 1928 (Verkhratsky and Butt 2007). Similar to Schwann cells in the PNS, oligodendrocytes are highly specialised glial cells, primarily responsible for the production of myelin, which enwraps axon cylinders. However, they also play an important role in supporting the long term integrity of axons, as well as stimulating the growth of axon diameter (Nave 2010). Contrary to the origination of their name, a single oligodendrocyte can send out many processes which account for segments on up to 60 neighbouring axons (Doyle, Simon et al. 2008).

Oligodendrocytes develop from proliferating oligodendrocyte precursor cells (OPCs) which migrate from the ventricular zones of the CNS (Barres and Raff 1994). From here, a combination of chemorepellent and chemotactic signals guide their migration along axons and radial glia to their final destinations (Sugimoto, Taniguchi et al. 2001). OPC development into mature, myelin-forming oligodendrocytes involves a series of developmental stages which can be defined by the presence of a number of cell surface markers (stage-specific antibodies), including NG2, A_2B_5, O4, O1 and MBP (Fig.1.3) (Zhang 2001). In addition to the sequential expression of cell markers, they undergo a morphological transformation from bipolar progenitors to myelinating oligodendrocytes bearing multiple processes (Zhang 2001).

Oligodendrocytes are the last cell type to develop in WM and they carry out the majority of myelination post-natally (Miller 2002).

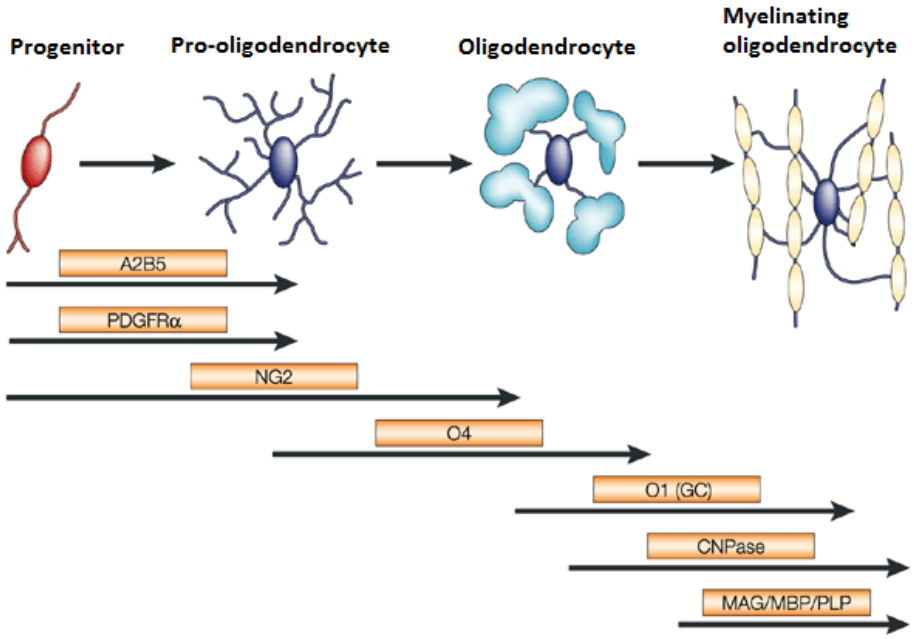

Fig. 1.3: **Oligodendrocyte development.**

Oligodendrocyte lineage showing the variety of cell makers expressed during different periods of development. Taken from (Zhang 2001).

1.1.2.2: Astrocytes

Astrocytes are the most abundant type of glial cell in the CNS (Lundgaard, Osorio et al. 2014). They play a crucial role in the maintenance of homeostatic conditions, including pH regulation, neurotransmitter re-uptake, free radical scavenging and extracellular K^+ buffering (Butt and Ransom 1993, Ransom 2003). In addition, they also play an important role in the maintenance of the blood brain barrier (BBB), as their end-feet processes cover approximately 90% of the cerebral vasculature (Lundgaard, Osorio et al. 2014).

Unlike the protoplasmic type found in GM, WM astrocytes are predominantly fibrous, having a relatively small cell body with extensive long processes which extend out from the body and run along nerve fibres (Shannon, Salter et al. 2007). In addition to maintaining homeostatic conditions, fibrous astrocytes have shown to be an important source of energy reserve for

neighbouring axons. Astrocytes contain stores of glycogen which can be converted to lactate and subsequently shuttled to axons by MCT transporters during periods of high energy demand and/or energy deprivation (Ransom and Fern 1997, Wender, Brown et al. 2000, Fern 2015). Mature GFAP-expressing astrocytes are first observed in WM regions around the same time that OPCs begin migrating (Lundgaard, Osorio et al. 2014). Astrocytes may play a role in guiding OPC migration and development as they are the primary producer of platelet-derived growth factor (PDGF), and PDGFα receptor signalling is known to inhibit oligodendrocyte differentiation (McKinnon, Waldron et al. 2005, Lundgaard, Osorio et al. 2014).

1.1.2.3: Microglia

Microglia are the resident immune cell within the CNS. Unlike neurons and macroglia (astrocytes and oligodendrocytes) which originate in the embryonic germ layer (the neuroectoderm), microglia enter the CNS from the circulating vasculature (Allen and Barres 2009). Microglia have a ubiquitous distribution throughout the CNS, accounting for approximately 5-20% of total cells in the mouse brain (Streit 2000). Their main function is to scavenge and engulf debris, damaged cells and infection. Under pathological conditions, microglia become activated or 'reactive' which induces an increase in mobility, a change in morphology and an upregulation of monocyte-macrophage molecules (Streit 2000). They are also proposed to play a role in synaptic remodelling, by removing unnecessary synaptic connections (Allen and Barres 2009). Interestingly, microglia communicate with the systemic immune system. For example, systemic infections can lead to the metabolic upregulation of microglia in the CNS (Dantzer, Bluthe et al. 1998, Perry and Teeling 2013).

1.1.2.4: NG2+ Glia/OPCs

The fourth glial cell type within the CNS is known as NG2 glia, based on their expression of NG2 chondroitin sulfate. NG2 glia have a stellate morphology, similar to astrocytes but are often referred to as oligodendrocyte precursor cells (OPC) as they regularly differentiate into oligodendrocytes. During development, a sub-population of NG2+ OPCs remain undifferentiated, accounting for a significant population in the adult CNS (Dawson, Polito et

al. 2003). Interestingly, NG2+ glia account for 8-9% of the total cell population in WM, but only 2-3% in GM (Verkhratsky, Butt *et al.* 2015). OPCs are the principle proliferative cell type in the mature CNS (Dawson, Polito et al. 2003). There is evidence to suggest that NG2+ cells generate oligodendrocytes following demyelination, suggesting that they act primarily as a reservoir of new oligodendrocytes (Polito and Reynolds 2005, Tripathi, Rivers et al. 2010). Aside from regenerating oligodendrocytes in the mature CNS, they form close synaptic-like contacts with nodes of Ranvier and receive direct synaptic input from neuronal cells which suggests that they may also have a functional role under physiological conditions (Butt, Duncan et al. 1999, Kukley, Capetillo-Zarate et al. 2007, Ziskin, Nishiyama et al. 2007).

1.1.3: Model WM tracts:

1.1.3.1: The isolated Optic Nerve (ON)

Throughout this project, the isolated rodent optic nerve (ON) is used as a model WM tract. Extensive use of the ON has provided invaluable insight into both physiological and pathological interactions between glial cells and axons in WM. The ON is an extruded central WM tract, essentially responsible for transmitting visual information from the eye to the brain (Drance and Anderson 1995). This information transmission is facilitated by several hundred thousand axons which project from retinal ganglion cells to the optic chiasm at the base of the brain. Many axons cross over at the optic chiasm and carry on as the optic tract, eventually terminating at the superior colliculus (or optic tectum) in the mid-brain (Raff 1989).

The ON offers a variety of advantages over alternative WM tracts. An important feature of the ON is the lack of intrinsic neuronal cell bodies, which eliminates any complications or interferences, associated with neighbouring GM regions. The ON contains a variety of supporting glial cells, namely oligodendrocytes, astrocytes, NG-2+ cells and microglia, so any cell bodies in the ON must be those of glia (Butt, Pugh et al. 2004). The lack of neuronal cell bodies allows for the study of physiological and pathological axo-glial interactions in WM (Butt, Pugh et al. 2004). In addition, it ensures that any recordings from the ON (e.g. extracellular glutamate) are purely of WM origin. The intact nerve is relatively simple to isolate and due to

the surrounding connective sheath, the cellular components remain bundled together and so it can be treated like an individual fibre. The isolated nerve can be maintained for several hours with minimal structural/functional loss, allowing for investigations over relatively long periods (Dong and Hare 2005). The functional homogeneity and structure of the ON allows for reliable electrophysiological recordings i.e. compound action potential recordings. This permits the study of a variety of nerve conduction properties including conduction velocity and functional recovery following an insult e.g. ischemia, anoxia, aglycemia.

The structural anatomy of the rat ON (RON) has been well characterised, both during development and in mature rodents. The RON originates from the optic stalk, an extension of the neural tube (Raff 1989). By embryonic day 14-16 (E14-16), the first axons begin to invade the optic stalk, originating from newly developed retinal ganglion cells (Sefton, Horsburgh et al. 1985). By birth (P0), a period which developmentally correlates with mid-term human WM, the number of axons in the rat ON reaches between 240,000 and 275,000 (Crespo, O'Leary et al. 1985, Sefton, Horsburgh et al. 1985). At this age, all axons are unmyelinated and have a diameter of <0.3μm (Sefton, Horsburgh et al. 1985), where AP propagation is mediated by a low density of NaVs distributed along the axolemma, with a conduction velocity of 0.2m/s (Foster, Connors et al. 1982, Waxman, Black et al. 1989). The RON contains two macroglial cell types; fibrous astrocytes and oligodendrocytes. Of the two, astrocytes represent the vast majority of glial cells in the ON at birth (Butt and Ransom 1993, Mi and Barres 1999). They are known to populate the optic stalk from E16, emerging from the retina-end and forming a perivascular, glial limiting membrane around the periphery of the nerve (C. Raff and H. Miller 1984, Small, Riddle et al. 1987). On the other hand, the first OPCs begin to emerge after P2 from the chiasm-end of the nerve (Raff 1989).

From early-mid gestation onwards, axons undergo selective deletion or pruning, which can reduce the number of WM axons by over half. Over the course of the first week and a half after birth, the number of RON axons dramatically declines to a more stable figure of 100,000 (Crespo, O'Leary et al. 1985). Prior to the initiation of myelination, the small pre-myelinated axons undergo a programme of radial expansion, where they increase in diameter (up to 3-fold) in preparation for contact with glial processes and ensheathment (Alix and Fern 2009). While OPCs appear at P2, the first post-mitotic, immature oligodendrocytes begin to emerge at P6, when their processes begin to navigate along pre-myelinated axons. Immature

oligodendrocytes extend a much higher number of processes compared to their more mature phenotype (typically 30 v 16 processes, respectively), which correlates to the high number of unmyelinated axons present in younger ONs (Butt and Ransom 1993). The first detectable wraps of myelin are observed between P6-P8 (Foster, Connors et al. 1982). By P10, only ~2% of axons are myelinated (Alix, Zammit et al. 2012). In addition, the first clusters of NaVs on axons begin to emerge between P9-P10, consistent with the redistribution of Na^+ channels to future nodes of Ranvier (Rasband and Shrager 2000). At this age, the ratio of astrocytes to oligodendrocytes is 50:50 (Wilke, Thomas et al. 2004). Myelination proceeds rapidly and by P28, approximately 85% of all axons with the nerve are myelinated (Foster, Connors et al. 1982). However, myelination continues up until ~P90, when 100% of RON axons are myelinated, analogous to a continuous increase in the number of oligodendrocytes into adulthood, where they eventually become the most abundant glial cell in the ON (Vaughn 1969). During this developmental period, the AP conduction velocity sharply increases from 0.2m/s at birth (P0), reaching 30 m/s in the fully-myelinated mature RON, a 150-fold increase (Foster, Connors et al. 1982).

The isolated ON is an *ex vivo* model and therefore should closely reflect any interactions or injury mechanisms which occur *in vivo*. Exposing the ON to modelled ischemia has provided invaluable information about the injury mechanisms involved in WM. Despite this, it is not without limitations. As mentioned previously, there are no physical barriers separating GM and WM regions in the CNS. While the absence of surrounding GM in the ON preparation ensures recordings are of pure WM origin, it also excludes any potential interactions with surrounding GM regions which are likely to have an influence *in vivo.*

1.1.3.2: Corpus Callosum (CC)

In addition to the ON, the corpus callosum (CC) was also used as a model WM tract during this project. The CC is the primary commissural WM tract in the brain, responsible for connecting the left and right cerebral hemispheres. It is the largest white matter tract in the mammalian brain, composed of between 200 and 250 million axonal projections in humans (Fitsiori, Nguyen et al. 2011). Although the majority of axons connect to homologous regions

in the opposite hemisphere, some axons project diagonally to contralateral association regions while some extend down through the CC from the supracallosal gyrus on the upper surface of the CC to the fornix, located on the under surface of the CC (Moody, Bell et al. 1988). The CC is classified into 3 spatial regions; the genu located anteriorly, the splenium found at the posterior region of the CC and the body, which is found in between these two structures.

Compared to the RON, developmental changes which occur in the rat CC are not as well characterised. The number of axons nearly triples from birth to P5 reaching approximately 11.4 million in the rat, but unlike the ON, this number is maintained until at least P60 in adult rats (Gravel, Sasseville et al. 1990). The first wraps of myelin sheath do not appear until P12 (Bjartmar, 1994). In addition, the mature CC consists of a mix of both myelinated and unmyelinated axons. Unlike the ON, the development of the CC is not homogenous across all regions (Luders, Thompson et al. 2010). Coronal brain slices, including the corpus callosum, have been previously used as a model WM as they have some advantages over isolated preparations such as the ON. While the ON excludes the cell body from which the axons originate, the whole CC slice includes the entire cell, including the cell body (Tekkok and Goldberg 2001). In addition, it also contains a mixed population of both myelinated and unmyelinated axons. Finally, intact brain slices include the surrounding GM which will likely affect WM regions *in vivo.*

1.2: Glutamate

Glutamate is the principle excitatory neurotransmitter in the mammalian CNS (Nedergaard, Takano et al. 2002). The excitatory actions of glutamate have been acknowledged since the mid-twentieth century when early studies found that the application of glutamate directly onto the motor cortex induced clonic-type convulsions in dogs and apes (Hayashi 1952). The vast majority (~90%) of excitatory neurons in the CNS are glutamatergic (Danbolt 2001). Glutamatergic signalling is associated with a variety of physiological processes including plasticity, learning and memory (Anderson and Swanson 2000, Danbolt 2001, Stys and Lipton 2007). In addition, more recent findings suggest that it is a key mediator of neuronal and glial cell development; regulating migration, proliferation, differentiation, synapse formation and myelination (Danbolt 2001, Lujan, Shigemoto et al. 2005, Lundgaard, Luzhynskaya et al. 2013).

Glutamate has a ubiquitous distribution throughout the brain and spinal cord. However, the actions of glutamate are not restricted to the CNS. Studies have shown that glutamate receptors are expressed in non-neuronal peripheral tissue including the heart, lungs, kidneys, bone marrow, ovary, testis and endocrine cells (Patton, Genever et al. 1998, Gill, Pulido et al. 1999, Gill and Pulido 2001). However, knowledge of the distinct functions of glutamatergic signalling in peripheral tissues is sparse (Nedergaard, Takano et al. 2002). For the relevance of this thesis, the following refers to glutamatergic signalling within the CNS.

1.2.1: Biosynthesis

1.2.1.1: De novo synthesis

Glutamate is a non-essential amino acid meaning that it is not a dietary requirement. It can be synthesised *de novo* though our own metabolism. Glutamate is unable to cross the blood brain barrier (BBB) and therefore, must be synthesised from local precursors within the CNS. Glucose is a major energy substrate in the brain. Glycolysis is an essential anaerobic biochemical pathway which converts a 6-carbon glucose molecule into two 3-carbon pyruvate molecules. The *de novo* synthesis of glutamate takes place in astrocytes due to the presence

of pyruvate carboxylase (PC), an enzyme which catalyses the production of oxaloacetate from pyruvate. In addition, pyruvate can also be metabolised to acetyl CoA by pyruvate dehydrogenase (PDH) (Schousboe, Scafidi et al. 2014). Both oxaloacetate and acetyl CoA enter the tricarboxylic acid cycle (TCA cycle) where they subsequently condense to form a net production of the intermediate, α-ketoglutarate. α-ketoglutarate is converted to glutamate via aspartate aminotransferase (ATT) (Westergaard, Drejer et al. 1996, Pardo, Contreras et al. 2013). While PC is abundant in astrocytes, neurons lack significant expression and therefore, lack the ability to synthesise large amounts of glutamate from glucose (Shank, Bennett et al. 1985). In astrocytes, glutamate is converted to glutamine (by the energy requiring enzyme, glutamine synthase), released into the ECS and taken up by neighbouring neurons, where it can be converted back to glutamate (Nedergaard, Takano et al. 2002) (See Fig. 1.4).

1.2.1.2: Pyruvate-Recycling Pathway

The *de novo* synthesis of glutamate is estimated to account for only 25-30% of the glutamate neurotransmitter pool (Schousboe, Bak et al. 2013). Alternatively, glutamate is taken up by a range of excitatory amino acid transporters (EAATS; see Section 1.2.2.1) and can enter the 'pyruvate-recycling pathway' where it is converted back into pyruvate again. Once taken up by astrocytes, glutamate is metabolised back into α-ketoglutarate by glutamate dehydrogenase (GDH). α-ketoglutarate dehydrogenase (KGDH) subsequently catalyses the oxidative decarboxylation of α-ketoglutarate to succinyl Co-A, which continues in the TCA cycle to form malate. Malate is then converted back into pyruvate via malic enzyme (ME). Pyruvate can be re-synthesised into glutamate, as required (Anderson and Swanson 2000, Platt 2007) (Fig. 1.4).

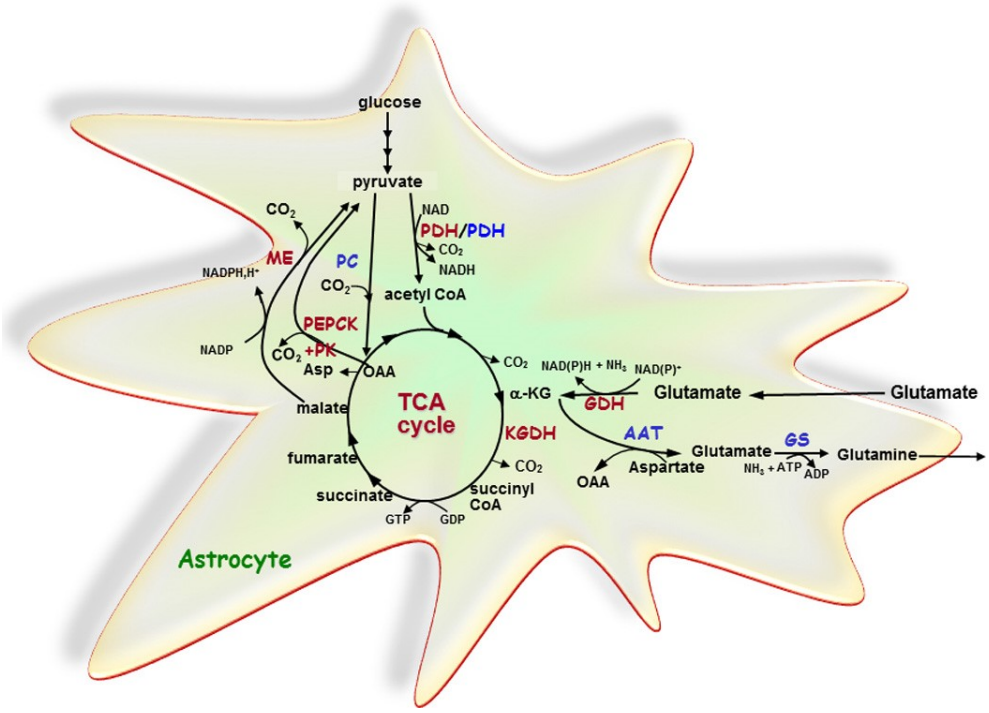

Fig. 1.4: Glutamate Biosynthesis.

A schematic representation outlining the *de novo* synthesis of glutamate from glucose (blue: essential enzymes) and the re-uptake of extracellular glutamate which enters the pyruvate-recycling pathway (red: essential enzymes). Taken from (Schousboe, Scafidi et al. 2014).

1.2.1.2: Glutamate-glutamine cycle

The glutamate-glutamine cycle is the major pathway by which glutamate is recycled in the CNS. This process requires an intimate relationship between neurons and astrocytes. Similar to the pyruvate-recycling pathway, once glutamate is released into the extracellular space, it is rapidly taken by EAATs located on astrocytes. Glutamate is then quickly converted into glutamine via glutamine synthase (GS), an enzyme which is absent in neurons (Chen and Swanson 2003). Glutamine is non-toxic, does not activate glutamate receptors and is the most common precursor of glutamate in the CNS. Glutamine can be shuttled out of astrocytes into the extracellular space by system-N transporters (SN1) and subsequently taken up from the extracellular space by glutamine specific, sodium-coupled amino acid transporters (SATs) located on neuronal membranes (Danbolt 2001, Chen and Swanson 2003). The up-taken glutamine is the main precursor of neuronal glutamate synthesis, as it can then be directly

converted back into glutamate via the mitochondrial enzyme, glutaminase (Danbolt 2001). Glutamate is then actively repackaged into vesicles (see section 1.2.2.2). Not only are astrocytes essential in the synthesis of glutamate, but they also play a vital role in the control of extracellular and intracellular glutamate concentrations.

1.2.2: Glutamate Transporters

1.2.2.1: Excitatory amino acid transporters (EAATs)

An essential characteristic of glutamatergic signalling is the maintenance of low resting extracellular concentrations. As mentioned, glutamate is abundant throughout the CNS however, the majority is kept within cells. Under physiological conditions, extracellular glutamate concentrations ($[Glut]_e$) are kept in the low micro-molar range, typically 1-4µM. In contrast, intracellular concentrations are over a thousand-fold higher (in the millimolar range, ~1-10mM), forming a steep concentration gradient (Danbolt 2001, Chen and Swanson 2003, Cavelier and Attwell 2007). The maintenance of low $[Glut]_e$ is predominantly due to glutamate uptake via a range of glutamate transporters, also referred to as excitatory amino acid transporters (EAATs). Synaptically released glutamate is rapidly removed by EAATs, with a time constant of approximately 1ms (Vyklicky, Korinek et al. 2014).

EAATs are thermodynamically-driven proteins which are located on the surface of cells throughout the CNS (Amara and Fontana 2002). The uptake of glutamate, against its concentration gradient, is predominantly driven by the steep Na^+ gradient across the plasma membrane (Sherwin and Fern 2005, Grewer, Gameiro et al. 2008). Thus, EAATs are secondary active transporters, using ionic gradients as a source of free energy for this process. The inward movement of glutamate is coupled with a net inward movement of between 2 and 3 Na^+ ions (depending on transporter subtype) with one H^+ ion, accompanied by the counter transport of one K^+ ion (Danbolt 2001, Amara and Fontana 2002, Grewer, Gameiro et al. 2008). Thus, EAATs are referred to as symporters. The stoichiometry of this process gives way to a net inward movement of positive charge. The electrogenic nature of this transport is further driven by a negative membrane potential across the plasma membrane (Amara and Fontana

2002, Grewer, Gameiro et al. 2008). This movement of ions is followed by the work of the Na^+/K^+ ATPase pump (sodium-pump) to restore the physiological Na^+-gradient and regain the resting V_m (Anderson and Swanson 2000). As discussed, glutamate taken up by astrocytes can either enter the pyruvate-recycling pathway or the glutamate-glutamine cycle. However, glutamate is also directly taken up by neurons, where it is packaged into vesicles (see below, section 1.2.2.2).

To date, 5 pharmacologically distinct Na^+-dependent glutamate transporter genes have been identified and cloned, known as EAAT1-5 in humans (Amara and Fontana 2002, Baud, Haynes et al. 2004). As it stands, EAAT-1 and EAAT-2 are the predominant glial transporters, EAAT-3 is a neuronal transporter, EAAT-4 is also a neuronal transporter but is restricted to GABAergic Purkinje cell neurons in the cerebellum, while EAAT-5 is restricted to bipolar cells and rod photoreceptors in the retina (Domercq, Sánchez-Gómez et al. 1999). However, they are all polypeptides which share about 50%-60% amino acid sequence similarity (Salter and Fern 2005). The non-human homologues of EAAT1-3 are referred to as GLAST (glutamate-aspartate transporter), GLT-1 (glial-type glutamate transporter) and EAAC-1 (excitatory amino acid carrier 1), respectively (Bridges and Esslinger 2005). Although these transporters are located on various cell types, astrocyte uptake is quantitatively most important (Anderson and Swanson 2000). GLAST and GLT-1 are abundantly distributed on astroglial membranes (Chaudhry, Lehre et al. 1995). Furthermore, these two-subtypes are the dominant regulators of glutamate uptake in the CNS (Rothstein, Dykes-Hoberg et al. 1996, Amara and Fontana 2002).

Similar to GM, EAATs regulate $[Glut]_e$ in WM. GLAST, GLT-1 and EAAC-1 are the major glutamate transporters found in the rodent ON (Domercq, Sánchez-Gómez et al. 1999). EAAC-1 (originally thought to be an exclusive neuronal transporter) was seen to be the major EAAT sub-type expressed on axons and oligodendrocytes (Arranz, Hussein et al. 2008). Conversely, EAAC-1 contributes to more l-glutamate ($[^3H]$-labelled) uptake than either of the other EAATs in developing oligodendrocyte cultures (derived from the P7 rat CC) (DeSilva, Kabakov et al. 2009). EAAT expression appears to be developmentally regulated, as GLT-1 expression is down-regulated as immature oligodendrocytes develop into mature myelin-producing oligodendrocytes *in vivo* (DeSilva, Kabakov et al. 2009). Similarly, another study also reported a strong expression of EAAT2 in developing oligodendrocytes in the 32-week gestational age

in human, whereas, expression was undetectable in 7 month olds (Desilva, Kinney et al. 2007). In contrast, the expression of EAAT1 and EAAT3 is constant throughout (Desilva, Kinney et al. 2007). Consistent with a high expression of EAATs during development, P14-P17 oligodendrocytes are capable of accumulating high levels of d-aspartate during exogenous perfusion (Arranz, Hussein et al. 2008). While GLT-1 is reportedly downregulated during development, Baltan *et al.* (2008) demonstrated that astrocytic GLT-1 expression increases in older mouse ONs (12 month old).

1.2.2.2: Vesicular Glutamate Transporters (VGLUTs)

While EAATs regulate $[Glut]_e$, vesicular glutamate transporters (VGLUTs) are responsible for regulating intracellular glutamate concentrations in neurons ($[Glut]_i$). The cytoplasmic concentration of neuronal glutamate can reach ~10mM. However, vesicular concentrations are typically several-fold higher, reaching concentrations of ~100mM (Cavelier and Attwell 2007). VGLUTs are vesicular-bound proteins which sequester cytoplasmic glutamate inside vesicles. Like EAATs, VGLUTs can also be classified into distinct subgroups; VGLUT1, VGLUT2 and VGLUT3. However, there are several major differences between the two groups of transporters. While EAATs have a very high affinity for glutamate, with a K_m between 4 and 40µM, VGLUTs have a much lower affinity, with a K_m of approximately 1mM (Shigeri, Seal et al. 2004). Unlike EAATs, VGLUTs are not Na^+-dependant transporters. VGLUT-mediated transport of glutamate is largely dependent on the activity of V-type H^+-ATPase, an ATP-dependant vesicular H^+ pump located on the vesicular membrane. The V-type H^+-ATPase is responsible for forming and maintaining a high concentration of protons inside the vesicular lumen, thus generating a proton gradient and an acidic environment inside vesicles (pH 5-5.5) (Cavelier and Attwell 2007). Furthermore, the proton gradient also forms an internal positive membrane gradient (approximately +50mV) across the vesicle (Beyenbach and Wieczorek 2006, Cavelier and Attwell 2007). It is this electrical transmembrane gradient, rather than the pH gradient, which drives the transport of negatively-charged glutamate by VGLUTs (Fremeau Jr, Troyer et al. 2001, Cavelier and Attwell 2007).

1.2.2.3: Glutamate-Cystine Antiporter

EAATs and VGLUTs represent the two major glutamate transporters within the CNS. However, it must be noted that the CNS expresses a number of proteins capable of glutamate transport. For example, the glutamate-cystine antiporter is an electroneutral exchanger which uses the glutamate transmembrane gradient to transport cystine into the cell. Unlike EAATs, the glutamate-cystine exchanger is Na^+-independent and transports glutamate out of the cell (Danbolt 2001, Bridges, Natale et al. 2012). This will be further discussed in section 4.1.3.5.

1.2.3: Glutamate Receptors

Excitatory neurotransmission is facilitated by a range of glutamate receptors located on the surface of neuronal and glial cells throughout the CNS. Thanks to the development of molecular biology and cloning, glutamate receptors can be broadly divided into two distinct families; ionotropic and metabotropic receptors. Ionotropic glutamate receptors (iGluRs) are ligand-gated ion channels which mediate rapid synaptic signalling, allowing the direct influx of ions such Na^{2+}, Cl^- and Ca^{2+} in response to agonist binding. On the other hand, metabotropic glutamate receptors (mGluRs) are G-protein coupled receptors and act via second messenger signalling pathways (Niswender and Conn 2010). While iGluRs mediate rapid glutamatergic signalling, mGluRs are commonly referred to as neuromodulatory glutamate receptors (Niswender and Conn 2010).

1.2.3.1: Ionotropic Glutamate Receptors (iGluR)

iGluRs are large, cation-specific ion channels which share a common tetrameric structure (i.e. made up of four protein sub-units). Each heterogeneous sub-class is composed of a variable combination of distinct receptor subunits (Fig. 1.5). Each receptor is composed of four hydrophobic subunits intercalated within the plasma membrane; including 4 transmembrane domains, one re-entrant pore loop, an extracellular N-terminus (expressing a ligand binding domain) and intracellular C-terminus (Paoletti and Neyton 2007). The variable subunit

composition for each receptor subtype heavily influences the receptors permeability to Na^+, K^+ and Ca^{2+} ions, electrophysiological properties and therefore, their functional properties. Changes in iGluR expression is particularly evident during development (Lujan, Shigemoto et al. 2005). Agonist binding induces a conformational change causing the channel to open. This allows the movement of charged ions through the transmembrane pore and causes a change in membrane potential referred to as an excitatory post synaptic potential (EPSP) (Platt 2007). iGluRs are ubiquitously distributed throughout the mammalian CNS, with evidence of functional expression on axons as well as astroglia, oligodendrocytes, NG-2 cells and even myelin itself (David, Yamada et al. 1996, Micu, Jiang et al. 2006, Ouardouz, Coderre et al. 2009, Ouardouz, Coderre et al. 2009, Li, Xiao et al. 2013).

Although all iGluRs share a common structure, they are classically sub-divided into three major subtypes based on their subunit composition and pharmacological characteristics; NMDA (N-methyl D-aspartate), AMPA (α-amino-3-hydroxy- 5-methyl-4-isoxazolepropionic acid) and kainate receptors (Ozawa, Kamiya et al. 1998). However, AMPA and kainate receptors are now regularly classified as 'non-NMDA receptors' as neither agonist (AMPA nor kainate) clearly distinguishes the receptors, since both agonists are capable of activating both receptors (Ozawa, Kamiya et al. 1998). AMPA receptors are assembled from a combination of GluR1-4 subunits, while kainate receptors contains a combination of GluR5-7 and KA1-2 (Traynelis, Wollmuth et al. 2010) (Fig 1.5). Non-NMDA receptors have a much lower affinity for endogenous glutamate compared to NMDA receptors (Dingledine, Borges et al. 1999, Platt 2007). They display very rapid gating kinetics and so, generate the early component of excitatory post synaptic currents (EPSC). Equally, they undergo rapid desensitisation (within 100ms), time-limiting the flow of ions (Dingledine, Borges et al. 1999, Platt 2007). Non-NMDA receptors are relatively permeable to monovalent cations, such as Na^+ and K^+, but are typically Ca^{2+} impermeable (Platt 2007). However, it must be noted that receptors which lack the Ca^{2+}-impermeable GluR2 subunit allow Ca^{2+} influx (Dean, Fraser et al. 2005). NMDA receptors are composed of a combination of 4 distinct sub-units from three families; NR1, NR2 and NR3 (Fig. 1.5). Interestingly, NMDA receptors have a voltage-dependant Mg^{2+} block, which can be relieved following sufficient depolarisation of the cell membrane. This can be provided by AMPA/kainate receptor activation. NMDA receptors will be discussed in more detail in section 5.1.2.

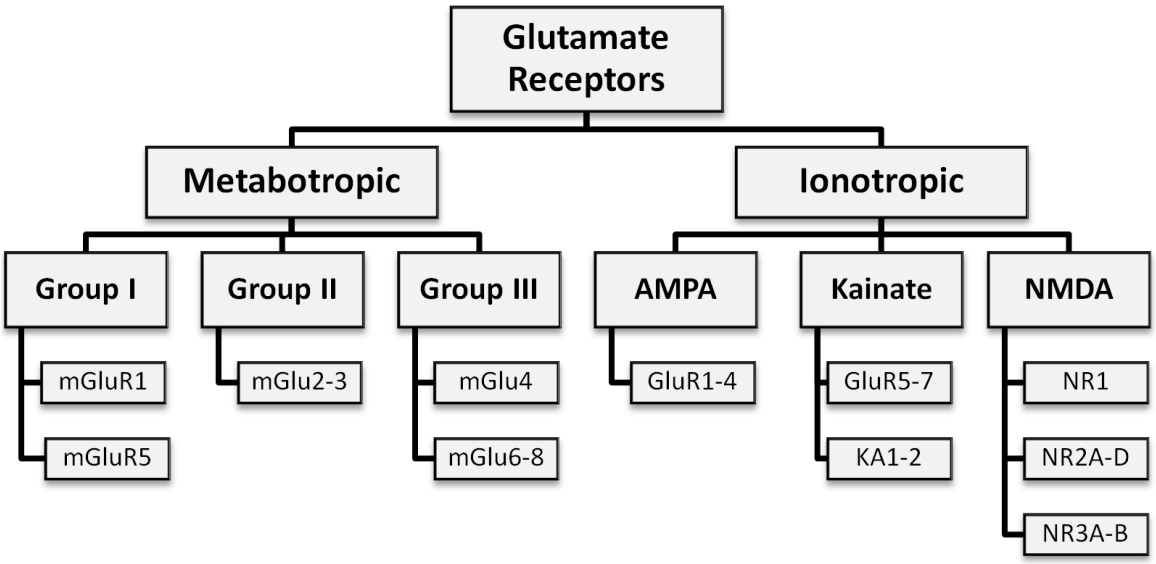

Fig 1.5: Classification of glutamate receptor class, sub-classes and subunit composition.

Glutamate receptors can be broadly divided into ionotropic and metabotropic receptors. Ionotropic receptors are further divided into AMPA, kainate and NMDA receptors. Metabotropic receptors are divided into group I, group II and group III. Each receptor is composed of a variable combination of distinct subunits.

1.2.3.2: Metabotropic Glutamate Receptors (mGluR)

mGluRs are G-protein coupled receptors which are responsible for the modulation of slow excitatory transmission. They consist of a dimer of two 7–transmembrane domains which when activated, initiate an intracellular cascade of events. mGluRs relay information though the activation of intermediate molecules known as G-proteins. G-proteins are intracellularly bound to mGluR and are composed of α, β and γ subunits. In its inactivated state, the α subunit is linked to GDP (guanine diphosphate) (Niswender and Conn 2010). However, the binding of an extracellular agonist to the receptor causes the exchange of GDP for GTP (guanine triphosphate), and the disassociation of the α subunit from the trimeric complex. The β, γ dimer and the GTP-bound α subunit are then free to activate a variety of downstream targets such ion channels or effectors, capable of mediating intracellular secondary messengers (Niswender and Conn 2010).

mGluRs are divided in three sub-types (Group I,II and III) based on their intracellular signalling mechanisms and pharmacology. Group 1 mGluRs are coupled to phospholipase C which classically leads to Ca^{2+} immobilisation. Whereas group II and III, directly regulate ion channels through the inhibition of adenylate cyclase (Niswender and Conn 2010). Within these groups, there are eight receptor sub-units (mGluR 1-8) (Fig 1.5).

1.2.4: Excitotoxicity

Under a variety of pathological conditions, the excessive release of endogenous glutamate and/or the failure of EAATs can have detremential effects. Elevated extracellular glutamate concentrations ($[Glut]_e$) can lead to the sustained activation of iGluRs, a phenomenon known as *excitotoxicity*. Excitotoxicity is defined as the pathological process of cell death resulting from the toxic actions of excitatory amino acids (Dong, Wang et al. 2009), or simply as "an exaggeration of the excitatory effect" (Olney, Rhee et al. 1974). This mechanism underlies the progression of a growing number of acute and chronic neurological disease states (Wang and Qin 2010). These include stroke, traumatic brain injury, hypoglycaemia, spinal cord injury, Alzheimer's and Parkinson's disease (Blandini, Porter et al. 1996, Reisberg , Doody et al. 2003, Xu, Hughes et al. 2004, Yi and Hazell 2006, Doyle, Simon et al. 2008, Alix and Fern 2009, Yang, Hamner et al. 2014).

The toxic actions of glutamate were first reported in 1957 by D.R. Lucas and J.P. Newhouse, who noticed that systemic injections of sodium l-glutamate induced cell death in the inner layer of the retina in mice (Lucas and Newhouse 1957). The term 'excitotoxicity', was later coined by John Olney in 1969 who confirmed the neurotoxic actions of glutamate after finding that subcutaneous injections also induced acute neuronal necrosis in a variety of regions in the CNS (Olney 1969). However, excitotoxic damage is not confined to neurons. Since then, a variety of studies have demonstrated the vulnerability of oligodendroglia to excitotoxicity (Fern and Moller 2000, Deng, Rosenberg et al. 2003, Xu, Hughes et al. 2004, Káradóttir, Cavelier et al. 2005, Salter and Fern 2005, Hamilton, Hubbard et al. 2009). There is also evidence of glutamate-receptor mediated injury to astrocytes, microglia and NG-2 cells (David, Yamada et al. 1996, Kingham, Cuzner et al. 1999, Hamilton, Hubbard et al. 2009).

Elevated concentrations of extracellular excitatory amino acids, such as glutamate and aspartate, promote the over-activation of iGluRs. This ultimately gates the post-synaptic receptor ion channel allowing an excessive influx of a range of extracellular ions including Na^+, Cl^- and Ca^{2+}. Na^+ influx through the ion channel (combined with K^+ efflux) meadiates the excessive depolaraisation of the post synaptic membrane (Dong, Wang et al. 2009). In addition, the accumulation of Na^+ and Cl^- ions contribute to rapid cellular swelling and osmotic disruption, a common feature of excitotoxicity (Olney, Price et al. 1986, Choi 1987). While the removal of extracellular Na^+ or Cl^- ions can prevent early neuronal cell swelling, it has no effect on the inevitable cell death which occurs after prolonged periods sustained receptor activation (Choi 1987). The rise in intracellular Ca^{2+} concentration ($[Ca^{2+}]_i$) is recognised as the central mediator of excitotoxic cell death (Choi 1985, Choi 1987). Under physiological conditions, $[Ca^{2+}]_i$ is kept low due to the activity of a varity of mechanisms, including the Ca^{2+}-ATPase and the Na^+-Ca^{2+} exchanger (NCX). However, under certain pathological conditions, the failure of these homeostatic mechanisms combined with the excessive influx of Ca^{2+} through iGluRs allow $[Ca^{2+}]_i$ to reach toxic levels. High $[Ca^{2+}]_i$ triggers a cascade of events, including the activation of a variety of deleterious, Ca^{2+}-dependant enzymes capable of causing apoptotic and necrotic cell death (Szydlowska and Tymianski 2010). The activation of lipases, proteases, phospahatases and endonucleases promote the degradation of cell organelles, cytoskeletal/membrane disruption and toxic downstream events (Szydlowska and Tymianski 2010). The excitotoxic rise in $[Ca^{2+}]_i$ is largely considered a consequence of direct entry through iGluRs. The activation of Ca^{2+}-permeable NMDA receptors and/or AMPA/Kainate receptors (particularly GluR2-lacking receptors) can elevate cystolic free Ca^{2+}, a process which is exacerbated under certain patholgical conditions. For example, the toxic rise in $[Ca^{2+}]_i$ in oligodendrocyte cell bodies during ischemia is largely facilitated through the activation of AMPA/kainate receptors (Fern 1998, Deng, Rosenberg et al. 2003, Wilke, Thomas et al. 2004, Salter and Fern 2005). Interestingly, NMDA receptors are known to permit a much larger Ca^{2+} influx (Mayer and Westbrook 1987) and therfore, have a greater potential in mediating the detrimental rise in $[Ca^{2+}]_i$ (Salter and Fern 2005, Micu, Jiang et al. 2006, Szydlowska and Tymianski 2010). However, it must be noted that AMPA/kainate receptor activation is known to mediate WM damage in the absence of extracellular Ca^{2+}, indicating that receptor activation may be sufficient to induce Ca^{2+} release from intracellular stores or that $[Na^+]_i$ accumulation alone may mediate cell death (Baltan, Besancon et al. 2008). As

cystosolic Na^+ and Ca^{2+} increases, alternative mechanisms are known to contribute to excitotoxic-induced Ca^{2+} overload. For example, excessive membrane depolarisation can activate voltage-gated Ca^{2+} channels (Lee, Zipfel et al. 1999). Similarily the sodium-calcium exchanger (NCX), which normally extrudes $[Ca^{2+}]_i$ in exchange for Na^+, is known to operate in reverse contributing to the initial rise in $[Ca^{2+}]_i$ observed following acute exposure to excitotoxins (Hoyt, Arden et al. 1998).

Mitochondria can sequester cytosolic Ca^{2+}, which depolarises the mitochondrial membrane potential ($\Delta\psi_m$). Excitotoxic Ca^{2+} influx can promote mitochondrial overload which can lead to the opening of the permeability transition pore (PTP) on the inner mitochondrial membrane. Under such conditions, the PTP sequentially begins to release Ca^{2+} back into the cytosol, along with apoptotic mediators like cytochrome-c (Nicholls and Budd 1998, Nicholls and Ward 2000, Szydlowska and Tymianski 2010). Mitochondrial Ca^{2+} accumulation also leads to the generation of excessive reactive oxygen species (ROS), like nitric oxide (NO), which can cause damage to cellular nucleic acids and promote mitochondrial dysfunction (Szydlowska and Tymianski 2010).

The involvement of metabotropic glutamate receptors in excitotoxicity is still somewhat controversial. There is evidence to suggest that prolonged activation of mGluRs (particularly group 1) reduces neuronal susceptability to NMDA-mediated excitotoxicity in both organotypic hippocampal and cortical culture (Koh, Palmer et al. 1991, Bruno, Copani et al. 1994, Baskys, Bayazitov et al. 2005). This is also the case for oligodendrocyte cultures exposed to ischemic conditions, an effect was was suggested to be a result of preventing intrecellular glutathione loss and inhibiting the build-up of ROS (Deng, Wang et al. 2004). On the otherhand, other studies have found them to exaccerbate axonal injury by promoting intracellular Ca^{2+} release via phospholipase-c activation (AGRAWAL, THERIAULT et al. 1998, Stys 2005).

1.3: Ischemia

1.3.1: White Matter Ischemia

The human brain represents approximately 2% of the total body mass, yet consumes 20% of the body's total energy production at rest (Engl and Attwell 2015). The majority of cerebral ATP (adenosine triphosphate) is generated through a combination of glycolysis (in the cytosol) and oxidative phosphorylation (in the mitochondria). Thus, the brain requires a continuous supply of the essential substrates required for cellular respiration, specifically O_2 and glucose. To achieve this, the brain receives nearly a quarter of our total cardiac output (Flynn, MacWalter et al. 2008), consuming ~20% of total oxygen intake and ~25% of circulating glucose (Harper and Jennett 1990, Doyle, Simon et al. 2008). Cerebral ischemia is defined as the inadequate supply of essential nutrients to the brain, which occurs through the cessation of blood flow. An insufficient supply of O_2 and glucose ultimately leads to depleted levels of cellular ATP which can have catastrophic consequences.

On the basis of O_2 consumption, WM has a lower metabolic rate when compared to cerebral GM (Nishizaki, Yamauchi et al. 1988). Consequently, it receives a lower blood supply. For example, while GM regions typically receives a blood flow of 50ml/100mg/min^{-1}, WM receives 30ml/100mg/min^{-1} (Mohr, Grotta et al. 2011). As a result, WM has a higher infarction threshold (Pantoni, Garcia et al. 1996, Tekkok and Ransom 2004). Even so, prolonged periods of ischemia can result in extensive WM damage. Due to the high density of packing within WM tracts, the formation of an infarct severely disrupts signal transmission and neuronal circuits, which will inevitably lead to devastating clinical impairments. Ischemic WM injury can lead to the reduced conductance velocity of WM axons or in severe cases, a complete block in action potential conduction. To date, a variety of neuroprotective compounds have shown promise in rodent stroke models but have failed in clinical trials (Song, Woodbury et al. 2014). While their failure is likely multifactorial, the under-appreciation of WM injury in stroke is now considered a primary reason. WM constitutes about 14% of total brain volume in the rodents, whereas, it occupies about 50% in humans (Song, Woodbury et al. 2014). Many studies have focused on GM protection, inadvertently neglecting WM. Considering the high

percentage of WM in the human brain, it comes as no surprise that stroke is rarely confined to GM (Goldberg and Ransom 2003). The occlusion of large intracranial arteries will affect both grey and white matter regions. Ischemic WM damage is now recognised as a major component of cerebral ischemia (Sozmen, Hinman et al. 2012). In fact, approximately 95% of all ischemic stroke patients exhibit some degree of WM injury (Ho, Reutens et al. 2005, Wang, Liu et al. 2016). Interestingly, WM damage occupies an average of 42% of the total infarct volume (Ho, Reutens et al. 2005). Furthermore, up to 30% of ischemic strokes predominantly involve subcortical WM infarcts due to the occlusion of penetrating arteries which supply deep WM regions (Rosenzweig and Carmichael 2013). In addition, the injury mechanisms which operate under ischemic conditions are distinct from those which contribute the GM damage, which may explain the lack of clinical benefits to date. There are a number of ways in which WM can be deprived of an adequate blood supply;

1.3.1.1: Stroke

Stroke is a devastating disease which occurs approximately 150,000 times every year in the UK alone (Writing Group, Roger et al. 2012). Despite major advances in recent years, it is currently the 4th leading cause of death in the UK (Hackett, Yang et al. 2010, Lerdal, Bakken et al. 2011). However, according to the World Health Organisation (WHO), it is the 2nd largest cause of mortality worldwide, accounting for approximately 6.7 million deaths every year (WHO, 2014). In addition, it is the leading cause of long-term disability, with nearly half of all stroke survivors suffering from physical and/or mental impairments (Ovbiagele and Nguyen-Huynh 2011). This accounts for a wide range of disabilities including speech, walking, co-ordination, swallowing and vision to name but a few. Furthermore, the burden of the disease is set to double worldwide by 2030 due to an ageing population (Feigin, Forouzanfar et al. 2014). While age is the single largest risk factor for stroke, other factors include smoking, excess alcohol, obesity, diabetes and high blood pressure (Scarborough, Bhatnagar et al. 2011).

It is estimated that approximately 30% of all stroke survivors experience a recurrent stroke (Mohan, Wolfe et al. 2011). In fact, it is estimated that recurrent strokes account for 25-33% of total cases (Stroke Association, Stroke statistics 2016). A study by Lee *et al.* found that of

patients who experienced a stroke, 24% had a second cerebrovascular event within 5 years (Lee, Shafe et al. 2011). Recurrent strokes are typically more severe, with approximately 16% being fatal within 56 days of the initial stroke (Lee, Shafe et al. 2011). Unfortunately, current treatments for acute stroke are relatively limited. Therefore, there is an urgent need for effective interventions in order to minimise irreversible damage.

There are two distinct types of cerebral stroke; haemorrhagic and ischemic. A haemorrhagic stroke involves the rupture of a weakened blood vessel and a subsequent bleed which occurs either within the brain (an intracerebral haemorrhage), or on the surface of the brain (a subarachnoid haemorrhage) (Gomes and Wachsman 2013). It results in the accumulation of blood, increasing pressure in the surrounding tissue and disruption normal blood flow. Haemorrhagic strokes are typically more severe than ischemic stroke, but only account for approximately 10-15% of all cases (Gomes and Wachsman 2013). The remaining 85-90% of cases are ischemic. Ischemic strokes involve the occlusion of a major artery or blood vessel within the brain which obstructs blood flow, and therefore, restricts the supply of essential nutrients. This is a consequence of clot formation within the artery, either via a thrombosis or an embolism. The degree of cell death depends on the severity and the duration of the ischemic insult (Doyle, Simon et al. 2008). Ischemic strokes typically lead to the formation of an infarct, which is a region of severe tissue damage within the brain (Doyle, Simon et al. 2008). The infarct core is characterised by rapid focal necrosis and irreversible damage. However, the surrounding area, known as the penumbra, can remain functionally viable for a short period due to the collateral blood supply (Gomes and Wachsman 2013). However, the collateral supply is incapable of supporting this region indefinitely, and so, cells within the penumbra will succumb to apoptosis/necrosis unless the blood supply is restored. This region is the most clinically salvageable area and therefore, is the focus of much research.

1.3.1.2: Periventricular White Matter Injury and Cerebral Palsy

Selective WM injury in the developing brain is the most common pathological substrate associated with a range of neurological disorders, including cerebral palsy (Khwaja and Volpe 2008). WM pathology in the neonatal brain was first reported by Virchow in 1867, who

described the 'softening' of developing WM (Jin, Londono et al. 2015). Some years later in 1962, Banker & Laroche described the necrosis of WM regions adjacent the lateral ventricles (Banker and Larroche 1962). While research into the etiology of immature WM pathology is still ongoing, ischemia is currently considered the most common predisposing factor related to this pattern of injury (Back 2014). Interestingly, ischemic insults to the early developing CNS selectively damage WM structures, while sparing GM regions (Fern 2011). As a result, ischemia regularly leads to the development of a selective pattern of injury known as periventricular white matter injury (PWMI).

As the name suggests, PWMI is found deep in developing WM adjacent the lateral ventricles (Shannon, Salter et al. 2007). The hallmark characteristic of PWMI is the death of developing oligodendrocytes. However, irreversible injury to pre-myelinated axons, diffuse gliosis and enlarged ventricles is also evident. Severe cases involve ischemic-type lesions, known as periventricular leukomalacia (PVL), which display a focal necrotic core, surrounded by areas of diffuse injury, characterised by the selective loss of developing oligodendrocytes (Banker and Larroche 1962, Volpe 2001). Pre-term infants are the largest patient cohort who suffer PWMI, with the high-risk period being those born between weeks 23 and 32 of gestation. It is apparent in approximately 50% of pre-term infants born before 32 weeks and/or under 1500g birth-weight (Khwaja and Volpe 2008). Advances in neonatal care have dramatically improved the survival rate of pre-term infants, yet there has been no significant reduction in the incidence of this debilitating WM injury (Alix and Fern 2009). Infants who develop PWMI, regularly exhibit problems such as seizures, sensory/cognitive deficits and/or motor disabilities, including cerebral palsy (CP). CP is a non-progressive disorder which accounts for a wide range of incurable motor and sensory impairment syndromes, which manifest at a young age, and continue unabated throughout a lifetime (Volpe 2001). It is the most common human birth disorder, with a prevalence of 1 in every 400 live births (Kuban and Leviton 1994). This translates to approximately 1800 new cases of CP every year in the UK alone (cerebralpalsy.org.uk). PWMI is the leading cause of CP in surviving premature infants (Salter and Fern 2008). It is estimated that between 60-100% of CP cases, show signs of PWMI (Anderson and Swanson 2000). However, at the moment there are not effective treatments or prophylactic remedies for dealing with this.

This raises the question as to why the developing brain would be deprived of blood, and what makes WM so susceptible? The propensity for PWMI is closely associated with an incomplete vascular supply at this age (Volpe 2001, Khwaja and Volpe 2008). Focal necrotic lesions in PVL are typically located in the arterial end zones of long penetrating vessels. The distal end zones of penetrating arteries are not fully developed during the early-mid gestational period of human development, which leaves deep WM regions particularly susceptible to periods of prolonged ischemia if blood flow decreases. In addition, blood flow to WM regions in the developing brain is surprisingly low, ranging from 1.6 to 3ml. 100 $g^{-1}.min^{-1}$, which is approximately 25% of what GM regions receive at this age (Khwaja and Volpe 2008). Therefore, the margin by which cerebral blood flow (CBF) can drop before injury begins to occur is minimal (Volpe 2001). There is also evidence to suggest that that immature infants show an impaired autoregulation of CBF during periods of low blood pressure (Khwaja and Volpe 2008). This is likely related to the absence of muscles in penetrating arteries (Kuban and Gilles 1985). A second cohort of full-term infants suffer birth-asphyxia, which is the temporary interruption of oxygen availability during birth (Morales, Bustamante et al. 2011). This may can occur from a prolapsed umbilical cord before birth, delivery complications or underdeveloped lungs (cerebralpalsysymptoms.com). In addition, genetic factors, such as congenital heart disease (CHD), may also leave infants susceptible to prolonged periods of ischemia (Back and Rosenberg 2014).

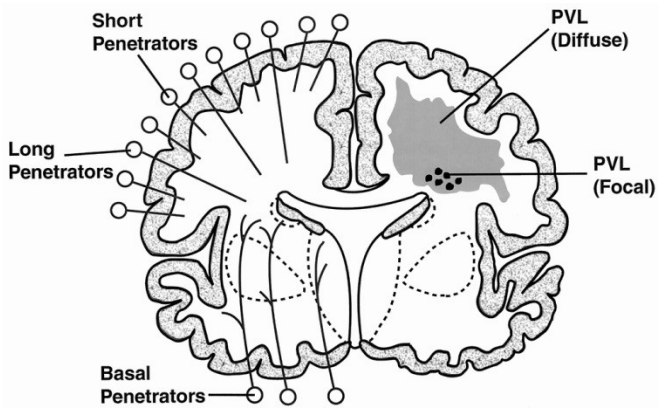

Fig 1.6: Cerebral blood supply and periventricular white matter injury.

Schematic representation of a coronal section through the cerebrum. The left hemisphere indicates the cerebral vascular supply, including long and short penetrating arteries. The right hemisphere indicates the location of both focal necrotic regions (black) and the diffuse penumbra region (grey) seen with PVL. Note the location of focal regions adjacent the lateral ventricles (centre). The outer overlaying grey shading depicts grey matter, whereas the under-laying white region depicts white matter. Taken from (Volpe 2001).

1.3.1.3: Cardiac arrest, vascular dementia and spinal cord injury

As discussed, stoke and PWMI regularly lead to the formation of focal ischemic lesions. However, global cerebral ischemia, which encompasses the entire brain, can also occur when blood flow to the brain is completely stopped. This is regularly a consequence of cardiac arrest. Ischemic heart disease is the leading cause of death worldwide, accounting for approximately 8.76 million deaths per year (WHO, 2014). Furthermore, approximately 40% of patients who survive cardiac arrest are left in a vegetative state (Madl, Kramer et al. 2000). Cerebral ischemia is considered the leading cause of disability and death following cardiac arrest (Mangus, Huang et al. 2014). The cessation of systemic circulation during cardiac arrest leaves the cerebrum susceptible to global ischemic brain injury. If blood supply in not restored quickly, this ultimately leads to extensive neuronal and glial damage.

Vascular dementia is the second leading cause of dementia, after Alzehimers' disease. It currently affects approximately 150,000 people in the UK. Interestingly, approximately 20% of patients who survive a stroke will develop vascular dementia. Subcortical vascular dementia is typically caused by cerebrovascular disease, such as hypertensive small vessel disease (Strub 2003). It typically arises from the development of thick walled arteries, and stiff and twisted blood vessels which ultimately reduce blood supply. It is the most common form of vascular dementia and predominantly occurs in people over the age of 65 (Alzehimers Society, Vascular dementia).

A reported 2.5 million people are currently living with spinal cord injury, with that number increasing by approximately 130,000 every year (Thuret, Moon et al. 2006). Similar to stroke, it is a major debilitating pathology. The primary insult typically arises from physical trauma. However, secondary injury is regularly observed due to vascular and biochemical events which occur following the initial insult (Oyinbo 2011). The vascular mechanisms of secondary injury include impaired autoregulation of blood flow, systemic hypotension and ischemia-reperfusion. A reduction in blood flow immediately after the primary trauma can contribute to exacerbating the injury.

1.3.2: Pathophysiological events during WM Ischemia

1.3.2.1: Early events: Ischemic depolarisation

Depleted levels of ATP during ischemia initiate a deleterious cascade of events which ultimately lead to cell death if the blood supply is not restored. ATP is utilised by a variety of energy-dependant proteins and pumps involved in maintaining homeostatic conditions. A significant fraction of cerebral ATP is used by the Na^+/K^+ ATPase to maintain ionic gradients within the CNS. It is estimated that the Na^+/K^+ ATPase consumes up to 50% of the brains energy levels (Attwell and Laughlin 2001). The Na^+ and K^+ gradients between the intracellular compartment and extracellular space, power a variety of homeostatic transporters, including several Na^+-coupled transport systems such as the sodium-calcium exchanger (NCX) and excitatory amino acid transporters (EAATs). As mentioned in section 1.1.1.2, these ionic gradients are also essential for action potential conduction in WM.

During ischemia, cellular ATP levels are consumed within a matter of minutes which leads to the failure of a variety of ATP-dependant pumps, including the Na^+/K^+ ATPase. The failure of the Na^+/K^+ ATPase and the gating of ATP-sensitive K^+ channels cause a dramatic rise in $[K^+]_e$ (Ransom, Walz et al. 1992, Sun and Feng 2013), accompanied by a depolarising shift in membrane potential, which subsequently gates a number of voltage-dependant channels (Stys 1998, Alix 2006). Na^+ influx proceeds through the opening of non-inactivating voltage-gated Na^+ channels (VGNCs) (Malek, Adorante et al. 2005, Stys 2005). While axons are incapable of AP conduction following the collapse of Na^+/K^+ gradients, the early loss in excitability does not directly lead to irreversible injury. It is under these conditions which a variety of deleterious events occur.

In an effort to maintain sufficient levels of ATP, astrocytic glycogen stores may be utilized via an increase in anaerobic metabolism. However, the amount of ATP produced by anaerobic respiration alone is minimal. It leads an accumulation of extracellular lactic acid and an acid shift in extracellular pH (~0.31 drop) (acidosis) (Ransom, Walz et al. 1992). In addition, the high intracellular levels of Na^+ also promote the reverse operation of the Na^+-H^+ antiporter, further acidifying the intracellular compartment (Stys 1998).

1.3.2.2: Axonal Ionic Injury Mechanisms: 'Ca^{2+} dyshomeostasis'

The collapse of cellular Na^+ and K^+ gradients predisposes a variety of mechanisms which mediate irreversible cell injury and death in WM. Ca^{2+} is a major intracellular second messenger in neurons and glia. Intracellular Ca^{2+} signalling is dependent on the maintenance of low cytosolic concentrations in quiescent cells (Alberdi, Ruiz et al. 2014). While extracellular Ca^{2+} concentrations ($[Ca^{2+}]_e$) are approximatly 2mM, intracellular Ca^{2+} concentrations ($[Ca^{2+}]_i$) are maintained in the nanomolar range (typically <150nM) by several proteins, including the Ca^{2+}-ATPase which sequesters Ca^{2+} into intracellular stores and Na^+/Ca^{2+} exchanger, which extrudes Ca^{2+} across the plasma membrane. In addition, numerous cytosolic, Ca^{2+}-binding proteins (or 'Ca^{2+} buffers') serve as chelators of free Ca^{2+} ions, which modulates the temporal and spatial transient rises in cytosolic Ca^{2+} (Schwaller 2010). Examples of Ca^{2+} buffers include calretinin, calbindin-D9k/-D28k and parvalbumins.

During ischemia, the failure of these mechanisms combined with the excessive influx of $[Ca^{2+}]_e$ across the plasma membrane and/or the release of Ca^{2+} ions from intracellular stores, leads to toxic elevations in cytosolic Ca^{2+}. As previously mentioned in section 1.2.4, Ca^{2+} overload promotes several toxic downstream events, including the activation of a variety of deleterious Ca^{2+}-dependant enzymes e.g. protease and lipases (Marcoli, Bonfanti et al. 2004, Montana, Ni et al. 2004, Káradóttir, Cavelier et al. 2005). Ca^{2+} overload is recognised at the central deleterious event in ischemic WM.

Numerous studies have shown that irreversible WM injury is a Ca^{2+}-dependant process. However, the source and pathway of cytosolic Ca^{2+} is somewhat controversial. The influx of $[Ca^{2+}]_e$ is a major mediator of anoxic injury in the myelinated ON (Stys, Ransom et al. 1990, LoPachin and Stys 1995). Studies have shown that the degree of anoxic injury is directly proportion to the concentration of $[Ca^{2+}]_e$, with complete protection seen with 0mM Ca^{2+} (plus the calcium chelator, EGTA) (Stys, Ransom et al. 1990). Furthermore, anoxia leads to a sustained decrease in extracellular Ca^{2+} levels by approximately 0.42mM, consistent with the influx of extracellular ions (Brown, Westenbroek et al. 2001). In contrast, Ouardouz *et al.* found that the ischemic rise in axonal Ca^{2+} in the dorsal column predominantly originates from intracellular stores (Ouardouz, Nikolaeva et al. 2003). In fact, Ca^{2+} free solutions are known to exacerbate injury in older WM tracts (optic nerve) (Baltan, Besancon et al. 2008). Nikolaeva

et al. reported that the chemical ischemia-induced rise in ON axonal Ca^{2+} is only abolished when $[Ca^{2+}]_e$ was omitted, and IP_3/ryanodine receptors on intracellular stores were simultaneously blocked (Nikolaeva, Mukherjee et al. 2005). Therefore, it is plausible that Ca^{2+} dyshomeostasis during ischemia occurs via multiple pathways.

1.3.2.2a: Reversal of the Na^+/Ca^{2+} Exchanger (NCX)

Interestingly, Na^+ influx through non-inactivating VGNCs is also necessary for irreversible anoxic injury in the RON (Stys, Waxman et al. 1992). Axoplasmic Na^+ levels gradually rise over the course of 60 minutes of anoxia, increasing by approximately 5-fold, reaching concentrations near 100mM (LoPachin and Stys 1995, Stys, Lehning et al. 1997). Na^+ channel blockade (with either TTX or STX) or Na^+ replacement (with either Cl^- or Li^+) significantly improves post-anoxic compound action potential (CAP) recovery in the myelinated RON (Stys, Waxman et al. 1992, Brown, Westenbroek et al. 2001). A major mechanism for coupling the fluxes of both Ca^{2+} and Na^+ ions is the NCX. The NCX is an transmembrane antiporter which usually extrudes $[Ca^{2+}]_i$ ions from a cell in exchange for $[Na^+]_e$ ions. However, the accumulation of $[Na^+]_i$ combined with a positive shift in membrane potential favours the reverse operation of the NCX and thus, promotes transport of Ca^{2+} into a cell. Pharmacological inhibition of the NCX is highly protective, resulting in a significant improvement in CAP recovery post-anoxia (Stys, Waxman et al. 1992, Li, Jiang et al. 2000). Likewise, inhibition of the NCX (with bepridil) also prevents a significant component of the anoxia-induced drop in $[Ca^{2+}]_e$ during anoxia (Brown, Westenbroek et al. 2001). Therefore, a primary route of axonal Ca^{2+} influx during anoxia is through the reversal of the NCX.

1.3.2.2b: Voltage-Gated Ca^{2+} Channel (VGCCs) activation

An early study by Stys *et al.*, found that the application of a range of non-specific Ca^{2+} channel blockers (Mn^{2+}, Co^{2+} and La^{3+}) had no significant effect on ON functional recovery following anoxia (Stys, Ransom et al. 1990). However, it was suggested that any potential protection may have been clouded by the toxic effect of applying inorganic ions (Stys 1998). Therefore, the involvement of voltage-gated Ca^{2+} channels (VGCCs) was re-examined some years later

due to a lack of appropriate controls. More recent studies using non-toxic L-type VGCC antagonists (nifedipine, diltiazem and verapamil) found a significant improvement in CAP recovery post-anoxia (Fern, Ransom et al. 1995). Furthermore, the co-application of N-type channel antagonist, SNX-124, with diltiazem added further protection post-anoxia suggesting that multiple sub-types of VGCCs mediate a toxic rise in $[Ca^{2+}]_i$ (Fern, Ransom et al. 1995). Similar to NCX inhibition (with bepridil), inhibiting L-type VGCCs (with diltiazem) also reduced the drop in $[Ca^{2+}]_e$ levels in the adult RON during anoxia (Brown, Westenbroek et al. 2001). Thus, a combination of influx through VGCCs and the NCX contribute to the toxic Ca^{2+} rise in myelinated axons.

Moreover, Ca^{2+} influx through VGCCs mediate the ischemic injury of developing pre-myelinated axons. Diffuse expression of VGCCs along the axolemma of pre-myelinated axons is known to contribute to AP conduction during development (Alix, Dolphin et al. 2008). However, the expansion of central pre-myelinated axons prior to the initiation of myelination is accompanied by the formation of clustered Ca^{2+} channels (P- and Q- type) which populate future nodes of Ranvier (Flynn, MacWalter et al. 2008, Alix, Zammit et al. 2012). Interestingly, these large diameter central axons are particularly susceptible to ischemic injury, which is mediated via Ca^{2+} influx through these VGCCs (Alix, Zammit et al. 2012).

1.3.2.2c: Mobilisation of Intracellular Ca^{2+} Stores

While Ca^{2+} influx through the NCX and VGCCs mediates a significant component of the axonal Ca^{2+} rise, several studies have reported a rise in the absence of extracellular Ca^{2+} (Ouardouz, Nikolaeva et al. 2003). This is associated with the release of Ca^{2+} from intracellular stores, such as the endoplasmic reticulum (ER). Intracellular Ca^{2+} storage compartments contain relatively high concentrations of Ca^{2+} (0.1-1mM). Interestingly, when myelinated ONs are exposed to caffeine, an agonist of ryanodine receptors, it leads to a dramatic increase in Ca^{2+}-sensitive OGB-2 fluorescence, suggesting that intracellular release is capable of elevating axoplasmic Ca^{2+} levels (Ren, Ridsdale et al. 2000). The major sources of intracellular Ca^{2+} release from ER is through ryanodine receptors (RyR), inositol-1,4,5-triphosphate receptors (IP3R), NAADP-sensitive receptors and SCaMPER (sphingolipid Ca^{2+} release-mediating protein of the ER) (Stys 2005). In contrast to previous studies, Ouardouz *et al*. found that the omission

of bath Ca^{2+} had no protective effect on dorsal column axons which were exposed to 60 minutes of ischemia (Ouardouz, Nikolaeva et al. 2003). However, when intracellular stores were depleted with the Ca^{2+}-ATPase inhibitor thapsigargin, there was a significant improvement in CAP recovery (Ouardouz, Nikolaeva et al. 2003, Ouardouz, Malek et al. 2006). Furthermore, the rise in $[Ca^{2+}]_i$ in a Ca^{2+} free aCSF solution was abolished in the presence of blockers of ryanodine and IP3 receptors (Ouardouz, Malek et al. 2006).

The L-type Ca^{2+} channel blockers, diltiazem and nimodipine, which block the channels voltage sensor, provided a significant degree of protection post-ischemia in the rat spinal cord (Ouardouz, Nikolaeva et al. 2003). Curiously, this effect was not observed in the presence of the pore-blocking agent, cadmium (Cd^{2+}). IHC demonstrated a close link between $Ca_v1.2/3$ (L-type channel subunits) and RyR1/2 (ryanodine receptors). This paradigm suggests that L-type channels sense membrane depolarisation, and signal to RyRs causing them to open and release Ca^{2+} (Ouardouz, Nikolaeva et al. 2003, Stys 2005). Ouardouz *et al.* proposed that the mechanism of intracellular release involves a "complex interplay" between AMPA-receptor mediated depolarisation which is detected by VGCC which subsequently promotes Ca^{2+} mobilization from intracellular stores (Ouardouz, Malek et al. 2006). Interestingly, blocking intracellular Ca^{2+} release with thapsigargin or with diltiazem, which blocks the voltage sensor of L-type VGCCs (which should prevent Ca^{2+} mediated release from ryanodine receptors), failed to improve functional recovery in the absence of extracellular Ca^{2+} in the P10 RON (Alix, Zammit et al. 2012). This suggests that intracellular release may be developmentally regulated.

1.3.2.3: Astrocyte Injury Mechanisms

Fibrous astrocytes are considered relatively resistant to ischemia when compared to axons and oligodendrocytes (Thomas, Salter et al. 2004). This is closely associated with their high energy reserves in the form of glycogen deposits, fatty acids and lactate (Rossi, Brady et al. 2007, Doyle, Simon et al. 2008). However, astrocytes undergo a programme of reactive astrocytosis during ischemia, which may have obscured previous *in vivo* studies. In fact, histological studies have shown evidence that astrocytes may be much sensitive to energy deprivation than originally thought (Fern 2015). Interestingly, fibrous WM astrocytes are

considered more sensitive to acute ischemic injury than protoplasmic GM astrocytes (Shannon, Salter et al. 2007).

Similar to axons, increases in $[Ca^{2+}]_i$ mediates the death of neonatal *in situ* astrocytes (Fern 1998). Prior to the migration of oligodendrocytes into the ON (P0-2), fura-2 loaded astrocytes show an dramatic increase in $[Ca^{2+}]_i$ after 5-10 minutes of ischemia, with cell death evident after only 15-20 minutes (Fern 1998). Astrocyte death at this age is Ca^{2+}-dependant process, mediated via Ca^{2+} influx is through the activation of both T- (early influx) and L- (late influx) type VGCC. It was also noted that neonatal astrocytes have a low Na^+ conductance, and therefore, the Na^+/Ca^{2+} acted to remove intracellular Ca^{2+} during ischemia (Fern 1998).

However, the Ca^{2+}-dependant mechanism of astrocyte injury is a maturation-dependant process. By P10, an age which coincides the high-risk period for PWMI, the removal of $[Ca^{2+}]_e$ exacerbated astrocyte cell death (Thomas, Salter et al. 2004). Although a rise in $[Ca^{2+}]_i$ is observed during ischemia, it does not mediate cell death at this age. Interestingly, the change in injury mechanism coincides with the down-regulation of VGCCs and an upregulation of the Na-K-Cl- co-transporter (NKCC) from the age of P5. Inhibition of the NKCC (with bumetanide) or the removal of Na^+ or Cl^-, prevents a large degree of astrocyte injury. This suggests the cellular swelling becomes a major mechanism of astrocyte injury. Astrocyte injury is initially prevented by blocking NKCC, which was protective for a period of up to 40 minutes of OGD. Complete protection was found at all time periods (up to 60 minutes) by removing extracellular Na^+ and K^+, and was found to be mediated by DIDS-sensitive HCO_3^- transport at later stages (Salter and Fern 2008). Consistent with these findings, the inhibition of VGCCs and iGluRs does not prevent astrocyte pathology during OGD at this age (Alix, Zammit et al. 2012).

1.3.3: Concluding Remarks: Excitotoxic WM injury

The process of ischemic WM injury involves a complex combination of distinct injury pathways. However, excitotoxic WM damage is now considered a central mechanism involved in the death of oligodendrocytes and irreversible functional injury. The involvement of excitotoxicty in ischemic WM will be explored in more detail in chapter 4 and 5.

1.4: Overall Research Aims

As outlined, ischemic WM pathology is an area of high clinical relevance. Despite recent advances, there is still a surprising lack of effective interventions. Ischemic WM injury features rapid myelin disruption which ultimately leads to the failure of action potential conduction. However, the fundamental mechanism(s) of ischemic myelin damage is controversial. Recent studies have also revealed the extensive nature of glutamatergic signalling in WM, including between the axon and myelin sheath (the axo-myelinic synapse). The overall aims of this project are to determine the mechanisms of glutamate release in WM and to test the hypothesis that myelinic NMDA receptor activation mediates ischemic myelin damage.

Chapter 3: Experiments in chapter 3 investigate the significance of vesicular glutamate release in WM, specifically in axons and fibrous astrocytes. The overall aim is to test whether myelinated central axons are capable of vesicular glutamate release.

Chapter 4: Chapter 4 examines the potential mechanisms underlying a key event in the pathophysiology of WM stroke; ischemic glutamate release. The aim is to determine the pathway of glutamate release under acute ischemic conditions.

Chapter 5: Chapter 5 examines the mechanism of ischemia-induced myelin damage in central WM. The specific aim is to test the hypothesis that the over-activation of myelinic NMDA receptors mediates myelin damage and irreversible injury during ischemia. Furthermore, I test a novel sub-unit specific NMDA receptor antagonist, QNZ-46.

The work in this thesis will hopefully contribute to a better understanding of the injury mechanisms involved in ischemic WM. It is hoped that these findings will also contribute to the development of an effective intervention for patients.

Chapter 2:

Materials & Methods

2.1: Animals

All animal procedures conformed to local ethical guidelines. UK home office regulations were followed and all experiments were conducted in accordance with the UK Animals (Scientific Procedures) ACT 1986. All animals were sacrificed via schedule 1. Wistar rats, PLP-GFP and C57Bl/6 wild-type mice and were sacrificed via cervical dislocation (rats aged <P10) or exposed to a rising concentration of CO_2, prior to cervical dislocation or exsanguination. All THY1/YFP (line H) and GFAP-GFP transgenic mice were sacrificed at the University of Malta, where animals were anesthetised using isoflurane (Vetflurane 100mg/g, Virbac.) prior to decapitation.

For experiments requiring the use of optic nerve (ON), nerves were dissected from either neonatal Wistar rats (P8-12), adult Wistar rats (P90-120), adult PLP-GFP or C57Bl/6 wild-type mice (P80-110). For corpus callosum (CC) experiments, coronal slices were obtained from adult Wistar rats (P90-120), adult THY-1/YFP (Line H), GFAP-GFP or C57Bl/6 wild-type mice (P80–110).

2.2: Optic Nerve and Corpus Callosum Isolation

Following decapitation, the scalp was removed and the ON was severed at the optic disc by cutting behind the eyeballs. The skullcap was removed and the brain was quickly dissected into a petri dish containing oxygenated artificial cerebrospinal fluid (aCSF; see table 2.1 for composition). Both ONs were dissected free at the optic chiasm and placed in an oxygenated interface perfusion chamber (Harvard Apparatus Inc.). Following decapitation, the entire procedure typically took less than 2 minutes.

For experiments requiring the use of brain slices, the brain was initially dissected into a petri dish containing oxygenated aCSF. The cerebellum and brain stem were removed, and the entire brain was subsequently embedded in 0.5% agrose (made-up in aCSF) and put on ice for 5-7 minutes. The embedded brain was mounted on the platform of a vibratome (Leica VT1200g) using superglue and immediately immersed in an oxygenated, ice-cold HEPES

cutting solution (see Table 2.1 for composition. Note; brain slices carried out in the University of Malta were immersed in ice-cold aCSF supplemented with 75mM sucrose). The embedded brain was stabilised against a 4% agrose block (made up in H_20), which was also superglued to the stage. The brain was oriented to cut coronal slices from the genu of the corpus callosum through the caudal extent of the hippocampus. Coronal slices (400µm thick), including the corpus callosum, were cut and transferred to a Haas-type interface brain slice chamber (Harvard Apparatus Inc.) containing oxygenated HEPES cutting solution at room temperature. Only slices in which the anatomical structure of the CC was clearly visible, and had a continued appearance across the midline were included in experiments.

For the majority of experiments carried out on the CC, whole brain slices were transferred to an interface perfusion chamber. However, for electrophysiological CAP experiments, the CC was dissected out from the brain slice under a stereomicroscope. Slices were kept in ice-cold HEPES cutting solution and the surrounding tissue was carefully removed from the CC using a microscissors and forceps (Fig. 2.1). The isolated CC was immediately transferred to the interface perfusion chamber. The procedure typically took less than 5 minutes. Li *et al.* have since published a paper (including a supplementary video) outlining the steps involved (Li, Velumian et al. 2016). In order to include a sufficient number of axons running within the plane of a slice, CC slices between the bregma (identified by the anterior commissure at the base of the slice) and 1.2mm away (caudal direction) were included in CAP recordings.

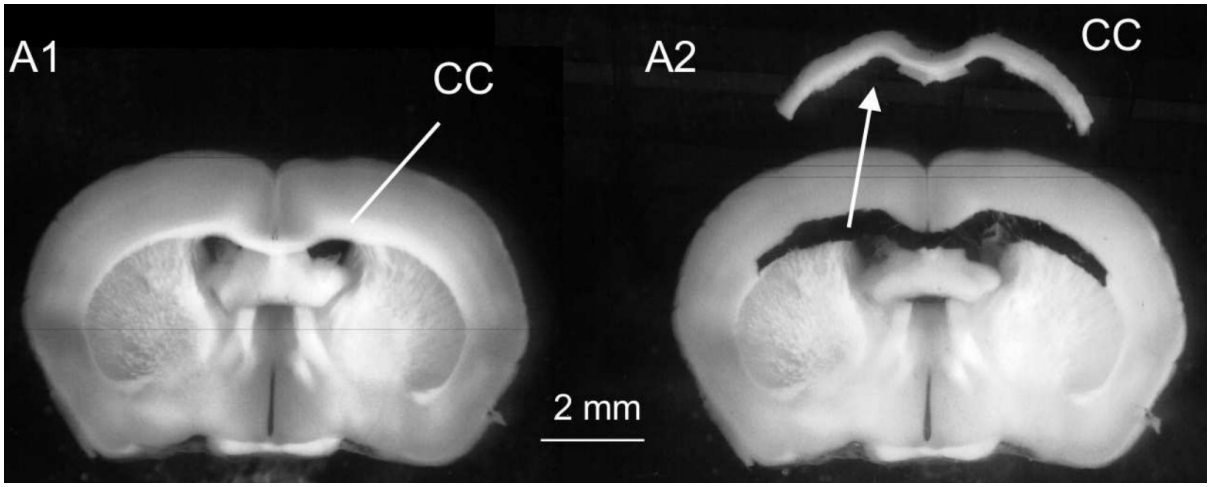

Fig. 2.1: Corpus callosum isolation from coronal brain slices.

a1) 400µm thick coronal brain slices were kept in ice-cold cutting solution. **a2)** Using a micro-scissors and forceps, the surrounding tissue was carefully separated from the CC. Once the surrounding tissue was removed and discarded; the isolated CC was transferred to the recording chamber. Taken from (Li, Velumian et al. 2016).

2.3: Solutions and Drugs

Solutions were made up using Millipore deionised water and kept in the fridge for no longer than one night before use. The osmolarity was tested using a vaporpressure osmometer (Wescor, Vapro), and corrected to 300mOsm (±10mOsm), if required. All control aCSF/HEPES solutions were bubbled with a 95% O_2/5% CO_2 gas mixture for at least 60 minutes before use, and continued throughout the day. Alternatively, oxygen-glucose deprivation (OGD) solutions were bubbled with 95% N_2/5% CO_2.

Below is the composition of all solutions (Table 2.1) and pharmacological reagents (Table 2.2) used;

	aCSF	OGD aCSF	Zero-Na^+ aCSF*	Zero-Ca^{2+} aCSF	High K^+ aCSF (50mM)	Hyd. buffer	10X PBS	HEPES cutting aCSF
NaCl	126	126	_	126	79	100	1.37M	92
KCl	3	3	3	3	50	_	27	2.5
NaH_2PO_4	2	2	_	2	2	1.9	100	1.2
$MgCl_2$	2	2	2	2	2	1	_	_
$NaHCO_3$	26	26	_	26	26	_	_	30
Glucose	10	_	10	10	10	_	_	25
Sucrose	_	7	_	_	_	_	_	_
$CaCl_2$	2	2	2	_	2	_	_	2
NMDG/Cl	_	_	124	_	_	_	_	_
Choline-HCO_3	_	_	26	_	_	_	_	_
EGTA	_	_	_	50µM	_	_	_	_
Glycerol	_	_	_	_	_	2	_	_
HEPES	_	_	_	_	_	_	_	20
$C_6H_7NaO_6$	_	_	_	_	_	_	_	5
Thiourea	_	_	_	_	_	_	_	2
$C_3H_3NaO_3$	_	_	_	_	_	_	_	3
$MgSO_4.7H_2O$	_	_	_	_	_	_	_	2
KH_2PO_4	_	_	2	_	_	_	20	_
Na_2HPO_4	_	_	_	_	_	8.1	_	_

Table 2.1: **Composition of solutions used.**

All concentrations are in mM, unless otherwise stated. pH was adjusted to 7.4 if necessary. aCSF=artificial cerebrospinal fluid, OGD=oxygen-glucose deprivation, PBS=phosphate buffered saline and Hyd. buffer= hydration buffer used for biosensors. *****When preparing zero-Na^+ aCSF, 124mM NMDG was initially made up in 500ml water and pH was adjusted to 7.4 using concentrated hydrochloric acid (HCl) before the remaining ingredients were added. All the above reagents were purchased from Sigma-Aldrich.

To prepare 500ml 4% paraformaldehyde (PFA), 20g PFA powder was added to a beaker with 450ml warm, distilled H_2O with stirring. The beaker was covered with parafilm and gradually heated to 60°C. Note; the solution should not exceed 70°C, as this will break down PFA. 5 drops of 2N NaOH (~1 drop per 100ml) were added to aid dissolution. Once dissolved, the beaker was removed from the hot plate, 50ml of 10X PBS was added and it was left cool to room temperature. pH was adjusted to 7.4 with HCl, the solution was filtered and aliquots were stored at -20°C.

Name	Supplier	Solvent	Storage Temp. (°C)	Working Conc.
(+)-**MK 801** maleate	Tocris (Bio-techne)	DMSO	-20 (alloq.)	10/50 μM
A-967079¥	Abcam	DMSO	-20 (alloq.)	10 μM
Antimycin-a	Sigma-Aldrich	DMSO	-20 (alloq.)	25 μM
Bafilomycin a1	Viva Bioscience	DMSO	-20 (alloq.)	50nM
BAPTA-AM	Sigma-Aldrich	DMSO	-20 (alloq.)	50 μM
Carbenoxolone (**CBX**)	Sigma-Aldrich	Water	2-8	100 μM
CIQ	Tocris (Bio-techne)	DMSO	-20 (alloq.)	20 μM
Diltiazem Hydrochloride¥	Tocris (Bio-techne)	H_20	Room temp.	100 μM
EGTA	Sigma-Aldrich	Water	Room temp.	50 μM
FM4-64	Life Technologies	H_20	2-8	10 μM
Furosemide¥	Sigma-Aldrich	DMSO	Room temp.	5mM
Goat Serum	Sigma-Aldrich	-	-20	10%-PBGST
L-aspartic acid (**aspartate**)	Sigma-Aldrich	Water	Room temp.	10 μM
L-glutamaine	Sigma-Aldrich	Water	Room temp.	10 μM
L-glutamic acid (**glutamate**)	Sigma-Aldrich	Water	Room temp.	10-100 μM
NBQX disodium Salt¥	Tocris (Bio-techne)	H_20	-20 (alloq.)	20 μM
NBQX¥	Tocris (Bio-techne)	DMSO	-20 (alloq.)	20 μM

NPPB	Sigma-Aldrich	DMSO	-20 (alloq.)	100 μM
Paraformaldehyde (**PFA**)	Sigma-Aldrich	0.1M PBS	-20	4% (w/v)
PPDA	Tocris (Bio-techne)	DMSO	-20 (alloq.)	1-50 μM
Pregnanolone hemisuccinate¥	Steraloids Inc.	DMSO	-20 (alloq.)	100 μM
Prostaglandin E_2 (**PGE_2**)	TRC	DMSO	-20 (alloq.)	100 μM
QNZ-46¥	Tocris (Bio-techne)	DMSO	-20 (alloq.)	1-50 μM
Rose Bengal (**RB**) ¥	Sigma-Aldrich	H_20	Room temp.	0.5 μM
Rotenone	Sigma-Aldrich	DMSO	Room temp.	1nM-5μM
Sulfasalazine (**SAS**)	Sigma-Aldrich	DMSO	Room temp.	250 μM
TBOA	Sigma-Aldrich	DMSO	-20 (alloq.)	200 μM
Triton X-100	Sigma-Aldrich	-	RT	0.5%-PBGST
Veratridine	Tocris (Bio-techne)	DMSO	-20 (alloq.)	10 μM
β Cyclodextrin	Sigma-Aldrich	PBS	RT	1mM

Table 2.2: List of pharmacological reagents used.

TRC= Toronto Research Chemicals, DMSO= Dimethyl sulfoxide, alloq.= aliquoted, PBS= phosphate buffered saline, PBGST= PBS/goat serum/triton mixture. ¥= experiments preformed in a darkened room.

All reagents were added to the appropriate aCSF solutions on the day of experiment. Some reagents were dissolved, aliquoted and frozen down as stock solutions. In experiments using furosemide, the aCSF solution was adjusted accordingly to accommodate 5mM furosemide (i.e. NaCl concentration was reduced to 123.5mM from 126mM). When reagents were dissolved in DMSO, the final concentration was kept below 0.5% volume per unit volume (v/v). For experiments using BAPTA-AM, RONs were incubated into a petri-dish containing zero-Ca^{2+} aCSF and 50μM BAPTA-AM for 90 minutes (30 minutes at room temperature, 60 minutes at 2-8°C). Afterwards, RONs were placed in the perfusion chamber and perfused with solutions without the drug. BAPTA-AM is an acetoxymethyl ester derivative of the calcium chelator BAPTA, and once the compound enters the cell, intracellular esterases cleave the acetoxymethyl group, leaving the compound permanently internalised.

2.4: Experimental Protocol: *In vitro* ischemia

Following ON/CC isolation, the tissue was placed in an interface perfusion chamber (Harvard Apparatus Inc.) and continuously perfused with oxygenated aCSF at a rate of 0.6-1.5ml/min. The chamber was humidified via continuously bubbling with 95% O_2/5% CO_2 (gas flow: 1LPM) and the temperature was gradually warmed to 37±0.5°C over 60 minutes (101C Temp Controller, Warner Instruments). In order to regain homeostatic control following the dissection, nerves/slices were allowed to equilibrate for a minimum of 60 minutes before initial control recordings (Fig. 2.5c). At the beginning of every experiment, baseline recordings were made for a minimum of 10 minutes under normoxic conditions. As previously reported, both ON and CC slices can be maintained under control conditions for several hours with minimal functional or structural loss (Alix and Fern 2009, Li, Velumian et al. 2016).

As previously discussed, ischemia is defined as an inadequate supply of essential substrates required for cellular metabolism. In living tissue, this is a consequence of an insufficient blood supply. To simulate ischemic conditions, the isolated tissue was perfused with a zero-glucose (substituted with 7mM sucrose), deoxygenated (pre-bubbled for 60 minutes with 95% N_2/5% CO_2) aCSF solution (Fig. 2.2). The chamber bath was simultaneously bubbled with the 95% N_2/5% CO_2 gas mixture to remove atmospheric O_2. In addition, the recording chamber was partially covered to prevent the diffusion of atmospheric O_2 to the tissue. Previous studies report that the concentration of O_2 in the recording chamber reaches zero after approximately 2 minutes (Stys, Waxman et al. 1992). This is referred to as 'oxygen-glucose deprivation' or 'OGD' throughout. Nerves were typically exposed to OGD for 60 minutes, following which, normoxic conditions were re-introduced (reperfusion) for 60-90 minutes to ensure maximum functional recovery. Temperature, gas and aCSF flow-rates were maintained constant throughout.

It must be noted that this is a global model of ischemia, where the entire tissue is subject to an equal degree of insult. Therefore, this does not allow for any interactions which may occur between a focal ischemia core, a surround penumbra and/or normoxic tissue, which may occur *in vivo.*

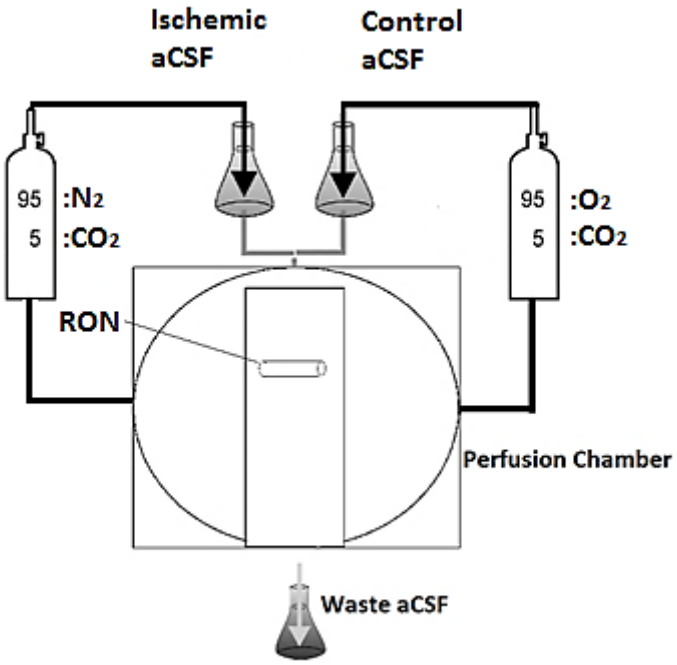

Fig. 2.2: Schematic representation of RON in perfusion chamber.

Nerves were perfused with an oxygenated aCSF solution containing 10mM glucose under control conditions (right). To mimic ischemia, nerves were exposed to a deoxygenated aCSF solution with zero-glucose (left). RON= rat optic nerve, aCSF= artificial cerebrospinal fluid.

For experiments using enzymatic biosensors, stable recording could not be obtained under anoxic conditions (see section 2.6.3 for details). Therefore, *chemical ischemia* was employed as our model; combining metabolic inhibition with glucose deprivation. To inhibit oxidative phosphorylation, either rotenone (1nM, neonates) or antimycin-a (25µM, adults) was added to an oxygenated/zero-glucose aCSF solution. Rotenone is commonly used as a broad-spectrum insecticide and pesticide due to its potent ability to selectively inhibit complex-I of the mitochondrial electron transport chain (ETC). More specifically, rotenone reversibly inhibits NADH dehydrogenase, preventing the transfer of electrons to ubiquinone. It has previously shown to mimic the effects of hypoxia (Wyatt and Buckler 2004) and therefore, has been used by many authors as a model of chemical ischemia (Litsky, Hohl et al. 1999, Allen, Káradóttir et al. 2005). Antimycin-a is a potent inhibitor of electron transport at complex III of the ETC, and has also previously been employed as a model of ischemia (Allen,

Káradóttir et al. 2005, Fern 2015). All other components remained the same throughout recordings.

Following every experiment, the chamber was rinsed with 1l of distilled H_20. Once a week, the chamber was sequentially rinsed with H_20, sodium phosphate tribasic, H_20, a dilute hydrochloric acid solution and finally with H_20 again. Any water in the chamber bath was removed at the end of every experiment.

2.5: Compound Action Potential (CAP) Recordings

2.5.1: Background

Electrophysiology is essentially the study of electrically excitable cells. As mentioned, WM tracts are primarily responsible for relaying electrical signals between different regions of the CNS. This form of communication is executed through the propagation of action potentials (AP) which involves the rapid change in membrane potential along an axon. The compound action potential (CAP) is defined as the sum of all action potentials fired from individual axons within a nerve bundle, when the nerve is electrically stimulated (Stys, Ransom et al. 1991). Electrophysiological CAP recordings from the isolated ON are widely used as a measure of electrical conductance, providing a quantitative measure of axonal function and conductance velocity. Continuous recordings act as a reliable measure of functional recovery following periods of energy deprivation, such as OGD. To access functional recovery from isolated WM tracts, CAPs were recorded from the rat/mouse ON and CC using the glass electrode preparation (Stys, Ransom et al. 1991). This technique was established in the 1930's by Ergland and Gasser (Erlanger and Gasser 1937) and involves the electrical stimulation of one end of a nerve and the subsequent recording of the propagated CAP at the opposite end.

An electrical model was developed in 1991 by Stys *et al.* which greatly contributed to the development of stable and reliable recordings which could be applied over long periods (Stys, Ransom et al. 1991). Treating the nerve as a single isolated fibre, the 'intracellular potential' of the nerve which is inside the recording electrode, is referred to as V_e. The intracellular potential of the nerve which is outside the electrode is assigned V_m (see Fig. 2.3). Without

stimulation, the resting potential is equal in both parts of the nerve (e.g. -70mV), with respect to ground. Thus, the recorded difference between V_m and V_e (V_o) is zero. A signal is only recorded when $V_o \neq 0$. When the fibre is electrically stimulated, V_m will depolarise (become less negative) resulting in a transient difference between V_e and V_m. The resulting output voltage drop (V_o) will be recorded by the recording electrode. Initially V_o will become positive as V_m depolarises. However, as the action potential propagates along the fibre, V_m will repolarise, while V_e depolarises, resulting in V_o becoming more negative. Thus, the recorded CAP is the transient difference between V_m and V_e and is typically biphasic. When both V_m and V_e have returned to their resting potential, no signal will be recorded (Stys, Ransom et al. 1991). However, resistive elements will strongly affect the flow of current between V_m and V_e. AP conduction will be met by both internal resistance (R_i) and external resistance (R_o) (see Fig. 2.3). R_i includes the series membrane resistance, while R_o accounts for the combined resistance of the extracellular space, glial cells, connective tissue and the fluid layer between the nerve and electrode. V_o can therefore be described by the following equation;

$$V_o = \frac{R_o (V_m - V_e)}{R_i}$$

V_o is directly proportional to R_o. Thus, increasing the external resistance will directly increase the size of the recorded signal, V_o, which can be achieved by inserting the nerve into a tight fitting electrode (Stys, Ransom et al. 1991).

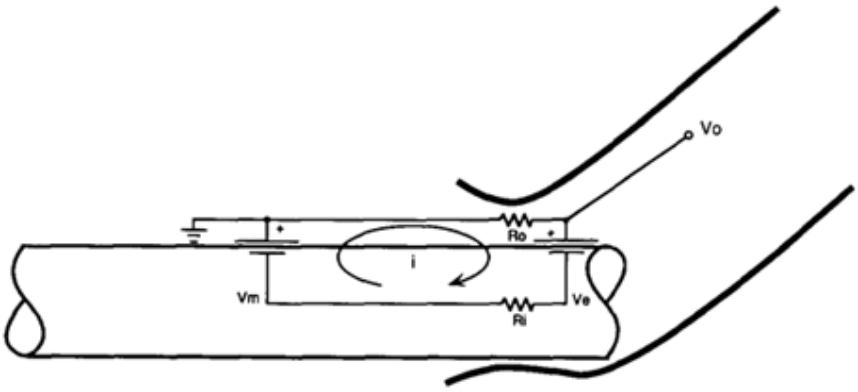

Fig. 2.3: Schematic representation of the theoretical electrical model of CAP recording from the ON.

Shown is an optic nerve inserted into the end barrel of a recording electrode. The recorded signal, V_o, is a result of a voltage drop across R_o following the flow of current, *i*, between V_m and V_e. V_m represents the transmembrane potential outside the electrode, while V_e represents the transmembrane potential inside the electrode. Adapted from (Stys, Ransom et al. 1991).

2.5.2: Set-up/Protocol

Both stimulating and recording glass electrodes (1-1.2mm diameter, Harvard Apparatus) were shaped via gentle heating over the flame of a Bunsen burner until the barrel bends under its own weight, forming a periscope shape. Sliver wire was coated with a thin chloride layer by immersing it in a solution containing chloride ions overnight (chlorine tablets dissolved in distilled water). The chlorided silver wire (Ag/AgCl) was then inserted into the lumen of each glass capillary. The stimulating electrode also had an Ag/AgCl wire wrapped around the outside of the glass capillary barrel near the opening in order for the wire to make contact with the perfusing aCSF solution. The electrodes were mounted in a manipulator and positioned at either end of the nerve. To minimise electrical interference (noise) and stimulus artefact field potentials, a third, identical electrode was placed parallel to the recording electrode, providing a differential recording.

The stimulating electrode is connected to an isolated stimulator (Iso Stim A320; World Precision Instruments) via both Ag/AgCl wires, forming a returning current. The Ag/AgCl wire

from both the recording and subtracting electrode are connected to an amplifier (Cyber Amp 320, Axon Instruments) via an electrode adaptor (AI405, Axon Instruments).

All electrodes are back-filled with oxygenated aCSF. Following the equilibration period after dissection, the ON/CC was gently nudged into the lumen of the stimulating electrode at one end, and the lumen of the recording electrode at the opposite end (Fig. 2.4b). A tight fit around the RON was necessary to ensure the nerve did not move during the course of an experiment. If needed, the mouth of the glass electrode was heated over a flame to alter the glass diameter. Once secure, recording started.

With younger, unmyelinated nerves, CAPs were evoked via square-wave constant current pulses (Iso stim A320, WPI) with a typical duration of 150-600µs. 50µs or lower pulses were used for the older myelinated nerves. Increasing the stimulus intensity (0-1.1mA) dramatically increases the size of the recorded CAP, until a plateau is reached. CAPs were elicited via 125% supra-maximal pulses to ensure all functional axons within the RON are recruited. Differential signals were amplified (Cyber Amp 320, Axon Instruments), filtered (low pass: 800-20,000 Hz), digitized (1401 micro3, Cambridge Electrical Design Ltd.) and displayed on a PC running Signal software (version 6, Cambridge Electrical Design Ltd.) (Fig. 2.4). CAPs were evoked and recorded every 30 seconds.

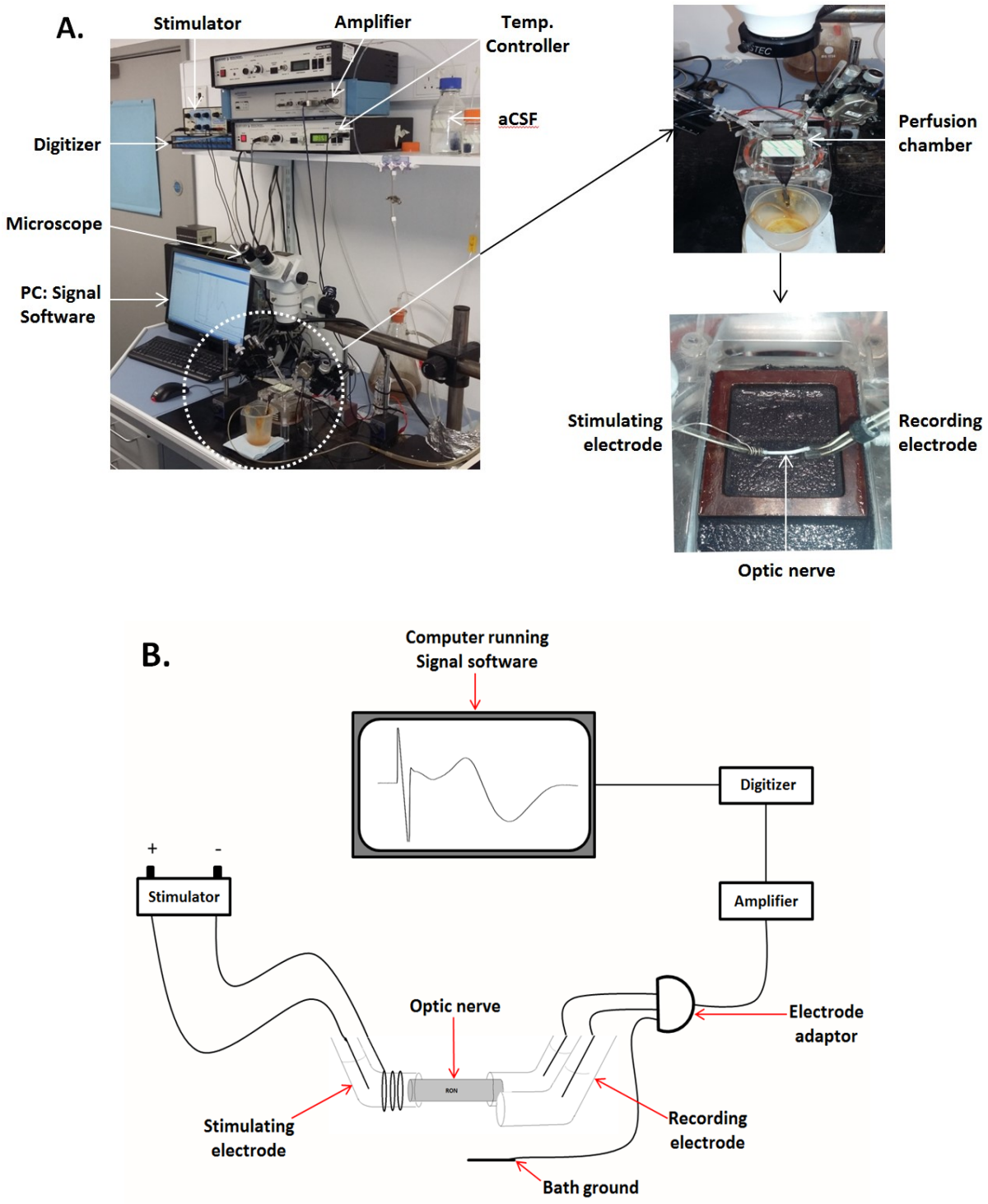

Fig. 2.4: CAP recording set-up.

a) Photo of CAP set-up in lab. The ON is maintained on a nylon mesh on the surface of an interface perfusion chamber. Stimulating and recordings electrodes are connected to each end of the nerve. **b)** Schematic illustration of CAP set-up.

2.5.2: CAP Analysis

As mentioned, the electrical model proposes a biphasic CAP (Stys, Ransom et al. 1991). This is the case with young unmyelinated ONs (<P12) as nearly all axons within the fibre conduct at similar velocity due to their uniform diameter and lack of myelin (Fig. 2.5a). However, unlike the homogenous population of axons in the pre-myelinated ON, the adult ON contains a population of axons with various diameters and thus, a variety of conductance velocities (Hildebrand and Waxman 1984). The resulting adult CAP consists of 3 positive peaks i.e. triphasic (Fig. 2.5b).

To quantitatively access functional integrity, the peak-to-peak amplitude of biphasic CAPs was measured every 30 seconds of recording (neonates, Fig. 2.5a). For triphasic CAPs, the rectified area under the curve was calculated up to where the waveform returned to baseline (adult, Fig. 2.5b). Both measurements were made using Signal software by placing a cursor before the first peak (but after the stimulus artefact) and a second cursor where the CAP returns to zero. The stimulus artefact was subtracted at the end of every experiment. To accurately access functional recovery after reperfusion, all CAPs were normalised to the initial 10 minutes of recordings under control conditions. Non-recoverable CAP loss indicates irreversible functional injury.

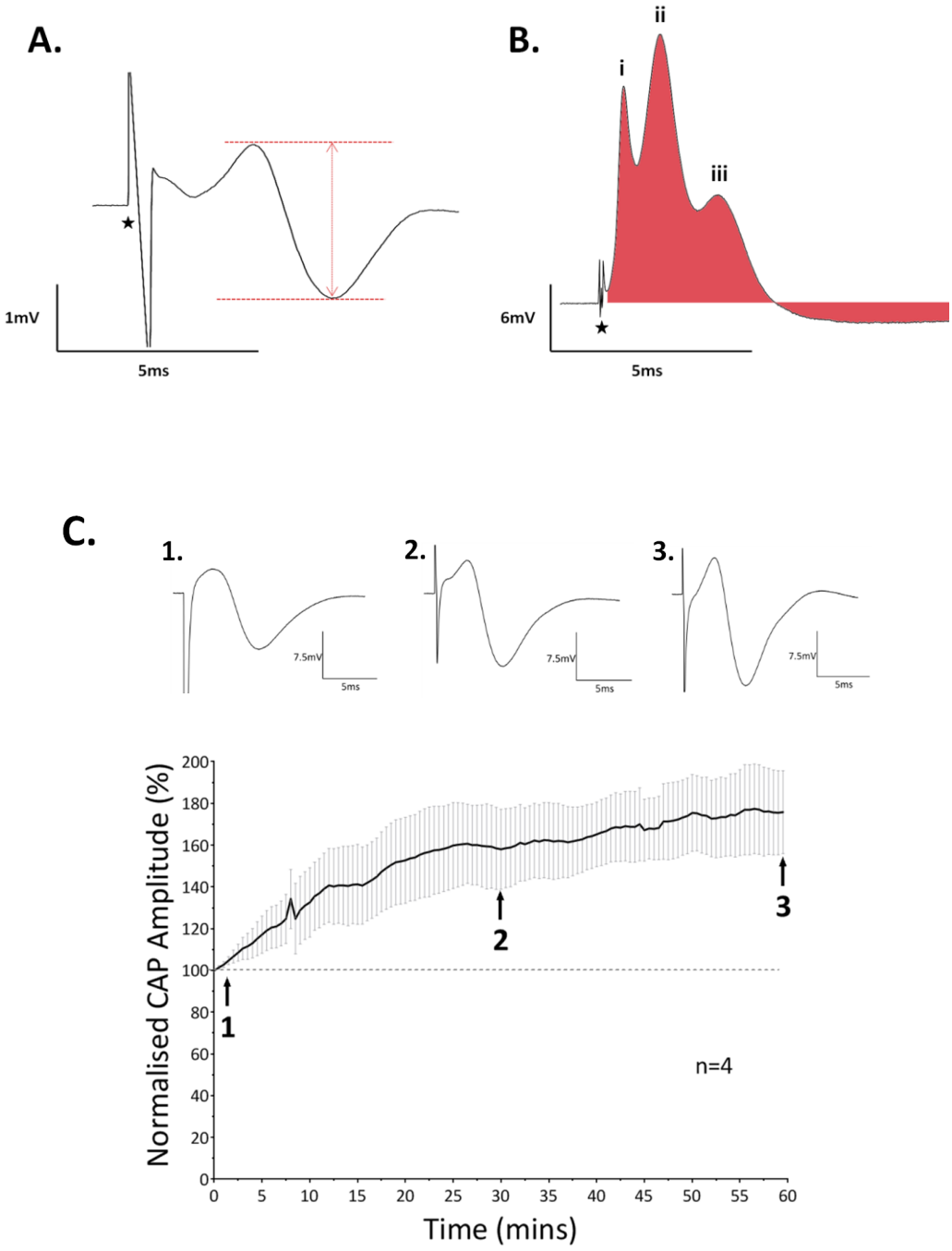

Fig. 2.5: Sample CAP trace recorded from a pre-myelinated optic nerve (P10) and a fully myelinated adult optic nerve.

a) P10 CAPs are typically biphasic in shape, with a positive and negative component. CAP amplitude is measured from peak-to-peak (red). **b)** Adult CAPs typically have 3 positive peaks (i-iii) followed by a delayed negative component. CAP area is measured as the rectified area under the curve (red). ***=** stimulus artefact. **c)** Following dissection, CAP amplitude recovers to a stable plateau over 60 minutes. (1=CAP recording was initiated 5 minutes after dissection). All remaining CAP experiments were initiated after 60 minutes recovery in control aCSF (3).

2.6: Extracellular Glutamate Recordings

2.6.1: Background

One of the primary objectives of this project is to examine the mechanism(s) of glutamate release in WM. A practicable way of achieving this involved the direct measurement of extracellular glutamate concentration ($[Glut]_e$) within the nerve. Sarissa Biomedical Ltd. (Warwick University, Coventry, UK) specialise in the development and production of microelectrode amperometric biosensors (sarissaprobes®) used for the detection of neuroactive chemicals, including l-glutamate (GLU-sensors) (Tian, Gourine et al. 2009). The electrochemical sensors allow for real-time detection of relatively low concentrations of l-glutamate (limit of detection; 100nM) with a broad linear range (from 0.1μM to 100μM). The sensors are specifically designed for *in vitro* and *in vivo* research, but also have clinical diagnostic applications, capable of measuring analytes in a droplet of blood (15µl). The sensors have previously been used for the detection of neurochemicals in cell culture (Trotman, Vermehren et al. 2015) and with *in situ* preparations, such as the isolated rodent optic nerve (Yang, Hamner et al. 2014).

Sarissaprobes® are enzymatic biosensors, which convert a substrate or analyte of interest (i.e. glutamate) into an active product, providing an amperometric signal which is directly proportional to the concentration of the substrate. The sensors are made of a hollow glass body containing a platinum (Pt) wire, connected to a pin at one end (see Fig. 2.6). At the opposite end, the exposed Pt wire (sensing area) is coated with an immobilised layer of glutamate oxidase, which when exposed to l-glutamate, generates hydrogen peroxide (H_2O_2) in the following oxidation reaction (Tian, Gourine et al. 2009);

$$\text{l-glutamate} + O_2 + H_2O \rightleftharpoons \text{2-oxoglutarate} + NH_3 + \mathbf{H_2O_2}$$

The detection principle of the GLU-sensor is based on the production of H_2O_2, which can be detected by the polarised platinum (Pt) wire (+500mV relative to an Ag/AgCl reference electrode);

$$H_2O_2 \xrightarrow{\text{Pt wire (+500mV)}} O_2 + H^+ + \mathbf{2e}$$

The resulting current is amplified via a potentiostat (Duo-Stat ME200+, Sycopel International), which is connected to the sensor. Currents are recorded and displayed on a PC using Signal software.

There are several features which ensure a highly selective ('true') glutamate signal. The microelectrode tip is coated with a very thin perm-selective polymer, which allows H_2O_2 to freely diffuse through to the electrode surface where it is subsequently detected by the Pt wire. However, it rejects any possible compounds which may interfere with readings (see 'inner permeable selective layer', Fig. 2.6). The layer of glutamate oxidase is covalently linked to the polymer which securely immobilises the enzyme to the sensor surface and prevents leaching. In addition, the sensing tip is also coated with an outer perm-selective layer which excludes electroactive interferents, such as l-ascorbic acid, uric acid, dopamine and 5-HT, which may be oxidised themselves at the Pt wire (Dale, Hatz et al. 2005). However, l-glutamate can freely diffuse through the outer perm-selective layer to the inner enzymatic layer. Finally, null sensors are used in every experiment. Null sensors are identical to GLU-sensors, but lack the layer of glutamate oxidase. During recordings, both biosensor and null signals are recorded, but the null signal is subsequently subtracted from the biosensor signal to eliminate current generated from nonspecific interferants. Thus, any increase in current will reflect a direct increase in extracellular glutamate concentrations ($[Glut]_e$). The GLU-sensors are 50μM in diameter and 0.5mm in length (product number; SBS-GLU-05-50) and have a shelf life (dry storage) of at least 4 months when kept at 4-8°C.

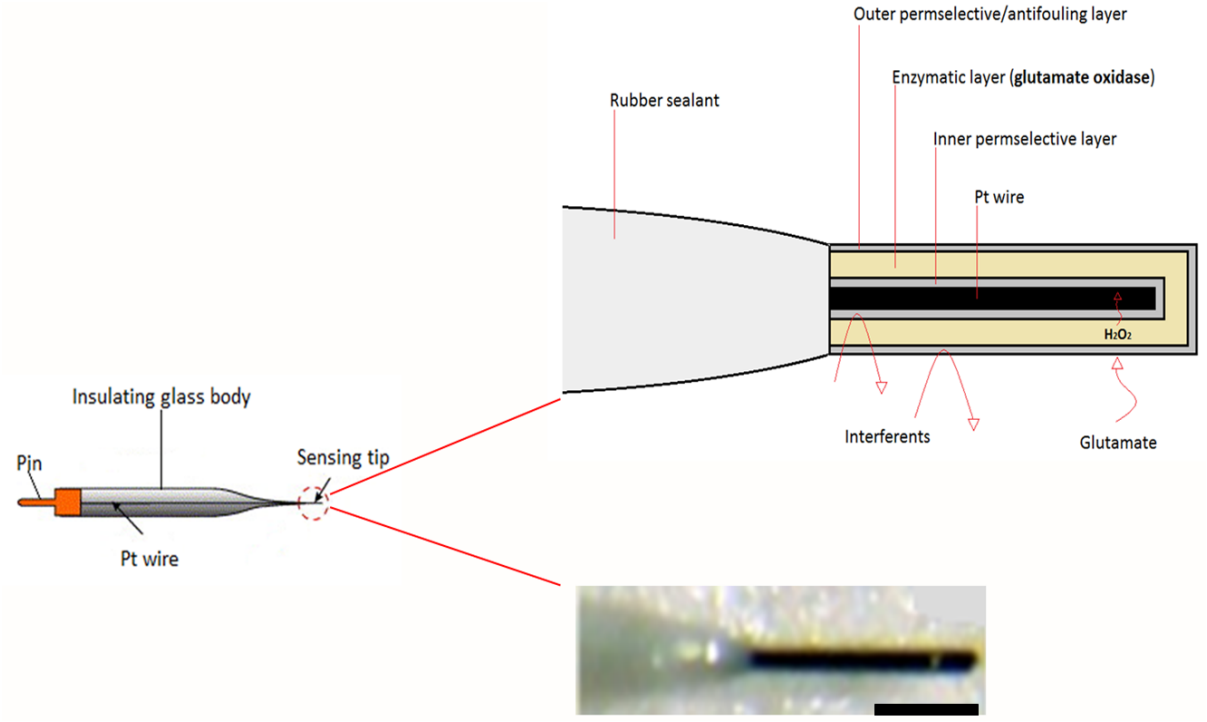

Fig. 2.6: Physical structure and principle underlying glutamate microelectrode biosensors.

Scale bar= 1mm. Adapted from (Dale, Hatz et al. 2005) and sarissa-biomedical.com.

2.6.2: Set-up/Protocol

Before first use, the sensor tips were carefully bent so that the sensing tip ran parallel to the nerves longitudinal axis (Fig. 2.7b). To do this, the rubber sealant was grasped close to the sensing tip with a fine forceps and bent to the desired angle. In addition, the sensors are immersed in a hydration buffer (see Table 2.1) for a minimum of 10 minutes before use. Microlectrodes are then mounted on a manipulator and carefully lowered into the chamber. Sensor-selectivity was tested against compounds which have a similar structure to glutamate. The sensors were highly responsive when exposed to 10µM l-glutamic acid (glutamate), yet there was no response to either glutamine or aspartic acid (both 10µM) (Fig. 2.8a).

For ON experiments, the tough outer membrane prevented the simple insertion of the sensor tip without stripping the perm-selective layers. Therefore, a small incision was made on the upper surface of the nerve (approximately 10-20% of the nerve diameter) using a micro-

scissors. The CC did not require such a procedure. Sensor tips were fully inserted and moved laterally towards the centre of the nerve, away from the incision site (Fig. 2.7b). This was carried out for both GLU-sensor and null sensor. Following sensor insertion, nerves/slices were allowed to equilibrate for long periods before an experiment. The initial recorded current ($[Glut]_e$) was high following electrode insertion, presumably due to localised tissue damage. $[Glut]_e$ gradually declined to a low stable baseline over a long stabilization period of 120-180 mins (neonatal ON), 300-420 mins (adult ON) or 180-240 mins (adult CC slice) (Fig. 2.8b). A stable baseline was recorded for a minimum of 10 minutes at the start of every experiment. An Ag/AgCl reference electrode was present in the chamber for all experiments.

In order to convert sensor current into glutamate concentration, a calibration was necessary at the end of each experiment. To do this, electrodes were withdrawn from the nerve, as the tissue would impede free access of exogenous glutamate. The sensor tips were then lowered into the chamber and exposed to a known concentration of l-glutamic acid. It was important to ensure that the entire surface area of the sensor is immersed in solution. All calibrations were carried out in the same physiological solutions which were used that day i.e. aCSF at 37°C. Calibrations were initially repeated with multiple concentrations of l-glutamic acid, but due to the reliable linear response, single point calibrations were sufficient (Fig. 2.9a-b). Repeated use of the sensors led to a gradual decrease in biosensor sensitivity. According to Sarissa Biomedical, this is a likely a consequence of enzyme degradation from proteases within the tissue and physical removal of enzyme at the sensor surface (sarissa-biomedical.com) (Fig. 2.9a-b). Stock l-glutamic acid solutions were kept for no longer than 3 months (at 4°C, Fig. 2.9c). Following calibration, the sensors were removed, stored in small pots containing the hydration buffer and kept at 4-8°C. Once rehydrated, they have a wet shelf-life of between 3 to 5 days. Exposure to air was kept to a minimum as this is known to decrease sensor activity.

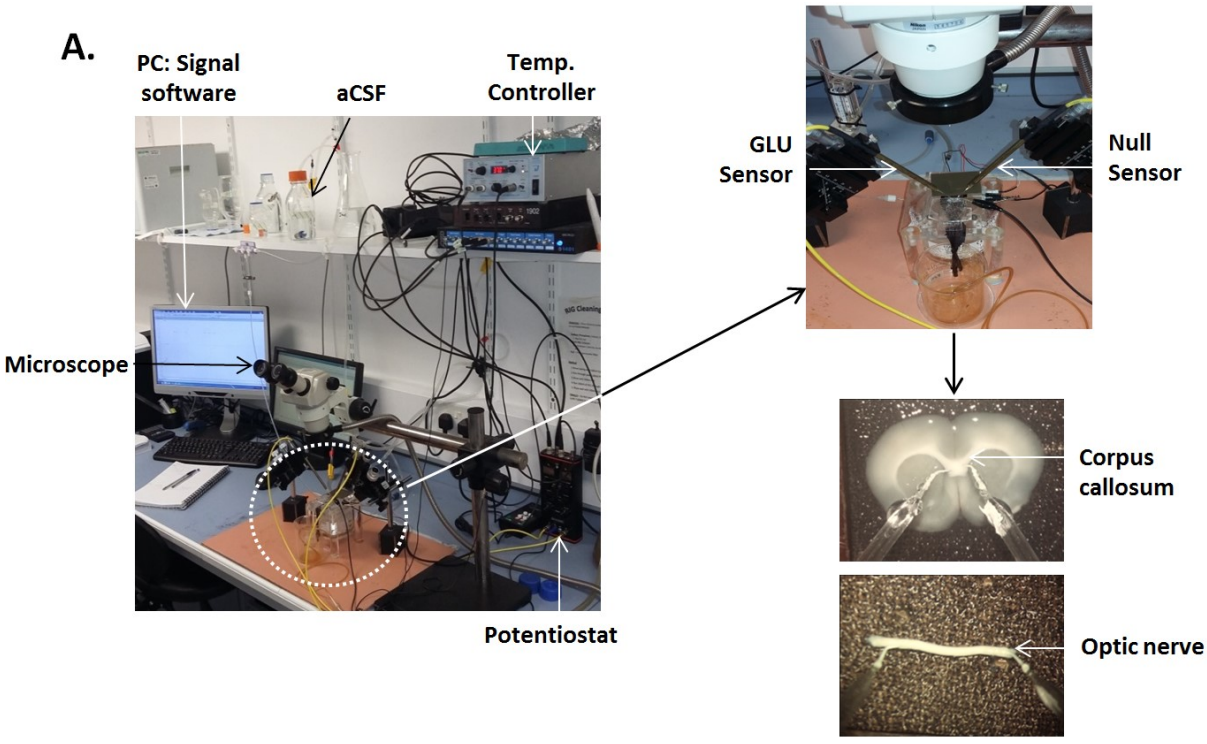

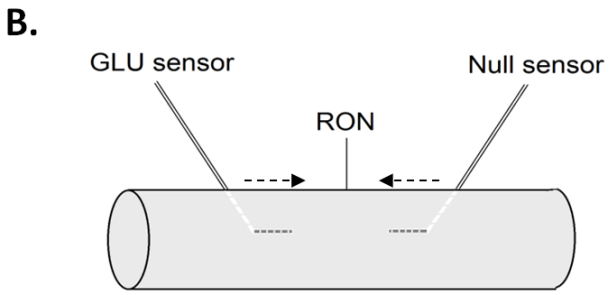

Fig. 2.7: Glutamate biosensor set-up.

a) Photo of glutamate biosensor set-up in lab. The ON/CC is maintained in an interface perfusion chamber. Both GLU and null biosensors are inserted inside the tissue. **b)** Schematic representation of sensor positioning inside the RON.

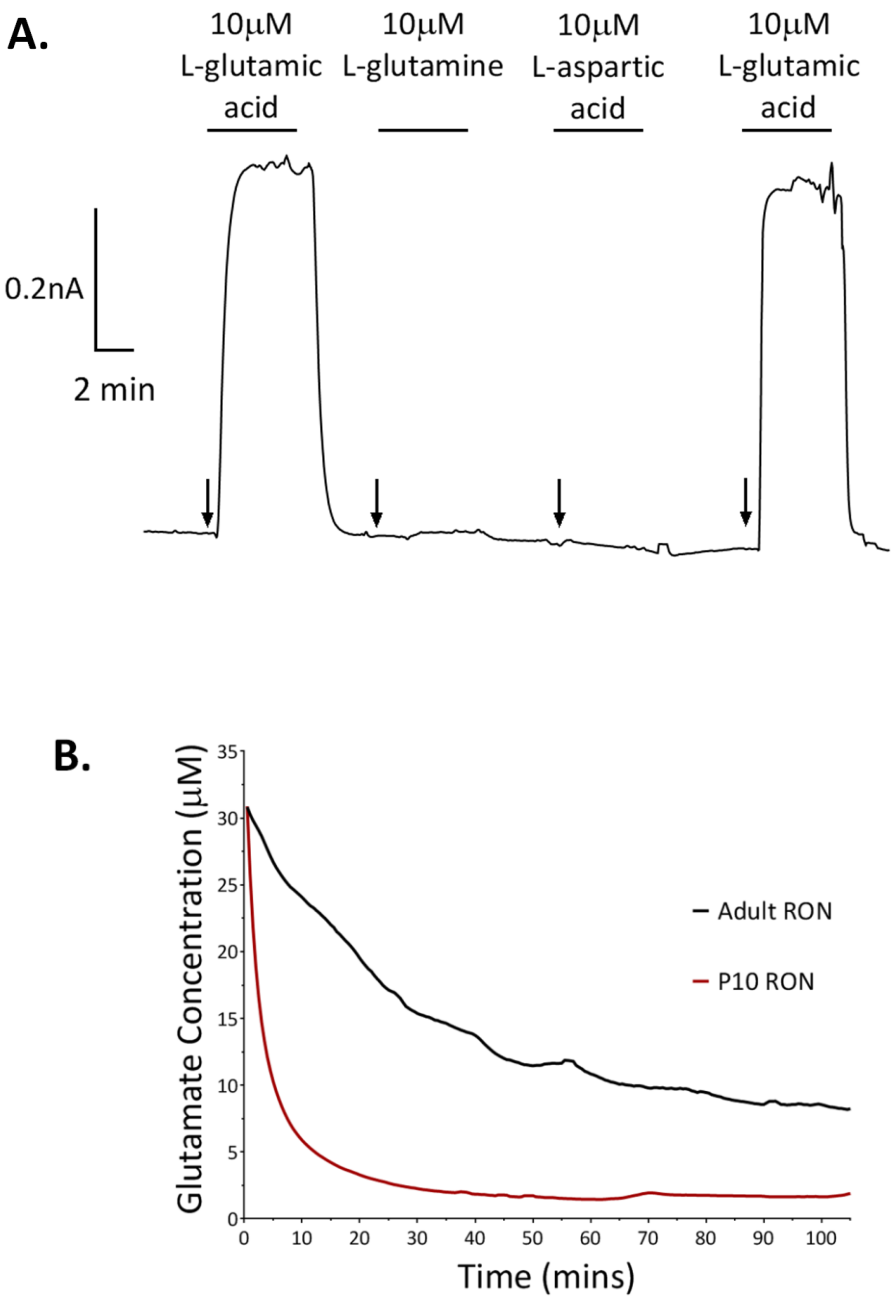

Fig. 2.8: Selectivity of GLU-biosensors and long stabilization period.

a) Selectivity of GLU- biosensors against equivalent concentrations of l-glutamic acid, l-glutamine and l-aspartic acid (10μM). Note the large current response to l-glutamic acid, which was absent during exposure to the other compounds. **b)** Sample trace of elevated $[Glut]_e$ in adult (black) and neonatal (grey) ON (recordings initiated 20 minutes after electrode insertion). Note how the adult ON required a longer period of stabilization when compared the neonate.

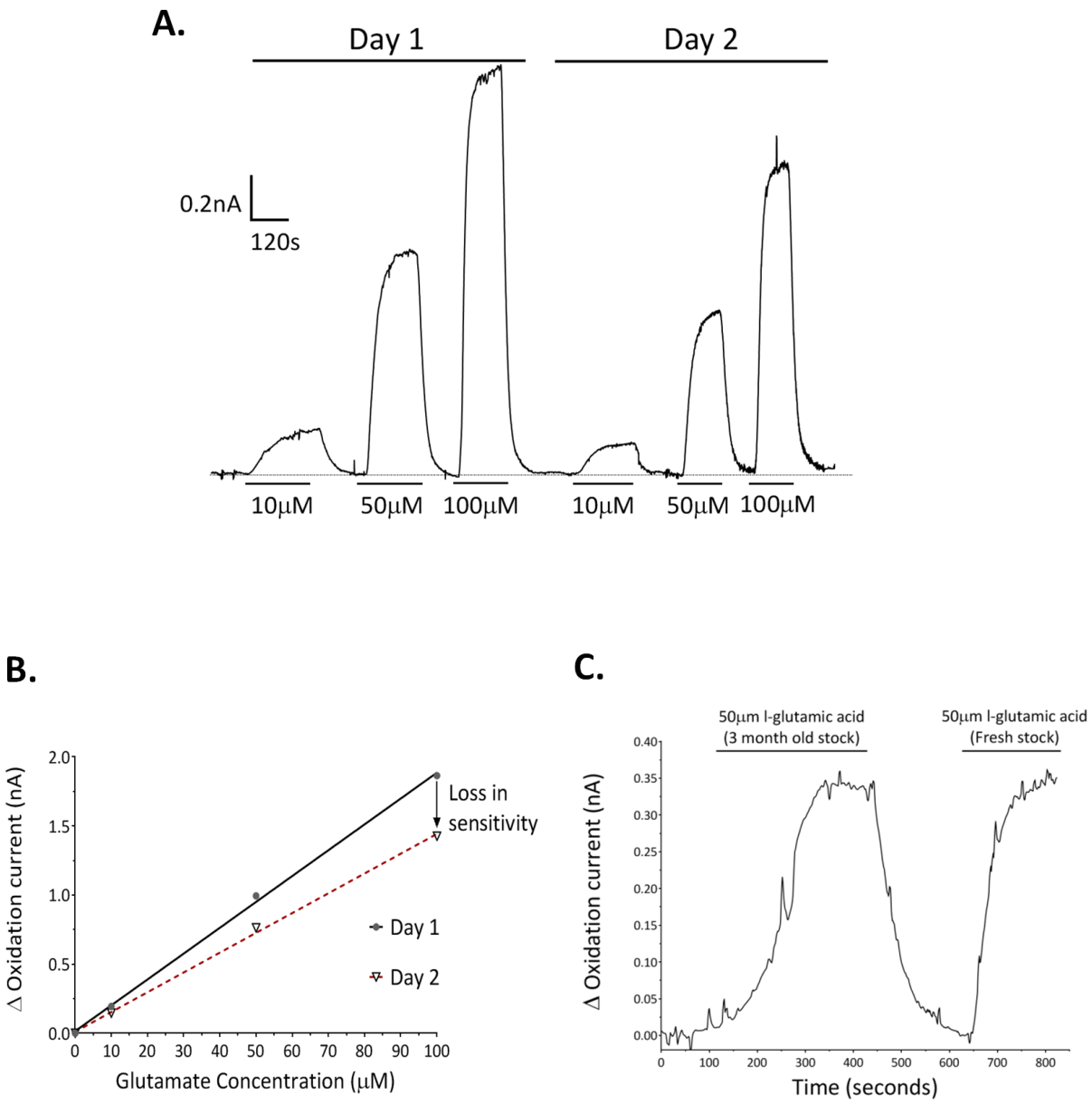

Fig. 2.9: GLU-biosensor calibration.

a,b) GLU-biosensor *i*-t response curve to various concentrations of l-glutamic acid. Note the linear response to concentrations up to 100μM. GLU-biosensor sensitivity decreased with time (Day 1 v Day 2). **c)** When stored at 4°C, stock l-glutamic acid was useable for at least 3 months.

2.6.3: Oxygen-dependency

As mentioned, the oxidation reaction responsible for H_2O_2 production requires the substrates l-glutamate, oxygen and water (l-glutamate+O_2+H_2O⇌2-oxoglutarate+NH_3+H_20_2). Despite previous papers reporting reliable recordings under hypoxic conditions (Dale, Hatz et al. 2005, Tian, Gourine et al. 2009); we could not get stable recordings following O_2 withdrawal. GLU-biosensor sensitivity was dramatically reduced following the removal of O_2 from the chamber (Fig 2.10a-b). In addition, this would occasionally increase the signal-to-noise ratio. This discrepancy may be related to the severity of oxygen withdrawal. Whereas previous papers using sarissaprobes® perfused samples with a deoxygenated solution (pre-bubbled with 95%N_2/5%CO_2) (Dale, Pearson et al. 2000, Frenguelli, Llaudet et al. 2003, Tian, Gourine et al. 2009), our preparation was perfused with a deoxygenated aCSF and had atmospheric O_2 removed from the chamber via bubbling the chamber bath with 95% N_2/5% CO_2. This protocol may be closer to anoxic conditions, which may account for the decrease in GLU-sensor sensitivity during OGD. For this reason, chemical ischemia was employed as our model of ischemia for experiments using GLU-biosensors.

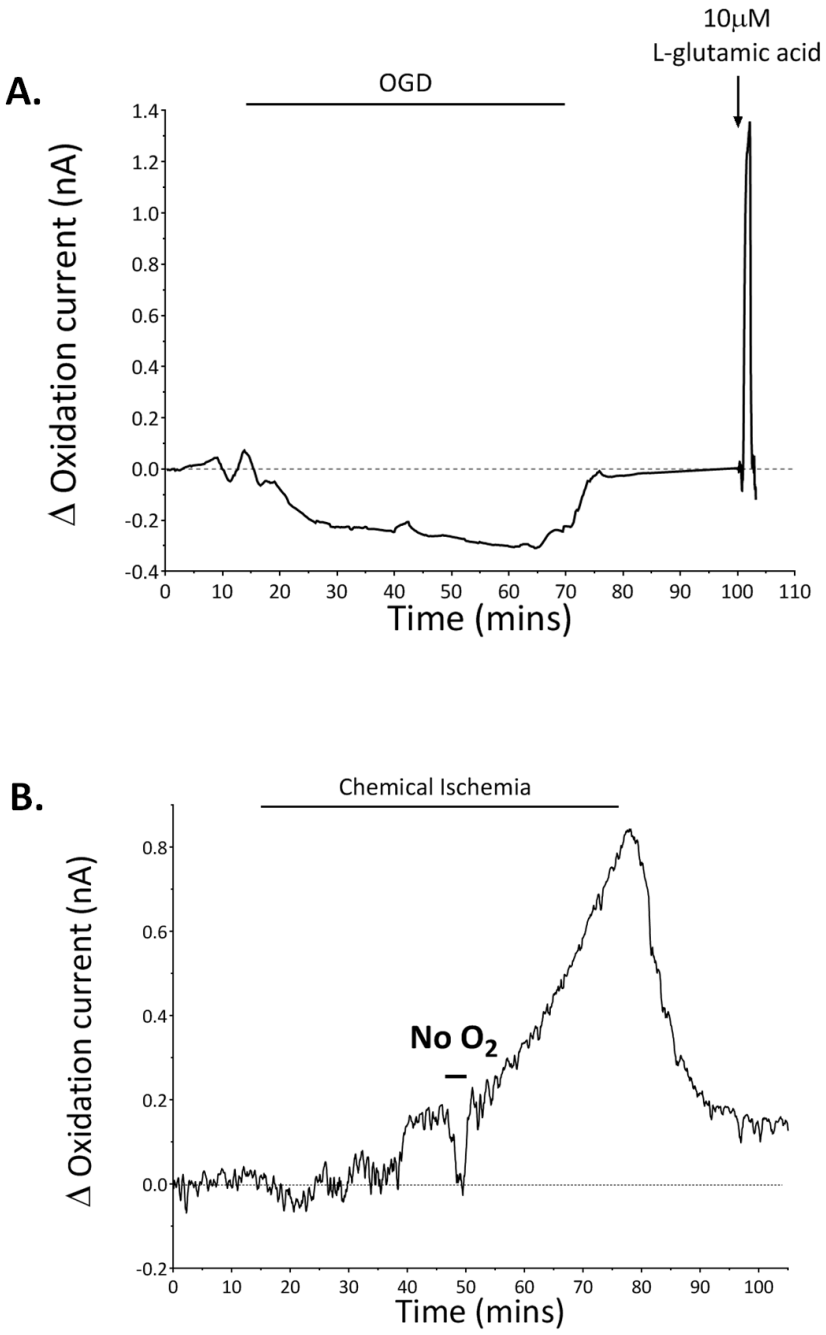

Fig. 2.10: GLU-biosensors are O_2 dependent.

a) Sample *i*-t response curve during exposure to OGD. Not the drop in current during O_2 withdrawal. Yet, GLU-biosensors were still responsive to l-glutamaic acid (10μM) under normoxic conditions. **b)** An alternative sample *i*-t response curve, showing a clear loss in sensitivity when O_2 was removed from the chamber for 5 minutes during exposure to chemical ischemia.

2.7: Immunohistochemistry (IHC)

2.7.1: Background

Immunohistochemistry (ICH) is a technique used to visualise the distribution and localisation of specific target antigens within tissue. The first ICH study was performed by Albert H. Coons *et al.* in 1941 (Coons, Creech et al. 1941). The technique is based on antigen-antibody interactions within biological tissue, which can subsequently be visualised with fluorescent markers (fluorophores). An antibody, or immunoglobulin (Ig), is a 'Y' shaped protein consisting of a constant Fc region and two variable fab fragments. The antigen-binding site (paratope) is located on the fab fragment of the antibody. The antigen-binding site selectively binds to the epitope of the target antigen. There are two methods of detecting bound antigens; the direct and indirect method. The direct method uses an antibody which is directly conjugated to a flurorophore or fluorochrome, which allows visualisation under a fluorescent microscope. The indirect method uses a second, fluorescent antibody; the unlabelled 'primary' antibody which binds directly to the antigen, and a second fluorophore-conjugated 'secondary' antibody which subsequently binds to the primary antibody.

Primary antibodies are produced by inoculating a host animal (e.g. rabbit, mouse, goat) with the antigen of interest. The host's immune system will produce specific antibodies against the foreign antigen, which can later be withdrawn and purified. These antibodies can be either polyclonal or monoclonal. Polyclonal antibodies recognise many epitopes on a single antigen, whereas monoclonal antibodies only recognise one. The secondary antibody is generated by inoculating another host species with antibodies from the host species in which the primary antibody was produced.

2.7.2: Protocol

ONs were immersed in a petri-dish containing 4% paraformaldehyde (PFA) for 20-30 minutes at room temperature. PFA forms covalent cross-links between proteins which prevents decomposition and stabilises cell morphology. Nerves were then transferred to a 20% (w/v) sucrose solution (in 1X PBS) for a further 20 minutes (cryoprotection). The tissue is

subsequently embedded in OCT medium (Tissue-Tek, Sakura) and frozen at -20°C. 20µm thick cryostat-cut (Leica) sections were mounted on SuperFrost Plus slides (ThermoFisher Scientific) and left to dry at room temperature. If slides were not immediately used for staining, they were stored at -20°C for a maximum of 1 month.

Each slice was encircled with a hydrophobic, PAP pen and washed in 1X PBS for 5 minutes. To facilitate antibody access and prevent non-specific binding of secondary antibodies, sections were permeabilised and blocked in a 1X PBS solution containing 10% goat serum and 0.5% triton X (referred to as PBGST) for 2 hours at room temperature. All primary and secondary antibodies are diluted in PBGST. Sections were then incubated with primary antibodies overnight at 4°C. The sections were then washed three times in PBGST for 5 minutes, and incubated in the secondary antibody for 1 hour at room temperature. This was followed by a series of washes; 3 X 5 minute washes in PBGST, followed by 3 X 5 minute washes in 1XPBS. Slides were mounted with Citifluor (glycerol/PBS solution), cover-slipped and allowed to dry. Negative controls were carried out to ensure there was no non-specific binding of the secondary antibody. For this, primary antibodies were excluded.

Antibody	Dilution	Species	Clonality	Company
Neurofilament heavy (200kDa)	1:500	Mouse	Monoclonal	Sigma
Neurofilament-light (70kDa)	1:500	Mouse	Monoclonal	Sigma
L-glutamate	Various	Rabbit	Polyclonal	Abcam

Table 2.3: List of primary antibodies used in ICH studies

Antibody	Dilution	Species	Company
Alexa Fluor 488, Anti-mouse	1:1000	Goat	Sigma-Aldrich
Alexa Fluor 568, Anti-rabbit	1:200	Goat	Sigma-Aldrich

Table 2.4: List of secondary antibodies used in ICH studies.

Attempts were made to examine glutamate distribution in the RON using an anti-l glutamate antibody (ab9440). The immunogen for this antibody is l-glutamate conjugated to glutaraldehyde. However, due to excessive auto-fluorescence from glutaraldehyde-fixed nerves (0.1-2.5%), reliable images were not obtained. A variety of antibody concentrations, fixes (glutaraldehyde, PFA, methanol-acetone, and methanol) and fix-durations were tested, but to no avail. In addition, sudan black was used to quench auto-fluorescence. However, this was unsuccessful and glutamate-staining was no longer pursued.

2.7.3: Confocal Imaging and Analysis

RON slices were imaged via single-photon, laser scanning confocal microscopy (Leica TCS SP8 inverted microscope) using a x40/x63 oil objective lens. For each set of experiments, all slices were treated in the same way with respect to laser intensity, gain and format. Neurofilament staining was analysed using Image J (National Institutes of Health) and mean pixel intensity levels were measured from at least 3 random regions of interest (ROI) from every slice.

2.8: Fluromyelin and QNZ-46 Imaging

2.8.1: Fixed-slices

Fluromyelin Red (Life Technologies) is an established red-fluorescent myelin stain. As with the IHC protocol, RON fixed-sections were initially blocked and permeabilised (2hrs in PBGST). Slices were then incubated with fluromyelin (1:300) for 20 minutes at room temperature. Following this, sections were washed 3 times in PBGST (5 minutes each) and 3 times in 1X PBS (5 minutes each), before being cover-slipped. Images were acquired using an inverted Nikon epifluorescent microscope. Mean pixel intensity was analysed with Image-J.

2.8.2: Live-tissue: Bath-loading

For dual live-imaging of fluromyelin and QNZ-46, adult rat ON or brain slices (400µM thick) were incubated with fluromyelin (1:20) and QNZ-46 (50µM) in cutting solution for 120 minutes at 4°C. Following which, slices were transferred to fresh cutting solution (fluromylein/QNZ-46 free) and images were collected via laser scanning confocal microscopy. Wide-field QNZ-46 imaging was performed using a Zeiss epifluorescence microscope.

Fluorescent emission scans during excitation at 405 nm were conducted using 10nm bin width and the lambda-scan function; with 10mM QNZ-46 in DMSO diluted 50:50 in immersion oil. QNZ-46 has a peak emission at 450nm in a lipid environment (Fig. 2.11b*). *Lambda scan was performed by Prof. Robert Fern and Prof. Mario Valentino. For remaining experiments, QNZ-46 was imaged following excitation at 405nm using filter settings standard for DAPI emission.

2.8.3: In vivo

Adult C57Bl/6 mice were injected IP. with a 200µl of 50% DMSO solution containing 1mM β-cyclodextrin + 20mg/Kg QNZ-46 (50:50), or a vehicle control without the QNZ-46. Injections were performed blind by animal house staff and mice were left for 240 minutes on a warming pad. Other than mild sedation in both groups, attributed to the DMSO, the animals showed no signs of distress or aberrant behaviour. ON or brain slices were collected as above, in solutions that did not contain QNZ-46. Images were acquired via laser scanning confocal or epifluorescence microscopy.

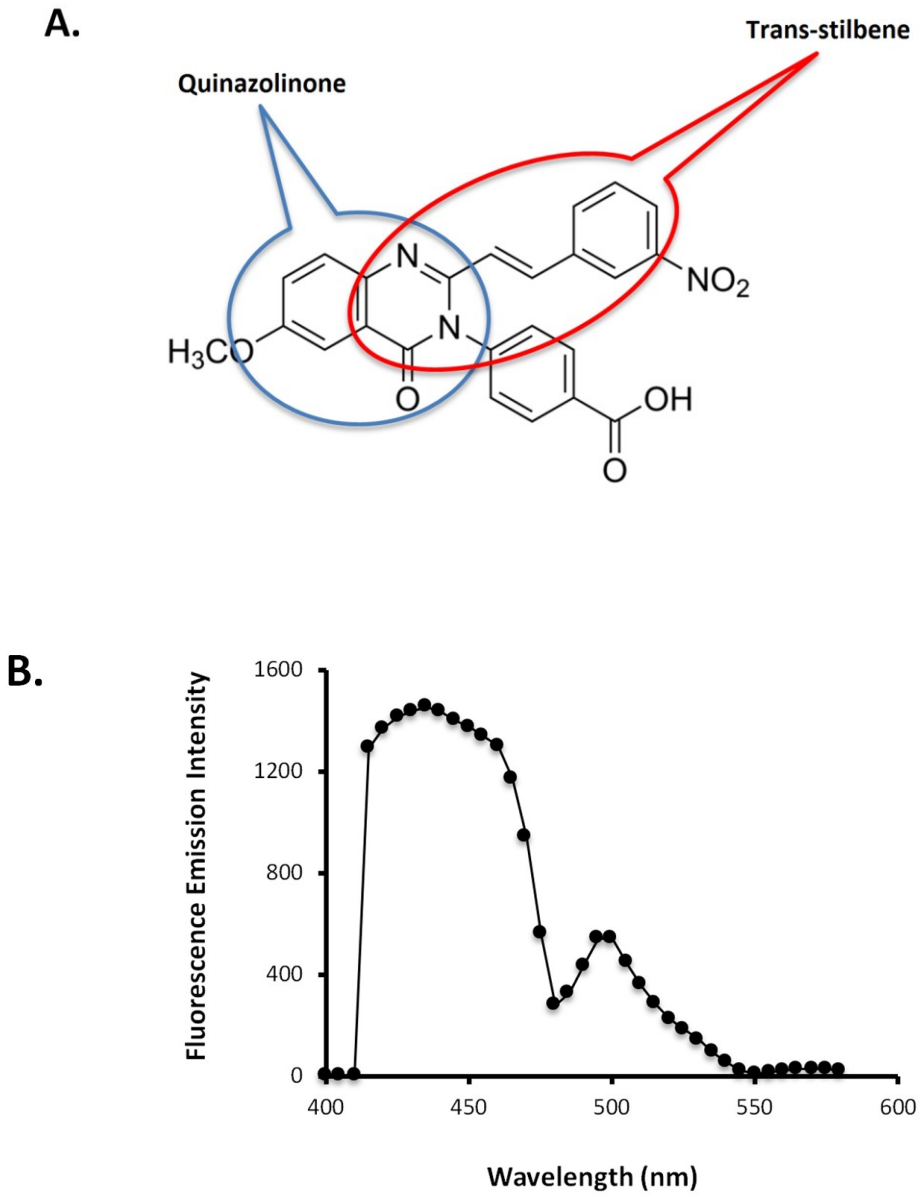

Fig. 2.11: QNZ-46 fluorescence.

a) Molecular structure of QNZ-46 indicating the fluorescent quinazolinone backbone (blue) and the myelin targeting trans-stilbene region (red). **b)** Lambda scan of QNZ-46 fluorescence following excitation at 405nm in a lipid environment (10mM QNZ-46 in immersion oil). QNZ-46 fluorescence peaks at 450nm in a lipid environment.

2.9: FM-dye Imaging

2.9.1: Background

FM dyes are non-toxic, lipophilic styryl-compounds which have been extensively used to study the kinetics of vesicular fusion and recycling. The use of FM dyes as a vesicular marker relies on their ability to reversibly partition into lipid membranes without penetrating (Hoopmann, Rizzoli et al. 2012). All FM dyes have the same general structure. The dye is composed of a lipophilic tail, which causes the dye to partition into lipids environments, such as plasma or vesicular membranes (Gaffield and Betz 2006). The length of the tail region determines the dyes affinity for lipid membranes, with long-tailed variants, such as FM 4-64 (dye*N*- (3-triethylammoniumpropyl)- 4 -(6-(4-(diethylamino)phenyl)hexatrienyl) pyridinium dibromide), binding more tightly (Verstreken, Ohyama et al. 2008). The tail-end is connected to a water-soluble (lipophobic) head group which prevents the dye from crossing the plasma membrane. The head and tail groups are connected via two aromatic rings linked by a variable double bond region, which together create the fluorophore (Gaffield and Betz 2006, Hoopmann, Rizzoli et al. 2012). The number of double bonds connecting the two rings determines the dye's fluorescence spectrum. Dyes with a high number of double bonds, such as FM 4-64, typically have a red-shifted emission spectrum (Gaffield and Betz 2006).

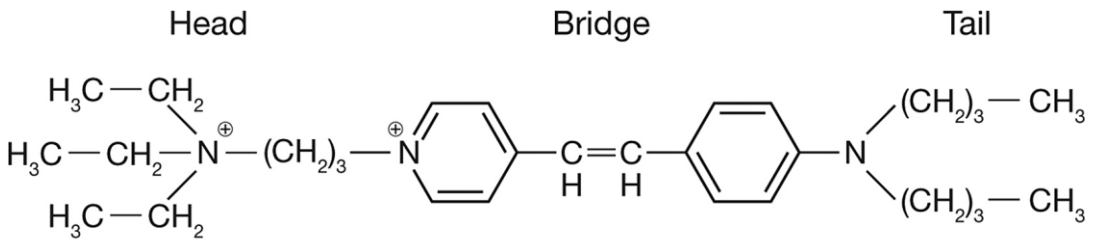

Fig. 2.12: **Chemical structure of FM4-64.**

Structure of FM4-64 showing the lipophilic tail end, and the positively-charged lipophobic head group. Both components are connected to aromatic rings which are linked via a variable double bond bridge. (Hoopmann, Rizzoli et al. 2012).

FM-dyes are particularly useful in the study of vesicular recycling. The dyes excited state relies on the transfer of charge across the double-bond bridge and is highly dependent on solvent polarity (Gaffield and Betz 2006). The dye is practically non-fluorescent in polar, aqueous solution, such as water. However, once its hydrophobic tail is inserted into the outer leaflet of a lipid membrane (non-polar), lipophilic interactions cause the probe to become intensely fluorescent (Newton and Murthy 2006). In preparations capable of vesicular neurotransmitter release and reuptake, the dye becomes internalised within recycled vesicles, allowing for optical imaging of vesicular uptake/release. Measurement of vesicular exocytosis can be accomplished by quantifying FM-fluorescence during stimulation, where a decrease in fluorescence reflects the release of the vesicular-bound probe into the bath (see Fig. 2.13).

As mentioned, FM4-64 has a pronounced red-shifted emission spectrum, well separated from the green/yellow emission spectra of green-fluorescent protein (GFP) and yellow fluorescent protein (YFP). This is highly advantageous, allowing for dual-excitation imaging of both FM-fluorescence and endogenous fluorophores. Experiments using FM 4-64 were carried out on transgenic mice with either neuronal-specific expression of YFP, controlled by the THY1-promoter (THY1-YFP (line H)), or astrocyte-specific expression of GFAP, controlled by the GFP promoter (GFP-GFAP (line M)).

FM-dye imaging in intact brain slices can be difficult due to excessive background fluorescence (Winterer, Stanton et al. 2006). The high density of surface membrane lipid makes it difficult to eliminate residual membrane-bound dye, even after extensive washing (Pyle, Kavalali et al. 1999). It is particularly difficult to wash out the dye from damaged membranes in acute slices. Non-specific fluorescence may be significantly strong enough to dampen any vesicular-bound fluorescence. To help overcome these issues, a long recovery period is allowed following brain slicing. Moreover, imaging was acquired via two-photon microscopy (TPM), capable of providing an unrivalled signal over background fluorescence by suppressing out-of-focus, background fluorescence (Winterer, Stanton et al. 2006, Valentino, Zammit et al. 2011).

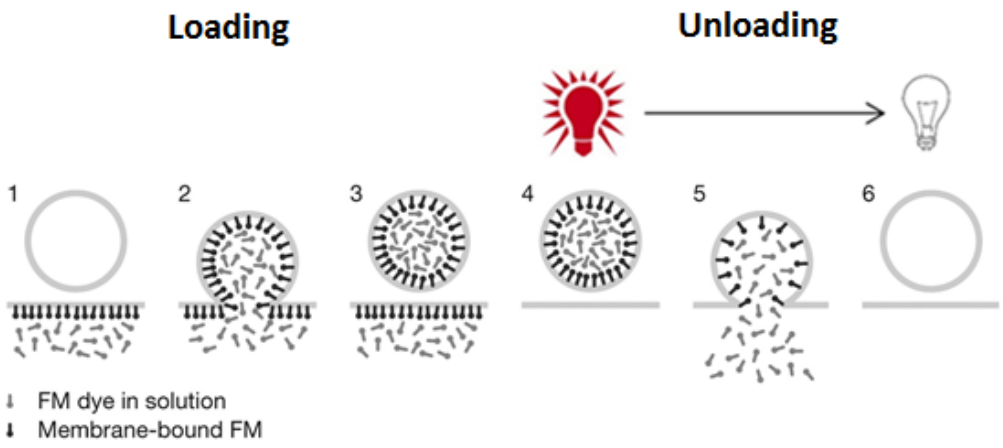

Fig. 2.13: Theory behind FM-dye vesicular imaging.

1. FM-dye is applied to a cell or tissue, causing it to reversibly insert into the outer leaflet of the plasma membrane. This dramatically increases fluorescence intensity, labelling the extracellular membrane. **2.** To induce exocytosis/endocytosis, the preparation is stimulated in the presence of the dye. This causes vesicles to fuse with the membrane, coming into contact with the dye. **3.** Subsequently, endocytosis will trap some of the dye molecules in retrieved vesicles. **4.** The remaining extracellular dye is washed away, leaving only the entrapped dye in internalised vesicles. **5.** The preparation is stimulated again in the absence of the dye, causing the fusion of vesicles with the outer-membrane, releasing vesicular dye into the ECS (destaining). **6.** The released dye is washed away. Adapted from (Hoopmann, Rizzoli et al. 2012).

2.9.1: Protocol

Stock FM4-64 (Life Technologies) solutions (1mM) were dissolved in deionised water and stored for several months at 2-8°C when protected from light (Gaffield and Betz 2006). Coronal brain slices (400µm thick) from transgenic animals were placed in an oxygenated HAAS-type interface holding chamber (Scientific Systems Design Inc.) for a minimum of 90 minutes (at room temperature). A brain slice was then transferred to a mini submerged chamber (0.5ml) with a coverglass bottom (Warner Instrument Corporation, Hamden, CT) mounted on the stage of a custom modified, upright BX50W1 Olympus Multiphoton microscope (Olympus, Tokyo, Japan). Slices were held in place by means of a slice anchor ('harp') with nylon thread and perfused with room temperature oxygenated (95% O2/5% CO2) aCSF at a flow rate of approximately 3.5 ml/minute. Final temperature control (37 ±1°C) was maintained using an in-line heater (Warner Instrument Corporation, Hamden, CT) equipped

with a feedback thermistor placed in the chamber and the temperature raised gradually over 1 hour. Slices were initially examined to identify a suitable region of the CC. The multiphoton system housed Keplerian beam expanders with IR introduction light paths to achieve perfect excitation efficiency and highly resolved images. A mode-locked MaiTai HP DeepSee laser system (Spectra- Physics) with a tuneable Ti: sapphire oscillator (690-1040nm) was used as the excitation light source (pulse width < 100fs; pulse repetition rate 80Mhz) and controlled through an acousto-optical-modulator to allow for precise changes in laser intensity. The Group Velocity Dispersion was electronically compensated by a prism coupled pre-chirper and the beam diameter adjusted by a Keplar telescope.

Slices were perfused with 10µM FM4-64 (in aCSF) for 10 minutes. To stimulate vesicular exocytosis, slices were subjected to a 50mM K^+ aCSF solution (depolarising solution) + 10µM FM4-64 for 5 minutes (Kukley, Capetillo-Zarate et al. 2007). After which, slices were returned to aCSF + 10µM FM4-64 for a further 20 minutes to ensure complete endocytosis. Next, slices were washed in aCSF (without FM4-64) for a minimum of 15-20 minutes and a suitable region of the CC was identified. Finally, slices were exposed to 50mM K^+ aCSF for 10 minutes (or ischemia for 30 minutes) to promote vesicular fusion/FM4-64 unloading. Control images were acquired for at least 60 seconds before FM4-64 unloading. Images were acquired every 10 seconds following laser excitation at 890nm and collected using standard red and green filter settings.

2.9.1: FM-dye Analysis

Image acquisition was performed using the Olympus FluoView software. To compare any changes in FM-fluorescence, pixel intensity was calculated in defined regions of interest, i.e. YFP+ axon cylinders or GFP+ astrocytes. Data is expressed as the percentage change in fluorescence intensity relative to resting fluorescence intensity before stimulation (%ΔF/F) over time (minutes). Control experiments were repeated in control aCSF to account for possible photo-bleaching and/or spontaneous vesicular release. Any significant decrease in FM-fluorescence was indicative of stimulation-evoked release of vesicular-bound FM 4-64.

2.10: Statistics

$[Glut]_e$ and CAP experiments were plotted as a 120-second rolling average over time and random spikes were removed. All data is presented as mean ± SEM. Significance was determined by unpaired t-test or one-way ANOVA with Holm-Šídák *post hoc*-test, as appropriate (GraphPad Prism 6). Ischemia and control experiments were interdigitated. For experiments requiring long periods of drug pre-treatment, appropriate control experiments were performed to allow direct comparison. ns $P \geq 0.05$, * $P \leq 0.05$, ** $P \leq 0.01$, *** $P \leq 0.001$, **** $P \leq 0.0001$.

Chapter 3:

Vesicular Glutamate Release in White Matter

3.1: Introduction

3.1.1: Synaptic White Matter

Synaptic transmission is a highly specialised, unidirectional mechanism of intercellular signalling within the CNS. It is achieved via the release of vesicular neurotransmitters, followed by the subsequent interaction with receptors located on a dedicated post-synaptic membrane. In conventional GM synapses, the arrival of an action potential leads to a depolarising shift in membrane potential, which opens voltage-gated Ca^{2+}-channels (VGCCs) located on the pre-synaptic bouton. The subsequent rise in $[Ca^{2+}]_i$, is detected by synaptotagmin-1, which induces a conformational change in SNARE protein associations and leads to the fusion of neurotransmitter-laden vesicles with the pre-synaptic membrane. Once released, the neurotransmitter freely diffuses across the synaptic cleft and binds to specialised target receptors embedded in the post-synaptic membrane.

The absence of conventional neuronal synapses in WM led to the common belief that vesicular exocytosis was confined to GM regions, as an exclusive mechanism of inter-neuronal signalling. However, there is now compelling evidence which demonstrates that vesicular neurotransmission is prominent in deep WM regions, distant from classical GM synapses. Many key features of conventional neurotransmission are evident in WM, including the expression of SNARE proteins and a range of neurotransmitter receptors. Axons are considered the pre-synaptic element in WM and are known to express the necessary machinery required for vesicular exocytosis, including a high density of neurotransmitter-laden vesicles. Furthermore, axonal glutamate release is capable of evoking receptor-mediated responses in neighbouring glial cells and myelin, acknowledged as the post-synaptic component of the WM synapse (Kukley, Capetillo-Zarate et al. 2007, Ziskin, Nishiyama et al. 2007, Alix, Dolphin et al. 2008, Hamilton, Vayro et al. 2010, Alix and Domingues 2011, Gautier, Evans et al. 2015, Micu, Plemel et al. 2016).

The majority of axonal projections in the CNS are glutamatergic (Spitzer, Volbracht et al. 2016). Consequently, glutamatergic neurotransmission appears to be the dominant form of synaptic signalling within WM, facilitating direct communication between axons and their neighbouring glial partners. However, the functional significance of glutamate signalling at

the WM synapse is not fully understood. While there are many similarities between GM and WM synapses, the structural and functional differences are indisputable (Matute, Domercq et al. 2013).

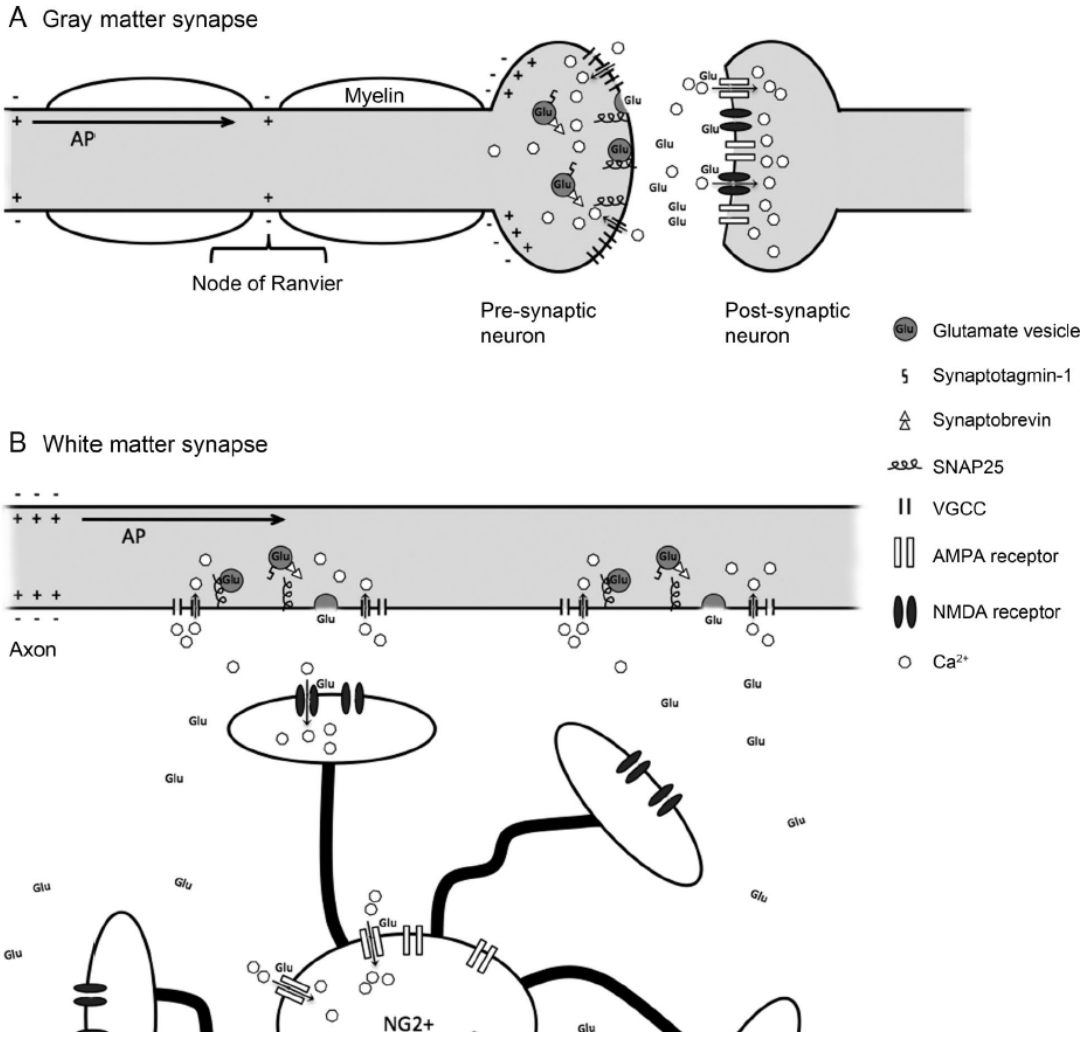

Fig. 3.1: **The synapse**.

Simplified representation of **a)** the conventional GM synapse, and **b)** the WM synapse (in an unmyelinated tract). In both cases, the arrival of an action potential (AP) opens voltage-gated Ca^{2+} channels (VGCCs), which leads to the fusion of glutamate-laden vesicles with pre-synaptic membrane (/axolemma). Released glutamate binds to receptors located on the post-synaptic membrane, either the post-synaptic neuron or NG2+ glia in this case. Taken from (Alix and Domingues 2011).

3.1.2: The Pre-synaptic Partner in WM

3.1.2.1: The Axon

Axons are responsible for the rapid transmission of electrical signals within the nervous system. The first direct evidence of synaptic neurotransmission in WM came in 2007, when two independent groups demonstrated AMPA receptor-mediated synaptic currents in oligodendrocyte precursor cells (OPCs) following the electrical stimulation of unmyelinated axons in the corpus callosum and optic nerve (Kukley, Capetillo-Zarate et al. 2007, Ziskin, Nishiyama et al. 2007). Similar to neuronal synapses, spontaneous excitatory post-synaptic currents (EPSCs) were also recorded in OPCs at rest (Ziskin, Nishiyama et al. 2007).

Interestingly, unmyelinated axons and OPCs form anatomically defined contacts, appropriate for synaptic transmission. Electron microscopy has revealed the accumulation of vesicles distributed along the axon-side of the axolemma, with a similar size and configuration as those observed in cortical GM synapses (Kukley, Capetillo-Zarate et al. 2007, Ziskin, Nishiyama et al. 2007, Micu, Plemel et al. 2016). Similarly, axonal varicosities containing intracellular vesicles are observed along unmyelinated axons following electrical stimulation, particularly at specialised junctions with OPC processes (Shepherd and Raastad 2003, Wake, Ortiz et al. 2015). 'Omega-like' profiles of vesicular fusion with the axolemma have been documented along the internode of myelinated axons which were rapidly fixed following electrical stimulation (Micu, Plemel et al. 2016). Consistent with axons being the primary pre-synaptic element in WM, vesicular endocytosis (recycling) is observed in both myelinated and unmyelinated axons using FM-dyes (Kukley, Capetillo-Zarate et al. 2007, Wake, Lee et al. 2011, Wake, Ortiz et al. 2015, Micu, Plemel et al. 2016).

Vesicular fusion requires the expression and cooperation of a number of highly specialised proteins embedded in the pre-synaptic and vesicular membranes. Numerous studies have identified the expression of axolemma-bound SNARE proteins (e.g. SNAP-25) and vesicular glutamate transports (VGLUTs) in both unmyelinated and myelinated axons (Alix, Dolphin et al. 2008, Micu, Plemel et al. 2016). Axonal punctae which co-labelled for synaptophysin/SNAP-25 (Kukley, Capetillo-Zarate et al. 2007) and synaptophysin/VGLUT1 (Ziskin, Nishiyama et al. 2007) indicate that SNARE protein expression in axons is not simply a

consequence of anterograde transport towards the nerve terminal. In addition, pre-myelinated axons are known to express functional VGCCs which open during action potential conduction (Alix, Dolphin et al. 2008). Clustered VGCC are closely associated with the molecular components of vesicular docking, including V-ATPase and SNAP-25 (Alix, Dolphin et al. 2008). As expected for vesicular exocytosis, localised rises in intra-axonal Ca^{2+} are also observed during AP conduction (Verbny, Zhang et al. 2002, Zhang, Wilson et al. 2006, Kukley, Capetillo-Zarate et al. 2007).

3.1.2.2: Astrocytes

To date, there is no evidence to suggest that fibrous astrocytes contribute to vesicular neurotransmitter release in WM. However, this does not exclude them as a potential pre-synaptic element. Cultured GM astrocytes are capable of exocytotic neurotransmitter release, also referred to as 'gliotransmitter' release (Bezzi, Gundersen et al. 2004, Montana, Malarkey et al. 2006). Protoplasmic astrocytes express the secretory machinery required for vesicular fusion, including a range of SNARE proteins (Bezzi, Gundersen et al. 2004, Volterra and Meldolesi 2005). In addition, electron microscopy has revealed that astrocytes contain dense core vesicles, which are released in a botulinum toxin B (BoNT/B) sensitive fashion (Prada, Marchaland et al. 2011). Although astrocytes are generally regarded as electrically silent, they express a number of VGCCs, capable of elevating $[Ca^{2+}]_i$ (Bezzi, Carmignoto et al. 1998). The rise in $[Ca^{2+}]_i$ is both necessary and sufficient to induce vesicular glutamate release from cultured astrocytes (Parpura, Basarsky et al. 1994, Montana, Malarkey et al. 2006). Conversely, the stimulation of a range of receptors which elevate $[Ca^{2+}]_i$ (e.g. metabotropic glutamate, prostaglandin and purinergic receptors) also evoke glutamate release (Bezzi, Carmignoto et al. 1998, Hamilton, Vayro et al. 2010). Intracellular Ca^{2+} modulates a range of trafficking events which may promote the insertion of proteins which promote non-vesicular neurotransmitter release. However, the kinetics of such events are likely to be too slow to explain the rapid release of neurotransmitter observed in several cultured or slice preparations (Hamilton and Attwell 2010).

While still somewhat controversial, the exocytotic release of gliotransmitters from astrocytes is proposed to modulate neuronal excitability and/or neuronal transmitter release (Montana, Malarkey et al. 2006, Hamilton and Attwell 2010). Interestingly, the co-activation of AMPA/kainate and metabotropic glutamate receptors on astrocytes stimulates the release of glutamate in a Ca^{2+}-dependant manner, which could represent a mechanism of back-signalling to neurons (Bezzi, Carmignoto et al. 1998). In addition, high levels of $[K^+]_e$ trigger the release of vesicular glutamate by activating VGCCs and elevating astrocytic Ca^{2+} levels (Yaguchi and Nishizaki 2010). Considering action potential conduction elevates $[K^+]_e$, it is plausible that vesicular glutamate release from fibrous WM astrocytes may modulate actively firing axons. In support of such a theory, Sasaki *et al.* reported that the local application of glutamate along the axon of hippocampal neurons increases the width of the action potential waveform (Sasaki, Matsuki et al. 2011). Additionally, elevating $[Ca^{2+}]_i$ in periaxonal astrocytes also leads to the broadening of action potentials, through the activation of axonal glutamate receptors (Sasaki, Matsuki et al. 2011).

The expression of the synaptic protein, synaptophysin, on NG2+ glia (oligodendrocyte precursor cells), also raises the question of whether OPCs are also capable of vesicular fusion (Bakiri, Burzomato et al. 2009). Thus, it remains to be determined whether axons are the sole mediator of vesicular fusion in WM, or if WM glial cells are also capable of this specialised mechanism of communication.

3.1.3: The Post-synaptic Partner in WM

3.1.3.1: Oligodendrocyte Precursor Cells

As mentioned, OPCs come into close contact with axons, and thus are ideally positioned to monitor action potential firing (Hamilton, Vayro et al. 2010). Prior to the initiation of myelination, developing oligodendrocytes navigate along pre-myelinated axons, forming synaptic-like contacts with the bare axolemma (Káradóttir, Cavelier et al. 2005, Salter and Fern 2005, Alix and Fern 2009). Likewise, NG2+ cells in the mature CNS are known to send out processes which make precise contacts with the node of Ranvier in myelinated tracts (Butt,

Duncan et al. 1999, Ziskin, Nishiyama et al. 2007, Hamilton, Vayro et al. 2010). Similar to conventional neuronal synapses, developing (and mature) oligodendrocytes display a high post-synaptic density at sites of contact with unmyelinated axons (Kukley, Capetillo-Zarate et al. 2007, Ziskin, Nishiyama et al. 2007) and are endowed with functional AMPA/kainate receptors (Patneau, Wright et al. 1994, Tekkok and Goldberg 2001, Deng, Rosenberg et al. 2003), NMDA receptors (Káradóttir, Cavelier et al. 2005, Salter and Fern 2005, Micu, Jiang et al. 2006, Micu, Plemel et al. 2016) and all three groups of metabotropic glutamate receptors (Deng, Wang et al. 2004). The amplitude and kinetics of EPSCs recorded from corpus callosum OPCs during exposure to hyperosmotic solution (500mM sucrose supplemented) is not significantly different to the response recorded in from OPCs in alternative regions of the brain, suggesting that the receptor density and subunit expression is similar to those found in GM (De Biase, Nishiyama et al. 2010). Together, these characteristics leave oligodendroglia as ideal biological detectors of axonal neurotransmitter release.

Several studies have recorded EPSCs in OPCs following the electrical stimulation of axons. The rapid kinetics of OPC-recorded signals are characteristic of synaptic neurotransmission. Consistent with spontaneous vesicular fusion from axons, spontaneous EPSCs (independent of action potentials) were recorded in the absence of electrical stimulation, a feature which was abolished in the presence of AMPA receptor antagonists or tetrodotoxin (TTX) (Kukley, Capetillo-Zarate et al. 2007, Ziskin, Nishiyama et al. 2007). Ziskin *et al.* showed that EPSCs could still be elicited in the presence of *dl*-TBOA, a glutamate transporter antagonist, and were increased following the application of α-latrotoxin, which enhances vesicular fusion (Ziskin, Nishiyama et al. 2007). In contrast, bafilomycin-a1, an inhibitor of V-type H^+ ATPase, significantly decreased the amplitude of evoked EPSCs (Ziskin, Nishiyama et al. 2007). Glutamate receptor-mediated signalling in WM evokes transient intracellular Ca^{2+} rises in NG2+ glia *in situ* (Hamilton, Vayro et al. 2010). More recent studies have also noted Ca^{2+} transients in the fine processes of OPCs, following the electrical stimulation of DRG neurons, a feature which was prevented following glutamate receptor blockade or BoNT/A application (Wake, Ortiz et al. 2015).

3.1.3.2: Myelin Sheath

In the mature CNS, a large population of axons are myelinated; meaning only about 1% of the axolemma is directly exposed to the extracellular milieu. This raises the question of whether myelin is capable of responding to vesicular glutamate release along the internodal axolemma. Until recently, myelin was considered a passive insulator which solely facilitated saltatory action potential conduction across the nervous system. However, recent findings suggest that myelin may be much more reactive and dynamic than once thought. For example, myelin expresses isoforms of two essential Ca^{2+} buffering systems, Na^{+}-Ca^{2+} exchanger (NCX) and Ca^{2+}-ATPase, suggesting that it may play a role in ionic regulation and/or signal transduction (Ishii, Dutta et al. 2009, Jahn, Tenzer et al. 2009).

Studies on early myelinating WM show a high degree of NMDA receptor subunit (NR1) expression on the axolemma-side of navigating oligodendrocyte processes (Alix and Fern 2009). As these synapses are lost during development, NR1 is reportedly translocated from the oligodendrocyte processes into myelin, with distinct evidence of NR1 expression within compact myelin itself (Alix and Fern 2009). Interestingly, immunoreactivity for NMDA receptor subunits demonstrate that NMDA receptor expression is predominantly found along the outer and inner periaxonal membranes, at levels which are comparable to neuronal synapses (Micu, Jiang et al. 2006, Micu, Plemel et al. 2016). Thus, myelinic NMDA receptors are ideally position to detect internodal vesicular glutamate release. *Micu et al.* were the first to demonstrate that directly exposing myelin to iGluR agonists (NMDA + glycine or AMPA + cyclothiazide) led to an increase in myelin Ca^{2+}, as did the removal of Mg^{2+} under resting conditions (Micu, Jiang et al. 2006). More recently, the same group demonstrated that electrically active axons elicit Ca^{2+} rises in the cytoplasmic compartment of myelin, a feature which is abolished in the presence of NMDA or AMPA/kainate receptor antagonists, TTX or bafilomycin-a1 (Micu, Plemel et al. 2016). These findings suggest that not only is myelin capable of detecting glutamate release, but also that internodal axon segments may be capable of releasing vesicular glutamate into the confined periaxonal space (equivalent to the synaptic cleft (Matute and Ransom 2012)).

3.1.3.3: Alternative Targets: Astrocytes and Axons?

Vesicular neurotransmitter release at conventional synapses is known to mediate Ca^{2+} signalling in protoplasmic astrocytes (Bazargani and Attwell 2016). Fibrous astrocytes form close associations with axons and are known to respond to axonal neurotransmitter release (particularly ATP) (Hamilton, Vayro et al. 2008). Action potential evoked ATP release from axons evokes a transient rise in intracellular Ca^{2+} (Hamilton, Vayro et al. 2008). While AMPA/kainate and NMDA receptor expression has been described in protoplasmic astrocytes (Verkhratsky and Steinhauser 2000, Lalo, Pankratov et al. 2006), the expression of functional glutamate receptors on WM astrocytes has not (Huria, Beeraka et al. 2015). Therefore, based on our current knowledge, it seems unlikely that astrocytes are a target of synaptic transmission in WM.

While developing oligodendrocytes and myelin appear to be a major target of vesicular release in WM, reports of glutamate receptor expression on axons, raise the question of whether autologous glutamate signalling occurs in WM. Myelinated spinal cord axons are reported to express functional AMPA and kainate receptors, capable of eliciting intra-axonal Ca^{2+} rises (Ouardouz, Malek et al. 2006, Ouardouz, Coderre et al. 2009, Ouardouz, Coderre et al. 2009). In addition, pre-myelinated optic nerve axons express functional NMDA receptors which contribute to functional injury under ischemic conditions (Huria, Beeraka et al. 2015). However, the significance of such glutamate receptors under physiological conditions remains to be determined.

3.1.4: Physiological Function of Vesicular Glutamate Release in WM

Glutamatergic signalling within WM provides a sophisticated method of communication between axons and their partner glial cells. However, the physiological significance of such signalling is still somewhat controversial. Although much more experimental work is required, glutamatergic WM signalling is implicated in a variety of physiological processes;

3.1.4.1: Guide OPC Migration

Founder OPCs arise in distinct regions of the ventricular zone and are known to migrate considerable distances towards target axons (Binamé, Sakry et al. 2013). A combination of chemo-repellent and chemo-tactic signals guide OPC migration along axons/nerves towards their final destinations. Glutamatergic input can be detected in OPCs as early as P5 in neonatal mice (Ziskin, Nishiyama et al. 2007). Therefore, it is possible that vesicular glutamate release from actively firing axons may serve as an extrinsic regulator of OPC migration (Bakiri, Burzomato et al. 2009).

OPCs express NG2, an integral membrane chondroitin sulphate (Butt, Duncan et al. 1999), and studies have shown that NG2 interactions with intracellular and extracellular ligands regulate cell migration (Stallcup 2002). Interestingly, NG2 is directly coupled to AMPA receptors in OPCs (Stegmüller, Werner et al. 2003, Ziskin, Nishiyama et al. 2007). Quantal glutamate release from axons is known to occur even in the absence of defined post-synaptic targets (De Biase, Nishiyama et al. 2010, Alix and Domingues 2011). The absence of defined synaptic junctions implies that vesicular glutamate release is directly into the extracellular space (ECS). Consistent with the high expression of glutamate receptors on OPCs, the establishment of an axon-derived glutamate concentration gradient in the ECS may play a vital role in regulating OPC migration towards the target axon. Inhibiting NMDA receptors dramatically attenuates OPC migration in an *in vitro* migration assay using neurohypophysial explants (Wang, Pralong et al. 1996). Alternatively, AMPA receptor-mediated signals promote OPC migration in a concentration dependent manner, starting with AMPA concentrations as low as 50nM (Gudz, Komuro et al. 2006). Together, this suggests that glutamate-mediated signals act as a chemoattractant signal, which may provide positional cues, stimulating OPC migration towards its destination. In support of such roles, OPC processes are less closely associated with electrically active axons in which vesicular fusion is blocked (with BnTX or TnTX) (Wake, Ortiz et al. 2015).

3.1.4.2: Promote Oligodendrocyte Maturation

OPC maturation is essential for myelination. Given the importance of myelination, it comes as no surprise that the development of oligodendrocytes is a highly regulated process (Emery 2010). While intrinsic cues such as a 'developmental clock' that counts the number of cell divisions (Temple and Raff 1986) play an important role in OPC development, a variety of extrinsic cues, such as secreted molecules and axonal surface ligands, are essential in the control of OPC maturation into mature myelinating oligodendrocytes. Soluble axon-derived signals and the formation of synapses with axons influence the differentiation of immature oligodendrocytes (Miller 2002, Lundgaard, Luzhynskaya et al. 2013). Several studies have reported that glutamate receptor activation modulates oligodendrocyte differentiation by inhibiting OPC proliferation while simultaneously promoting differentiation into their mature counterparts. The activation of NMDA receptors in subventricular zone-derived OPCs increases their rate of differentiation and maturation *in vitro* (Cavaliere, Urra et al. 2012). On the other hand, the application of NMDA receptor antagonists or knockdown of the obligatory NMDA receptor subunit, NR1, significantly attenuates NMDA-induced differentiation (Li, Xiao et al. 2013). More recently, Fannon *et al*. demonstrated that blocking neuronal activity or AMPA receptors impaired the morphological development of OPCs and decreased the expression of myelin basic protein (MBP) (Fannon, Tarmier et al. 2015). Therefore, glutamatergic signalling may play a part in the complex array of axon-derived signals which control and guide glial cell development (Yuan, Eisen et al. 1998, Kukley, Capetillo-Zarate et al. 2007).

3.1.4.3: Activity-dependent Myelination

Up until recently, the significance of activity-dependant myelination in WM tracts was a rather controversial topic, as myelination is known to occur in the absence of electrical activity (action potentials) (Shrager and Novakovic 1995). For example, OPCs differentiate and form compact myelin on paraformaldehyde-fixed axons (i.e. inactive/dead) (Rosenberg, Kelland et al. 2008). However, it is now widely accepted that neuronal activity has a significant effect on both the rate and degree of myelination (Demerens, Stankoff et al. 1996, Wake, Lee et al.

2011, Lundgaard, Luzhynskaya et al. 2013, Gautier, Evans et al. 2015). Early studies observed a decrease in myelination in the ON of mice which were reared in the dark, which was interpreted as a result of decreased 'functional stimulation' (Gyllensten and Malmfors 1963). In contrast, electrically active axons which are capable of releasing vesicular neurotransmitters are preferentially myelinated in a co-culture of DRG neurons and OPCs (Wake, Ortiz et al. 2015). Similarly, blocking synaptic vesicular release reduces the number of myelin sheaths in zebra fish axons, while stimulating neuronal activity increased the number of myelin layers produced by a single oligodendrocyte (Mensch, Baraban et al. 2015). Vesicular glutamate release along axons stimulates the formation of cholesterol-rich microdomains on post-synaptic OPCs and also promotes the local synthesis of myelin basic protein (MBP), a major protein constituent of myelin sheath (Wake, Lee et al. 2011).

Using a myelinating co-culture system, Lundgaard *et al.* reported that myelination can occur via two distinct modes, resolving the prior controversy over the significance of activity-dependant myelination (Lundgaard, Luzhynskaya et al. 2013). The first intrinsic mode of myelination can occur in the absence of action potential conduction and glutamate release. However, the second mode requires the activity-dependent release of glutamate from axons and the subsequent activation of NMDA receptors on oligodendroglia. The switch to this 'activity-dependant mode' requires the release of either neuregulin (NRG) or brain-derived neurotrophic factor (BDNF) which enhances OPC sensitivity to axonal activity by increasing NMDA receptor mediated currents in OPCs (Lundgaard, Luzhynskaya et al. 2013). As a result, glutamatergic signalling enhances both the rate and degree of myelination in actively firing axons. Although glutamate release is not essential for myelination, it plays a central role in the preferential myelination of electrically active axons. Consistent with such data, there is a high expression of NMDA receptors on the myelinating processes of immature oligodendrocytes (Káradóttir, Cavelier et al. 2005, Salter and Fern 2005). Vesicular signalling in WM may also constitute a signal for myelin length regulation, as attenuating synaptic glutamate release from retinal ganglion cells increases the number of nodes and reduces the length of internodal myelin in the mouse ON (Etxeberria, Hokanson et al. 2016).

3.1.4.4: Re-myelination

During development, a population of NG2+ OPCs fail to differentiate, but instead form a distinct population of cells in the mature CNS (Nishiyama, Chang et al. 1999, Dawson, Polito et al. 2003). Following demyelination in multiple sclerosis (MS), OPCs undergo a process of rapid proliferation and subsequent differentiation in myelinating cells which replace myelin sheath (Reynolds, Dawson et al. 2002, Zawadzka, Rivers et al. 2010). Recruited OPCs form *de novo* contacts with demyelinated axons suggesting that WM synapses may play an import role in restarting myelination (Alix and Domingues 2011, Gautier, Evans et al. 2015). Blocking vesicular fusion from active axons or applying glutamate receptor antagonists significantly attenuates re-myelination in a toxin-induced focal demyelination model (Gautier, Evans et al. 2015). Similar to activity-dependent myelination, glutamatergic synaptic transmission between demyelinated axons and OPCs may regulate re-myelination in an activity-dependant fashion.

3.1.4.5: Maintain Axon Integrity

The precise role(s) of the proposed axo-myelin synapse remains elusive. In addition to axon ensheathment, oligodendrocytes maintain long-term axon integrity by providing metabolic support (Nave 2010, Lee, Morrison et al. 2012). For example, lactate derived from oligodendrocytes is metabolised in WM tracts during periods of energy deprivation (Funfschilling, Supplie et al. 2012). Oligodendroglial NMDA receptor activation promotes the release of lactate and the redistribution of glucose transporter, GLUT1, into the myelin compartment (Saab, Tzvetavona et al. 2016). Alternatively, the chronic ablation of the obligatory NMDA receptor subunit, NR1, in oligodendrocytes leads to GLUT1 depletion in myelin, and gradual WM degeneration (Saab, Tzvetavona et al. 2016). Furthermore, the activity-dependant release of vesicular glutamate from axons triggers the secretion of oligodendroglial exosomes which are subsequently internalised by the axon (Fruhbeis, Frohlich et al. 2013). Exosomes contain a multiple protein and RNA cargo which support axonal metabolism under oxidative stress (Fruhbeis, Frohlich et al. 2013). It is therefore possible that glutamatergic synapses between the axon and myelin may act as a signal for

axonal energy requirements. Such signalling may promote the transfer of energy substrates to fuel axons during electrical activity.

3.1.4.6: WM plasticity

Recent evidence suggests that axo-myelin signalling may also play a role in the long-term maintenance and re-modelling of myelin sheath (Wang and Young 2014). Long-term changes in myelinic nanostructure are closely associated with memory and learning (Lundgaard, Luzhynskaya et al. 2013, McKenzie, Ohayon et al. 2014). For example, training-related increases in myelination are regularly observed in WM (Scholz, Klein et al. 2009, Zatorre, Fields et al. 2012). The axo-myelinic synapse may provide a mechanism by which architectural changes in the structure of myelin occur based on axonal firing patterns. Double transgenic mice lacking both NR-2D and -3A display an increased myelin thickness resulting from an increased spacing between the myelin lamella (decompaction), rather than changes in the number of myelin layers (Micu, Plemel et al. 2016). This suggests that NMDA receptor-mediated currents in myelin may regulate the expression of structural myelin proteins, which in turn may alter axonal conduction properties. Although it is unlikely to work in isolation, glutamatergic signalling between the axon and myelin may prove to play a vital role in increasing our cognitive capabilities through myelin reorganisation (Wang and Young 2014).

3.1.5: Objective

The overall objective of this chapter is to investigate depolarisation-evoked vesicular fusion in WM. Previous studies have focused on post-synaptic signals as a way of detecting vesicular glutamate release. I aim to determine whether depolarisation-evoked vesicular release is capable of elevating extracellular glutamate concentrations.

Furthermore, recent studies have reported the possible existence of a novel type of chemical synapse between the axon and myelin sheath i.e. the axo-myelinic synapse. I will examine the pattern of vesicular exocytosis in myelinated axons in order to determine whether vesicular fusion occurs along the internodal segment of myelinated axons.

Finally, vesicular fusion in fibrous WM astrocytes has never been examined. I aim to compare depolarisation-induced vesicular release in axons and astrocytes, to determine whether fibrous astrocytes are capable of vesicular neurotransmitter release.

3.2 Results

3.2.1 High-K^+ induced depolarisation promotes vesicular glutamate release in adult white matter

Elevated concentrations of extracellular K^+ ($[K^+]_e$) is regularly used as a depolarising agent *in vitro* (Eng and Kocsis 1987, Takahashi, Shibata et al. 1997, Yaguchi and Nishizaki 2010). High $[K^+]_e$ (45mM) has previously been used to evoke vesicular fusion in the developing corpus callosum (Kukley, Capetillo-Zarate et al. 2007). In addition, $[K^+]_e$ is known to increase by 57.5mM under pathological conditions, such as ischemia (Szatkowski and Attwell 1994, Gido, Kristian et al. 1997). I initially examined the effect of 50mM $[K^+]_e$ (referred to as 'high-K^+') on WM conductivity using the isolated adult rat CC. A brief 5-minute exposure to high-K^+, reversibly attenuated CAP area to 3.62±3.62% (*n*=3), whereas, a 10-minute exposure completely abolished CAP conduction (0.03±0.05%, *n*=3) (Fig. 3.2a). Perfusion with high-K^+ did not lead to any irreversible functional injury, with CAP recovery reaching 123.3±7.18% (*n*=3, p=0.03) of its original area following wash-out (Fig. 3.2a(i)). A similar effect was observed in the adult RON (Fig. 3.2b, *n*=1).

Using enzymatic glutamate biosensors, extracellular glutamate concentrations ($[Glut]_e$) were recorded inside the adult CC during sequential exposures to high-K^+ (5 min and 10 min, respectively). Exposure to high-K^+ evoked a rapid rise in $[Glut]_e$, increasing by 12.95±3.57µM during a 5-minute stimulation (Fig. 3.3, *n*=10). Interestingly, $[Glut]_e$ peaked after 3.84±0.47 minutes of high-K^+, before returning towards baseline. Following a 60 minute rest period, slices were re-exposed to high-K^+ in the presence of EAAT inhibitor, TBOA (200µM) (Baltan, Besancon et al. 2008). The rise in $[Glut]_e$ was unaffected by EAAT inhibition, with maximum peak concentrations reaching 12.60±3.03µM (*n*=10). This was not significantly different from the initial first peak in the absence of TBOA (Fig. 3.3, p=0.94, note; both peak concentrations were measured within the initial 5 minutes of high-K^+).

To investigate whether the rise in $[Glut]_e$ is a result of vesicular docking, CC slices were treated with bafilomycin-a1 (50nM), a specific inhibitor of vesicular type H^+-ATPase (V-ATPase) (Cavelier and Attwell 2007, Hansen, Garrido-Comas et al. 2015, Micu, Plemel et al. 2016). In

order to ensure sufficient depletion of glutamatergic vesicles, slices were perfused with bafilomycin-a1 for a minimum of 120 minutes before exposure to high-K^+. Inhibition of vesicular loading with bafilomycin-a1 reduced the first high-K^+ evoked rise in $[Glut]_e$ to 3.89±1.94µM (*n*=5, Fig. 3.4a, p=0.11). Similarly, the second high-K^+ evoked rise (in TBOA) was significantly reduced to 4.06±0.74 µM (*n*=5, p=0.04, Fig. 3.4b). Together, this indicates that a major component of the K^+-induced rise in $[Glut]_e$ is of vesicular origin.

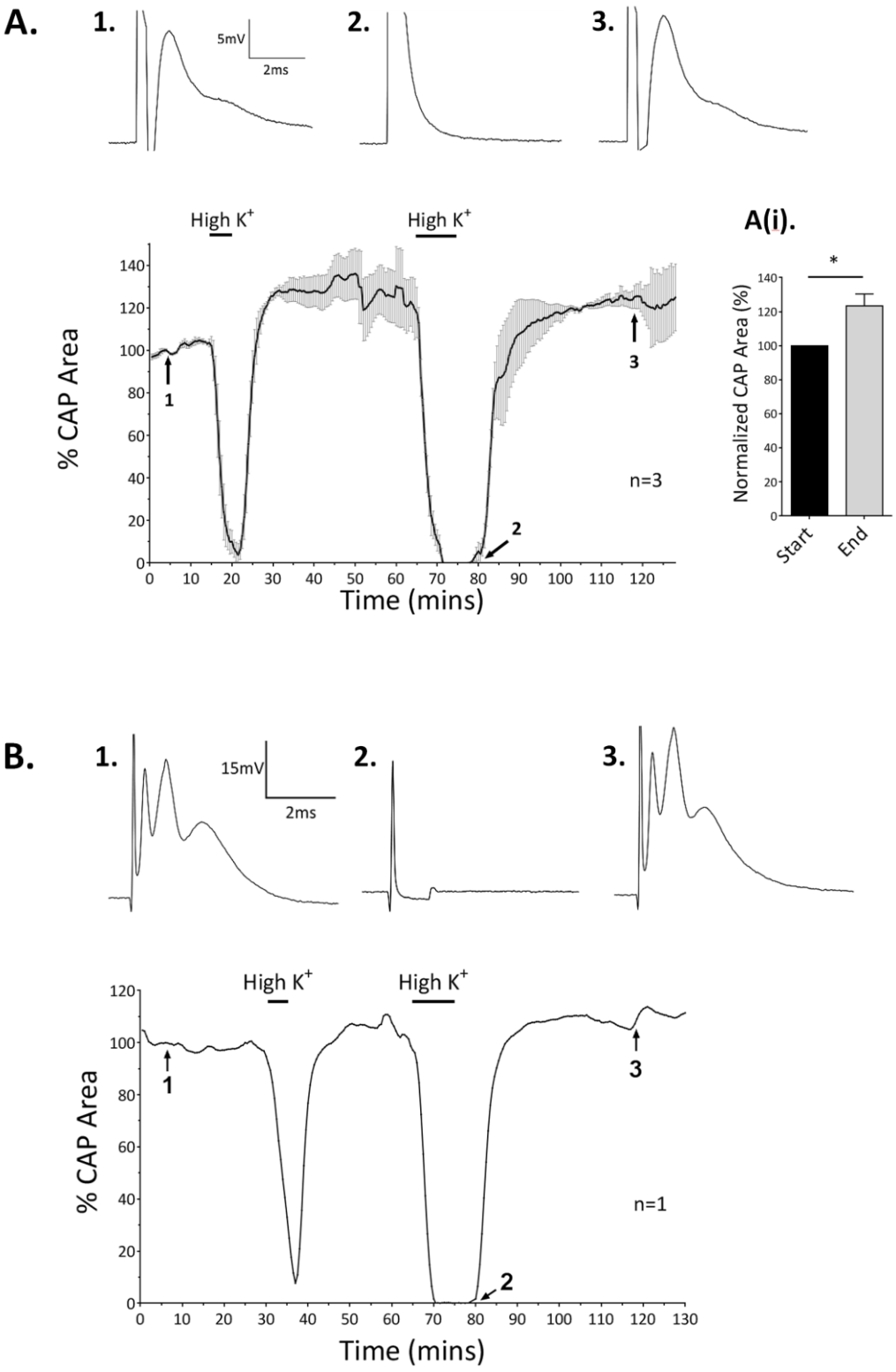

Fig. 3.2: High-extracellular K^+ reversibly blocks CAP conduction in adult WM tracts.

Time-course of CAP area recorded from the adult rat corpus callosum **(a)** and optic nerve **(b)**, including two brief exposures to high-K^+ (50mM KCl). Representative CAP traces (above) are shown at different time points, labelled 1-3. Perfusion with high-K^+ results in a rapid decline in CAP area, followed by a full recovery following wash-out (see inset **a(i)**: Histogram comparing mean CAP area before and after exposure to high-K^+).

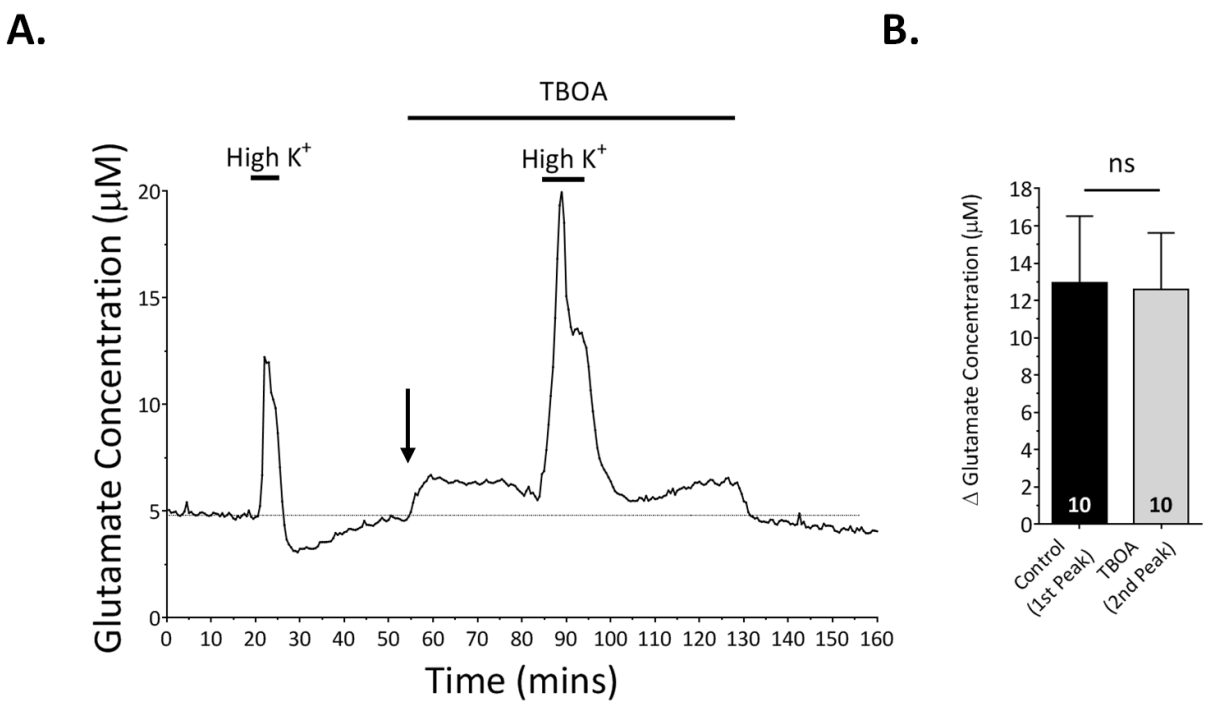

Fig. 3.3: High-K^+ evokes a TBOA-insensitive rise in extracellular glutamate.

a) Representative $[Glut]_e$ recording from inside the adult CC during exposure to high-K^+. Exposure to high-K^+ leads to a robust increase in $[Glut]_e$. Perfusion with the EAAT inhibitor, TBOA, led to a slight rise in resting $[Glut]_e$ (see arrow). Depolarisation-evoked release was unaffected in the presence of TBOA. **b)** Histogram comparing the maximum peak concentration reached in the absence and presence of TBOA (both measurements are taken within the initial 5 minutes of high-K^+). ns $p>0.05$.

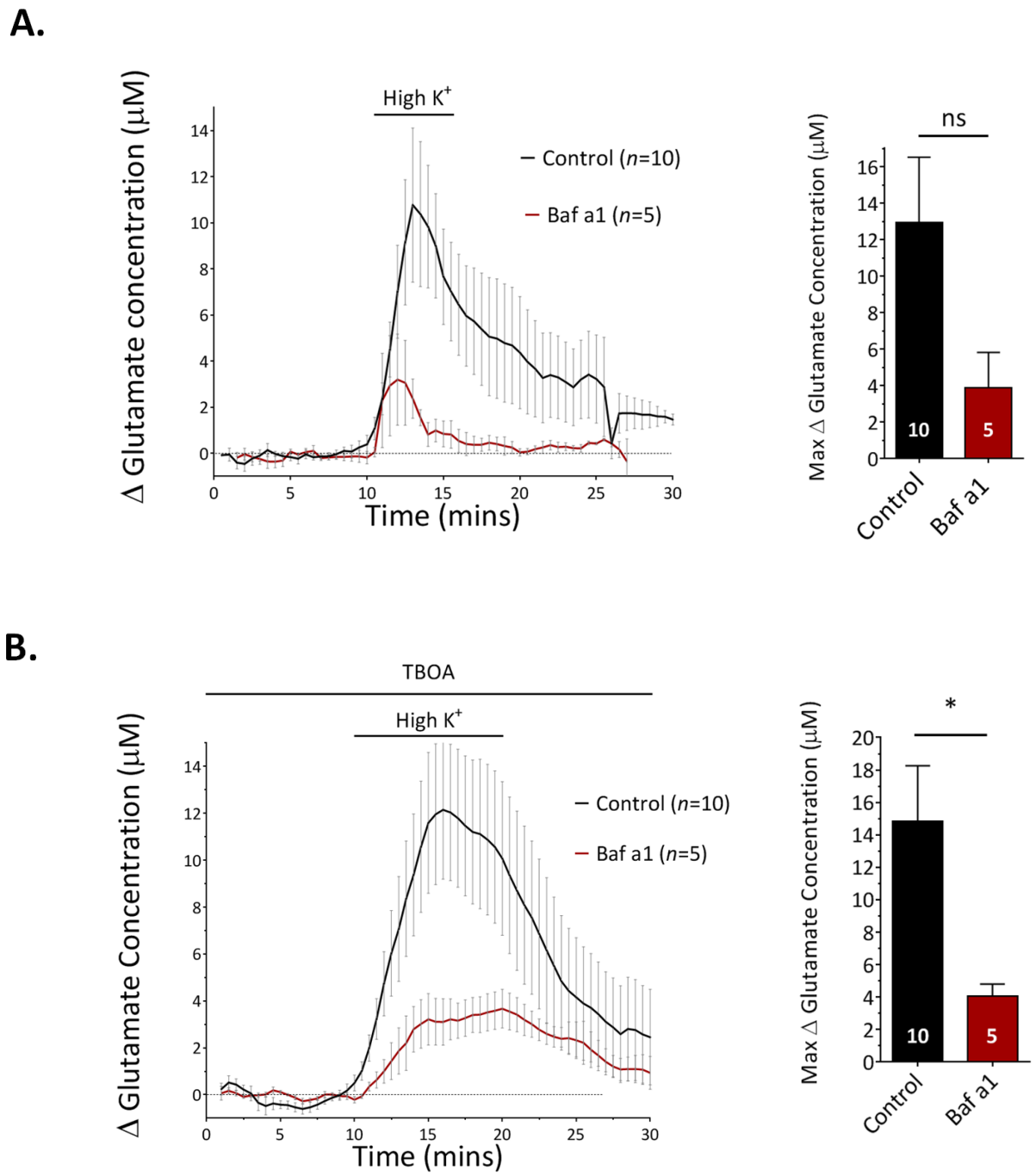

Fig. 3.4: High-K^+ evoked glutamate release is significantly attenuated following vesicular glutamate depletion with bafilomycin-a1.

$[Glut]_e$ time-course during a 5-minute **(a)** and 10-minute **(b)** exposure to high-K^+. Note; the maximum rise in $[Glut]_e$ is dramatically reduced in the presence of bafilomycin-a1 (baf-a1, red, see histogram). ns>0.5, *p<0.5.

3.2.2 High-K^+ evoked vesicular docking in adult white matter

The CC sits adjacent to GM structures with extensive glutamatergic input (Fig. 3.5a1). Considering there are no physical barriers separating the two regions, it is possible that the rise in $[Glut]_e$ recorded in the CC may be a result of synaptic glutamate release in neighbouring GM regions. To address this issue, I directly examined vesicular docking in the adult CC using the vesicular dye, FM4-64. Coronal brain slices, including the CC, were obtained from adult Thy-1/YFP^+ mice and imaged using two-photon confocal microscopy. The mean diameter of all YFP^+ axons is 0.86±0.02µm (Fig. 3.5a,b, *n*=167 axons), which is considerably higher than the mean diameter of unmyelinated axons in the adult mouse CC (0.25±0.01µm, (Sturrock 1980)). Therefore, it is highly likely that all YFP^+ axons in the CC are myelinated.

Using an established high-K^+ loading protocol (see section 2.9.2, (Kukley, Capetillo-Zarate et al. 2007)), low magnification images revealed extensive FM4-64 (vesicular) loading throughout the CC, indicative of vesicular recycling (Fig. 3.6a). Furthermore, FM-loaded YFP^+ axons were clearly identified at higher magnification (Fig. 3.6b,c). It is worth noting that fluorescent longitudinal cylinders, which were not YFP^+ axons, were also evident (Fig. 3.6c see arrows), which may represent FM-loading in unmyelinated axons. Contrary to Micu *et al.* (Micu, Plemel et al. 2016), punctate fluorescence was not observed along the axon cylinder. Considering the average vesicle size is ~50nm in diameter, it was not possible to identify individual vesicles using red light microscopy which has a limit of resolution of approximately 200-350nm (Schermelleh, Heintzmann et al. 2010).

To monitor FM4-64 stability, FM-fluorescence in the whole CC was initially monitored under control conditions (note; fluorescence was measured in random circular regions of interest (ROI) within the CC which will include all cell types, not just YFP^+ axons). FM-fluorescence decreased by 4.50±0.97% (*n*=15 random ROI/5 slices) after 10 minutes (Fig.3.8). Similar to $[Glut]_e$ experiments, FM4-64 fluorescence was also monitored during perfusion with high-K^+. Following 60 seconds of baseline recording in control aCSF, exposure to high-K^+ evoked a pronounced drop in FM-fluorescence which became significant after 60 seconds (p=0.02) (Fig. 3.7 and 3.8). Over a 10-minute period, FM-fluorescence was reduced by 16.34±0.96% (*n*=24 random ROI/8 slices), significantly lower than time-matched controls (p≤0.0001, Fig. 3.8).

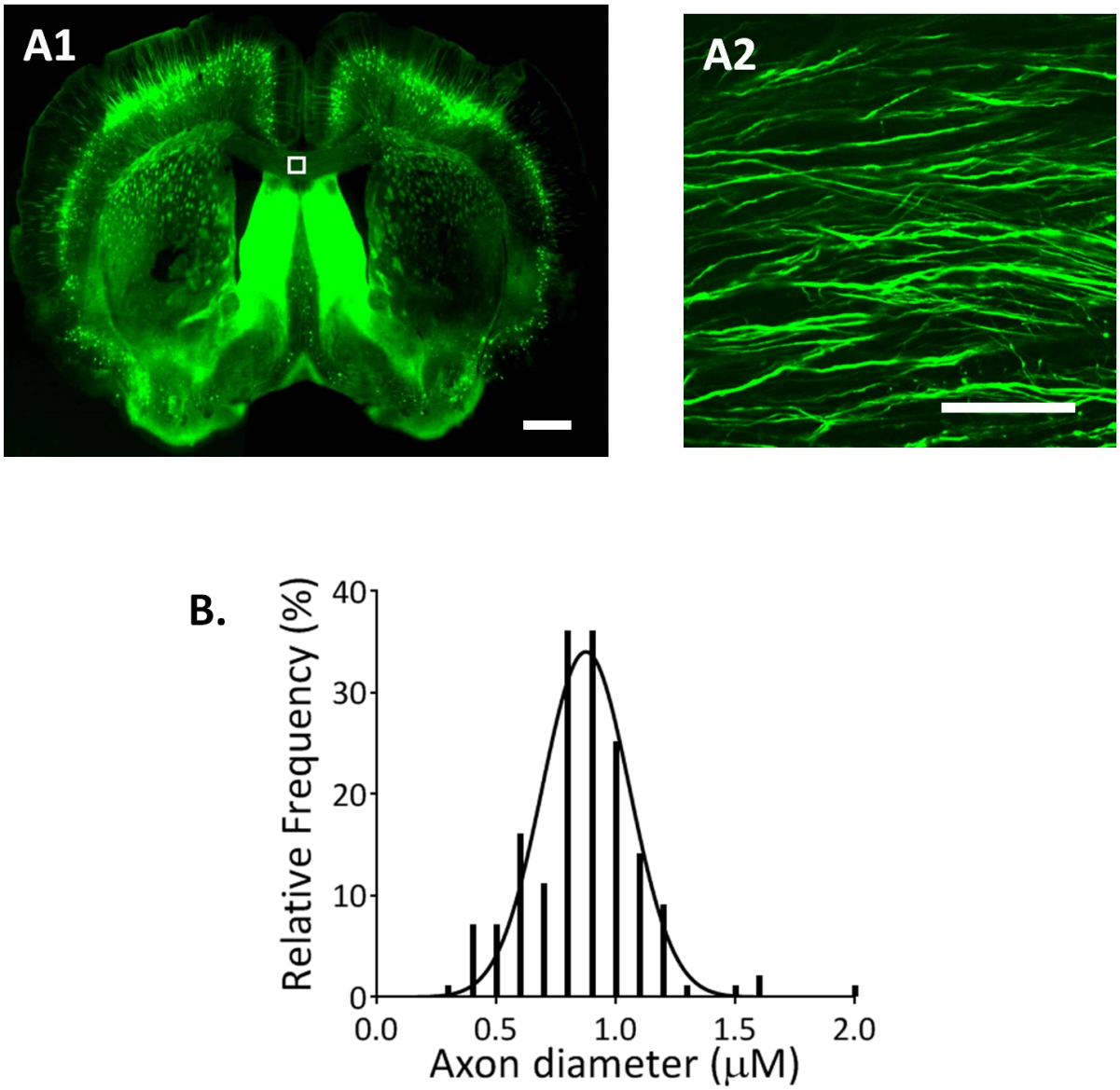

Fig. 3.5: Thy-1/YFP$^+$ axons in the adult mouse CC are large diameter, myelinated axons.

a1) YFP expression (green) in a coronal brain slice of an adult mouse (scale bar=2mm). Insert **(a2)** shows YFP$^+$ axons in the CC (scale bar=40µm). **b)** Frequency distribution curve of YFP$^+$ axons according to axonal diameter (*n*=167 axons from 45 brain slices).

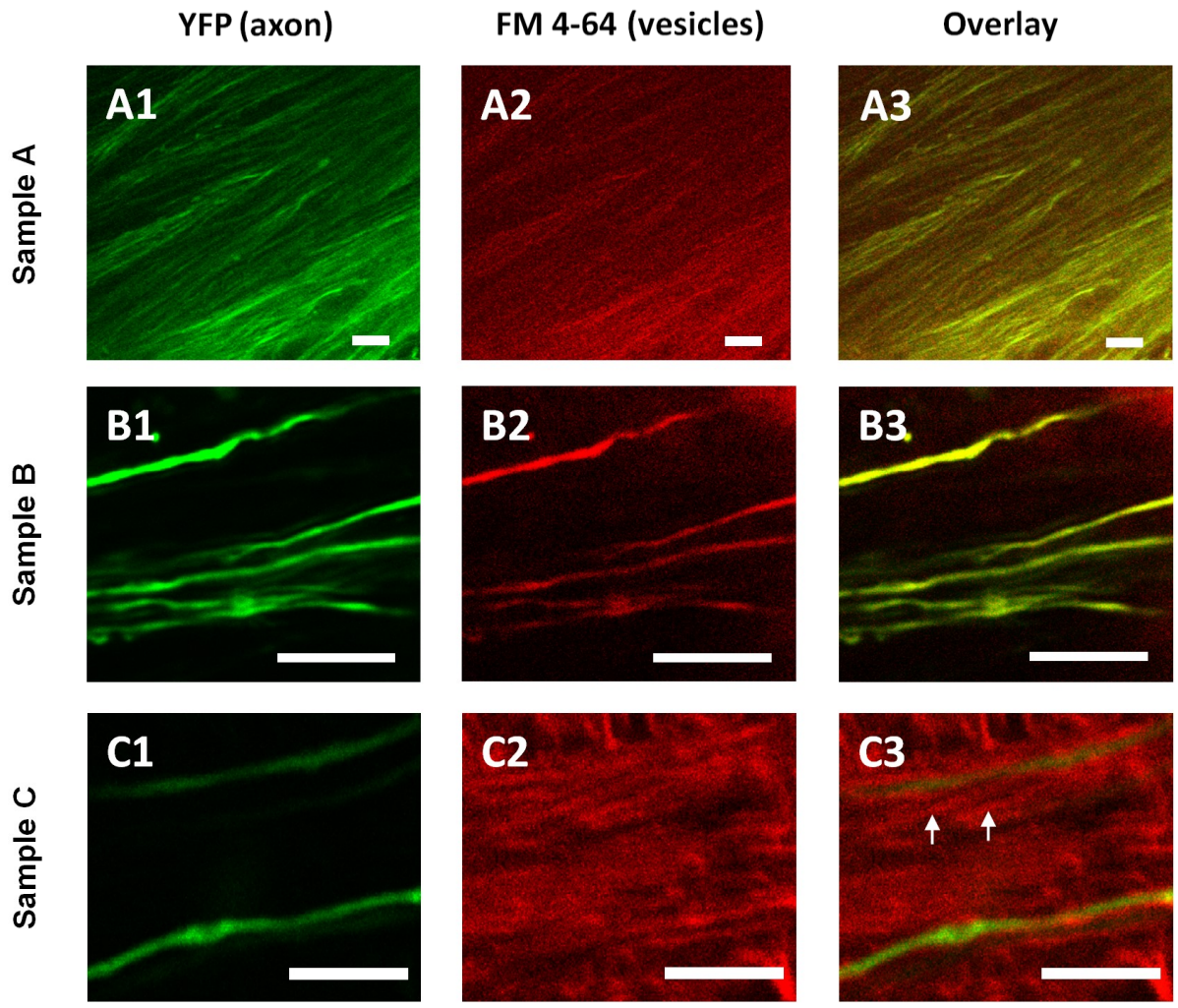

Fig. 3.6: Extensive FM4-64 loading is evident in myelinated axons throughout the adult corpus callosum.

a) Low magnification image of the YFP+ CC, demonstrating widespread loading of the vesicular dye, FM4-64 (red), in adult WM. Individual axons (green) are reliably imaged at higher magnification (sample **b,c**) showing a clear overlay of YFP+ with FM4-64. Note: sample **(c)** shows FM4-64 fluorescent longitudinal cylinders which are not YFP+ axons (C3; arrows), which may represent vesicular loading in YFP-negative axons (unmyelinated). Scale bar=10um.

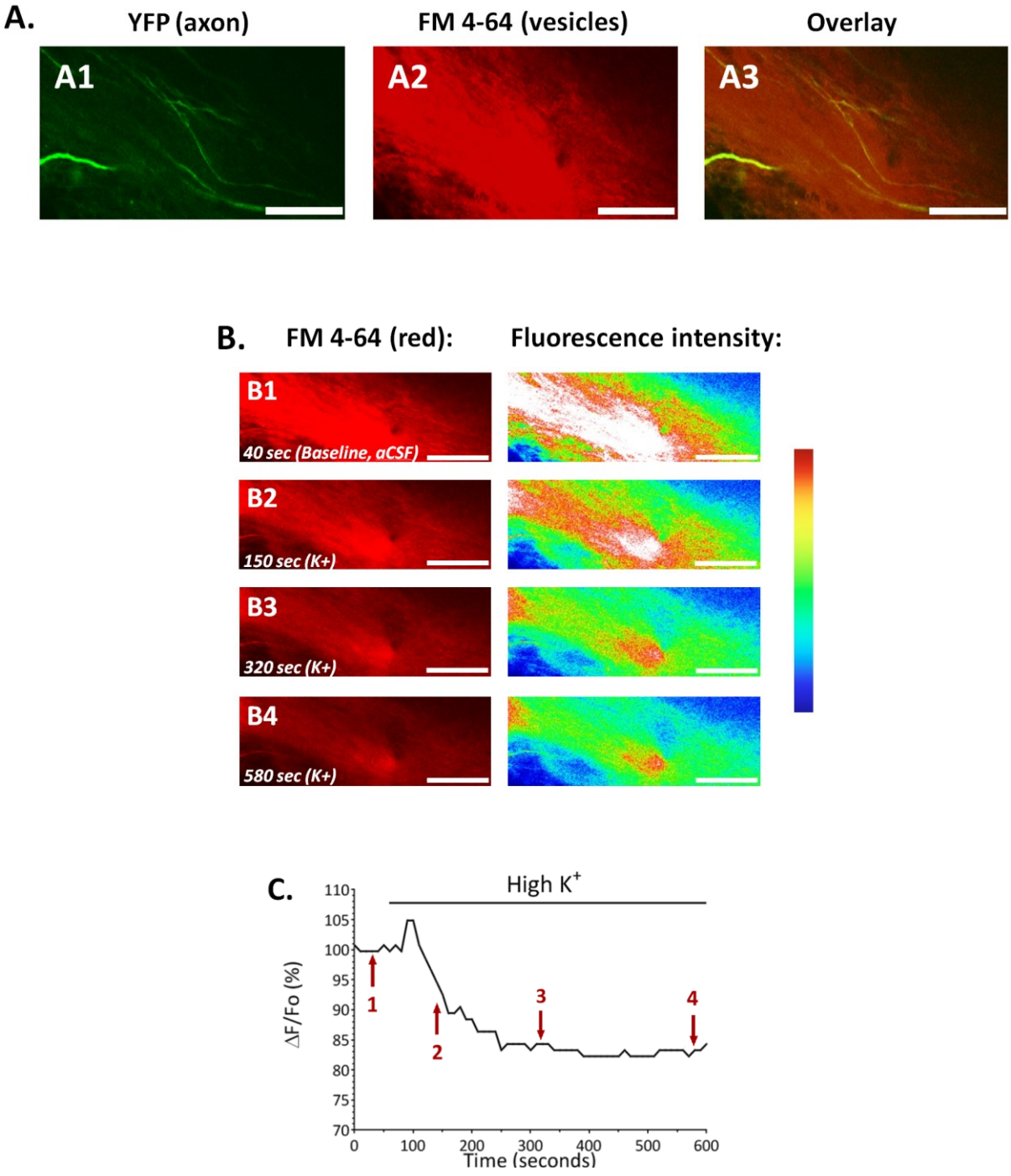

Fig. 3.7: High-K^+ evoked de-staining of FM4-64 from a sample region of the corpus callosum.

a) Widespread FM4-64 loading in a region of the YFP^+ CC. **b)** Representative images of FM4-64 emission captured at different time-points during perfusion with high K^+**.** Note the drop in FM4-64 fluorescence intensity (right). **c)** Time-course of FM4-64 fluorescence recorded from a sample region of the CC. Numbers (1-4) correspond to the representative images above (**b**). Scale bar=40µm.

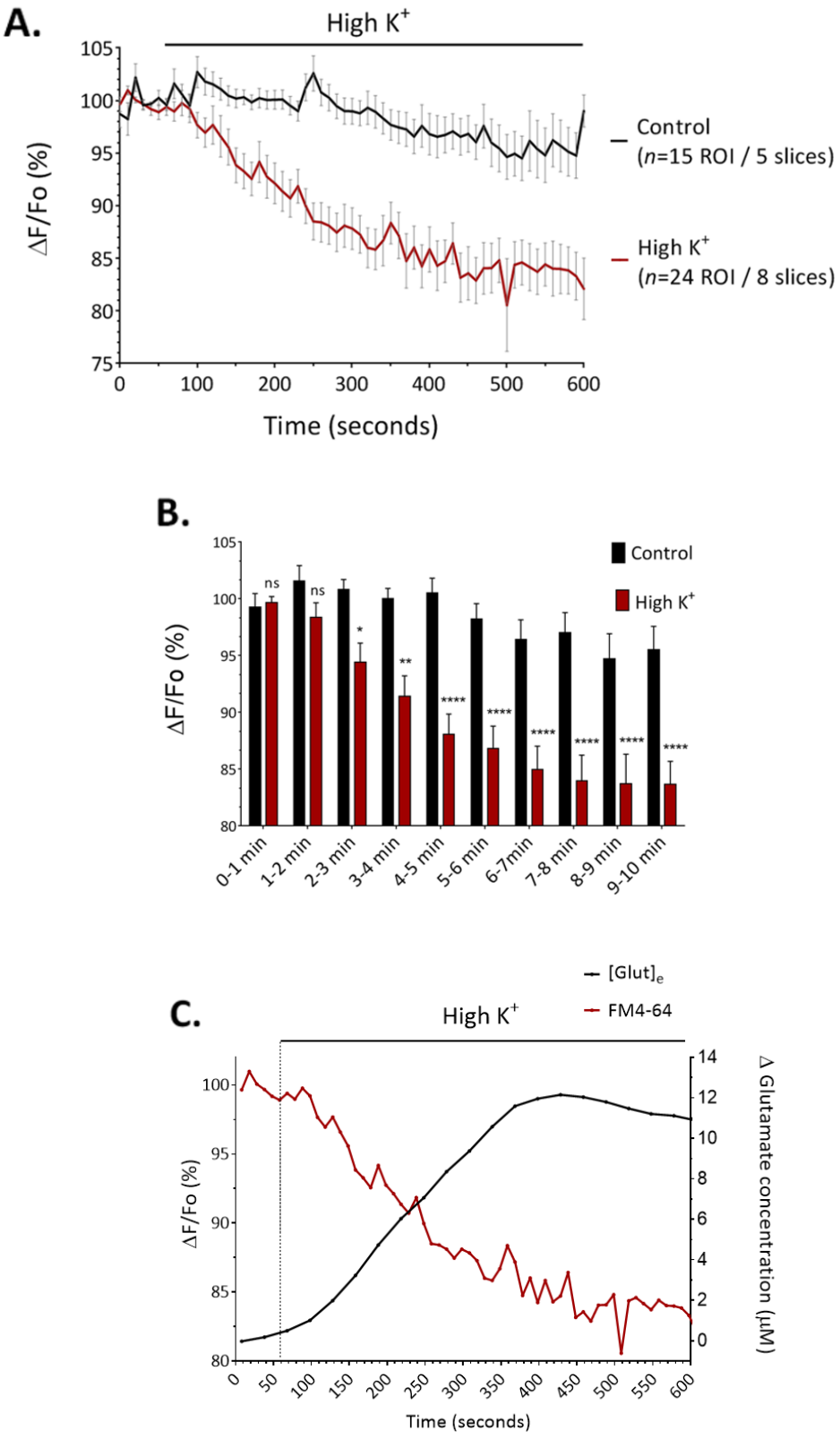

Fig. 3.8: High-K⁺ evoked vesicular docking in the adult corpus callosum.

a, b) Time-course/histogram of the mean (±SEM) fluorescence intensity of FM4-64 in the adult mouse CC. Under control conditions, fluorescence intensity remains relatively stable for 10 minutes (black). Exposure to high-K⁺ leads a significant drop in relative FM4-64 fluorescence (red). **c)** Overlay of FM4-64 fluorescence (red) and extracellular glutamate concentration (black). Note how the drop in FM4-64 fluorescence coincides with the early rise in glutamate concentration. ns>0.5, *p<0.05, **p<0.01, ****p<0.0001.

3.2.4 Vesicular glutamate release in white matter originates from axons

As previously demonstrated high-K^+ produced widespread axonal depolarisation, sufficient in blocking AP conduction (Fig. 3.2). However, high-K^+ will also depolarise all cells within WM, including astrocytes (Meeks and Mennerick 2007, Yaguchi and Nishizaki 2010). In an attempt to determine the source of K^+-evoked vesicular release, FM-fluorescence was monitored in axons and fibrous astrocytes.

Using Thy-1/YFP^+ mice, FM-fluorescence was initially examined in individual myelinated axon segments. FM-loaded YFP^+ axons were reliably imaged and displayed a relatively high level of FM-fluorescence (see Fig. 3.9a). Fluorescence intensity in axons remained stable under control conditions, exhibiting a 3.43±1.64% decrease after 10 minutes (Fig. 3.9/3.11, *n*=17 axons/5 slices). On the other hand, high-K^+ evoked a significant drop in FM-fluorescence, decreasing by 14.00±1.29% after 10 minutes (Fig. 3.10/3.11, *n*=22 axons/8 slices p=0.01). Similar to the whole CC, significance was reached within the initial 60 seconds of high-K^+ ($p \leq 0.05$, Fig. 3.11). The overt drop in axonal FM-fluorescence closely resembles the decrease recorded from the whole CC. Furthermore, there was no evidence of localised de-staining along the axon cylinder.

To access vesicular docking in WM astrocytes, experiments were repeated using GFAP-GFP+ mice. In contrast to axons, GFP^+ astrocytes displayed a much lower level of FM4-64 staining (Fig. 3.12a-f). Interestingly, numerous FM-loaded axon cylinders were clearly detected in close proximity to astrocytes, which expressed a significantly higher level of FM-fluorescence (Fig. 3.12f, n= 19, $p<0.0001$). Furthermore, there was no significant drop in astrocyte FM-fluorescence during exposure to high-K^+ (-6.40±0.80%, *n*=22 astrocytes/9 slices) when compared to time-matched controls (-5.03±0.64%, *n*=12 astrocytes/6 slices, Fig. 3.13/3.14, p=0.59)

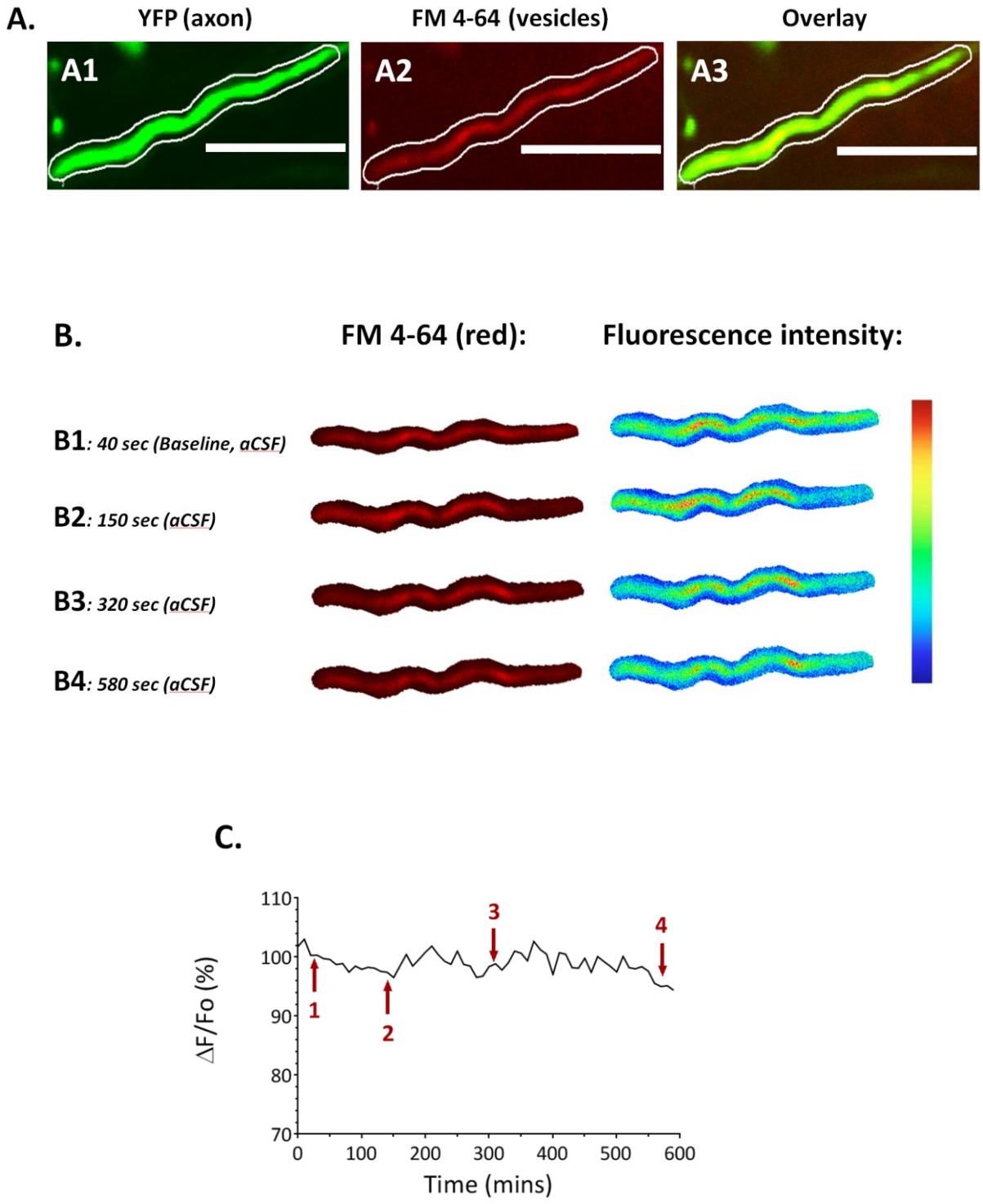

Fig. 3.9: Axonal FM4-64 fluorescence remains stable under control conditions.

a) Sample image of FM4-64 loading in an individual axon segment in the CC. **b)** Representative images captured at different time-points under control conditions**. c)** Time-course of axonal FM4-64 fluorescence under control conditions. Numbers (1-4) correspond to representative images above (B). Scale bar=10µm.

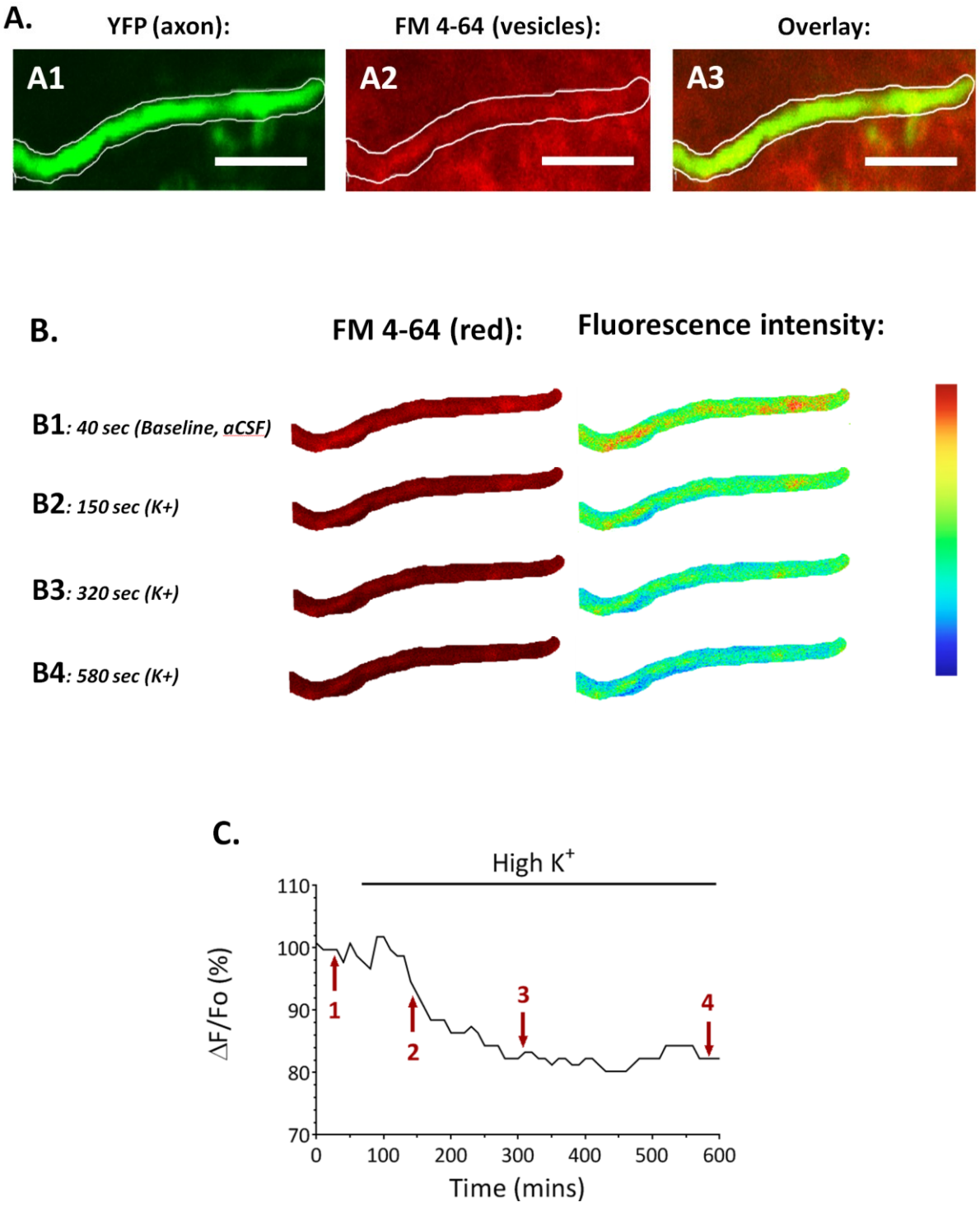

Fig. 3.10: High-K^+ evoked de-staining of FM4-64 in a sample axon segment.

a) Sample image of a FM4-64 loading in an individual axon segment in the CC. **b)** Representative images captured at different time-points during perfusion with high-K^+**. c)** Time-course of axonal FM4-64 fluorescence during high-K^+. Numbers (1-4) correspond to representative images above (b). Scale bar=10µm.

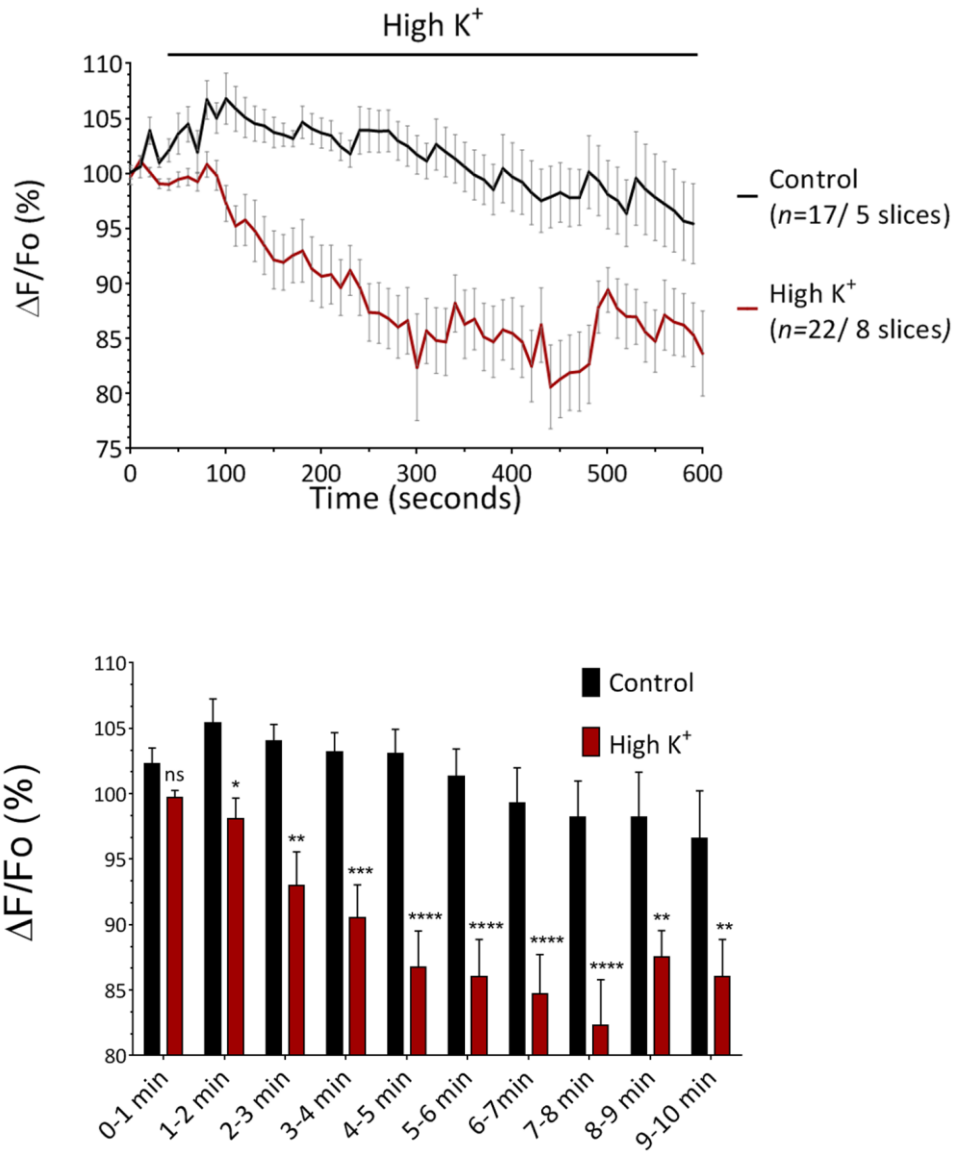

Fig. 3.11: High-K⁺ evoked vesicular docking in individual axons.

Time-course/histogram of the mean (±SEM) fluorescence intensity of FM4-64 in individual axon segments. Under control conditions, fluorescence intensity remains relatively stable for 10 minutes (black). Exposure to high K⁺ leads a significant drop in axonal FM4-64 fluorescence (red). ns>0.5, *p<0.05, **p<0.01, ****p<0.0001.

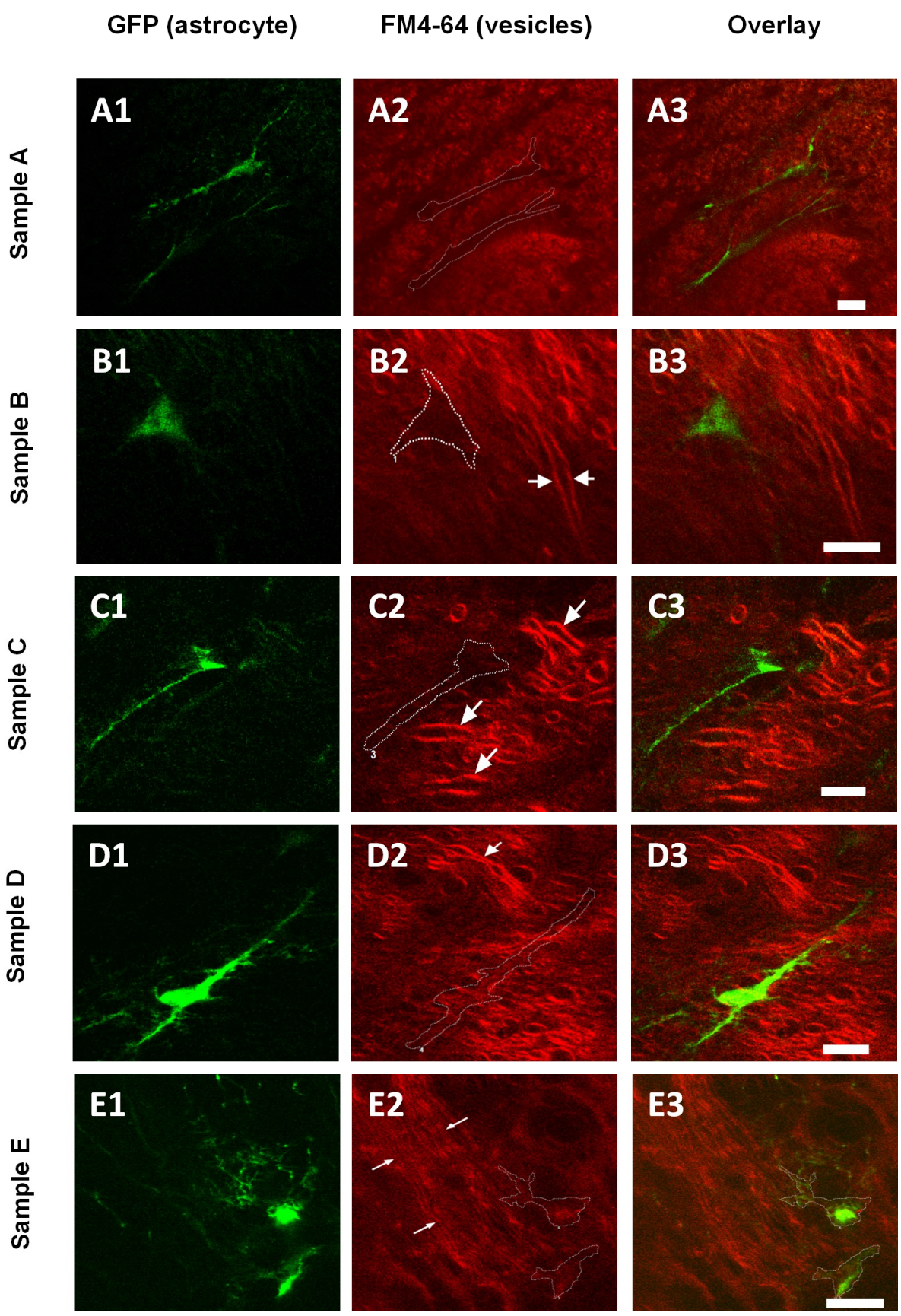
GFP (astrocyte)
FM4-64 (vesicles)
Overlay
Sample A
Sample B
Sample C
Sample D
Sample E
A1
A2
A3
B1
B2
B3
C1
C2
C3
D1
D2
D3
E1
E2
E3

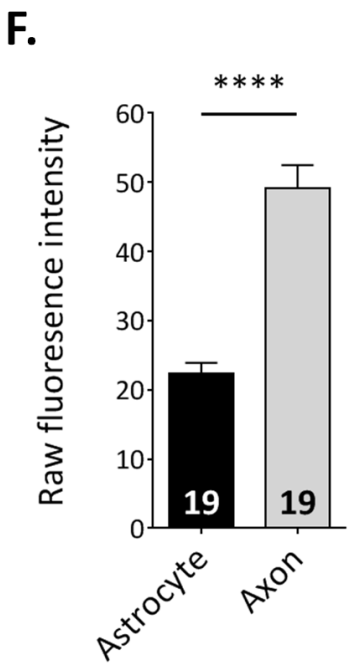

Fig. 3.12: GFP+ astrocytes display almost no FM4-64 staining.

a-e: Sample images of individual GFP+ astrocytes in the adult mouse CC. Note the low levels of astrocytic FM4-64 staining (astrocyte outline= dotted white line). Also, note the high levels of FM4-64 staining in several cylinder compartments nearby the astrocytes (arrow). This likely represents FM4-64 loaded axons. Scale bar=10µm. **f:** Raw FM4-64 fluorescence measured from astrocytes and from neighbouring axons (same area size recorded from each). ****p<0.0001.

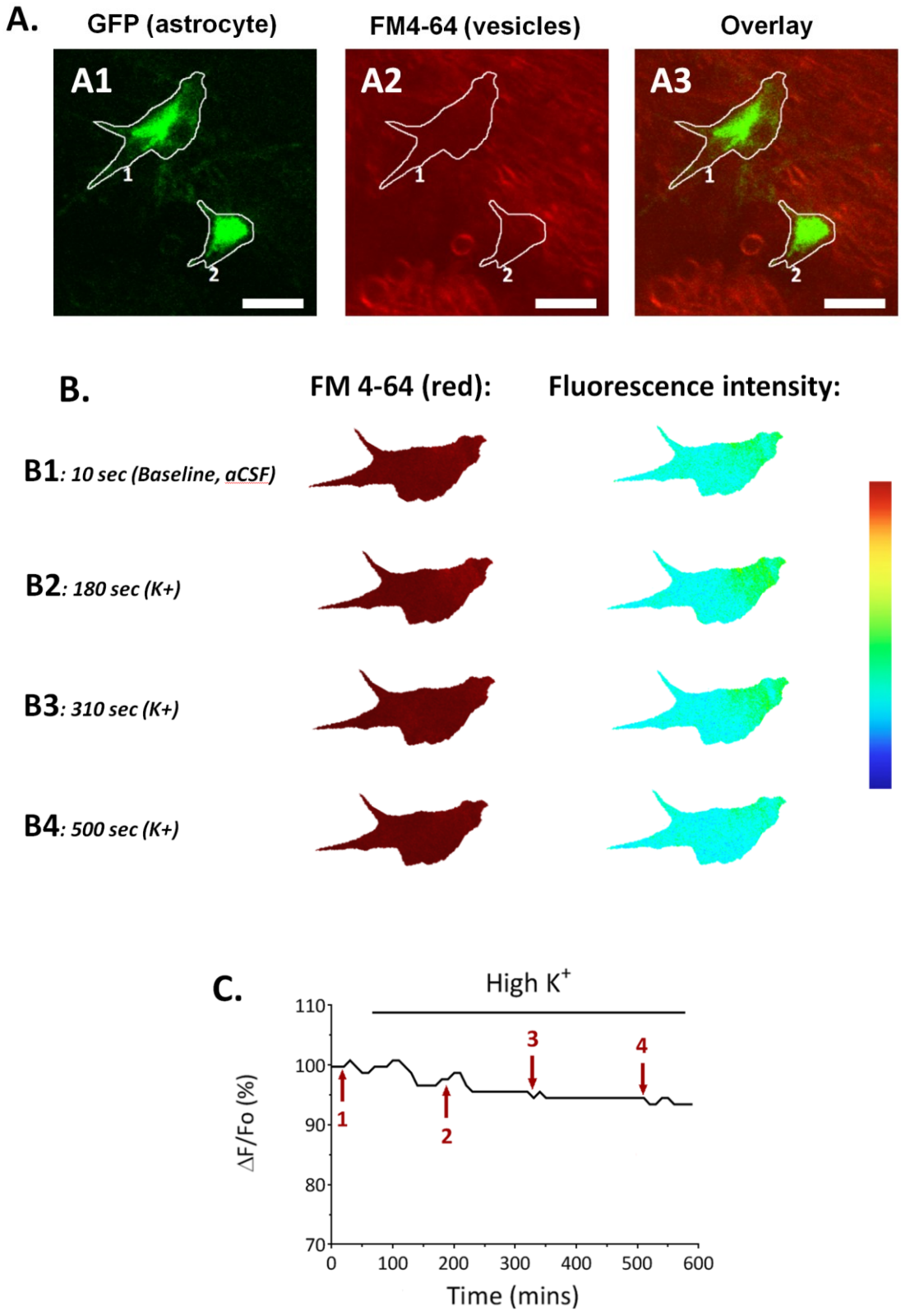

Fig. 3.13: FM4-64 fluorescence from a sample astrocyte remains stable during exposure to high-K^+.

a) Sample image of FM4-64 loading in two neighbouring astrocytes (1 and 2). **b)** Representative images captured from astrocyte (1) at different time-points during perfusion with high K^+**. c)** Time-course of astrocytic FM4-64 fluorescence during high K^+. Numbers (1-4) correspond to representative images above (B). Scale bar=10µm.

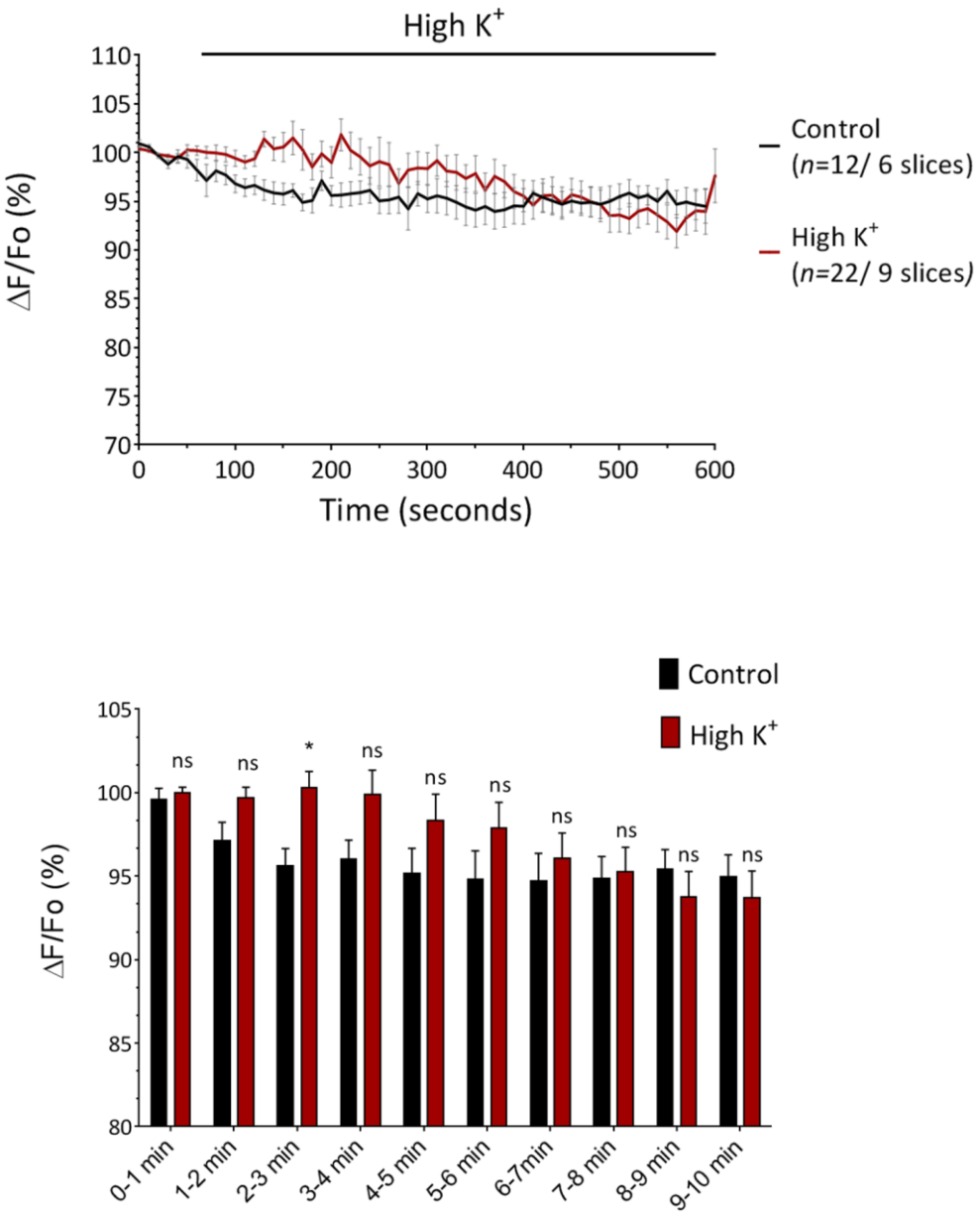

Fig. 3.14: High-K^+ does not evoke vesicular docking in white matter astrocytes.

Time-course/histogram of the mean (±SEM) fluorescence intensity of FM4-64 in individual WM astrocytes. Under control conditions, fluorescence intensity remains relatively stable for 10 minutes (black). Exposure to high-K^+ does not decrease FM4-64 fluorescence (red). ns>0.5, *p<0.05.

3.2.5: Attempts to evoke vesicular glutamate release in the juvenile RON

Considering high-K^+ evoked vesicular fusion originates from axons in the adult CC, I next attempted to evoke vesicular glutamate release from axons in an alternative WM tract, the juvenile rat optic nerve (RON). While the adult mouse CC contains a large population of unmyelinated axons, the adult RON is fully myelinated. As we have shown, vesicular fusion in myelinated axons will presumably release glutamate directly into the peri-axonal space between the axon and overlaying myelin sheath. This will limit, or completely prevent, any change in $[Glut]_e$. However, there are no such barriers in unmyelinated axons, where vesicular glutamate will empty directly into the extracellular space. For this reason, $[Glut]_e$ was recorded from the juvenile RON (P7-P17), which is predominantly unmyelinated at this age. Similar to the adult CC, high-K^+ evoked a significant rise in $[Glut]_e$ in the developing RON. However, the maximum peak concentration was much lower in the RON, increasing by 0.51±0.24µM (Fig. 3.15a,b, n=3, $p<0.05$). After a rest period of 30 minutes, a subsequent second stimulation with high-K^+, evoked a smaller rise in $[Glut]_e$ (see Fig. 3.15c). Experiments were performed in the presence of TBOA to prevent re-uptake and/or reverse transport.

To investigate whether action potential conduction evokes vesicular glutamate release, $[Glut]_e$ was recorded from inside the RON following electrical stimulation. To do this, each end of the nerve was inserted into the barrel of a stimulating and recording glass electrode. Following which, a single slit was made on the upper surface of the nerve. Both GLU and null sensing tips were inserted and directed towards the stimulating electrode (see Fig. 3.16a). However, this procedure was technically challenging and required delicate handling. CAPs were successfully recorded following sensor insertion, confirming that axons were still functional following the physical trauma of sensor insertion. Nerves were subject to a train of action potentials (50Hz x 1-60 seconds) and CAP amplitude was recorded every second. High-frequency electrical stimulation resulted in a reversible drop in CAP amplitude to 52.15% after 60 seconds, reflecting a partial failure in action potential conduction. Following which, CAP amplitude quickly recovered within 2 minutes (Fig. 3.16b). For this reason, all electrical stimulations (tests) were kept well under 60 seconds. Electrical stimulation evoked a change in the differential biosensor current recorded inside the nerve, indicating a rise in extracellular

glutamate. However, identical recordings were observed when the sensors were placed in the bath perfusate at a similar distance from the stimulating electrode (i.e. the RON was absent) (Fig. 3.16c). Attempts were made to re-position the sensors to eliminate this recorded artefact, but to no avail. Unfortunately, there was no additive current recorded from inside the ON.

To investigate whether increasing axonal $[Na^+]_i$ is capable of eliciting a rise in $[Glut]_e$, juvenile RONs were exposed to veratridine (10µM), an alkaloid neurotoxin which prevents voltage-gated Na^+ channel inactivation. Exposure to veratridine, gradually blocked nerve excitability after 21.83±2.49 mins (Fig. 3.17a, *n*=3). CAP amplitude failed to recover following wash-out. In order to prevent reverse glutamate transport following Na^+ influx, $[Glut]_e$ recordings were performed in the presence of TBOA (200µM). Perfusion with veratridine evoked a small rise in $[Glut]_e$ (Fig. 3.16b,c, +0.26±0.17µM, *n*=5). However, this was not significantly different to time-matched controls which decreased by 0.17±0.10µM (Fig. 3.17b,c, *n*=4, p=0.08).

Finally, in an attempt to evoke vesicular glutamate release from astrocytes, nerves were perfused with prostaglandin E2 (PGE2, 100µM), which is known to evoke Ca^{2+}-dependant glutamate release in cultured astrocytes (Bezzi, Carmignoto et al. 1998). Again, experiments were performed in the presence of TBOA. However, perfusion with PGE2 led to no significant change in $[Glut]_e$, with concentrations decreasing by 0.0004±0.06µM after 20-30 minutes (Fig. 3.18, *n*=3, p=0.25). Further techniques to evoke vesicular release in the neonatal RON were not attempted.

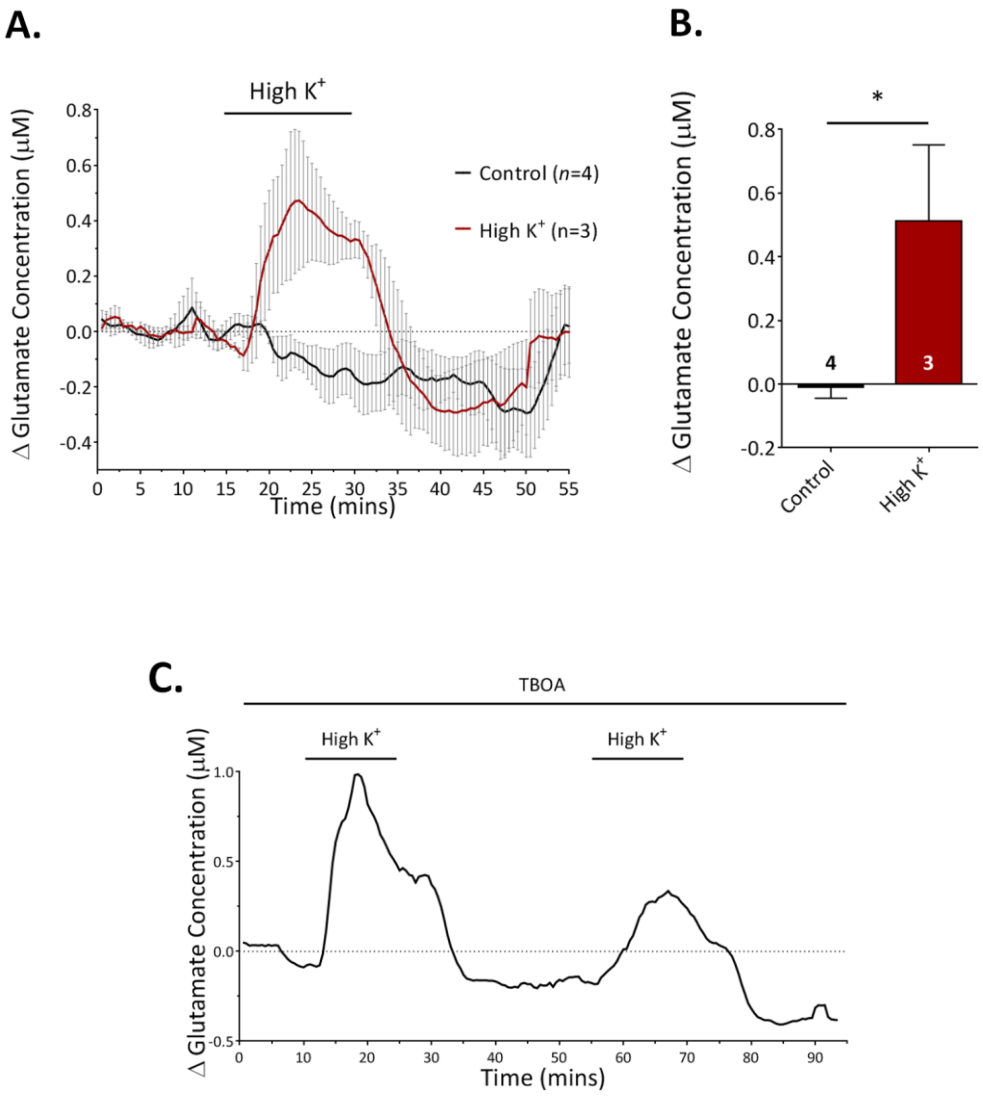

Fig. 3.15: High-K^+ evokes a small rise in extracellular glutamate in the developing RON.

a) Time-course of $[Glut]_e$ recorded in the pre-myelinated RON during exposure to high-K^+ (red) and under control conditions (black). **b)** Histogram comparing the maximum glutamate concentration reached during high-K^+ and under control conditions. Perfusion with high-K^+ significantly increased $[Glut]_e$. $p<0.05$. **c)** Sample time-course of $[Glut]_e$ recorded including two sequential exposures to high-K^+. Note the reduced rise in glutamate during the second stimulation which may reflect vesicular depletion.

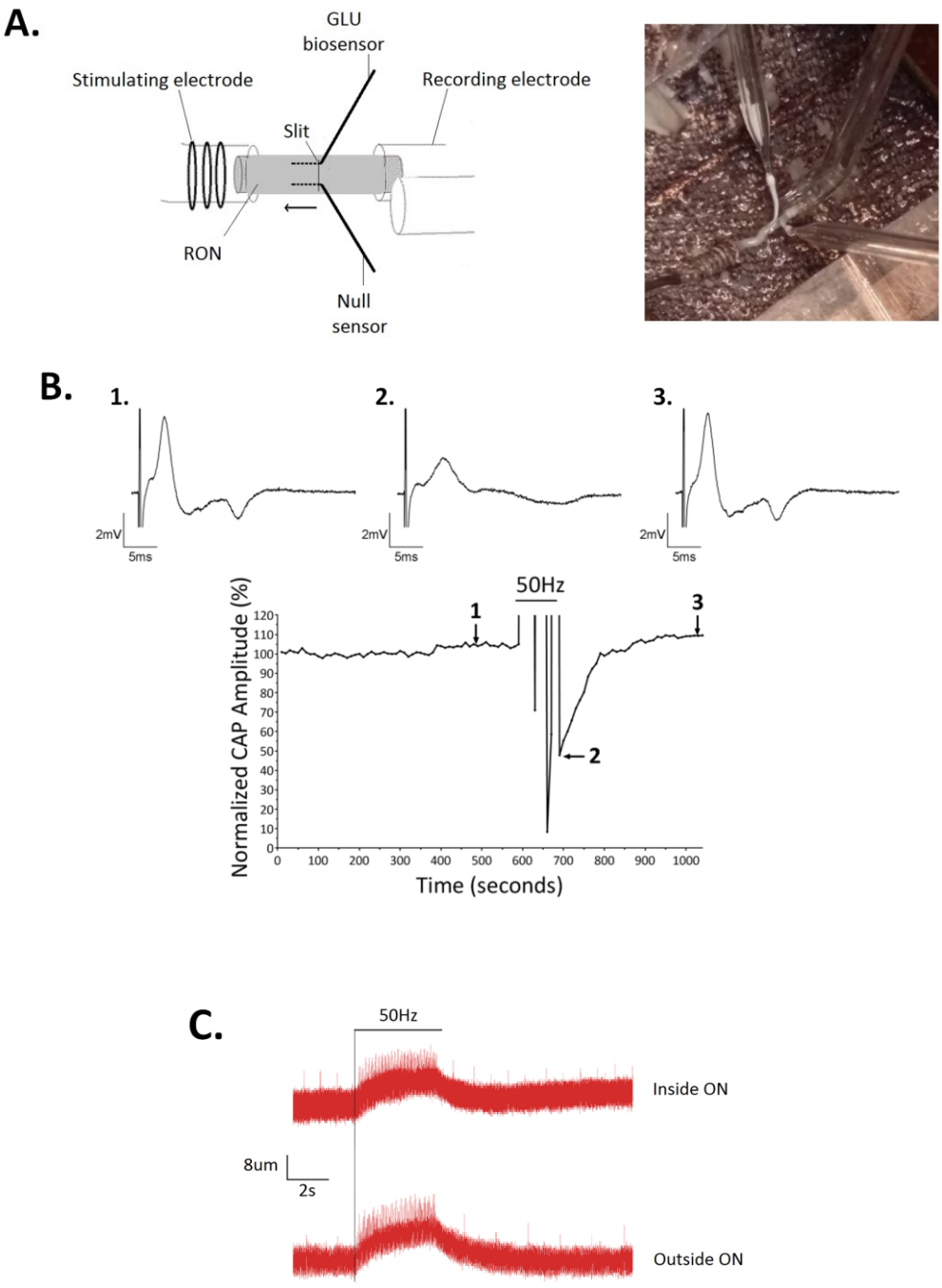

Fig. 3.16: A stimulus artefact prevented reliable recordings of activity-dependent glutamate release in the RON.

a) Positioning of bio-sensors in the RON during electrical stimulation. Note the direction of the sensor tips moving away from the site of insertion, towards to stimulating electrode. **b)** Time-course of CAP amplitude recorded from a P16 RON, including a 60second 50Hz electrical stimulation. Shown above are representative CAP traces recorded before (**1**), immediately after (**2**) and several minutes after (**3**) stimulation. **c)** Biosensor current recordings from inside the RON and in the bath perfusate (outside RON) during a brief 50Hz stimulation. Note the rise in biosensor current recorded when sensors are outside the nerve i.e. an electrical artefact.

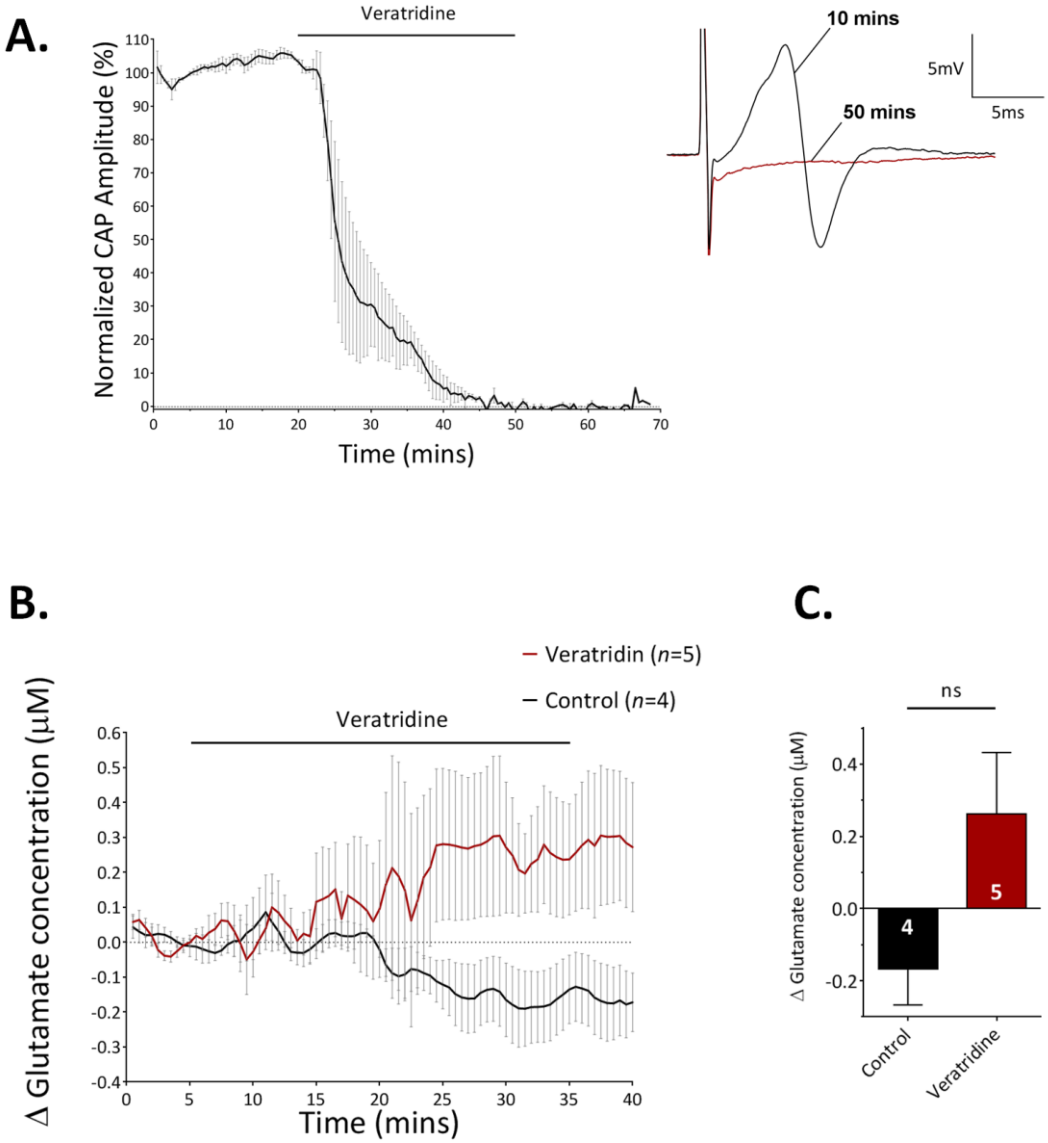

Fig. 3.17: Sodium-channel inactivation blocker, veratridine, blocks CAP conduction but does not significantly elevate $[Glut]_e$ in the neonatal RON.

a) Time-course of CAP amplitude during exposure to 10μM veratridine. Insert: Representative CAP image before (10mins) and after (50mins) veratridine. **b)** $[Glut]_e$ recordings during exposure to veratridine (red) and in control aCSF (black). **c)** Histogram comparing the mean glutamate concentration during the last 10 minutes of veratridine (from 25-35 mins) against the same period in control aCSF. ns $p>0.5$.

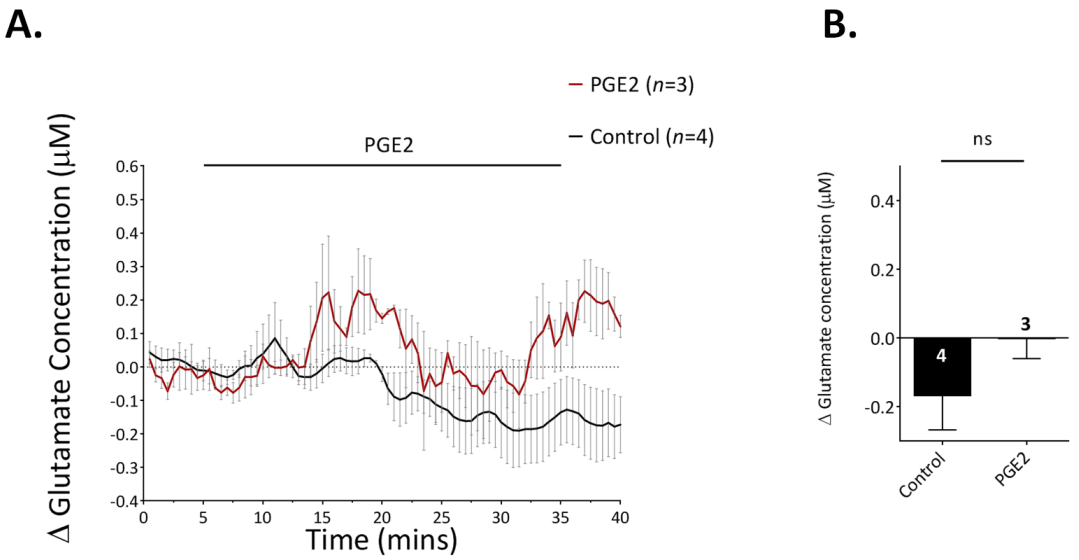

Fig. 3.18: Prostaglandin E2 does not evoke glutamate release in the neonatal RON.

a) $[Glut]_e$ recordings during exposure to PGE2 and in control aCSF. **b)** Histogram comparing mean glutamate concentration during the last 10 minutes of PGE2 (from 25-35 mins) against the same period in control aCSF. ns $p>0.5$.

3.3: Discussion

3.3.1: Synopsis

Neurotransmitter signalling is a highly-specialised method of intercellular communication within the CNS. For years, it was considered a neuronal-specific phenomenon, exclusive to conventional synapses in GM. However, recent reports have revealed that glutamatergic signalling is also an essential feature of axo-glial communication in WM. In this chapter, I have examined vesicular glutamate release in the adult mouse corpus callosum. The data demonstrates that axonal depolarisation (with high-K^+) evokes a substantial rise in extracellular glutamate concentrations. Furthermore, glutamate release was not via the reversal of glutamate transporters, but rather via vesicular exocytosis. Vesicular imaging revealed that axons are the primary source of vesicular docking in white matter. Interestingly, vesicular fusion occurs along the internodal axolemma of myelinated axons. In contrast, I found no evidence to suggest that astrocytes contribute to vesicular glutamate release during elevated levels of K^+. Together, this data provides the first direct comparison of vesicular fusion in different cellular elements in white matter and supports the existence of functional axo-myelinic synapses.

3.3.2: Depolarisation-evoked vesicular release in WM elevates extracellular glutamate concentrations

In recent years, several studies have demonstrated the existence of functional WM synapses. Many of these studies recorded post-synaptic responses, such as EPSCs in OPCs or changes in myelinic [Ca^{2+}] (Kukley, Capetillo-Zarate et al. 2007, Ziskin, Nishiyama et al. 2007, Micu, Plemel et al. 2016). However, the change in extracellular glutamate concentrations following vesicular fusion has never been directly measured. The absence of confined synaptic boutons in WM suggests that vesicular glutamate release along the axon cylinder may lead to diffuse rises in $[Glut]_e$.

As reviewed in Chapter 1, the efflux of K^+ ions hyperpolarises the axonal membrane potential during AP conduction. Thus, the accumulation of $[K^+]_e$ is closely associated with axonal activity (Connors, Ransom et al. 1982, Ransom, Ransom et al. 2000). Furthermore, anoxia/ischemia causes a rapid rise in $[K^+]_e$ levels, capable of reaching 50-60mM in the ischemic core (Hansen 1985, Ransom, Walz et al. 1992, Belhage, Hansen et al. 1993, Gido, Kristian et al. 1997). Exposure to high extracellular K^+ is an established technique used to depolarise membrane potentials and promote vesicular fusion (Gaffield and Betz 2006, Kukley, Capetillo-Zarate et al. 2007, Yaguchi and Nishizaki 2010). The data presented demonstrates that exposing adult WM tracts to high-K^+ leads to rapid axonal depolarisation, capable of blocking nerve excitability. Furthermore, elevating $[K^+]_e$ for up to 10 minutes does not produce any irreversible functional injury. Using real-time glutamate biosensors, a sharp rise in corpus callosum $[Glut]_e$ was observed during high-K^+. Interestingly, the rapid rise in glutamate was followed by an immediate drop, with glutamate levels quickly returning towards resting concentrations. This demonstrates that axonal depolarisation is capable of evoking endogenous glutamate release from WM cells. In addition, the characteristic profile of K^+-evoked glutamate release suggests that axonal depolarisation evokes a burst of neurotransmitter release followed by the depletion of glutamate stores and/or the upregulation of glutamate uptake. However, a similar release profile was observed in the presence of TBOA, a glutamate transport inhibitor, which argues against the latter. Thus, the data suggests that WM glutamate stores are quickly depleted following strong axonal depolarisation.

During ischemia, the run-down of Na^+ and K^+ gradients, combined with a depolarising shift in membrane potential, favours the reverse operation of glutamate transporters (Rossi, Oshima et al. 2000, Grewer, Gameiro et al. 2008). Therefore, reverse EAATs pose as a potential mechanism of glutamate release during exposure to high-K^+. In fact, the application of high-K^+ was traditionally used in the study of reverse EAATs (Szatkowski, Barbour et al. 1990, Zerangue and Kavanaugh 1996). However, the depolarisation-evoked rise in $[Glut]_e$ was insensitive to EAAT inhibition, demonstrating that that the counter transport of glutamate does not contribute to release. In contrast, release was strongly reduced via the inhibition of vesicular loading with V-ATPase inhibitor, bafilomycin-a1. This indicates that high $[K^+]_e$ triggers extensive vesicular fusion in WM, leading to a diffuse rise in extracellular glutamate

concentrations. In agreement with previous findings, it also demonstrates that glutamate-rich vesicles are present in mature WM and supports the existence of WM synapses in the mature brain (Ziskin, Nishiyama et al. 2007, Micu, Plemel et al. 2016). The residual rise in $[Glut]_e$ in the presence of bafilomycin-a1 may reflect an incomplete depletion of vesicular glutamate stores with bafilomycin-a1. Alternatively, swelling-mediated release may contribute under such conditions (Su, Kintner et al. 2002).

High-K^+ evoked a significant rise in $[Glut]_e$ in the early myelinating RON, indicating that developing pre-myelinated WM also contains glutamatergic vesicles. Curiously, the rise in $[Glut]_e$ was much lower in immature WM, when compared to adult WM (0.51 v 12.95µM, respectively). This may reflect an expanded extracellular space in the developing RON (Huria, Beeraka et al. 2015). In addition, it is also possible that developing WM contains a smaller pool of ready-releasable glutamatergic vesicles. This may also explain the lack of significant glutamate release during Na^+-channel inactivation (veratridine).

3.3.3: Axons are the principle site of vesicular fusion in WM.

These findings raise further questions. **(i)** Does the depolarisation-evoked rise in $[Glut]_e$ actually originate from WM vesicles, or is it a consequence of spill-over from neighbouring GM synapses? The corpus callous is surrounded by neighbouring GM structures with extensive glutamatergic synapses. Moreover, there are no physical barriers between the GM-WM boarder. Thus, it is possible that excessive vesicular fusion at GM synapses diffuses into neighbouring structures, including the corpus callosum. **(ii)** Does vesicular fusion occur in myelinated axons? And if so, does it occur in localised regions, such as the node of Ranvier, or can it occur along the internodal axolemma? Unlike the rodent optic nerve, the adult mouse corpus callosum contains a mixed population of both myelinated and unmyelinated axons, with a respective ratio of 1:2 (Sturrock 1980). A rise in $[Glut]_e$ may reflect vesicular release from exposed regions of the axolemma, be that from unmyelinated axons and/or at node of Ranvier. However, measuring extracellular glutamate may not detect glutamate release into the confined periaxonal space. **(iii)** Finally, which cell type is primarily responsible for vesicular release in WM? As outlined in section 3.1.2.1, numerous studies have shown that

axons are the primary source of vesicular glutamate release in WM (Kukley, Capetillo-Zarate et al. 2007, Ziskin, Nishiyama et al. 2007, Alix, Dolphin et al. 2008, Micu, Plemel et al. 2016). However, astrocytes also contain the necessary machinery required for exocytotic release (Bezzi, Gundersen et al. 2004, Montana, Malarkey et al. 2006). In addition, activity-dependant $[K^+]_e$ accumulation also promotes astrocyte depolarisation (Ransom and Goldring 1973, Meeks and Mennerick 2007). A recent study demonstrated that high $[K^+]_e$-evoked depolarisation of cultured astrocytes causes a rise in astrocytic Ca^{2+} levels, which subsequently triggers vesicular glutamate release (Yaguchi and Nishizaki 2010). Therefore, it is possible that vesicular glutamate originates from both astrocytes and axons during exposure to high-K^+. To date, there has been no direct comparison of vesicular fusion within different cellular components in WM.

Two-photon confocal imaging of FM4-64 (vesicular dye) emission, revealed extensive FM4-64 loading throughout the whole corpus callosum. High-K^+ evoked a robust drop in FM-fluorescence, consistent the release of the vesicular probe into the aqueous bath solution. This demonstrates the extent of vesicular fusion and recycling throughout the adult corpus callosum. With this in mind, it is likely that a significant component, if not all, of the K^+-evoked rise in $[Glut]_e$ originates from WM cells.

Experiments using Thy-1/YFP+ mice allowed for the examination of vesicular docking in myelinated axons. Consistent with previous studies (Alix, Zammit et al. 2012), YFP+ axons in the mouse corpus callosum have a diameter range which is considerably higher than the upper limit for unmyelinated axons (Sturrock 1980). Therefore, all YFP+ axons used in this model are myelinated. Similar to the whole CC, high magnification images of YFP+ axons revealed extensive FM4-64 loading along the axon cylinder, indicative of active vesicular recycling in axons. Furthermore, axonal depolarisation produced rapid vesicular docking in myelinated axons. Interestingly, the rate of vesicular fusion/FM-unloading was highest during the initial minutes of high-K^+; FM-emission decreased at a rate of 3.4% per minute during the initial 3:50 minutes, whereas, it decreased at a rate of 0.55% per minute during the final 5:10 minutes. This is remarkably consistent with the rapid peak rise in $[Glut]_e$ recorded in the adult rat CC (3:50±0:28 minutes). Together, it demonstrates that depolarisation evokes an early burst in vesicular release from axons.

A recent study reported the expression of punctate FM4-64 fluorescence inside YFP+ axons following electrical stimulation (Micu, Plemel et al. 2016). However, I found no evidence of localised staining or de-staining along the axon cylinder. Therefore, the majority of vesicular docking must occur along internodal regions of the axolemma. This would suggest that the majority of vesicular neurotransmitter release is emptied directly into the periaxonal space between the overlaying myelin sheath and the axolemma. While I am unable to directly measure glutamate concentrations in the periaxonal space, one might hypothesise that due to its confined area, glutamate concentrations may reach levels much higher than those recorded in the extracellular space. Previous calculations estimate that if the average glutamatergic vesicle is 50nm in diameter, and contains approximately 100mM glutamate, the release of a single vesicle into the periaxonal space (approximate volume of 3.7μm^3) between the axolemma and ensheathing myelin (<20nm), it would yield an average concentration of approximately 2µM (Burger, Mehl et al. 1989, Ziskin, Nishiyama et al. 2007, Micu, Plemel et al. 2016). Internodal vesicular glutamate release strongly supports the proposed existence of an axo-myelinic synapse in WM (Micu, Plemel et al. 2016). As discussed in section 3.1.4, the physiological function of such synapses may represent an essential mechanism by which axons can signal to overlaying myelin, the importance of which remains to be seen. Proposed functions include signalling for metabolic support and regulation of myelin nanostructure. However, this also suggests that the periaxonal space may be a significant site of excitotoxic injury under certain pathological conditions.

Using a similar approach with GFAP-GFP+ mice, I examined potential vesicular fusion in fibrous astrocytes. In contrast to axons, FM4-64 loading was much lower in astrocytes. In addition, exposure to high-K^+ did not induce vesicular docking in WM astrocytes, which indicates that WM astrocytes are either incapable of vesicular release or that release is voltage-insensitive. Consistent with my findings, a previous study observed that eliciting transient Ca^{2+} rises in fibrous astrocytes (via the activation of metabotropic, purinergic and prostaglandin receptors) did not evoke vesicular release in the developing corpus callosum (Ziskin, Nishiyama et al. 2007). Based on these findings, corpus callosum astrocytes do not contribute to vesicular glutamate release. Astrocytic vesicular release is a controversial topic. As outlined in the introduction, numerous studies have demonstrated the expression of SNARE proteins and vesicles in astrocytes. Vesicular glutamate (and ATP) release from

astrocytes is observed at conventional neuronal synapses (forming the 'tripartite synapse') in response to neuronal activity (Volterra and Meldolesi 2005). It is plausible that regional differences may regulate gliotransmitter release. For instance, unlike protoplasmic astrocytes at the 'tripartite synapse', fibrous astrocytes may lack the ability to exocytose.

3.3.3: Source of Ca^{2+} during depolarisation?

An important feature of vesicular fusion is its Ca^{2+} dependency. Thus, a rise in axonal Ca^{2+} must precede vesicular glutamate release in the corpus callosum. Previous studies have demonstrated that axonal neurotransmitter release is strongly Ca^{2+} cooperative and involves highly localised Ca^{2+} micro-domain signalling (Kukley, Capetillo-Zarate et al. 2007). In addition, Ca^{2+} transients are observed in corpus callosum and optic nerve axons following electrical stimulation (Verbny, Zhang et al. 2002, Kukley, Capetillo-Zarate et al. 2007). However, the exact mechanism by which intra-axonal Ca^{2+} levels increase is controversial. Although my data provides no information on this, one can hypothesise on the source of Ca^{2+} based on the literature. Interestingly, Ca^{2+} transients in pre-myelinated axons are reduced in low extracellular Ca^{2+}. Similarly, excitatory post-synaptic currents (EPSC) are dramatically attenuated in OPCs under low extracellular Ca^{2+} conditions, which would support the direct influx of extracellular Ca^{2+} (Kukley, Capetillo-Zarate et al. 2007). Functional voltage-gated Ca^{2+} channels (VGCC) are expressed in the axolemma of pre-myelinated WM axons and are closely associated with vesicular apparatus such as SNAP-25 and V-ATPase (Alix, Dolphin et al. 2008). Similarly, K^{+}-mediated de-staining of FM1-43 is significantly prevented in the presence of calcium channel blocker, Cd^{2+}, which together suggests that Ca^{2+} influx through VGCCs on unmyelinated axons mediates vesicular fusion (Kukley, Capetillo-Zarate et al. 2007, Ziskin, Nishiyama et al. 2007).

While this strongly suggests that vesicular glutamate release is triggered by Ca^{2+} influx through VGCCs, the internodal axolemma of myelinated axons may have limited availability to $[Ca^{2+}]_e$ due to the ensheathing myelin layers. The average AP-evoked Ca^{2+} transient recorded in the mouse ON axon is approximately 10-fold lower in myelinated axons when compared to pre-myelinated axons (Verbny, Zhang et al. 2002). Previous reports have demonstrated that VGCCs redistribute to form clusters at the node of Ranvier during development (Alix, Dolphin

et al. 2008). Similarly, immunostaining for L-type Ca^{2+} channels (Cav1.2 subunit) in myelinated axons of rat molars, demonstrated that although VGCC expression was present along the axon membrane, staining intensity was highest at the node of Ranvier (Westenbroek, Anderson et al. 2004). Therefore, it is plausible that Ca^{2+} influx at the exposed node and the lateral diffusion of axonal Ca^{2+} may evoke internodal vesicular release. However, consistent with my findings that there is no evidence of localised vesicular fusion along the axon, there are no spatial variations in either the amplitude or shape of AP-induced Ca^{2+} transients along myelinated axons (Zhang, Wilson et al. 2006). Furthermore, the photolysis stimulation of axonal Ca^{2+} release at a designated point along the axon ("an artificial node") has a space constant of Ca^{2+} diffusion of between 30 and 40µm. Considering the average internodal length of a myelinated mouse ON axon is 138µm (Butt, Colquhoun et al. 1994), the lateral spread of Ca^{2+} from the node of Ranvier is insufficient to explain the spatially uniform rise in internodal Ca^{2+} during AP conduction (Zhang, Wilson et al. 2006). In agreement, Ca^{2+} diffusion coefficients in Myxicola axoplasm is relatively slow and is impeded by axoplasmic organelles (al-Baldawi and Abercrombie 1995). This raises the question of where the depolarisartion-induced rise in internodal Ca^{2+} originates. Although VGCCs reportedly redistribute to the node of Ranvier during development (Alix, Dolphin et al. 2008), several studies have reported that a low density of VGCCs are uniformly distributed along the internode of myelinated axons (Brown, Westenbroek et al. 2001, Ouardouz, Nikolaeva et al. 2003). Interestingly, the block of VGCCs abolish Ca^{2+} transients in myelinated axons (Jackson, Trout et al. 2001, Zhang, Wilson et al. 2006). However, myelinated axons also contain intracellular stores of Ca^{2+} capable of elevating axoplamic concentrations following release (Ren, Ridsdale et al. 2000). A recent study by Micu *et al.* reported that the axoplasmic rise in $[Ca^{2+}]_i$ during the electrical stimulation of myelinated axons, originates from intracellular Ca^{2+} stores (Micu, Plemel et al. 2016). They demonstrated that vesicular release from myelinated axons is attenuated by either the L-type voltage-gated Ca^{2+} channel inhibitor, nifedipine, or by antagonising Ca^{2+} release from ryanodine-sensitive intracellular stores. Consistent with previous studies (Ouardouz, Nikolaeva et al. 2003), these findings indicate that VGCCs along the internodal axon segment of myelinated axons sense depolarisation, which subsequently gates Ca^{2+} release from intra-axonal stores such as the axoplasmic reticulum (Micu, Plemel et al. 2016). It is plausible therefore, that depolarisation-evoked Ca^{2+} rises in axons originate from either extracellular influx or intracellular efflux, dependent on the presence of myelin. It would be

interesting to test whether the depolarisation-evoked rise in $[Glut]_e$ or vesicular docking in myelinated axons is affected by the removal of extracellular Ca^{2+}. Similarly, is the release of Ca^{2+} from the axoplasmic reticulum sufficient to induce vesicular fusion in myelinated axons?

In summary, this chapter demonstrates that K^+-evoked depolarisation of the adult corpus callosum evokes extensive vesicular fusion in axons which leads to elevated extracellular glutamate concentrations. In contrast, astrocytes do no contribute to vesicular neurotransmitter release. Vesicular fusion along the axolemma of myelinated axons supports novel findings which suggest that axons signal to the overlaying myelin in an activity/depolarisation dependent manner. However, the significance of axonal vesicular glutamate release under conditions of energy deprivation remains to be uncovered.

Chapter 4:

Glutamate Release Mechanisms in Ischemic White Matter

4.1: Introduction

4.1.1: Ischemia and Excitotoxicity

In the previous chapter, I reviewed the importance of glutamatergic signalling in WM and examined the significance of vesicular glutamate release in axons. As mentioned, resting extracellular glutamate concentrations ($[Glut]_e$) are kept in the low micromolar range (~1-2µM) under physiological conditions (Rutledge and Kimelberg 1996). This is primarily due to the actions of glutamate transporters (EAATs). However, under acute ischemic conditions, the excessive release of glutamate, combined with the failure of its re-uptake mechanisms, leads to a dramatic rise in $[Glut]_e$ throughout the CNS (Andiné, Sandberg et al. 1991, Pu, Li et al. 2000). Elevated $[Glut]_e$ triggers a cascade of deleterious events, including the pathological influx of Ca^{2+} ions through ionotropic glutamate receptors, a series of events collectively known as excitotoxicty (see section 1.2.4).

Glutamate was first implicated in the pathogenesis of ischemic brain injury in 1982 by Jørgenson and Diemer (Jorgensen and Diemer 1982). They noted that rats which were subject to cerebral ischemia, displayed a selective pattern of neuronal loss which closely resembled regions of high glutamate uptake. Shortly after, Benveniste *et al.* used microdialysis to measure an 8-fold increase in $[Glut]_e$ in the rat hippocampus during a 10 minute period of ischemia (Benveniste, Drejer et al. 1984). Initially, the involvement of glutamate-mediated damage was a controversial topic, as elevated $[Glut]_e$ was also recorded in regions which showed no signs of irreversible injury following cerebral ischemia (Globus, Busto et al. 1990). Choi and Rothman were among the first to report that blockers of iGluRs (i.e. AMPA/kainate/NMDA) reduced the infarct volume in animal models of focal ischemia (Choi and Rothman 1990). It is now well established that glutamate-mediated excitotoxicity plays a pivotal role in the development of irreversible ischemic brain injury. As outlined in the previous chapter, the unequivocal expression of iGluRs throughout WM leaves these structures particularly vulnerable to excitotoxic injury during energy deprivation. Similar to GM, excitotoxicity is now recognised as a crucial mechanism involved in the development of ischemic WM pathology.

4.1.1.1: Oligodendrocyte- AMPA/kainate receptor mediated injury

Oligodendrocytes are the myelinating cells of the CNS and are essential for the transmission of rapid saltatory action potential conduction (Bradl and Lassmann 2010). Oligodendrocyte cell death can have a profound effect on WM function, as a single oligodendrocyte is typically responsible for the myelination of up to 50 neighbouring axons (Velumian and Samoilova 2014). They are considered the most vulnerable cell type within the CNS and are highly sensitive to transient ischemia (Dewar, Underhill et al. 2003, Matute 2011). Numerous studies have shown that oligodendrocyte cell death during ischemia is primarily mediated via the sustained activation of AMPA and kainate receptors which are diffusely located on the oligodendrocyte cell soma. Excitotoxic injury of oligodendrocytes was first observed in 1993 by Oka *et al.* who found that exposing oligodendrocyte cell culture to glutamate (for 24 hours) lead to high levels of cell death (Oka, Belliveau et al. 1993).

Oligodendrocyte cell death is entirely dependent on the toxic influx of Ca^{2+} and its subsequent accumulation in the intracellular compartment. As a result, oligodendrocyte cell death during ischemia is prevented in the absence of extracellular Ca^{2+} (Matute, Sanchez-Gomez et al. 1997, Fern and Moller 2000). Several studies have shown that Ca^{2+} entry through activated AMPA/kainate receptors is the primary route of Ca^{2+} influx during acute ischemia (Matute, Sanchez-Gomez et al. 1997, Mcdonald, Althomsons et al. 1998, Li and Stys 2001, Micu, Jiang et al. 2006, Tekkok, Ye et al. 2007). Conversely, the pharmacological inhibition of AMPA/kainate receptors is sufficient in preventing OGD-induced cell death (Fern and Moller 2000, Tekkok and Goldberg 2001, Tekkok, Ye et al. 2007). *In vivo* studies have shown that the AMPA/kainate receptor antagonists, NBQX and topiramate, attenuate ischemia-induced WM injury in both developing and mature rodents (Follett, Rosenberg et al. 2000, Tekkök and Goldberg 2001, Rosenberg 2014).

Early oligodendrocyte cell death is the hallmark characteristic of periventricular white matter injury (PWMI) in the developing brain. The death of immature oligodendrocytes can lead to severe myelination disturbances, such as hypomyelination. Interestingly, the high risk period for PWMI (between weeks 23-32 of gestation in humans) coincides with a key point in oligodendrocyte development, when OPCs are progressing into immature oligodendrocytes and beginning to invade neighbouring axon tracts with their fine processes (Butt and Ransom

1993, Thomas, Salter et al. 2004, Fern 2011). At this age, developing oligodendrocytes are more sensitive than any other cell type, both in cell culture and *in situ* (Fern 2011). In addition, there are more sensitive than their earlier or later counterparts (Bergles, Roberts et al. 2000, Stys 2005). This raises the question as to why developing oligodendrocytes are so susceptible to injury at this age. Curiously, developing OPCs have an immature system for dealing with oxidative stress. For example, they have low levels of glutathione peroxidase and a poor ability to remove hydrogen peroxide from the cell, when compared with mature oligodendrocytes (Nave 2010). However, their heightened vulnerability during this period is predominantly associated with an elevated expression of Ca^{2+}-permeable AMPA/kainate receptors (Back, Han et al. 2002, Deng, Rosenberg et al. 2003). Furthermore, immature WM oligodendrocytes, and their mature counterparts, have a low expression of GluR2 subunits, which makes them particularly susceptible to Ca^{2+} influx when activated (Deng, Rosenberg et al. 2003).

4.1.1.2: Oligodendrocyte/Mylein- NMDA receptor mediated injury

While blocking AMPA/kainate receptors during ischemia prevents oligodendrocyte cell death, it does not preserve their myelinating processes. Interestingly, NMDA receptors are differentially expressed on the processes of immature oligodendroglia and also mediate toxic $[Ca^{2+}]_i$ rises during ischemia (Káradóttir, Cavelier et al. 2005, Salter and Fern 2005). For example, the application of MK-801 (NMDA receptor antagonist) prevents the detachment of oligodendrocyte processes during OGD (Salter and Fern 2005). In addition, oligodendrocyte NMDA receptors contain an unusual subunit composition. The presence of the NR3 subunit leaves them relatively resistant to Mg^{2+} blockade at a resting membrane potential, and therefore, susceptible to activation in the absence of strong depolarisation, typically provided by AMPA/kainate-receptor activation (Káradóttir, Cavelier et al. 2005). NMDA receptor blockade with memantine significantly attenuates the loss of developing oligodendrocytes in a rat model of PVL (Manning, Talos et al. 2008). Taken together, these findings demonstrate that the combined activation of both AMPA/kainate and NMDA-receptors, ultimately mediates to the demise of oligodendrocytes during acute periods of ischemia.

Myelin can protect underlying axons from physical mechanical damage by acting as a protective cushion, but it can also shield the axonal membrane from harmful substances in extracellular milieu under pathological conditions (Schäbitz, Li et al. 2000, Harukuni and Bhardwaj 2006). However, rapid myelin damage is a common feature of ischemic WM injury (Pantoni, Garcia et al. 1996). Interestingly, NMDA receptor subunits are shifted from oligodendrocyte cell processes to compact myelin sheath during myelination (Alix and Fern 2009). Chemical ischemia leads to an accumulation of Ca^{2+} in both oligodendrocyte cell bodies and the cytosolic compartment of myelin sheath in the adult RON (Micu, Jiang et al. 2006). This rise in Ca^{2+} is abolished in both compartments in the presence of kynurenic acid, a broad spectrum iGluR blocker. Consistent with previous findings, Micu *et al.* reported that the AMPA/kainate receptor antagonist, NBQX, prevented the Ca^{2+} rise in oligodendrocyte cell bodies. Interestingly, NBQX only had a modest effect on the myelinic Ca^{2+} rise indicating that the elevated Ca^{2+} levels in myelin must operate through a distinct mechanism and is not just a passive feature of Ca^{2+} diffusion from the cell soma. It was found that the rise in myelinic Ca^{2+} is a result of Ca^{2+} influx through activated NMDA receptors, as it was abolished following the application of NMDAR antagonists (MK-801, 7-CKA and D-AP5). Furthermore, NMDA receptor blockade (with 7-CKA) ameliorated the pathological loosening and fragmentation of myelin sheath during ischemia (Micu, Jiang et al. 2006). On the other hand, they found little evidence of axonal protection following NMDA receptor inhibition. Myelin is known to contain Ca^{2+}-dependant enzymes which may be activated following Ca^{2+} influx, promoting the breakdown of lipids and proteins (Fu, Wang et al. 2007). Similar to NMDA receptor expression on the myelinating processes of immature oligodendrocytes, NR3 subunits are also found in myelinic NMDA receptors. As a result, they are also relatively resistant to Mg^{2+} blockade, leaving them more susceptible to activation (Stys and Lipton 2007). Excitotoxic myelin injury will be examined in more detail in chapter 5.

4.1.1.3: Excitotoxic WM damage contributes to irreversible functional injury

While the above findings suggest that excitotoxic damage primarily effects oligodendrocytes and the myelin they manufacture, recent evidence demonstrates that the over-activation of glutamate receptors also contributes to the irreversible functional injury observed after

ischemia (Micu, Jiang et al. 2006, Ouardouz, Coderre et al. 2009, Ouardouz, Coderre et al. 2009). Importantly, it is the loss of action potential conduction which underlies a variety of clinical disabilities observed in patients who suffer either periventricular WM injury or stoke (Baltan, Carmichael et al. 2014).

Li and Stys (2000) were among the first to demonstrate that excitotoxic WM injury promotes the irreversible functional injury of myelinated WM tracts. They found that the sustained activation of iGluRs with either glutamate (1mM), AMPA (100µM) or kainate (500µM) lead to an irreversible decrease in CAP amplitude recorded from isolated spinal dorsal columns. Interestingly, they also noted that while axon cylinders were unaffected by glutamate, glial cell and myelin damage was clearly evident. In contrast, Tekkok *at al.* found that extended periods of perfusion with glutamate, AMPA or kainate had no effect on WM integrity in the mouse ON (MON), even when AMPA receptor desensitisation was blocked with cyclothiazide (Tekkok, Ye et al. 2007). However, they did find that exposure to a relatively short period of OGD (15 minutes) in the presence of glutamate, exacerbated functional recovery. In contrast, blockade of AMPA/kainate receptors during OGD dramatically reduced the degree of WM injury, increasing post-OGD CAP area from 21% to 72% (Tekkok, Ye et al. 2007). This has also been documented in alternative WM tracts; a selective AMPA/kainate receptor antagonist, NBQX, prevents the irreversible loss in CAP area and axonal structure (SMI-31 immunofluorescence) following 20 minutes of OGD in the adult corpus callosum (Tekkok and Goldberg 2001). Similarly, using an *in vivo* model of spinal cord ischemia, Kanellopoulos *et al.* demonstrated that the administration of NBQX reduced ischemia-induced WM damage (based on axonal counts) following aortic occlusion, and improved locomotor function 6 weeks after the insult (Kanellopoulos, Xu et al. 2000). While the over-activation of AMPA/kainate receptors play a crucial role in ischemia-induced WM injury, its effects seem to be magnified in older WM tracts (Baltan, Besancon et al. 2008). Baltan *et al*. discovered that the protective effect of NBQX was actually enhanced in MONs from animals aged between 12 and 24 months, a phenomenon which was attributed to an earlier and greater degree of glutamate release (Baltan, Besancon et al. 2008). In addition to AMPA/kainate receptor mediated injury, NMDA receptor blockade preserves post-OGD CAP amplitude in pre-myelinated and early myelinating WM tracts (Bakiri, Hamilton et al. 2008, Alix and Fern 2009, Huria, Beeraka et al. 2015).

This raises the question as to how glutamate receptors mediate functional injury. It is possible that the activation of glutamate receptors located on the axonal membrane may directly lead to irreversible axon damage. In the pre-myelinated RON, NR1 receptor subunits co-localised with small pre-myelinated axons and expression strongly correlated with areas of focal axonal injury (Huria, Beeraka et al. 2015). In addition, the activation of NMDA receptors on the axolemma of pre-myelinated axons mediates a significant degree of functional loss in the P2 RON (Huria, Beeraka et al. 2014). Similarly, the expression of Ca^{2+}-permeable AMPA and kainate receptors on dorsal column myelinated axons suggest that the direct activation of axonal glutamate receptors may mediate toxic Ca^{2+} influx during ischemia (Ouardouz, Coderre et al. 2009, Ouardouz, Coderre et al. 2009, Huria, Beeraka et al. 2014). However, axonal AMPA receptors are only weakly permeable to Ca^{2+} (Ouardouz, Coderre et al. 2009) and the application of iGluR agonists has little effect on CAP conduction (Tekkok, Ye et al. 2007). To date, there have been no reports of functional NMDA receptor expression on the axolemma of mature axons.

Alternatively, it is plausible that axonal injury may be secondary to oligodendrocyte damage and myelin breakdown. Interestingly, the focal breakdown of small pre-myelinated axons is observed at sites of contact with navigating oligodendrocyte processes (Alix and Fern 2009). The same study also reported that while NR1 (a NMDA receptor subunit) reactivity was high in navigating oligodendrocyte processes, the was no evidence of NR1 expression in the axonal membrane (Alix and Fern 2009). Consistent with the hypothesis that oligodendrocyte injury leads to axonal damage, the application of NMDA receptor antagonists during OGD leads to the complete protection of small diameter, unmyelinated axons, which significantly preserves CAP conduction (Alix and Fern 2009). iGluR-mediated injury of oligodendrocytes may enhance axonal injury through the release of toxic cellular components and/or the loss of trophic support (Tekkok and Goldberg 2001). For example, NMDA receptor-mediated injury of the navigating oligodendrocyte processes can lead to a local release of K^+ ions, which can in turn cause axonal depolarisation and lead to cytotoxic swelling (Alix and Fern 2009). Furthermore, saltatory action potential conduction is not supported following myelin degeneration (Smith 1994). Therefore, it is likely that the demise of oligodendrocyte/myelin plays an important role in mediating irreversible function damage in WM.

4.1.1.4: Sensitivity of Axo-glial Synapses

Immature oligodendrocytes and myelin sheaths express a variety of functional iGluRs, with levels comparable to those at conventional synapses (Kukley, Capetillo-Zarate et al. 2007, Micu, Plemel et al. 2016). As mentioned in the previous chapter, they are considered the post-synaptic element in the WM synapse. Interestingly, WM synapses are particularly vulnerable under pathological conditions such as hypoxia-ischemia. A consistent feature of ischemia-induced injury in WM is the high degree of damage to OPC processes, which form synaptic-like junctions with unmyelinated axons (Káradóttir, Cavelier et al. 2005, Salter and Fern 2005, Shen, Liu et al. 2012). In addition, the focal splitting and separation of myelin lamella is an early event during energy deprivation (Micu, Jiang et al. 2006, Fern, Matute et al. 2014). This heightened sensitivity has shown to be at least partly related to the high expression of glutamate receptors (particularly NMDARs) (Káradóttir, Cavelier et al. 2005, Salter and Fern 2005, Micu, Jiang et al. 2006).

When Shen *et al.* examined the fine structural changes in WM following hypoxia-ischemia (unilateral carotoid ligation), they noted that while the nucleus of oligodendroglia generally appeared normal, their processes were heavily vacuolated (Shen, Liu et al. 2012). In addition, while post-synaptic densities were abundant in control regions, there was a profound decrease in their number following ischemia, consistent with the selective degradation/retraction of oligodendrocyte processes. Similarly, during exposure to OGD, oligodendrocyte processes detachment and disintegration is apparent within 20 minutes, an event which precedes injury to the cell soma (Salter and Fern 2005). As mentioned, this process is prevented in the absence of $[Ca^{2+}]_e$ or by blocking NMDA receptors (Káradóttir, Cavelier et al. 2005, Salter and Fern 2005).

While glutamatergic signalling is considered a physiological process in WM, such findings indicate that axo-glial and axo-myelinic synapses are significant sites of excitotoxic damage under ischemic conditions. This heightened sensitivity is likely due to the close spatial relationship between axons and oligodendroglia/myelin, and the high expression of iGluRs on the post-synaptic membrane of WM synapses. In addition, it is possible that the confined dimensions of oligodendrocyte processes mean that even small rises in $[Ca^{2+}]_i$ can be toxic in such a restricted intracellular space.

4.1.2: Potential sources of endogenous glutamate:

Elevated $[Glut]_e$ clearly plays a central role in ischemic WM pathology. Glutamate release is therefore a crucial step in initiating the excitotoxic cascade. Excitotoxic injury is observed in isolated WM tracts, which indicates that the ischemic rise in $[Glut]_e$ must originate from WM cells. The three main cellular elements in WM; axons, astrocytes and oligodendrocytes all pose as potential sources of ischemic glutamate release. Several studies have analysed physiological glutamate levels in cells using immuno-electron microscopy. Interestingly, both axons and oligodendrocytes contain the highest levels of glutamate-like reactivity in developing periventricular WM and mature dorsal columns (Li and Stys 2001, Back, Craig et al. 2007). Wilke *et al.* also reported high glutamate levels in oligodendrocytes and 'non soma' regions of the developing ON (Wilke, Thomas et al. 2004). In contrast, astrocyte levels are relatively low in both developing and mature WM tracts (Li and Stys 2001, Wilke, Thomas et al. 2004, Back, Craig et al. 2007), which may relate to their high levels of glutamate synthase, which converts glutamate into glutamine, as part of the *glutamate-glutamine cycle*. Alternative sources of glutamate *in vivo* may originate from neighbouring GM regions, choroid epithelia and ependymal cells (Wilke, Thomas et al. 2004).

Axons are the primary functional element in WM and contain high concentrations of cytosolic glutamate (~4mM (Volpe 2008)) under control conditions. Therefore, they represent a major repository of glutamate in WM. Using semiquantitative glutamate immunohistochemistry, several studies have reported axons as a major source of ischemic glutamate release in WM. When the Na^+ and K^+ gradients are disrupted in the adult spinal cord, there is a significant release of endogenous glutamate from axon cylinders (Li and Stys 2001). Similarly, axonal glutamate levels in the adult spinal cord are significantly reduced following 60 minutes of anoxia (Li, Mealing et al. 1999). Axonal glutamate levels in periventricular WM are also reduced after hypoxia (by ~60%) (Back, Craig et al. 2007). As demonstrated in the previous chapter, axons are a significant source of glutamate-laden vesicles, which contain glutamate concentrations exceeding 50mM. Thus, axonal vesicular glutamate may also contribute to axonal glutamate release during ischemia (Kukley, Capetillo-Zarate et al. 2007, Alix, Dolphin et al. 2008, Micu, Plemel et al. 2016).

Oligodendrocyte glutamate levels are also attenuated during hypoxia (Li, Mealing et al. 1999, Back, Craig et al. 2007). Earlier studies have shown that oligodendrocytes are capable of releasing toxic levels of glutamate, which subsequently activates iGluRs located on the oligodendrocytes themselves (Fern and Moller 2000). However, Wilke *et al.* reported the net accumulation of oligodendrocyte glutamate levels following ischemia, rather than the depleted levels that would be observed with an overall net release (Wilke, Thomas et al. 2004). This suggests that oligodendrocytes ability to release glutamate may be dependent on their developmental stage and/or location (Fern, Matute et al. 2014). Although physiological astrocytic glutamate levels are low, their glutamate stores are slightly depleted following ischemia in developing WM (Wilke, Thomas et al. 2004, Back, Craig et al. 2007). However, in mature WM, astrocyte glutamate levels are unaltered by 60 minutes of anoxia (Li, Mealing et al. 1999). Thus, the source of ischemic WM glutamate release is still somewhat unresolved, as all three of the main cellular elements are capable of release.

4.1.3: Potential mechanisms of glutamate release during ischemia

Alongside the possible sources of endogenous glutamate, there are a variety of potential release mechanisms which can operate under acute ischemic conditions. The precise pathway(s) of glutamate release during ischemia is currently unknown.

4.1.3.1: Reverse Excitatory Amino Acid Transporters (EAATs)

EAATs are electrogenic, Na^+-dependant transporters which utilise the Na^+ gradient across the plasma membrane as a driving force for glutamate reuptake (Danbolt 2001). As discussed in chapter 1, EAATs are primarily responsible for maintaining low extracellular glutamate concentrations under physiological conditions. Intriguingly, the inhibition of EAATs (with TBOA) in oligodendrocyte cell cultures and in the ON leads to a significant rise in extracellular glutamate levels, which consequently leads to excitotoxic cell death, demyelination and axonal damage (Domercq, Etxebarria et al. 2005). Under acute ischemic conditions, inadequate levels of cellular ATP leads to the rapid failure of the Na^+/K^+-ATPase pump and

subsequently, the failure of EAAT uptake. However, the inevitable run-down of the Na^+ and K^+ gradients favour the reversal of EAATs, where glutamate is pumped into the extracellular space (Danbolt 2001). Due to the electrogenicity of EAATs, the associated depolarising shift in membrane potential also promotes their reversal. The reversal of EAATs was first demonstrated by Szatkowski *et al.* when they reported that elevating $[K^+]_e$ around glial cells evoked an outward membrane current reflecting glutamate release in whole-cell clamped Muller cells (Szatkowski, Barbour et al. 1990). The reverse operation of EAATs is now recognised as the major glutamate release pathway in ischemic GM (Rossi, Oshima et al. 2000, Grewer, Gameiro et al. 2008).

While the pathway of ischemic glutamate release in WM is still a topic of debate, several studies have reported that like GM, the reversal of EAATs contribute to ischemic glutamate release in WM (Li, Mealing et al. 1999, Li and Stys 2001, Tekkok, Ye et al. 2007, Hamilton, Kolodziejczyk et al. 2016). Both the developing and mature RON express the 3 main transporter sub-types; EAAC-1, GLT-1 and GLAST (Domercq, Sánchez-Gómez et al. 1999, Arranz, Hussein et al. 2008). In cultured oligodendrocytes, rapid ischemic cell death is mediated via the gating of AMPA/kainate receptors (Fern and Moller 2000). Interestingly, this study demonstrated that glutamate originated from the oligodendrocytes themselves via the reversal of EAATs. Early studies by Li and Stys found that the inhibition of EAAT with l-*trans*-PDC, led to a significant improvement in CAP recovery in the adult rat spinal dorsal column following Na^+/K^+-ATPase inhibition and anoxia, conferring a similar degree of protection to that observed in the presence of AMPA-receptor antagonist, GYKI52466 (Li, Mealing et al. 1999, Li and Stys 2001). Furthermore, they found that the anoxia-induced depletion of axonal and oligodendrocyte glutamate stores was prevented by l-*trans*-PDC (Li, Mealing et al. 1999). Similar results were observed in the adult ON where the application of TBOA, a non-transportable EAAT blocker, led to improved functional recovery in the MON, by completing preventing the pathological release of glutamate from the nerve (measured by HPLC) (Tekkok, Ye et al. 2007). As mentioned, older WM is more susceptible to irreversible ischemic injury due to an earlier and larger rise in glutamate levels (Baltan, Besancon et al. 2008). Baltan *et al*. found that the enhanced release of glutamate is a result of an increased expression of EAATs (particularly GLT-1) in older WM (Baltan, Besancon et al. 2008). Curiously, GLT-1 is most

heavily expressed on astrocytes in WM, which contain relatively low levels of glutamate (Arranz, Hussein et al. 2008, Schousboe, Scafidi et al. 2014).

Interestingly, the inhibition of EAATs during ischemia is also reported to exacerbate neuronal injury in organotypic cortical slices (Soria, Pérez-Samartín et al. 2014). Moreover, TBOA shortened the latency to anoxic depolarisation suggesting that glutamate transporters remain active and continue to uptake extracellular glutamate during the beginning of ischemia.

4.1.3.2: Vesicular exocytosis

The data presented in the previous chapter demonstrated the significance of vesicular glutamate release in WM. Depolarisation-evoked vesicular exocytosis is capable of significantly elevating extracellular glutamate concentrations (by ~13µM, see Fig.3.3). However, the contribution of vesicular glutamate release during ischemia is currently unknown.

Vesicular glutamate loading is an ATP-dependant process, powered by the action of V-type H^+ ATPase (V-ATPase). The V-ATPase pumps H^+ ions inside the vesicular lumen, forming a high-proton gradient and a positive vesicular membrane potential (Cavelier and Attwell 2007). Vesicular glutamate transporters (VGLUTs) utilize this positive membrane potential to load glutamate inside the vesicles. Therefore, under ischemic conditions, inadequate ATP levels will lead to the run-down of the H^+ gradient and membrane potential, which will eventually lead to a gradual loss of glutamate from its vesicular stores. However, the depletion of glutamate from vesicles can take several hours following V-ATPase inhibition (Cavelier and Attwell 2007), suggesting that Ca^{2+}-dependant vesicular exocytosis may occur in the absence of ATP. Moreover, a rise in axonal Ca^{2+} during anoxia/ischemia (see 1.3.2.2) will likely increase the frequency of vesicular exocytosis.

Several studies have reported that excessive vesicular fusion at neuronal synapses is the earliest mechanism of glutamate release, typically within 10 minutes following the onset of ischemia (Katchman and Hershkowitz 1993, Wahl, Obrenovitch et al. 1994, Dawson, Djali et al. 2000, Jabaudon, Scanziani et al. 2000, Fleidervish, Gebhardt et al. 2001, Kawakami,

Sekiguchi et al. 2001). Ischemia-induced vesicular fusion is likely a result of ischemic depolarisation, as an increase in $[K^+]_e$ depolarises membranes and leads to a rise in $[Ca^{2+}]_i$ levels. For example, the initial 15 minutes of ischemia is characterised by an increase in the frequency of EPSCs recorded in the calyx of Held synapse (Lee and Kim 2015). This increase in EPSCs was paralleled by an gradual rise in $[Ca^{2+}]_i$. The inhibition of VGCCs significantly inhibits ischemic glutamate release from cultured hippocampal neurons and attenuates neuronal injury (Kimura, Sawada et al. 1998). However, the protective effect of VGCC inhibitors is reduced when the length of ischemia is increased. This data suggests that vesicular exocytosis may occur for a sufficiently long period, until vesicular stores are depleted, following which alternative mechanisms come into play (Nishizawa 2001). However, vesicular release is not always an early event. Szatkowski and Attwell described two distinct phases of glutamate release following a reduction of blood flow (Szatkowski and Attwell 1994). The reversal of EAATs activate Ca^{2+}-permeable NMDA receptors which elevated intracellular Ca^{2+} levels. It is the rise in $[Ca^{2+}]_i$ that reportedly mediates the excessive fusion of vesicular glutamate.

Although vesicular glutamate release is likely to occur early on in ischemia, it can contribute to a significant component of total glutamate release. In cerebrocortical slice cultures, the OGD-induced rise in extracellular glutamate, and subsequent cell death, is significantly suppressed in the presence of VGCC blockers or inhibitors of vesicular exocytosis (Fujimoto, Katsuki et al. 2004). In addition, a significant component of glutamate (and aspartate) release from human cerebrocortical slices was inhibited in Ca^{2+}-free medium, characteristic of vesicular exocytosis (Marcoli, Bonfanti et al. 2004). Intravenous injections of a pre-synaptic N-type Ca^{2+} channel antagonist (SNX-111), significantly reduced both the concentration of $[Glut]_e$ and infarct volume in rats with middle cerebral artery occlusion (Takizawa, Matsushima et al. 1995).

While much of this work represents vesicular release at conventional synapses in GM, to date, there is little evidence of ischemia-induced vesicular release in WM. Interestingly, Káradóttir *et al.* noted a dramatic rise in the frequency of post-synaptic currents recorded in OPC upon exposure to ischemia, suggesting an increase in exocytotic neurotransmitter release (Káradóttir, Cavelier et al. 2005). Similar synaptic currents were recorded under control conditions and were abolished in the presence of tetrodotoxin (TTX), indicating that vesicular glutamate release originates from neighbouring axons (Káradóttir, Cavelier et al. 2005).

Therefore, the glutamate-rich vesicles present in these axons, pose as a potential source of glutamate efflux during OGD. In addition, the close associations and sensitivity of axo-glial synapses suggests that excessive vesicular fusion will dramatically elevate $[Glut]_e$ at these synapses, which may contribute to their sensitivity during ischemia.

4.1.3.3: Swelling-mediated glutamate release/ Clasmatodendrosis

Astrocyte swelling is one of the earliest responses to ischemia in the human CNS (Kimelberg 2005). During energy deprivation, the failure of the sodium-pump leads to a dramatic increase in $[K]_e$, combined with the accumulation of Na^+ (and Cl^-) ions within cells. $[K^+]_e$ is reported to increase from a resting level of 2.7-3.5mM (Somjen 2002), reaching between 50-80mM (Somjen 1979, Gido, Kristian et al. 1997). High $[K^+]_e$ can stimulate the activation of the Na^+ K^+ Cl^- co-transporter 1 (NKCC-1), which is expressed on fibrous WM astrocytes (Su, Kintner et al. 2002, Wilke, Thomas et al. 2004). The NKCC is a symporter which mediates the electroneutral transport of Na^+, K+ and Cl^- into cells (in a respective ratio of 1:1:2). The increased activity of NKCC-1 co-transporter contributes to the movement of excessive amounts of Na^+, K^+ and Cl^- into cells. An increase in intracellular osmolytes is rapidly followed by water which can easily diffuse across the water permeable cell membrane. However, this process is accelerated by the presence of aquaporin, particularly AQP-4 in astrocytes, which are a specialized class of water channels (Kimelberg 2005). NKCC null mice or bumetanide (a specific NKCC blocker) treated astrocytes show no cell swelling in response to high $[K^+]_e$, suggesting that NKCC activation is required to produce astrocyte swelling (Su, Kintner et al. 2002). In addition, the depolarising shift in membrane potential will attract the movement of negatively charged Cl^- ions into cells. Similarly, lactic acidosis is a well-documented feature of ischemia (Rehncrona, Rosén et al. 1981). Intracellular acidosis activates the Na^+/H^+ exchanger, which will try to alleviate intracellular proton build up. In exchange for proton efflux, sodium ions are transported into cells, contributing to a build-up of intracellular Na^+ and further exacerbating cellular swelling (Kimelberg 2005).

If astrocyte swelling is severe enough, it can lead to the rupture of cell membranes, and the enviable release of intracellular glutamate. However, in response to an increased cellular

volume, astrocytes try to compensate by opening volume-regulated anion channels (VRAC) (Kimelberg 2005, Malarkey and Parpura 2008). VRACs are outward rectifying channels which allow the release of intracellular osmolytes, down their concentration, into the extracellular space (Kimelberg 2005). VRACs are capable of releasing excitatory amino acids, like glutamate, when activated. Swelling-mediated release of glutamate was first reported by Kimelberg *et al.* in 1990, who monitored radiolabelled glutamate levels in response to hypotonic media (Kimelberg, Goderie et al. 1990). *In vivo* studies of ischemic GM indicate that cell swelling-induced increases in extracellular glutamate are mediated by anion channels (Seki, Feustel et al. 1999). High $[K^+]_e$-induced glutamate release is inhibited by anion channel blockers like L-6644711 and NPPB (Rutledge and Kimelberg 1996, Malarkey and Parpura 2008). Swelling-mediated glutamate release in WM leads to excitotoxic cell death in nearby developing oligodendrocytes during ischemia (Wilke, Thomas et al. 2004). Wilke *et al.* (2004) found that inhibiting the NKCC largely prevents the toxic rise in $[Ca^{2+}]_i$ in developing oligodendrocytes during ischemia.

In addition to VRACs, swelling-mediated glutamate release can also occur via a process known as clasmatodendrosis; the detachment and disintegration of astrocyte processes which occurs in parallel to astrocytic cell body swelling (Fern 2011). Fibrous astrocytes have numerous, highly ramified cell processes that extend from the soma. The loss of these fine cell processes is regularly reported during ischemia (Davies, Loddick et al. 1998, Thomas, Salter et al. 2004). Clasmatodendrosis was first recorded in 1961 when a reduction in blood flow led to the loss of distal astrocyte processes (Friede and van Houten 1961). Detachment of astrocyte processes leads to a loss in membrane integrity, which may liberate high levels of intracellular glutamate into the extracellular space.

4.1.3.4: Hemi-channels

Gap junction channels are a special class of ion channel which mediate the intercellular transfer of ions and molecules between neighbouring cells (Ye, Wyeth et al. 2003). They are typically composed of two aligned connexin hexamers on the membranes of two neighbouring cells. These pores can pass relatively large molecules of up to 1kDa in size (John,

Kondo et al. 1999). Gap junctions couple astrocytes and oligodendrocytes forming a 'glial syncytium' within the CNS (Orthmann-Murphy, Abrams et al. 2008). In addition, gap junctions are reported to mediate the transfer of ions and molecules across the lamella of myelin sheath, a process which is much faster than radial diffusion through myelin (Balice-Gordon, Bone et al. 1998, Nualart-Marti, Solsona et al. 2013).

However, single unopposed connexions can still act as functional channels known as hemi-channel. Functional hemi-channels exist *in situ* in WM (Ye, Wyeth et al. 2003). They are voltage-sensitive, where channels are typically closed at resting membrane potential, but can open following strong depolarisation (Trexler, Bennett et al. 1996). In addition, ambient levels of extracellular divalent cations (e.g. Ca^{2+}) keep hemi-channels in a closed state. Ye *et al.* (2003) discovered that exposure to a divalent cation-free solution induced the release of glutamate in cultured and *in situ* astrocytes in the mouse ON. Glutamate release could be prevented by several gap junction blockers such as heptanol, octanol and carbenoxolone. This raises the question of whether glutamate release through hemi-channels contributes to elevated $[Glut]_e$ under ischemic conditions.

Gap junction activation is reported to contribute to the development of ischemic brain injury (Rawanduzy, Hansen et al. 1997, Davidson, Green et al. 2012). Interestingly, metabolic inhibition activates a non-selective current in ventricular myocytes, a feature which is blocked by gap-junction blocker, La^{3+} (Kondo, Wang et al. 2000). Similarly, exposure to chemical ischemia promotes the uptake of positively and negatively charged gap junction permeant molecules (e.g. Lucifer yellow) into cultured astrocytes (Contreras, Sánchez et al. 2002). Uptake was significantly reduced in the presence of gap junction blockers indicating the opening of unopposed hemi-channels during ischemia. Ischemia leads to the dephosphorylation of Cx43, a major constituent of gap junctions (Contreras, Sánchez et al. 2002). Cx43 dephosphorylation can lead to a loss in gap junction coupling during ischemia and studies have found that neuronal cell death is reduced in Cx43 deficient mice (Frantseva, Kokarovtseva et al. 2002). In the ischemic ON, ATP release through hemi-channels activates P2X7 receptors which promote irreversible excitotoxic injury (Domercq, Perez-Samartin et al. 2010). Thus, glutamate release through hemi-channels during ischemia is a strong possibility.

4.1.3.5: Glutamate-cystine antiporter

The final potential pathway of glutamate release is through the glutamate/cystine antiporter (system X_c^-). This is a Na^+-independent, membrane-bound antiporter involved in the co-transport of cystine and glutamate in and out of cells, respectively. Glutamate release via the glutamate-cystine antiporter is reportedly a major source of extracellular glutamate under physiological conditions (Baker, Xi et al. 2002). However, Cavelier *et al.* suggested that physiological levels of extracellular cystine are too low to generate tonic glutamate release (Cavelier and Attwell 2005). Cystine is an essential substrate in glutathione synthesis, a major cellular antioxidant (McBean 2002). The maintenance of intracellular glutathione, particularly during periods of oxidative stress, promotes the activity of the glutamate/cystine antiporter, which mediates the cellular uptake of extracellular cystine in exchange for intracellular glutamate. As a result, the rapid upregulation of the antiporter during oxidative stress will promote glutamate release, potentially elevating $[Glut]_e$ to toxic levels (McBean 2002, Conrad and Sato 2012).

While physiological extracellular cystine levels may be too low to grant excessive glutamate release (Cavelier and Attwell 2005), there are several reports of increased activity under ischemic conditions. mRNA and protein levels of the exchanger are upregulated in cell culture following chemical ischemia (Reissner 2014). In addition, increased activity of the glutamate-cystine antiporter is observed in a rat model of MCAO (Soria, Pérez-Samartín et al. 2014). Interestingly, the blockade of the glutamate-cystine antiporter significantly reduced glutamate receptor-mediated currents in cortical neurons and reduced the degree of cell damage during OGD (Soria, Pérez-Samartín et al. 2014). Furthermore, lipopolysaccharide (LPS) activated microglial cells in the isolated RON, release excessive amounts of glutamate via the antiporter, which lead to widespread oligodendrocyte cell death (Domercq, Sánchez-Gómez et al. 2007).

4.1.4: Objective

The over-activation of iGluRs play a central role in ischemic WM pathology. Surprisingly, the rise in extracellular glutamate, responsible for iGluR activation, has never been directly measured in WM under ischemic conditions. Furthermore, the source and mechanism(s) of glutamate release under acute ischemic conditions are currently unknown.

The primary aim of this chapter is to determine whether extracellular glutamate concentrations increase during ischemia. Using enzymatic biosensors, I plan to establish a time-course of ischemic glutamate release in a model WM tract.

In doing so, I hope to determine the mechanism(s) of glutamate release under such conditions. Glutamate release will therefore be examined under a variety of conditions and pharmacological treatments aimed at blocking the different potential release pathways outlined in figure 4.1.

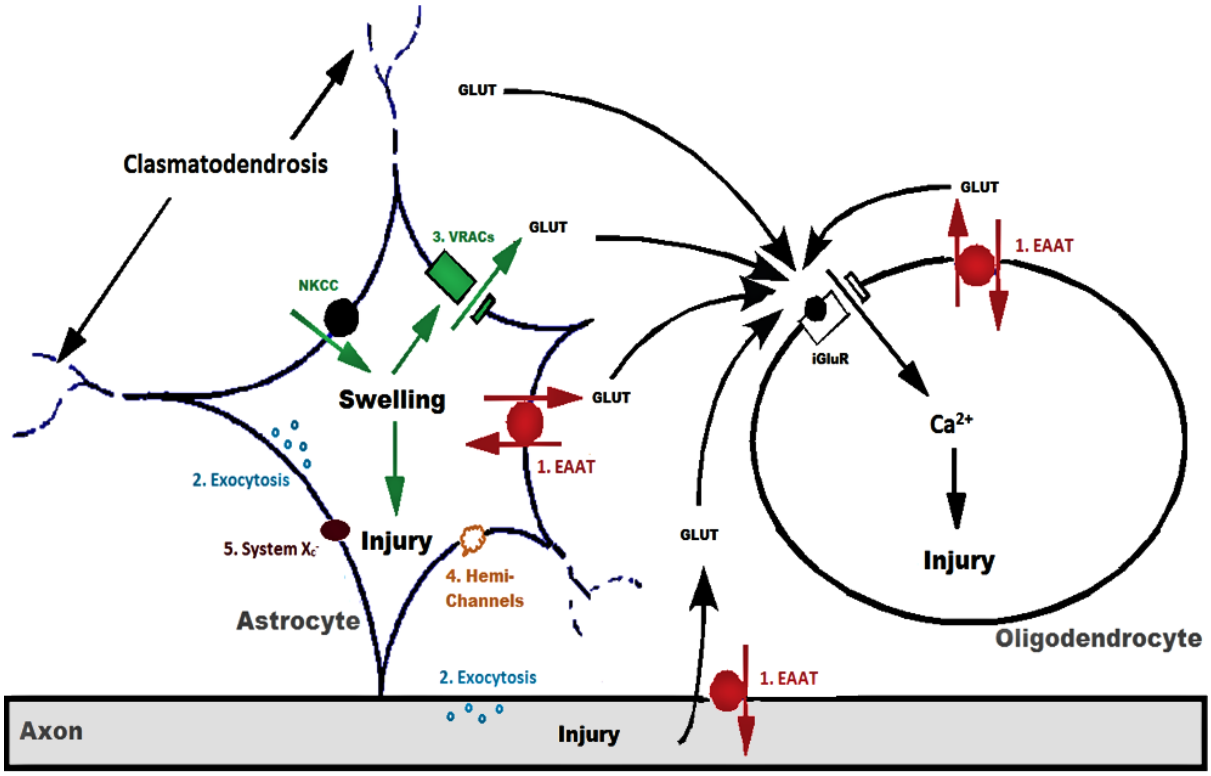

Fig. 4.1: Potential sources and mechanisms of ischemic glutamate release in white matter.

Schematic representation of glutamate release mechanisms from axons, astrocytes and oligodendrocytes. GLUT= glutamate, iGluR= ionotropic glutamate receptor, Ca^{2+}=calcium.

1: EAATs (excitatory amino acid transporters): Reverse glutamate transport

2: Exocytosis: Ca^{2+}-dependent vesicular release

3: VRAC (volume regulated anion channels): Swelling mediated release/clasmatodendrosis

4: Hemi-channels: Unopposed gap junctions

5: System X_c^-: Glutamate/cystine antiporter

Adapted with permission from (Fern 2011).

4.2 Results: Part (a): Developing WM

4.2.1 Ischemia-induced rise in extracellular glutamate in developing WM

Ischemia-induced glutamate release is a central event in the irreversible injury of developing WM (Wilke, Thomas et al. 2004, Back, Craig et al. 2007, Alix and Fern 2009, Alix, Zammit et al. 2012). In order determine the mechanism(s) of glutamate release; a time-course of $[Glut]_e$ was established in the developing P10 RON and CC, predominantly pre-myelinated WM tracts. The change in $[Glut]_e$ was monitored during exposure to chemical ischemia.

A stable resting $[Glut]_e$ was recorded in oxygenated aCSF for a minimum of 10 minutes before exposure to ischemic conditions. The mean resting $[Glut]_e$ within the extracellular space of the P10 RON was 1.36±0.31µM (*n*=70 RONs). Resting $[Glut]_e$ in the P10 corpus callosum (CC) was not significantly different, at 3.52±1.30µM (*n*=12, p=0.55, Fig 4.2). For comparison purposes, all release data was normalised to the initial baseline recordings under control conditions, and glutamate concentrations are plotted as the change in extracellular glutamate concentrations (ΔGlut).

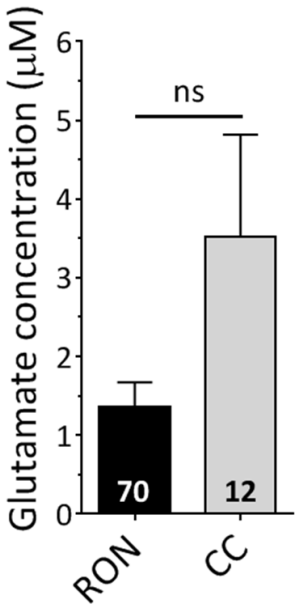

Fig. 4.2: Resting $[Glut]_e$ in early myelinating WM.

Bar chart comparing the resting $[Glut]_e$ in the P10 RON and the P10 CC. Measurements were taken in control oxygenated aCSF (mean ± SEM).

Due to the oxygen-dependency of the glutamate biosensors (see section 2.6.3), chemical-ischemia was employed as our model of energy deprivation. Electrophysiological compound action potential (CAP) recordings were used to access the functional injury induced by a range of rotenone concentrations, plus zero glucose. Under control normoxic conditions, CAP amplitude remained stable over the course of 105 minutes (108.50±4.53%, *n*=10, Fig. 4.3c,e-f). In contrast, exposing nerves to chemical ischemia, led to a rapid drop in CAP amplitude, eventually leading to a complete block in nerve excitability. There was no sign of functional recovery following 60 minutes of reperfusion using rotenone concentrations of 5nM and above (Fig 4.3a-b). However, using 1nM rotenone, CAP amplitude recovered to 6.49±2.23% (*n*=10, Fig. 4.3a-f). For all remaining experiments on the P10 RON/CC, 1nM rotenone and zero-glucose was used to mimic ischemic conditions.

Resting $[Glut]_e$ within the P10 RON remained relatively stable for at least 75 minutes under control conditions, with a maximum increase of 0.15±0.08µM (*n*=4) during the entire recording period (Fig 4.4a,c). However, upon exposure to chemical-ischemia, $[Glut]_e$ began to increase within 4-7 minutes and continued to do so at a steady rate throughout the entire ischemic period (Fig 4.4b-c). The maximum concentration recorded after 30 minutes of ischemia was 5.64±0.84µM (*n*=14) higher than the starting resting $[Glut]_e$. Upon reperfusion, $[Glut]_e$ quickly decreased, eventually returning to baseline levels after 30 minutes (Fig. 4.4b-c). Interestingly, the early rise in $[Glut]_e$ closely correlates to the early loss in CAP amplitude (taken as 10% of maximum glutamate rise and 10% decline in CAP amplitude, respectively, ns= 0.17, Fig. 4.4e-f).

To investigate whether the ischemia-evoked rise in $[Glut]_e$ is a common feature throughout developing WM, $[Glut]_e$ was also monitored in the P10 CC. Resting $[Glut]_e$ within the P10 CC remained stable under control conditions, increasing by a maximum of 0.48±0.34µM (*n*=3) over 75 minutes (Fig 4.5a,c-d). Chemical-ischemia evoked a robust increase in $[Glut]_e$, with concentrations reaching 9.27±1.41µM (*n*=4) after 30 minutes, not significantly different to the RON (*p*=0.11, Fig.4.5b,c-f). However, unlike the ON, $[Glut]_e$ remained significantly elevated in the CC following 30 minutes of reperfusion ($p<0.001$, Fig 4.5e,g).

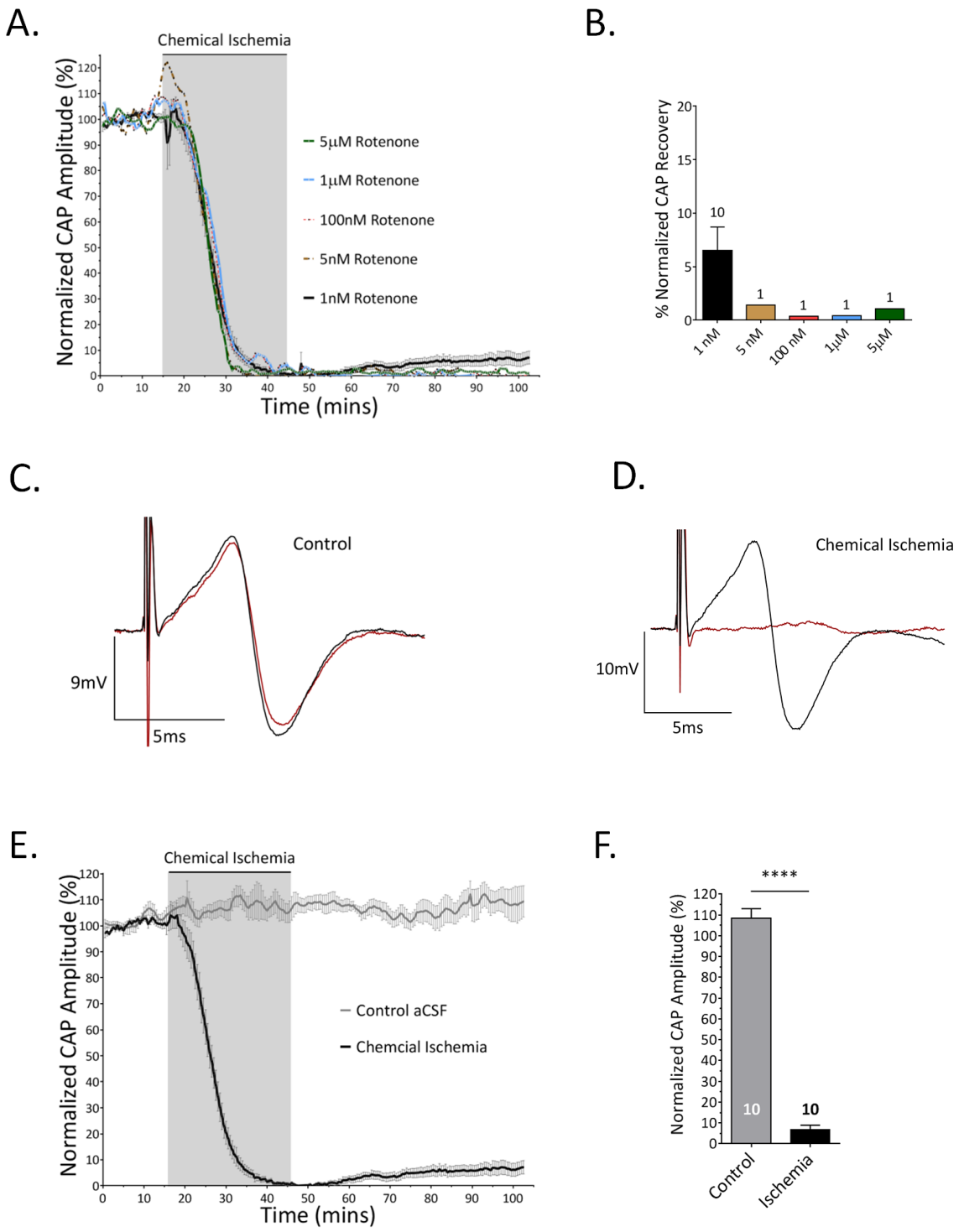

Fig. 4.3: Chemical-ischemia induced injury in the developing RON.

a) CAP time-course comparing the effects of zero-glucose and a variety of concentrations of rotenone (5µM to 1nM) on the P10 RON. **b)** CAP recovery following exposure to zero-glucose and a variety of concentrations of rotenone (5µM to 1nM). **c)** Representative CAP trace after 5 minutes (black) and 105 minutes (red) under control conditions. **d)** Representative CAP trace before (black) and after (red) 30 minutes of chemical ischemia (1nM rotenone/zero-glucose). **e)** CAP time-course comparing control conditions to chemical-ischemia (1nM rotenone/zero-glucose). **f)** CAP recovery under control conditions and following exposure to 30 minutes of chemical-ischemia. **** $p<0.0001$.

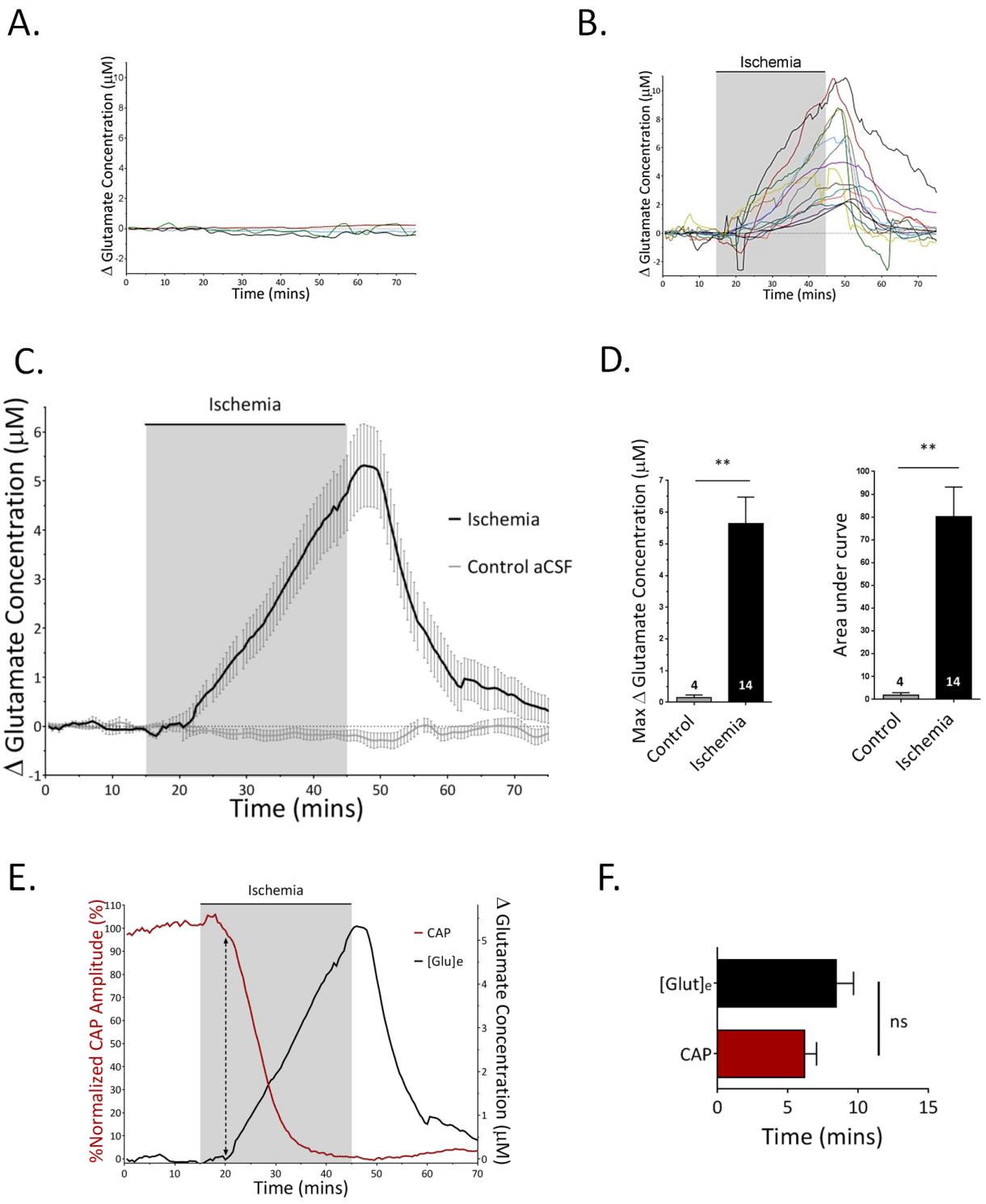

Fig. 4.4: Chemical-ischemia evokes a dramatic increase in extracellular glutamate concentration in the P10 RON.

a) Individual $[Glut]_e$ recordings under control conditions. **b)** Individual $[Glut]_e$ recordings during exposure to chemical-ischemia. **c)** Mean change (±SEM) in $[Glut]_e$ under ischemic and control conditions. **d)** Data summary comparing the maximum concentration change in extracellular glutamate and the area under the curve (total glutamate release) under both conditions. **e)** Overlay of CAP amplitude (red) and $[Glut]_e$ (black) time course showing the early rise in $[Glut]_e$ as CAP begins to decline. **f)** Histogram comparing the time taken for $[Glut]_e$ to increase by 10%, and for CAP to decrease by 10%. ns $p>0.05$, ** $p<0.01$.

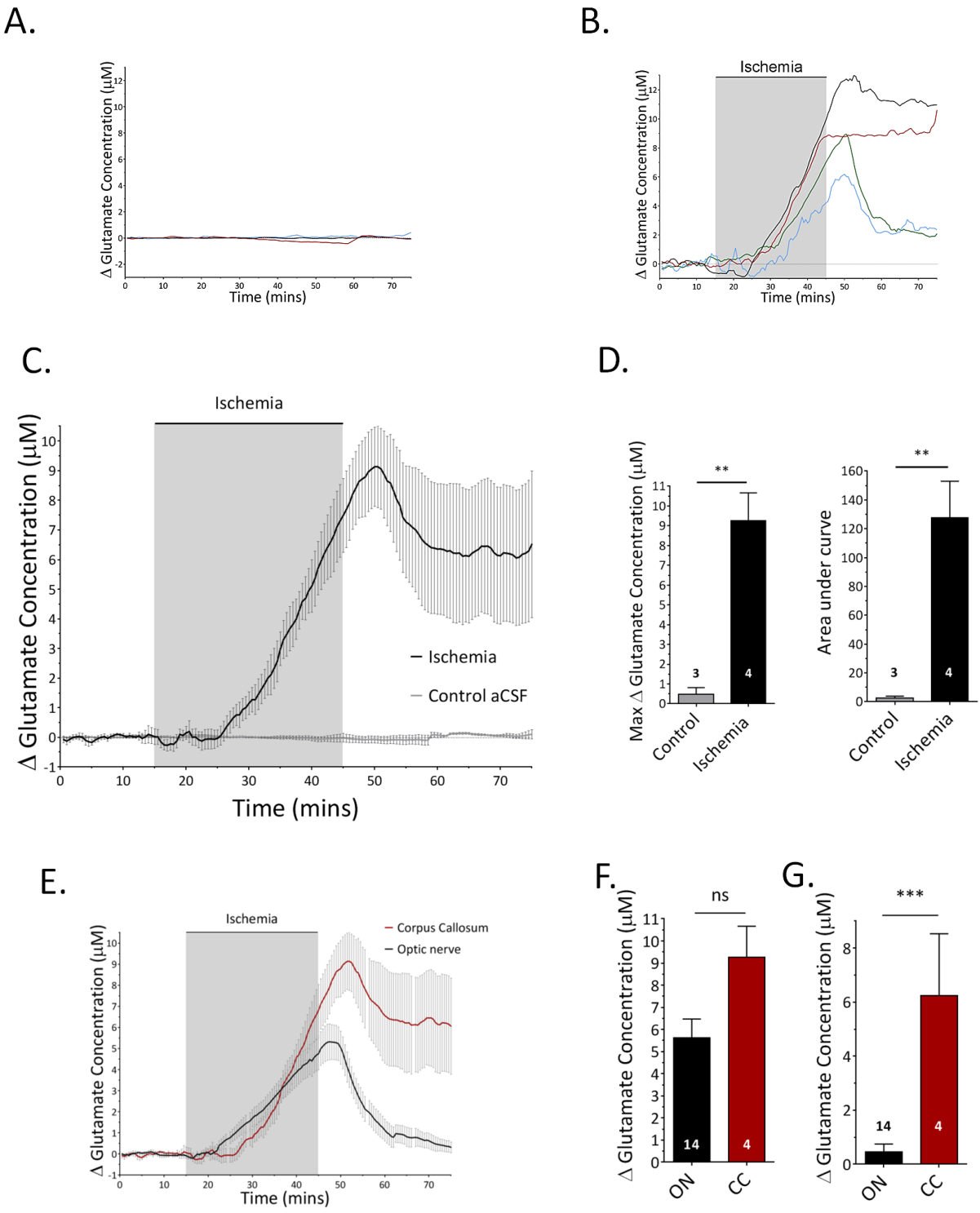

Fig. 4.5: Chemical-ischemia evokes a dramatic increase in extracellular glutamate concentration in the P10 rat CC.

a) Individual $[Glut]_e$ recordings under control conditions. **b)** Individual $[Glut]_e$ recordings during exposure to chemical-ischemia. **c)** Mean change (±SEM) in $[Glut]_e$ under ischemic and control conditions. **d)** Data summary comparing the maximum concentration change in extracellular glutamate and the area under the curve (total glutamate release) under both conditions. **e)** Overlay of ON (black) and CC (red) extracellular glutamate changes during chemical ischemia. Note the heightened $[Glut]_e$ during reperfusion in the CC. **f)** Histogram comparing the maximum peak concentration change in ON and CC. **g)** Histogram comparing the glutamate concentrations following 30 minutes of reperfusion in both tracts. ns $p>0.05$, ** $p<0.01$, *** $p<0.001$.

4.2.2 Reverse EAATs are not responsible for the ischemic rise in extracellular glutamate

Reverse glutamate transport is considered the primary mechanism of ischemic glutamate release in GM regions of the CNS (Rossi, Oshima et al. 2000, Baltan, Besancon et al. 2008). In an effort to reveal the mechanism(s) of glutamate release in developing WM, the reversal of EAATs posed as an attractive starting point. While the expression of functional EAATs has previously been reported in the developing ON (Arranz, Hussein et al. 2008), their capacity to maintain low extracellular concentrations has not. RONs were initially perfused with the potent glutamate transport blocker TBOA (200µM) under control conditions. Exposure to TBOA induced a significant rise in $[Glut]_e$, increasing by 0.43±0.06µM within 10 minutes (*n*=22, p<0.0001, Fig. 4.6b-c). $[Glut]_e$ remained elevated in the presence of TBOA. In contrast, there was no detectable rise in time-matched controls (*n*=4, Fig. 4.6a,c). These findings demonstrate the physiological regulation of extracellular glutamate by glutamate transporters in developing WM.

To access the potential involvement of reverse transport during ischemia, ONs were subject to chemical-ischemia in the presence of TBOA. Surprisingly, perfusion with TBOA (15 minutes before, during and 15 minutes after the insult) had no significant effect on either the onset or total glutamate release during ischemia, with concentrations increasing by 4.10±0.97µM (*n*=6, p=0.99 (*v control ischemia*), Fig. 4.7a-b). To further probe the involvement of EAATs, we took advantage of their Na^+-dependency and examined release under zero-Na^+ conditions (DeSilva, Kabakov et al. 2009). Nerves were perfused with a zero-Na^+ aCSF solution (NMDG substituted) for a minimum of 20 minutes before exposure to chemical-ischemia. Consistent with the TBOA findings, there was no significant reduction in overall glutamate release under these conditions, with concentrations increasing by 4.64±0.22µM (*n*=4, p=0.99, Fig. 4.8a-b).

Excitotoxic injury mediates a significant component of ischemia-induced functional injury in the P10 RON (Alix and Fern 2009). To further validate my findings, electrophysiological CAP recordings were examined in the presence of TBOA. Exposure to TBOA did not alter baseline CAP amplitude under control conditions. Moreover, it had no effect on either the latency to CAP failure during chemical-ischemia, nor did it improve CAP recovery following reperfusion (1.31±1.08%, *n*=4 (*v 6.49±2.23% (control)*), p=0.18, Fig. 4.9a-c). CAP recordings were also

examined using oxygen-glucose deprivation (OGD) as an alternative model of ischemia. CAP amplitude gradually declined over the course of 60-minutes of OGD, but did not block out, reaching 7.47±1.28% of its initial size. Following 90 minutes of reperfusion, CAP amplitude recovered to 36.27±5.44% (*n*=8, see Fig. 4.9e). Again, experiments were repeated in the presence of TBOA (15 minutes before, during and 15 minutes after). TBOA did not alter the rate of CAP decline during OGD, reaching 8.27±2.38% after 60 minutes. Furthermore, there was no significant improvement in CAP amplitude following reperfusion (31.52±5.67%, *n*=8, p=0.55, Fig. 4.9d-f). Together these experiments show that while EAATs regulate extracellular glutamate under physiological conditions, they are not the primary source of excitotoxic glutamate release under ischemic conditions.

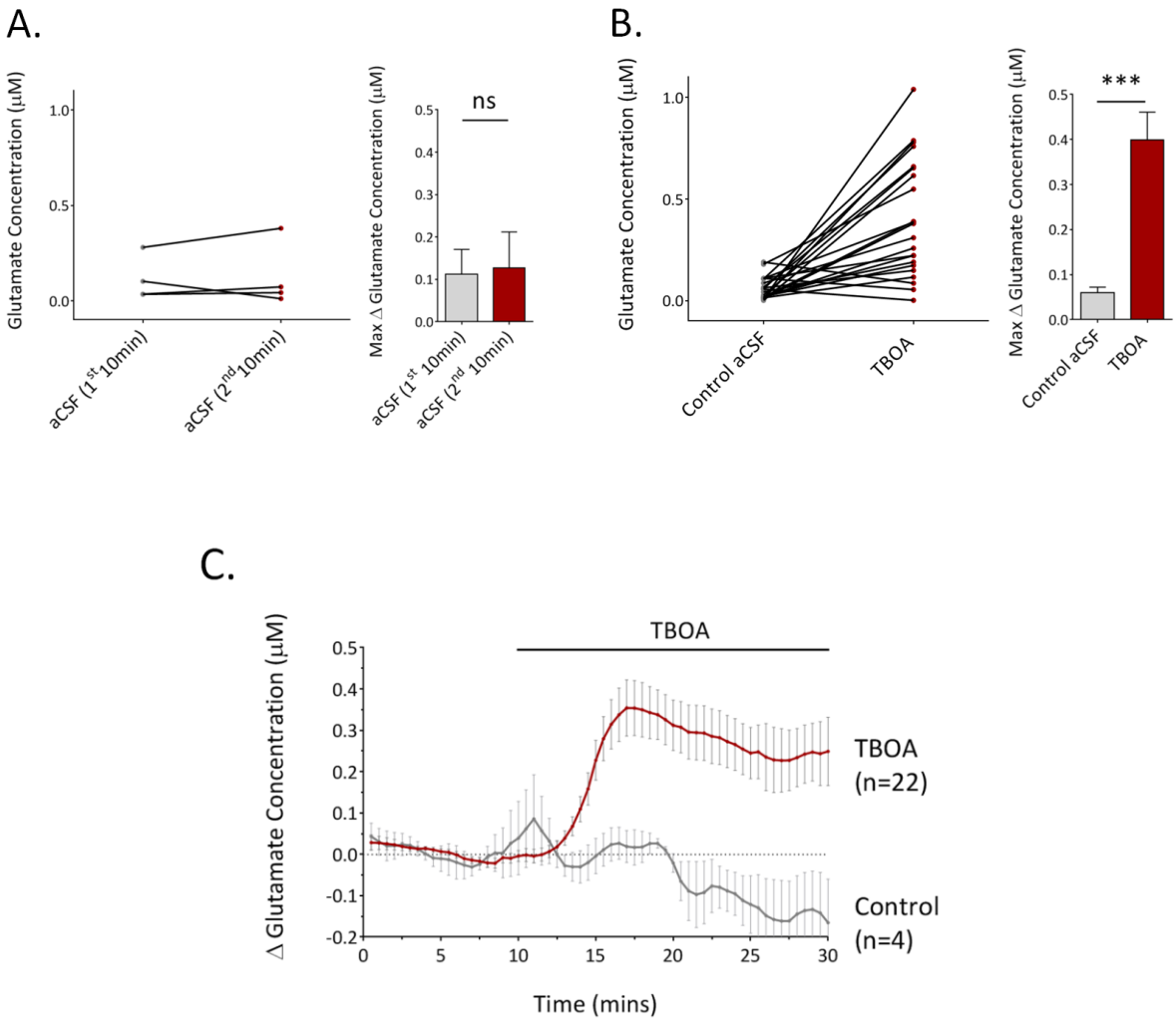

Fig. 4.6: Functional EAATs regulate extracellular glutamate under physiological conditions.

a) The maximum glutamate concentration recorded during two sequential time periods in control aCSF (i.e. 0-10mins (grey) v 10-20 mins (red)). **b)** The maximum glutamate concentration recorded in control aCSF (grey) and in the presence of TBOA (red). **c)** Time-course of extracellular glutamate demonstrating a rise in resting $[Glut]_e$ following exposure to TBOA. *** $p<0.001$.

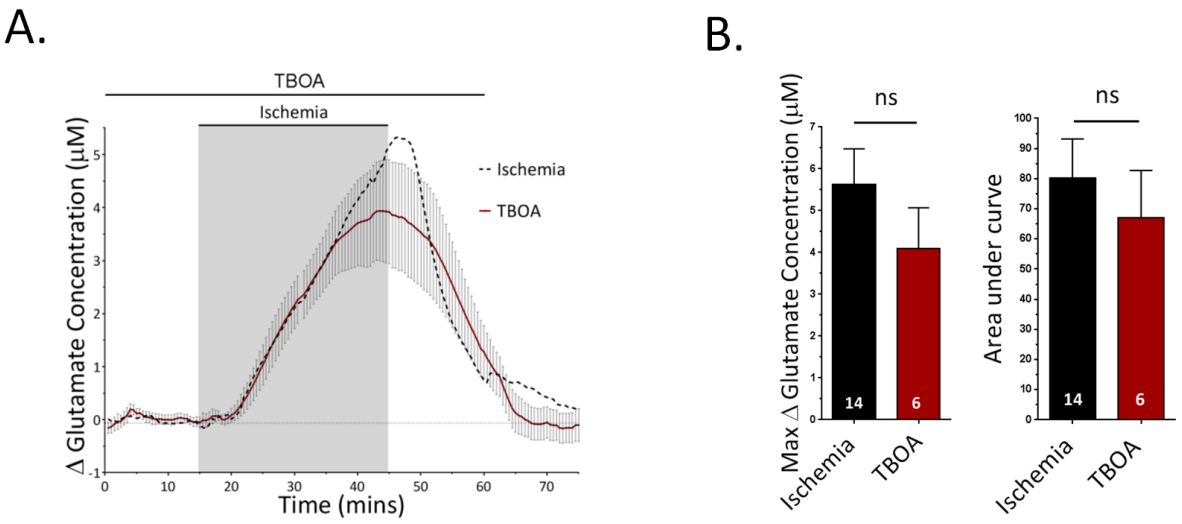

Fig. 4.7: Inhibition of EAATs with TBOA does not prevent the rise in extracellular glutamate under ischemic conditions.

a) Ischemia-induced glutamate release in the presence of TBOA. **b)** Histogram showing the effect of TBOA on ON $[Glut]_e$. ns $p>0.05$.

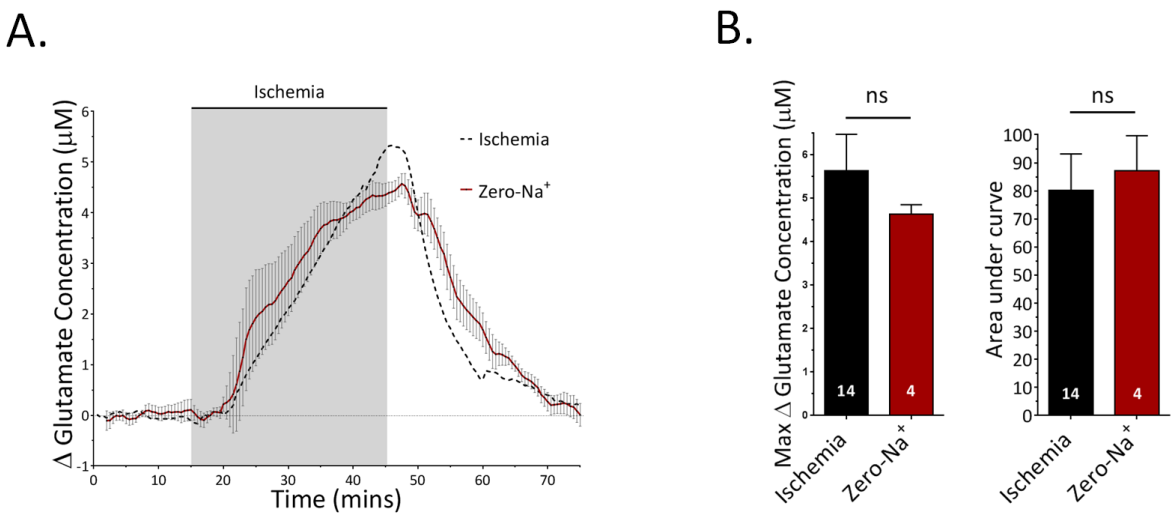

Fig. 4.8: Removal of extracellular Na^+ does not prevent the rise in extracellular glutamate under ischemic conditions.

a) Ischemia-induced glutamate release under zero-Na^+ conditions. **b)** Histogram showing the effect of zero-Na^+ on extracellular glutamate. ns $p>0.05$.

Fig. 4.9 →(*next page*): Inhibition of EAATs with TBOA, does not improve CAP recovery following chemical ischemia or OGD.

a) Representative CAP trace showing no improvement in functional recovery in the presence of TBOA, following 30 minutes of chemical-ischemia (black=before, red=after). **b,c)** CAP time-course and histogram demonstrating how TBOA does not prevent the irreversible CAP decline during chemical-ischemia. **d)** Representative CAP trace showing no improved functional recovery in the presence of TBOA following 60 minutes of OGD (black=before, red=after). **e,f)** CAP time-course and histogram demonstrating how TBOA does not prevent the irreversible CAP decline during OGD. ns $p>0.05$.

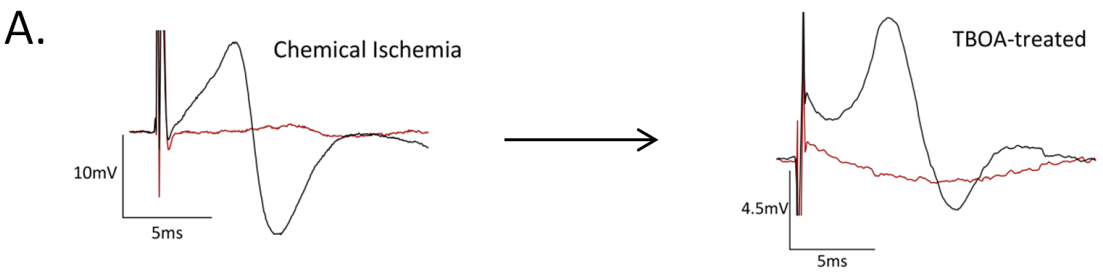
A.
Chemical Ischemia
10mV
5ms
TBOA-treated
4.5mV
5ms

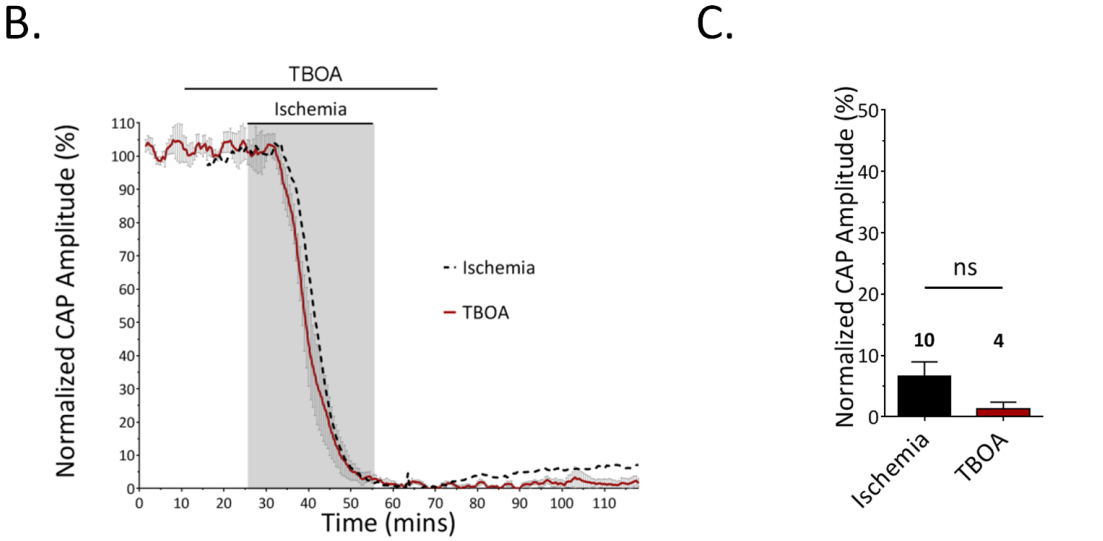
B.
TBOA
Ischemia
Normalized CAP Amplitude (%)
Ischemia
TBOA
Time (mins)
C.
Normalized CAP Amplitude (%)
ns
10
4
Ischemia
TBOA

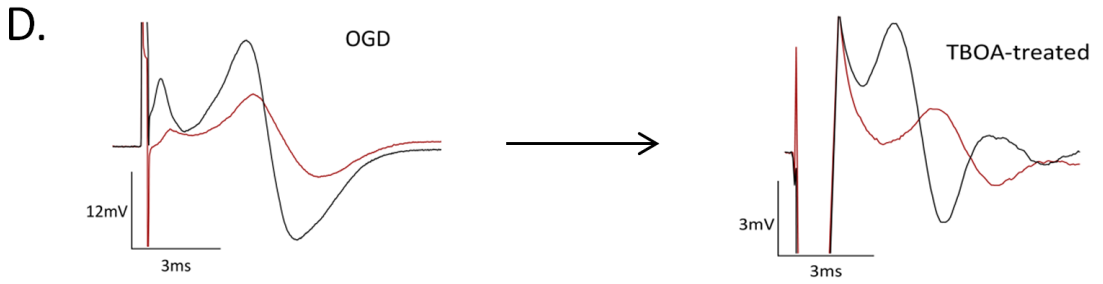
D.
OGD
12mV
3ms
TBOA-treated
3mV
3ms

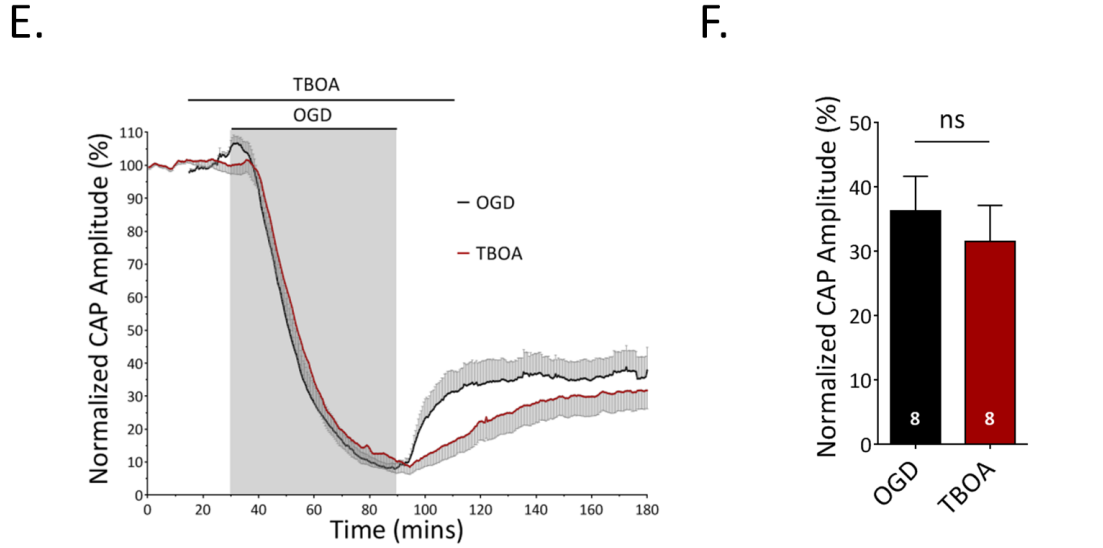
E.
TBOA
OGD
Normalized CAP Amplitude (%)
OGD
TBOA
Time (mins)
F.
Normalized CAP Amplitude (%)
ns
8
8
OGD
TBOA

4.2.3 Excessive vesicular fusion significantly contributes to elevated glutamate concentrations during ischemia.

Next, I investigated whether vesicular glutamate release contributes to the rise in $[Glut]_e$. Data from the previous chapter demonstrated that vesicular fusion along WM axons is capable of significantly elevating $[Glut]_e$. To examine the significance of Ca^{2+}-dependant vesicular release during modelled ischemia, $[Glut]_e$ was initially monitored under zero-Ca^{2+} conditions. Extracellular Ca^{2+} (i.e. $CaCl_2$) was omitted from the perfusing aCSF solution and EGTA (50µM) was added to chelate trace Ca^{2+} down to low nM concentrations (Alix and Fern 2009). RONs were exposed to zero-Ca^{2+} aCSF 20 minutes before the start of chemical-ischemia, during and for the initial 35 minutes of reperfusion, a protocol which was maximally protective in a previous study (Alix and Fern 2009). Under zero-Ca^{2+} conditions, $[Glut]_e$ gradually increased when nerves were rendered ischemic. Although significance was not reached, total glutamate release did appear reduced under these conditions (2.86±0.64µM, *n*=5, p=0.18, Fig. 4.10a-b).

We reasoned that the rise in intracellular Ca^{2+}, which is necessary for vesicular exocytosis, may also originate from intracellular stores (Ren, Ridsdale et al. 2000, Ransom and Brown 2003, Micu, Plemel et al. 2016). To eliminate any potential rises in intracellular Ca^{2+}, experiments were repeated using BAPTA-AM-treated nerves. Nerves were initially incubated in BAPTA-AM (50µM), a membrane permeable form of the intracellular Ca^{2+} chelator, BAPTA, for 90 minutes. Ischemia-induced glutamate release in BAPTA-AM treated nerves was significantly reduced under zero-Ca^{2+} conditions (1.88±0.38µM, *n*=4, p=0.03, Fig. 4.10c-d). However, there was no significant difference between BAPTA-AM treated and untreated nerves (p=0.98), and so the source of intracellular Ca^{2+} is inconclusive. Nonetheless, the extracellular rise in glutamate seemingly operates via a Ca^{2+}-dependant mechanism, as predicted for vesicular fusion.

In an effort to directly prevent vesicular glutamate release, I investigated the effect of bafilomycin-a1 (baf-a1, 50nM) (Hansen, Garrido-Comas et al. 2015). Baf-a1 is a selective inhibitor of the vacuolar-type H^+ ATPase (V-ATPase), responsible for producing a positive membrane potential and high concentration of H^+ ions within vesicles. As mentioned, VGLUTs utilize the high H^+ gradient to package glutamatergic vesicles. The inhibition of the V-ATPase

will lead to an inevitable run-down of the H^+ gradient, and thus, the gradual depletion of vesicular glutamate stores. RONs were perfused with baf-a1 for 120 minutes before exposure to ischemia. However, reports claim that the application of baf-a1 doesn't completely deplete glutamatergic vesicular stores unless vesicular turnover is promoted in the presence of baf-a1 (Cavelier and Attwell 2007). Considering the rationale behind vesicle-depletion with baf-a1 and the fact that high-K^+ evokes vesicular fusion in WM (see previous chapter), nerves were briefly perfused with a 'high-K^+' (10mM) aCSF solution (x2) during the 120 minute baf-a1 pre-treatment period. Exposure to high-K^+ caused a considerable drop in CAP amplitude, decreasing by 26.86±5.01% (*n*=3) after 5 minutes, and by 42.68±16.95% (*n*=3) after 10 minutes (Fig. 4.11a-c). However, it had no significant effect on CAP amplitude after wash-out (97.26±1.43% (start) v 98.13±11.46% (end), *n*=3, p=0.94, Fig. 4.11c).

Following this pre-treatment protocol, and in the continued presence of baf-a1, glutamate release was significantly attenuated during 30 minutes of chemical-ischemia, with a maximum increase of 1.15±0.29µM (*n*=4), versus 4.55±0.82µM (*n*=6) in time-matched controls (p=0.0056, Fig. 4.12a-b). Using the same pre-treatment protocol (i.e. brief exposures to high-K^+), glutamate release was also monitored in the presence of rose bengal (RB; 50µM), a potent inhibitor of VGLUTs. Similarly, RB significantly reduced the rise in $[Glut]_e$ during ischemia (1.98±0.47µM, *n*=6, p=0.013, Fig. 4.12c-d), confirming the involvement of vesicular exocytosis.

Given that vesicular glutamate release mediates a significant component of the elevated $[Glut]_e$, I next attempted to determine whether depleting nerves of their vesicular stores can reduce irreversible injury during ischemia. The 'high-K^+' pre-treatment protocol had no significant effect on CAP recovery following 60 minutes of OGD, when compared to control OGD experiments (control OGD: 45.98±5.69% (*n*=14), v high-K^+ OGD: 51.55±6.54% (*n*=4), p=0.63, Fig. 4.13a-b). For this reason, the OGD data was pooled (pooled OGD: 47.04±4.58% (*n*=18)). In the presence of baf-a1, there was a significant improvement in CAP amplitude recovery post-OGD (68.44±8.03%, *n*=9, p=0.04, Fig. 4.13c-e). Together, these findings strongly indicate that excessive vesicular fusion mediates a significant component of the early rise in extracellular glutamate levels.

While inhibiting vesicular fusion significantly reduced glutamate release, it did not completely abolish the rise in $[Glut]_e$. This suggests that an alternative mechanism of release may be

operating alongside vesicular fusion. I therefore, re-examined the involvement of reverse EAATs. $[Glut]_e$ was measured from baf-a1 treated nerves, in the presence of TBOA (200µm). As expected, glutamate release was significantly reduced when compared to control nerves (1.34±0.18µM, *n*=5, p=0.002, Fig. 4.14a-b). However, there was no additive reduction in total glutamate release when compared to baf-a1 treated nerves in the absence of TBOA (p=0.57).

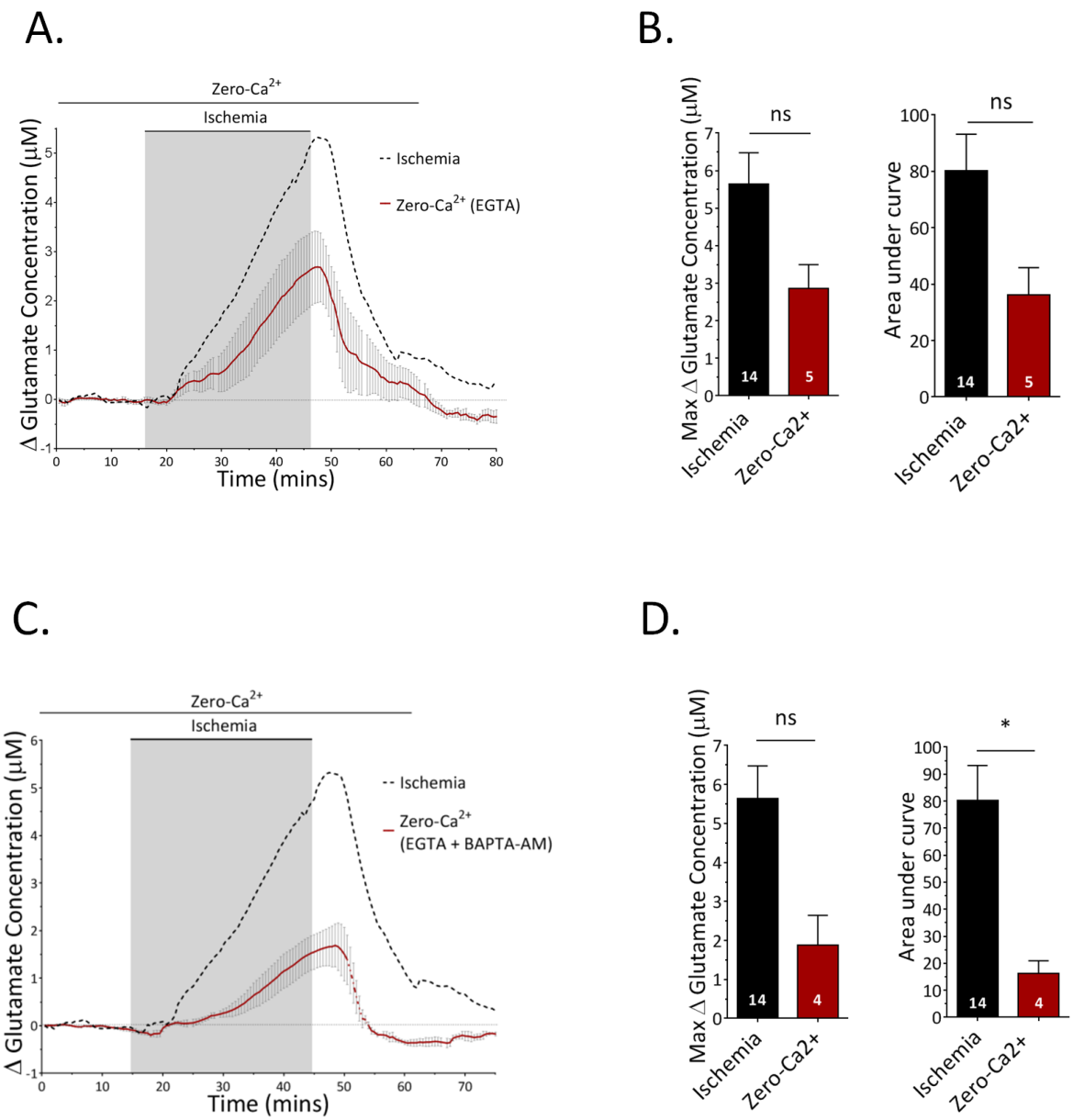

Fig. 4.10: Glutamate release is significantly attenuated under zero-Ca^{2+} conditions.

a) Ischemia-induced glutamate release in a zero-Ca^{2+} aCSF solution containing 50μM EGTA. **b)** Histogram demonstrating the effect of zero-Ca^{2+} on $[Glut]_e$. **c)** Ischemia-induced glutamate release from BAPTA-AM treated ONs in a zero-Ca^{2+} aCSF solution containing 50μM EGTA. **d)** Histogram demonstrating the effect of chelating extracellular and intracellular Ca^{2+} on $[Glut]_e$. ns $p>0.05$, *$p<0.05$.

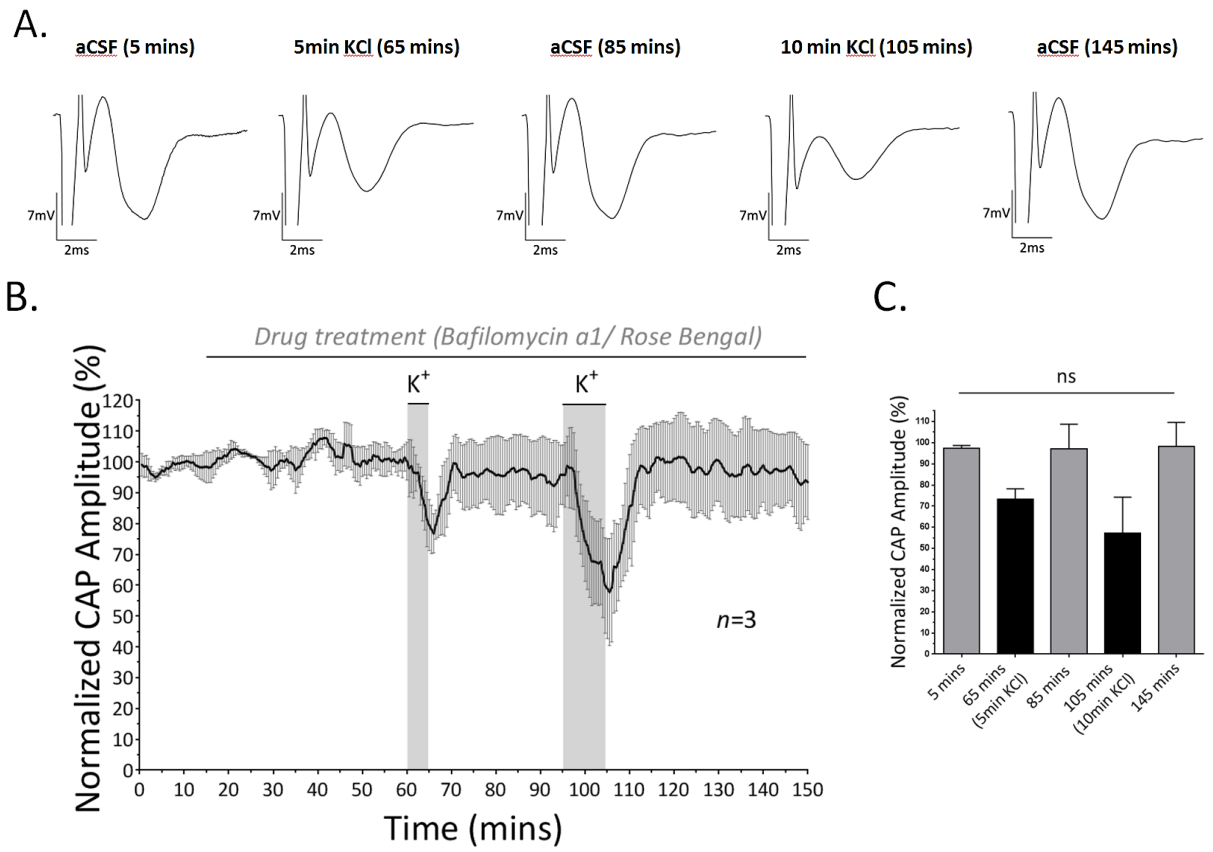

Fig. 4.11: Perfusing nerves with 10mM KCl aCSF to promote vesicular turnover, reversibly decreases CAP amplitude.

a) Representative CAP images recorded from the P10 RON in control aCSF and following either 5 or 10 minutes of 10mM KCl aCSF. Time points correspond to the CAP time-course below (b). **b)** CAP amplitude plotted against time showing a decrease in amplitude during perfusion with 10mM KCl. **c)** Histogram showing no significant difference in CAP amplitude after two successive exposures to 10mM KC. ns $p>0.5$.

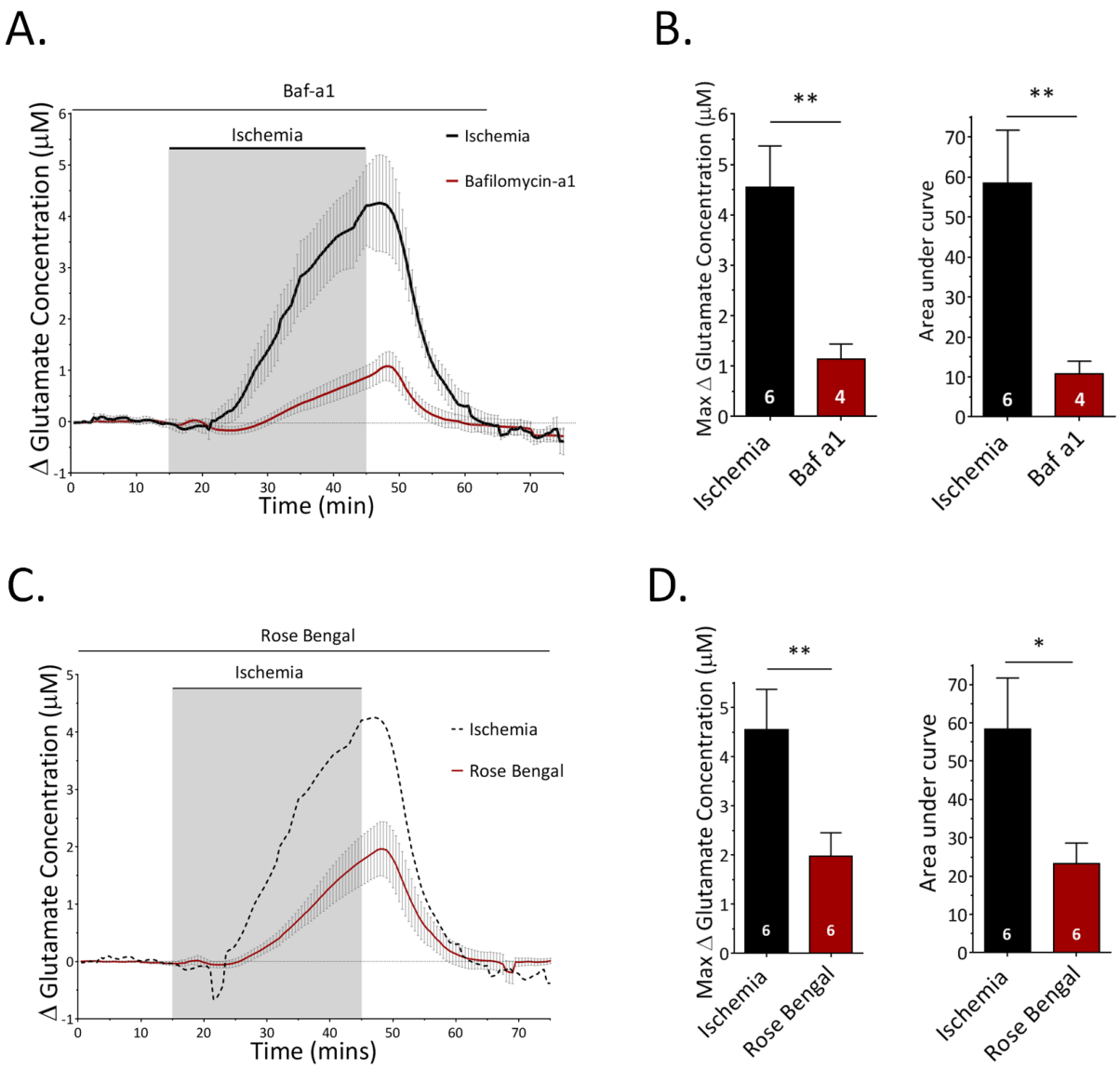

Fig. 4.12: The rise in extracellular glutamate is significantly reduced in vesicle-depleted nerves.

a) Ischemia-induced glutamate release in bafilomycin-a1 treated nerves. **b)** Histogram demonstrating the effect of bafilomycin-a1 on $[Glut]_e$. **c)** Ischemia-induced glutamate release in rose bengal treated nerves. **d)** Histogram demonstrating the effect of rose bengal on $[Glut]_e$. *p<0.05, **p<0.01.

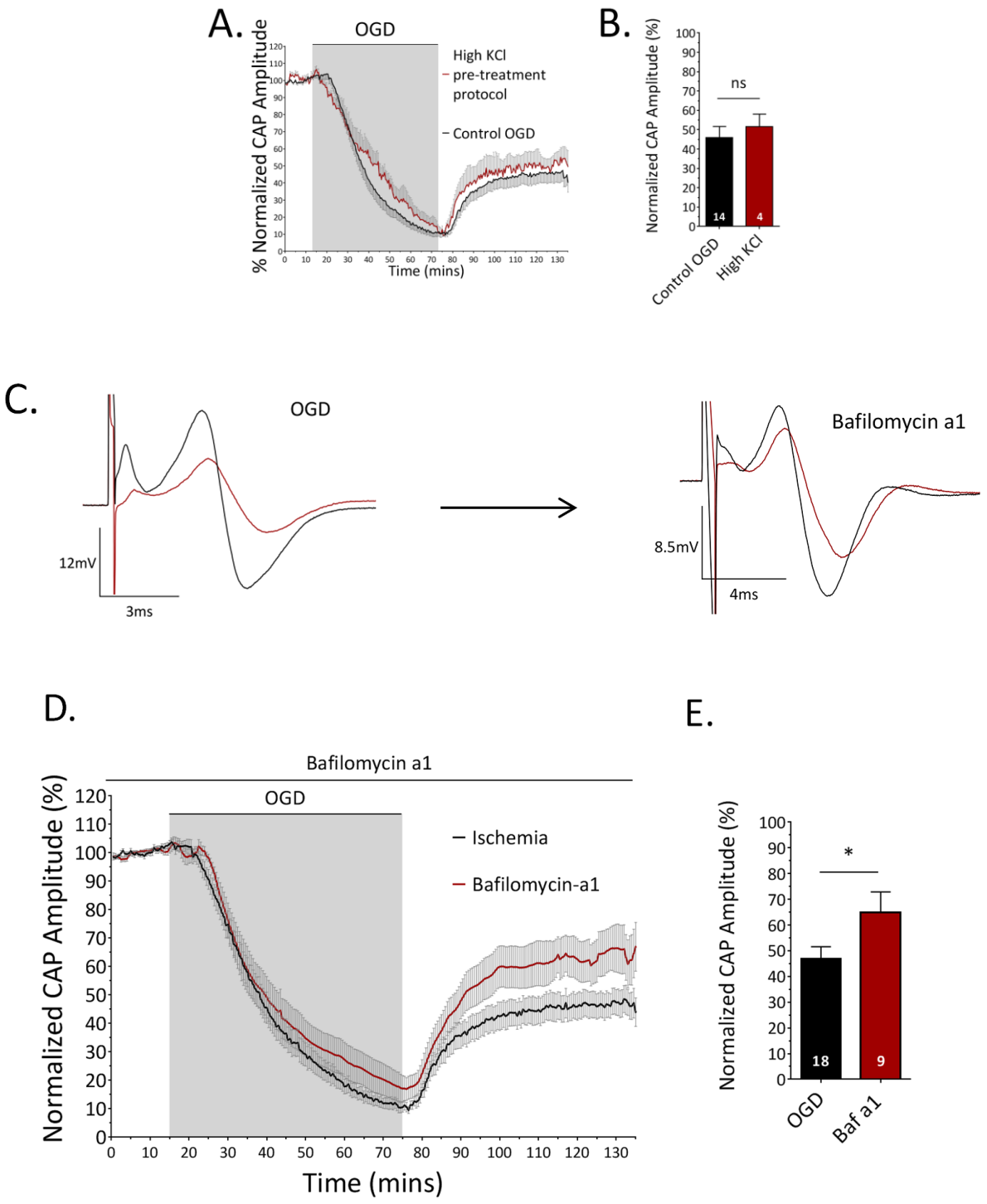

Fig. 4.13: Depleting nerves of their vesicular stores, significantly improves functional recovery following 60 minutes of OGD.

a) CAP time-course showing no significant difference in OGD sensitivity between nerves which were pre-exposed to 10mM KCl and those which were not (control OGD). **b)** Histogram showing no significant difference in CAP amplitude between the two groups. **c)** Representative CAP traces from control OGD and bafilomycin-a1 treated OGD (black: before, red: after) **d)** Bafilomycin-a1 treated nerves (vesicle depleted) show an improvement in CAP recovery after 60 minutes of OGD**. e)** Data summary of CAP recovery showing significant functional protection following bafimomycin-a1 treatment. ns $p>0.05$, * $p<0.05$.

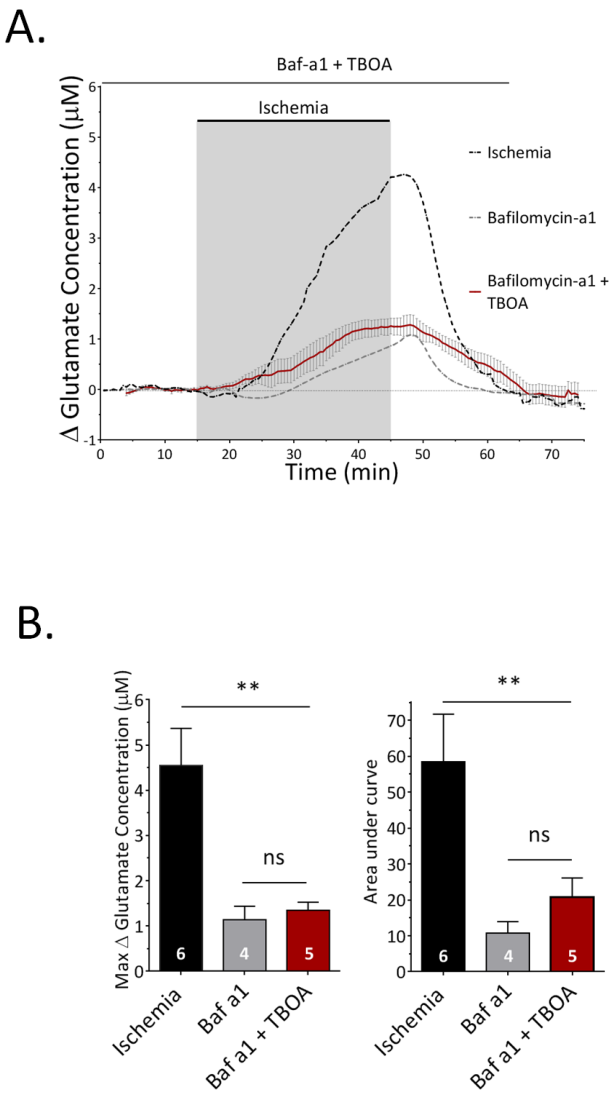

Fig. 4.14: Blocking EAATs with TBOA does not abolish the remaining rise in glutamate from bafilomycin-a1 treated nerves.

a) Ischemia-induced glutamate release from bafilomycin-a1 treated nerves in the presence of TBOA. **b)** Histogram demonstrating the effect of bafilomycin-a1 and TBOA on $[Glut]_e$. ns $p>0.05$, $^{**}p<0.01$.

4.2.4 Blocking alternative glutamate release pathways did not significantly reduce the ischemic rise in extracellular glutamate

Considering vesicular fusion does not fully account for the rise in $[Glut]_e$, I investigated three alternative glutamate release mechanisms which could potentially contribute to the high $[Glut]_e$ in developing WM. As previously mentioned, the activation of the NKCC co-transporter during ischemia promotes astrocyte cell swelling. In addition, swelling opens a range of VRACs, which are capable of glutamate release. To determine whether swelling-mediated mechanisms of glutamate release operate during acute ischemia, $[Glut]_e$ was monitored in the presence of furosemide (5mM), an effective NKCC inhibitor. However, the application of furosemide had no significant effect on glutamate release, with concentrations reaching 6.53±1.62µM (*n*=6, p=0.99, Fig. 4.15a-b). In addition, glutamate release was also examined in the presence of NPPB (100µM), a VRAC blocker. Yet again, this had no significant effect on $[Glut]_e$ (3.43±0.88µM, *n*=5, p=0.78, Fig. 4.15c-d). Together, this indicates that swelling-mediated glutamate release does not contribute to the excitotoxic build-up of extracellular glutamate.

Next, I proceeded to test the potential for glutamate efflux via gap junction hemi-channels. Glutamate release was monitored in the presence of the gap-junction blocking agent, carbenoxolone (100µM)(Ye, Wyeth et al. 2003). However, this had no significant effect on the $[Glut]_e$ time-course during ischemia, with concentrations reaching 4.41±0.81µM (*n*=6) following 30 minutes of chemical ischemia (p=0.67, Fig. 4.16a-b).

Finally, I examined potential glutamate release via the glutamate-cystine antiporter. To do this, $[Glut]_e$ was monitored in the presence of sulfasalazine (250µM) (Soria, Pérez-Samartín et al. 2014), a non-substrate inhibitor of the glutamate-cystine antiporter. Again, sulfasalazine did not have a significant effect on either the latency or magnitude of glutamate release during ischemia, with peak concentrations reaching 6.01±1.10µM (n=5, p=0.99, Fig. 4.16c-d).

Together it demonstrates that vesicular exocytosis is the primary mechanism of ischemic glutamate release in developing WM (Fig. 4.17a-b). However, it must be noted that although no significant contribution was found with EAATs, swelling-mediated release, hemi-channels

or the glutamate-cystine antiporter, the blockade of vesicular release did not completely prevent the rise in $[Glut]_e$.

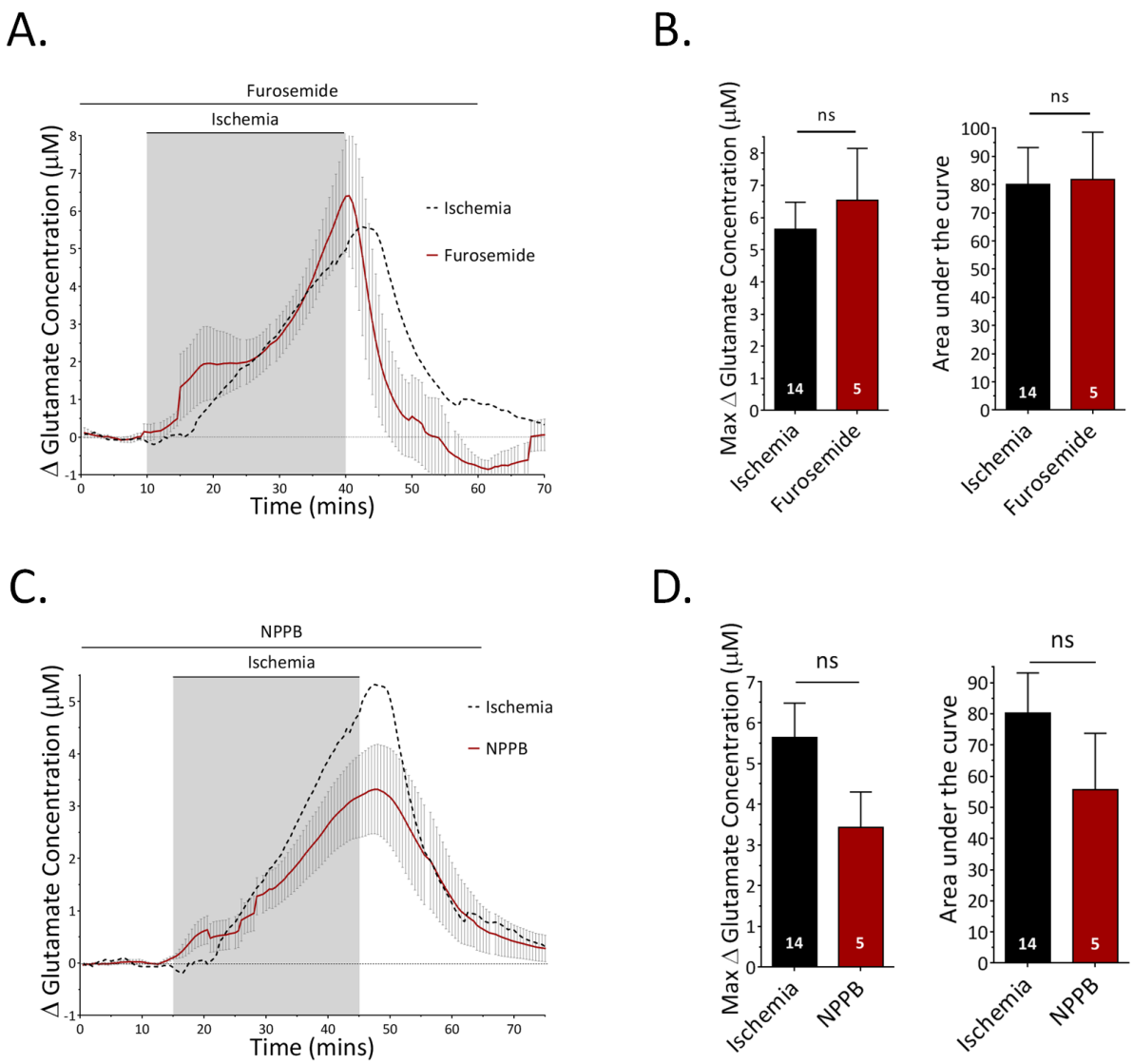

Fig. 4.15: Swelling-mediated glutamate release does not significantly contribute to the rise in extracellular glutamate.

a) Ischemia-induced glutamate release in the presence of furosemide. **b)** Histogram showing the effect of furosemide on $[Glut]_e$. **c)** Ischemia induced glutamate release in the presence of NPPB. **d)** Histogram showing the effect of NPPB on $[Glut]_e$. ns $p>0.05$.

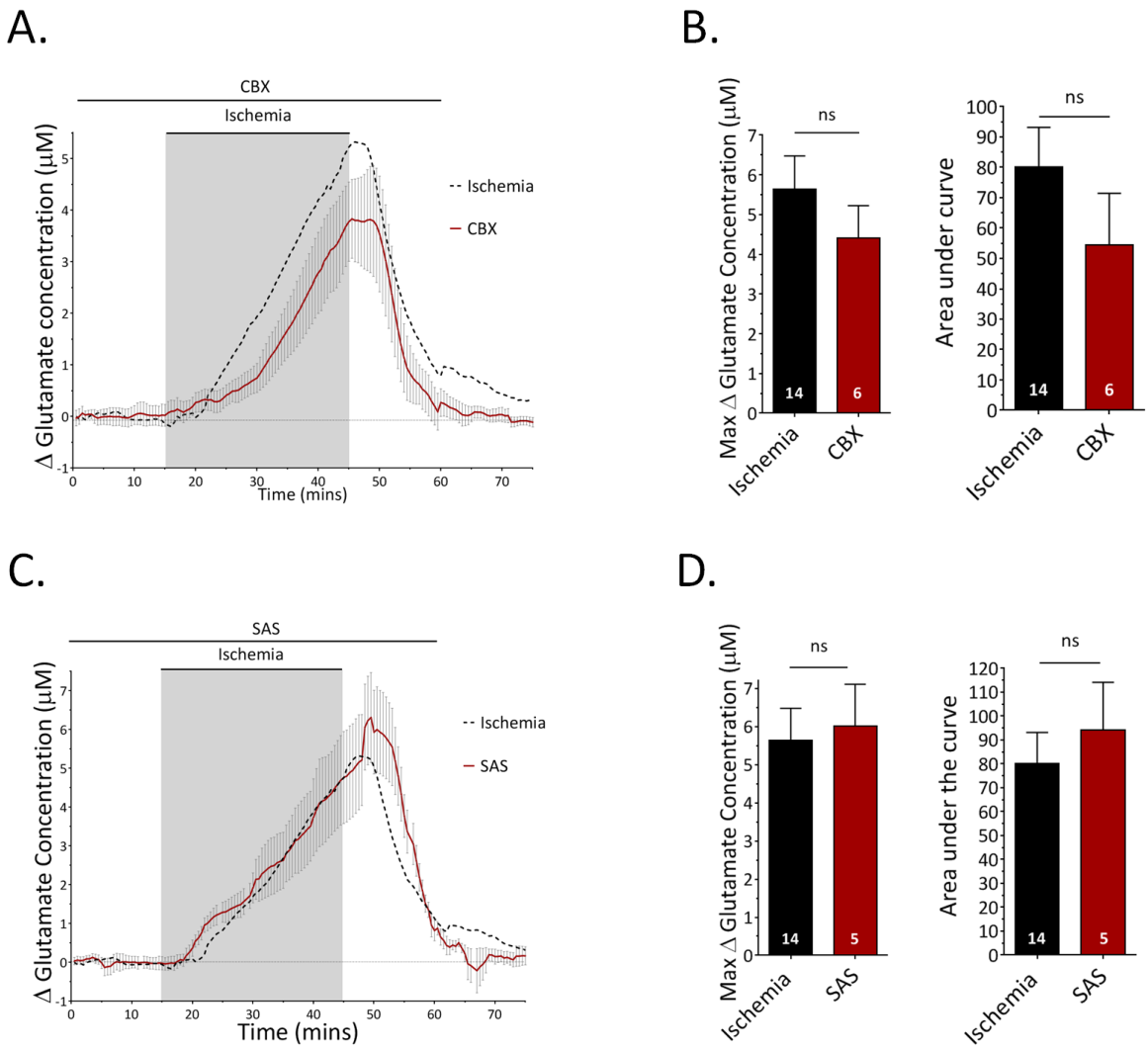

Fig. 4.16: Blocking either hemichannels or the glutamate-cystine antiporter does not prevent the rise in $[Glut]_e$.

a) Ischemia-induced glutamate release in the presence of carbenoxolone (CBX). **b)** Histogram showing the effect of carbenoxolone on $[Glut]_e$. **c)** Ischemia induced glutamate release in the presence of sulfasalazine (SAS). **d)** Histogram showing the effect of sulfasalazine $[Glut]_e$. ns $p>0.05$.

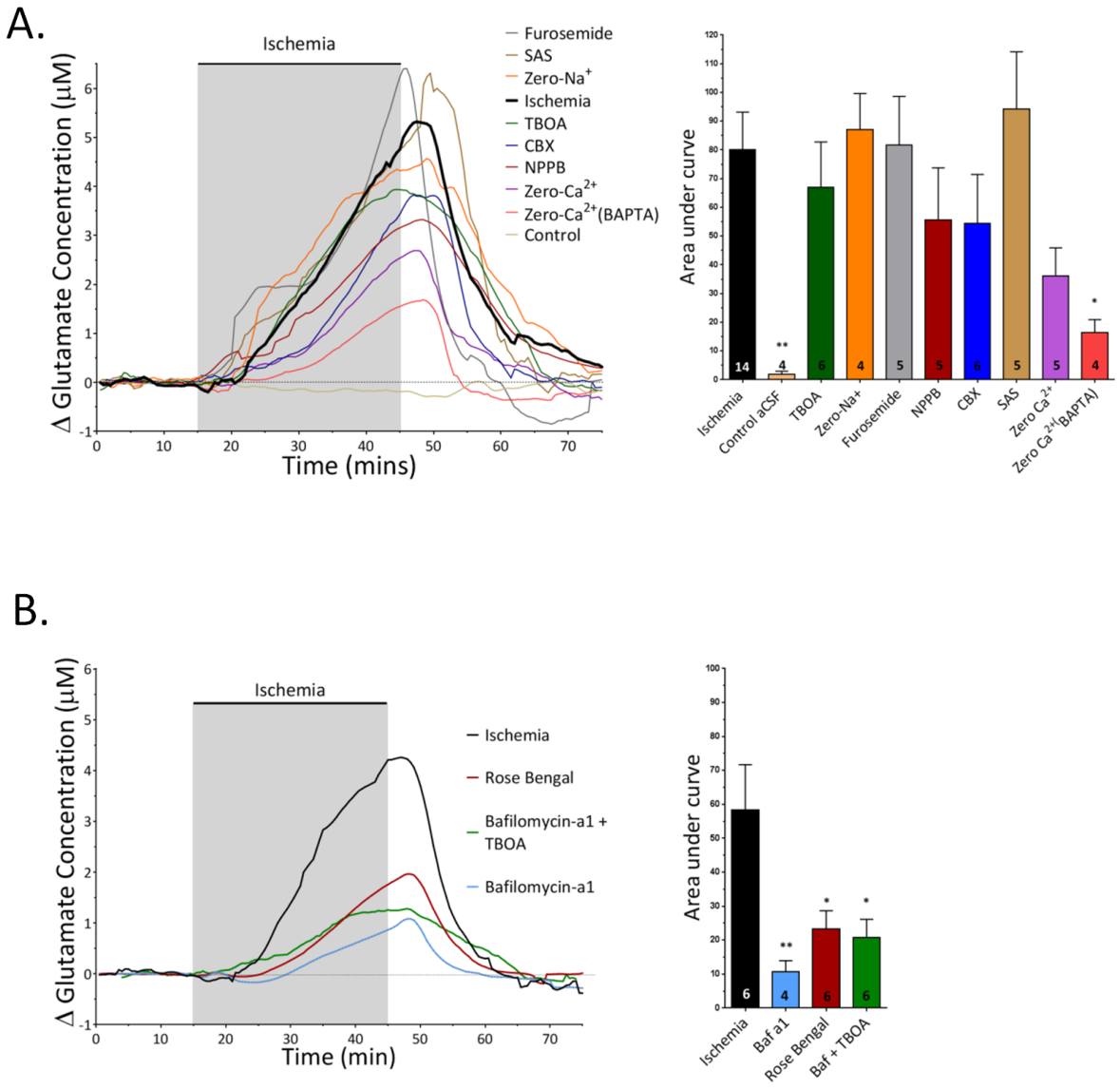

Fig. 4.17: Summary of $[Glut]_e$ recordings during exposure to modelled ischemia under all conditions and pharmacological treatments.

Techniques aimed at preventing vesicular glutamate release significantly reduce the rise in extracellular glutamate during 30 minutes of ischemia.

4.3 Results: Part (b): Adult WM

4.3.1 Ischemia-induced rise in extracellular glutamate in adult WM

Glutamate receptor-mediated injury is also implicated in the development of ischemic WM damage in mature WM (Stys 1998, Tekkok, Ye et al. 2007, Baltan, Besancon et al. 2008). Given that ischemia evokes a robust rise in $[Glut]_e$ in the developing RON, I sought to determine whether the same can be said for the adult RON. And if so, is release via the same mechanism?

Initially, resting $[Glut]_e$ was measured within the adult RON (>P90) in oxygenated aCSF. The mean resting $[Glut]_e$ was 8.9±1.4µM (*n*=40), significantly higher than the P10 RON (1.36±0.31µM, *n*=70, p<0.01, Fig. 4.18). Resting $[Glut]_e$ in the adult RON was also significantly higher than the adult CC and adult mouse optic nerve (MON) which were 1.61±1.8µM (*n*=15) and 2.87±1.4µM (*n*=5), respectively.

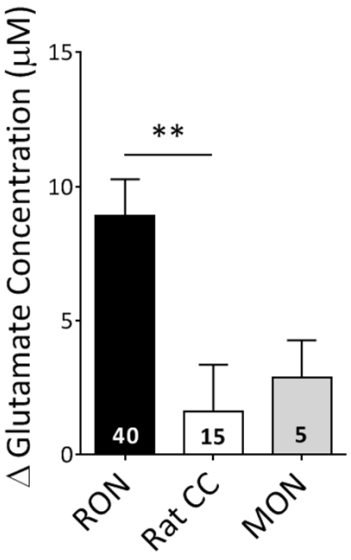

Fig. 4.18: Resting $[Glut]_e$ in adult WM.

Bar chart comparing the resting $[Glut]_e$ in the adult RON, CC and MON. Measurements were taken in control oxygenated aCSF (mean ± SEM). **= p<0.01.

Unlike the P10 RON, 30-minutes perfusion with 1nM rotenone/zero-glucose did not lead to irreversible functional damage (data not shown). For this reason, nerves were perfused with a known effective concentration of antimycin-a (25µM) and zero-glucose aCSF (chemical-ischemia) (Allen, Káradóttir et al. 2005, Bakiri, Hamilton et al. 2008). To access functional

recovery following exposure to chemical-ischemia, CAP area was monitored over time. CAP area remained relatively stable under control conditions, showing a slight increase following 165 minutes (116.0±5.75%, *n*=4, Fig. 4.19a,c-d). In contrast, simulation of ischemia (with antimycin-a/zero-glucose) resulted in a gradual decline in CAP area over the course of 60 minutes. CAP area did not recover following 60 minutes reperfusion (0.07±0.1%, *n*=3, p<0.0001, Fig. 4.19b-d).

$[Glut]_e$ remained stable under control conditions, with a maximum increase of 1.62±0.5µM (*n*=4) during 105 minutes of recording in oxygenated aCSF (Fig. 4.20a,c-d). Upon exposure to chemical-ischemia, there was a dramatic increase in $[Glut]_e$ within 5 minutes. Similar to the developing RON, the onset of glutamate release closely coincides with the early decline in CAP area (Fig. 4.20e-f, p=0.27). $[Glut]_e$ continuously increased throughout the ischemic period, reaching a maximum concentration of 26.96±6.0µM (*n*=13, p=0.04, Fig. 4.20b-d). Upon reperfusion, $[Glut]_e$ quickly decreased towards baseline levels. Due to the high variability in the adult RON, ischemic glutamate release data was split into two interleaved groups for analysis.

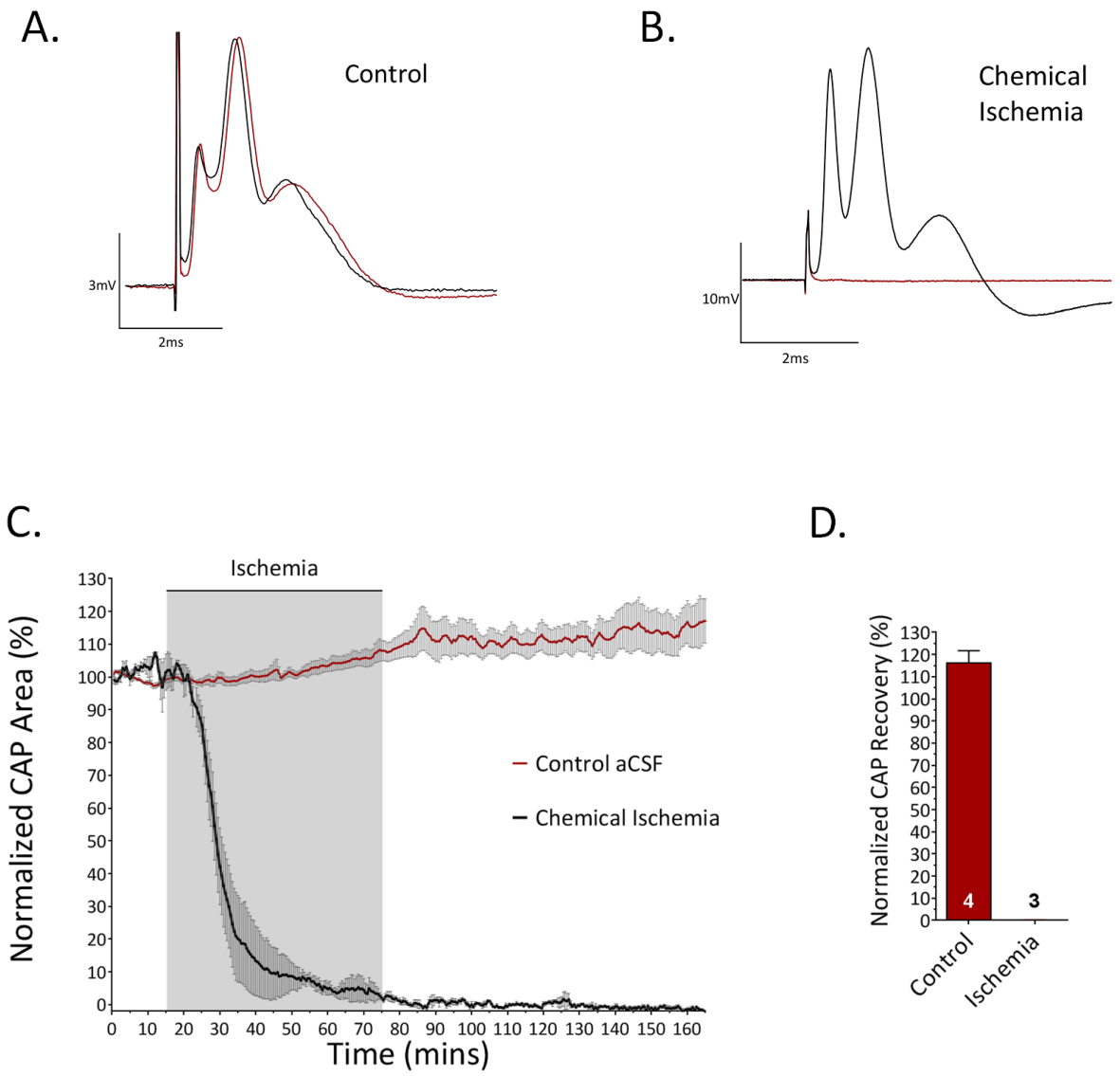

Fig. 4.19: Chemical-ischemia induced injury in the myelinated RON.

a) Representative CAP trace after 5 minutes (black) and 165 minutes (red) under control conditions. **b)** Representative CAP trace before (black; 5 mins) and after 60 minutes of chemical ischemia (red; 165 mins). **c)** CAP time-course comparing control conditions to chemical ischemia. **d)** CAP recovery under control conditions and following exposure to 60 minutes of chemical ischemia. **** p<0.0001.

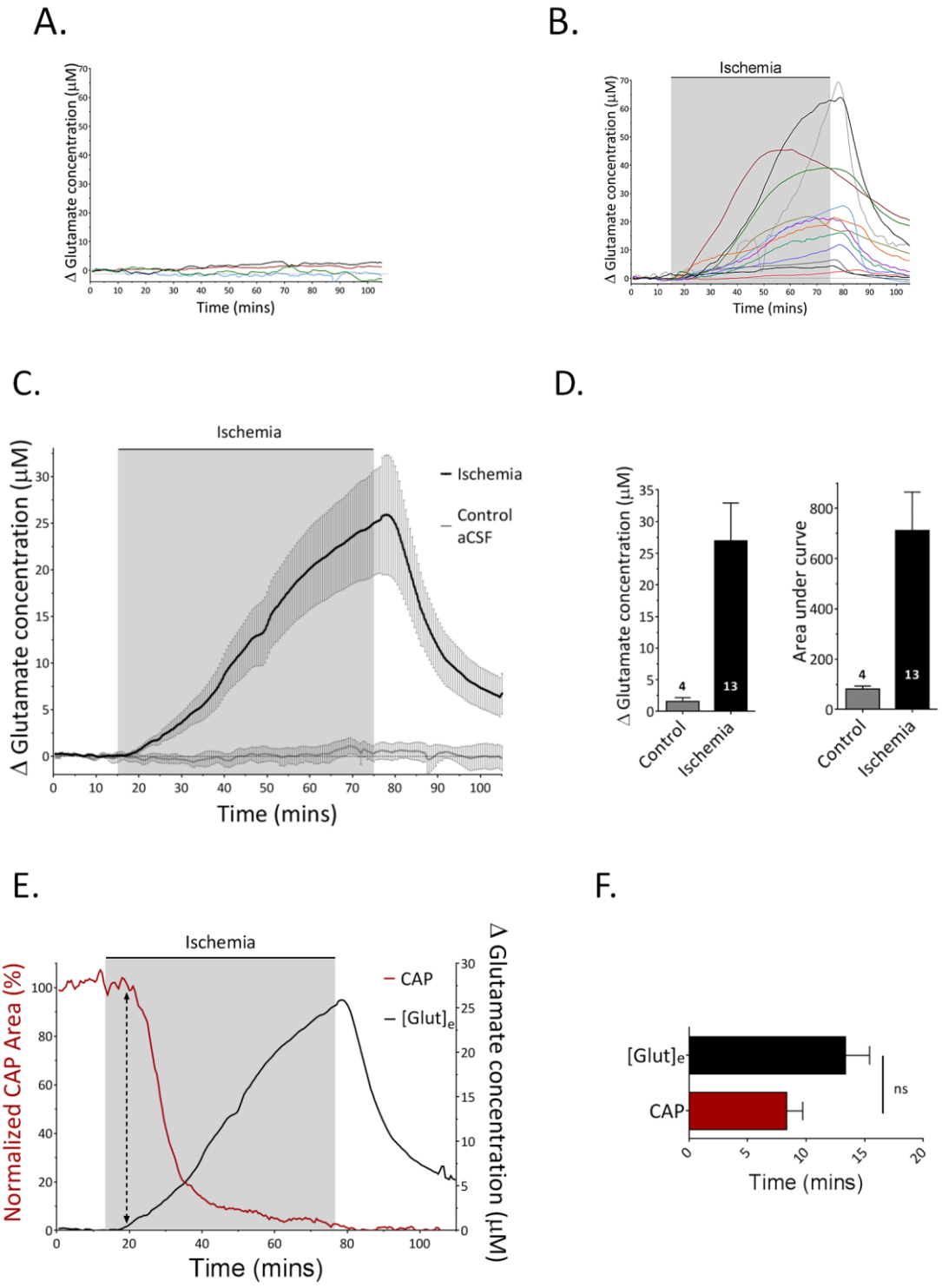

Fig. 4.20: Exposure to chemical-ischemia dramatically elevates extracellular glutamate concentrations in the adult RON.

a) Individual $[Glut]_e$ recordings under control conditions. **b)** Individual $[Glut]_e$ recordings during exposure to 60 minutes of chemical ischemia. **c)** Mean change (±SEM) in $[Glut]_e$ under control and ischemic conditions. **d)** Data summary comparing the maximum concentration change in $[Glut]_e$ and the area under the curve under control and ischemic conditions. **e)** Overlay of CAP amplitude (red) and $[Glut]_e$ (black) time course showing the early rise in $[Glut]_e$ as CAP begins to decline. **f)** Histogram comparing the time taken for $[Glut]_e$ to increase by 10%, and for CAP to decrease by 10%. ns $p>0.05$, ** $p<0.01$. ** $p<0.01$.

4.3.2 Reverse EAATs are not responsible for the ischemia-induced rise in extracellular glutamate in adult WM

The previous experiments on the developing RON showed that the reversal of EAATs do not contribute to the ischemia-induced rise in glutamate levels. This result was somewhat surprising considering several papers have reported EAATs as the source of glutamate release in mature WM tracts (Tekkok, Ye et al. 2007, Hamilton, Kolodziejczyk et al. 2016). Therefore, it is plausible that developmental changes of the molecular architecture within the ON, could lead to changes in the mechanisms of ischemic glutamate release. Moreover, it has been reported that there is an up-regulation of GLT-1 expression in older WM (Baltan, Besancon et al. 2008).

To investigate the significance of EAATs in adult WM, I initially examined the effect of EAAT inhibition under control conditions. Unlike the P10 RON, perfusing the adult RON with TBOA (200µM) had no significant effect on resting $[Glut]_e$, with concentrations slightly decreasing by 0.14±0.2µM (*n*=6) during the initial 10 minutes of TBOA exposure (p=0.52, Fig.4.21a-b). In contrast, exposure to TBOA induced a significant increase in resting $[Glut]_e$ in the adult corpus callosum (0.88±0.41µM, *n*=9, p=0.04, Fig.4.21c-d).

To test whether reverse EAATs contribute to the elevated $[Glut]_e$ during ischemia, $[Glut]_e$ was measured in the presence of TBOA (15 minutes before, during and 15 minutes after chemical ischemia). TBOA had no significant effect on either the early onset of release or total extracellular concentrations after 60 minutes of chemical-ischemia (TBOA: 22.53±3.73µM, *n*=6, *versus* control: 27.98±6.8µM, *n*=7; p=0.99, Fig. 4.22a-b). To further probe the involvement of EAATs, $[Glut]_e$ was also recorded under zero-Na^+ conditions (NMDG-substituted). However, this treatment resulted in a significant exacerbation of ischemia-induced glutamate release, with concentrations reaching 53.77±13.70µM (*n*=5, *versus* control: 27.98±6.8µM, *n*=7; p=0.005, Fig.4.22c-d). Consistent with my findings in the P10 RON, the results suggest that reverse EAATs do not contribute to glutamate release in the adult RON.

Previous studies which have reported the involvement of reverse EAATs in ischemic WM pathology have used the adult MON as their model WM tract (Tekkok, Ye et al. 2007, Baltan, Besancon et al. 2008). I therefore decided to investigate whether the differences in our

findings may be due to inter-species differences between the rat and mouse. Resting $[Glut]_e$ within the adult MON was recorded for 15 minutes before exposure to 60 minutes of chemical-ischemia. Ischemia induced a dramatic rise in $[Glut]_e$, which surprisingly peaked after only 26.63±1.09 minutes, reaching 35.60±9.85µM before rapidly falling back towards baseline levels (Fig. 4.23a-b, *n*=4). Unlike the adult RON, where glutamate release is continuous throughout the 60-minute insult, the distinctive glutamate release profile recorded in the adult MON suggests that glutamate stores may become depleted after 25-30 minutes, which may be related to its smaller size. Nonetheless, glutamate release in the MON was examined in the presence of TBOA (200µM). Although TBOA did appear to reduce the overall rise in $[Glut]_e$, statistical significance was not reached (18.07±6.98µM, *n*=5, p=0.22, Fig. 4.23a-b). Not enough nerves were examined to convincingly show the involvement of EAATs in the adult MON.

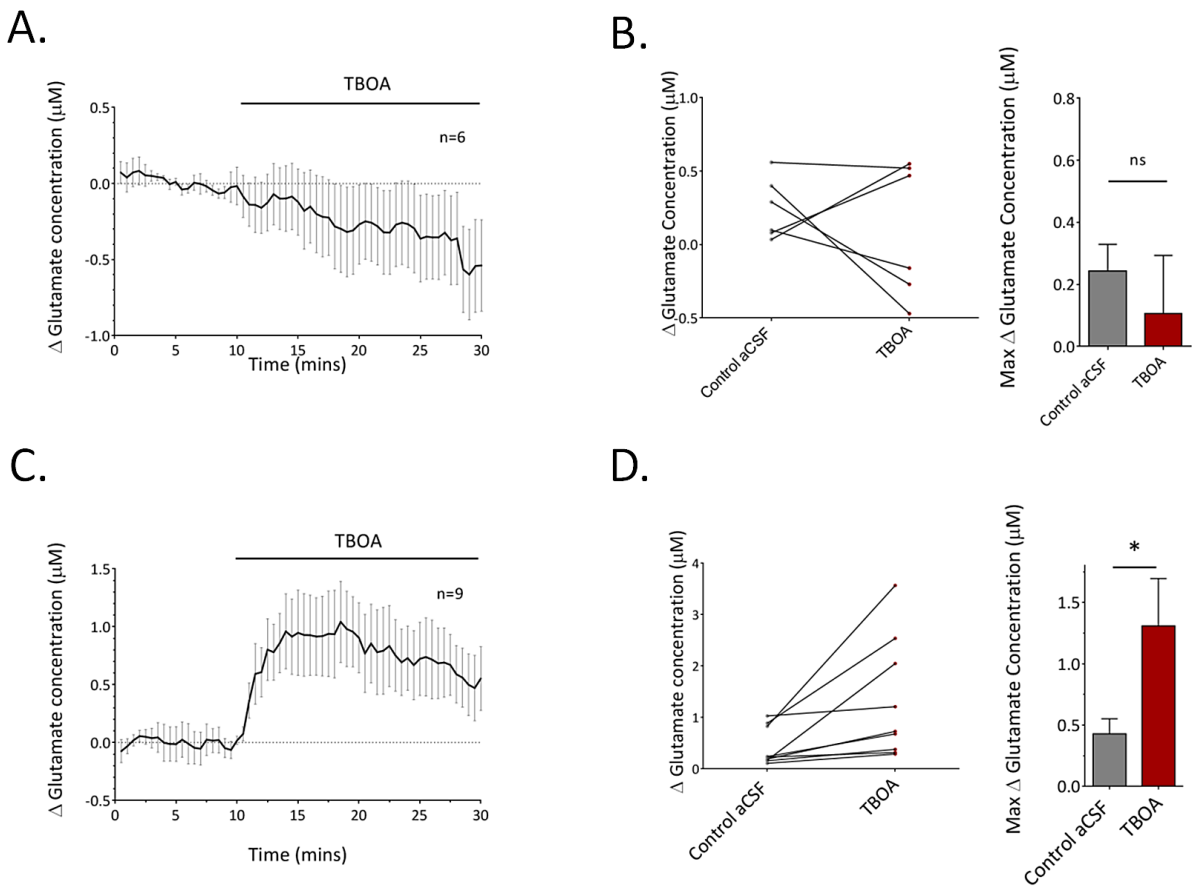

Fig. 4.21: Exposure to TBOA under physiological conditions does not elevate resting $[Glut]_e$ in the adult RON, but does in the CC.

a) Exposure to TBOA under control conditions does not change basal $[Glut]_e$ levels in the RON. **b)** Data summary comparing the maximum concentration during 10 minutes of control aCSF with the first 10 minutes of exposure to TBOA in the ON. **c)** Exposure to TBOA under control conditions significantly increases basal $[Glut]_e$ levels in the adult CC. **d)** Histogram comparing the maximum concentration during 10 minutes of control aCSF with the first 10 minutes of exposure to TBOA in the CC. ns $p>0.5$, *$p<0.05$.

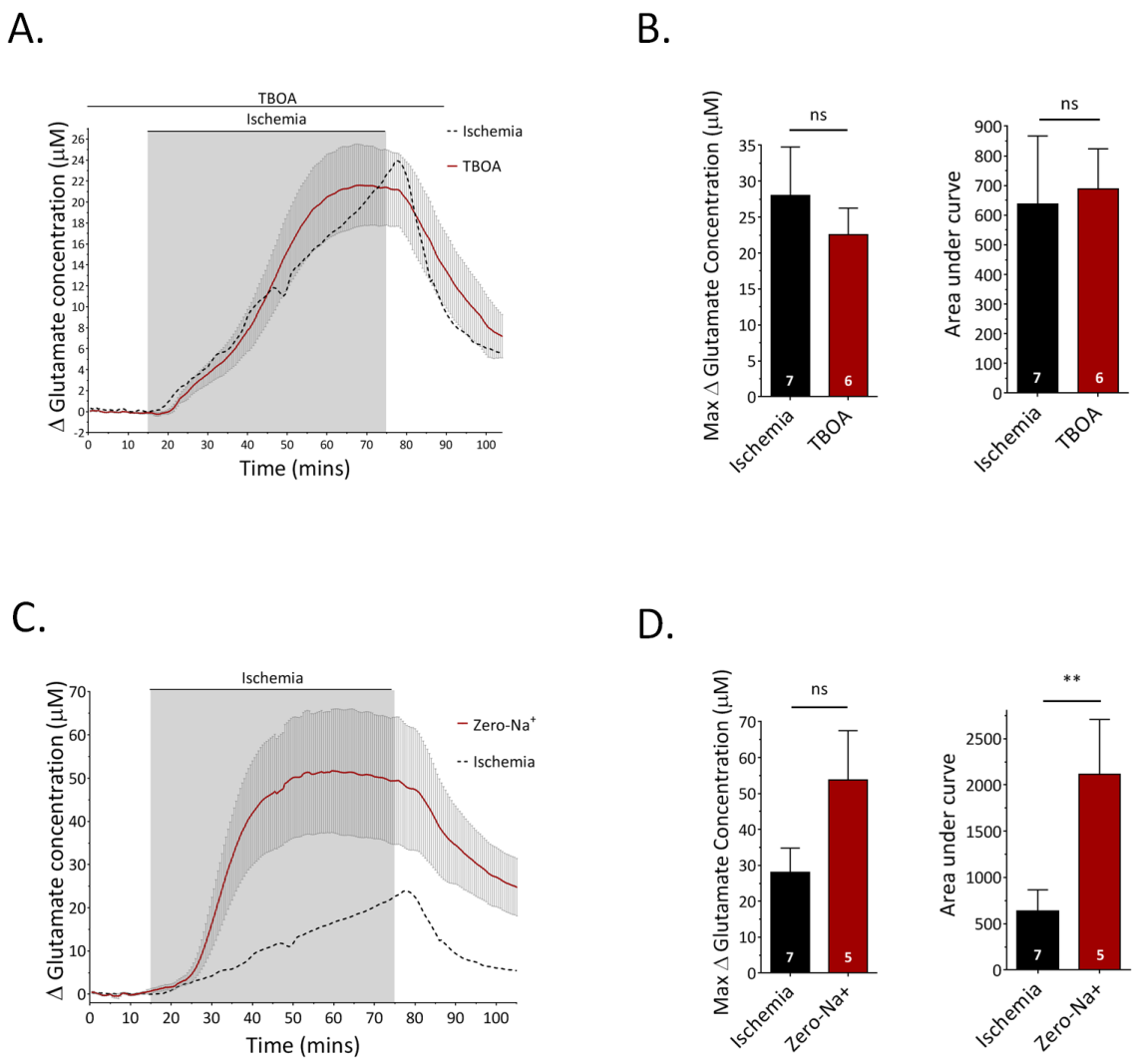

Fig. 4.22: Inhibition of EAATs with TBOA or under zero-Na$^+$ conditions does not prevent the ischemia-induced rise in extracellular glutamate in the adult RON.

a) Ischemia-induced glutamate release in the presence of TBOA in the ON. **d)** Histogram showing the effect of TBOA on $[Glut]_e$. **c)** Ischemia-induced glutamate release under zero-Na$^+$ conditions. **d)** Histogram showing the effect of zero-Na$^+$ on $[Glut]_e$. ns $p>0.05$, ** $p>0.01$.

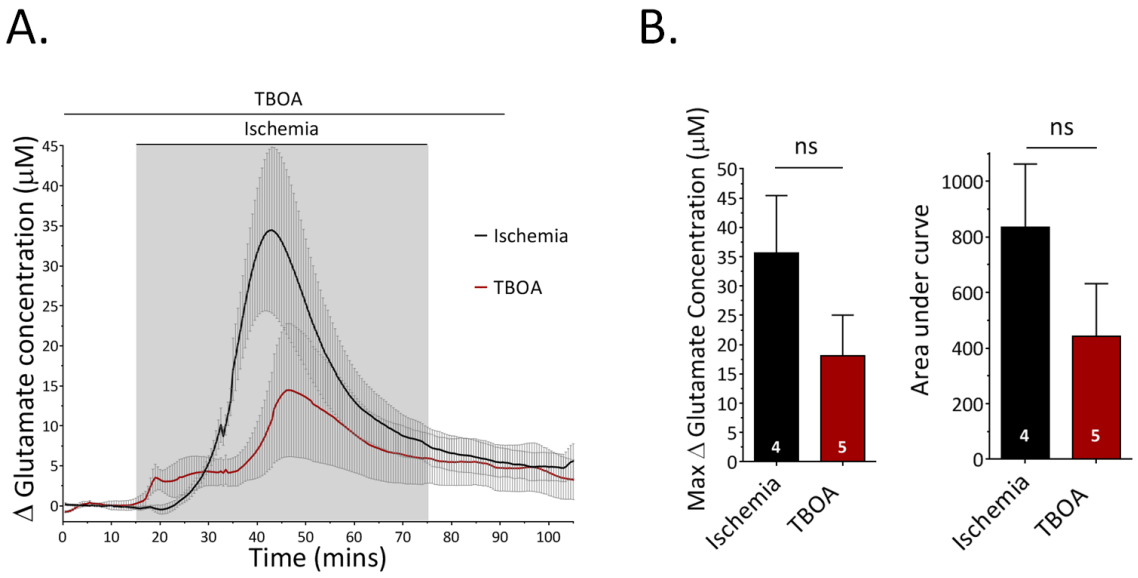

Fig. 4.23: Ischemia-induced glutamate release in the adult MON peaks after 25-30 minutes, and is not significantly reduced by TBOA.

a) $[Glut]_e$ time-course showing the rise in glutamate during ischemia and the effect of TBOA on glutamate release in the myelinated MON. **b)** Histogram showing the effect of TBOA on $[Glut]_e$. ns $p>0.05$.

4.3.3 Vesicular glutamate contributes to the ischemia-induced rise in extracellular glutamate in adult WM

Previous experiments on the unmyelinated P10 RON show that excessive vesicular fusion is capable of elevating extracellular glutamate levels, a phenomenon which occurs early in ischemia. In addition, experiments from chapter 3 show that myelinated axons are also capable vesicular docking. Therefore, I next accessed whether vesicular fusion contributes to the rise in $[Glut]_e$ during ischemia in the adult RON.

To test the significance of vesicular release in the adult RON, $[Glut]_e$ was recorded under zero-Ca^{2+} conditions. RONs were perfused with a zero-Ca^{2+} aCSF solution containing EGTA (50µM) for 20 minutes before, during and 35 minutes after ischemia. Similar to the P10 RON, a significant decrease in $[Glut]_e$ was observed in the absence of extracellular Ca^{2+}. $[Glut]_e$ reached 10.48±1.4µM (*n*=6) following 60 minutes of chemical ischemia, significantly lower than the time-matched control (25.78±11.05µM, *n*=6, p=0.04, Fig. 4.24a-b).

Provided the removal of extracellular Ca^{2+} is sufficient to reduce glutamate release, I next attempted to uncover the route of Ca^{2+} influx during ischemia. Ca^{2+} influx through voltage gated Ca^{2+} channels (VGCCs) is reported to mediate anoxic damage in the mature RON (Brown, Westenbroek et al. 2001). The application of diltiazem (100µM), an L-type Ca^{2+} channel blocker, had a similar effect on ischemic $[Glut]_e$ as zero-Ca^{2+}, attenuating glutamate concentrations to 12.89±3.73µM (*n*=7, Fig. 4.24c-d). However, statistical significance was not achieved (p=0.09). Nonetheless, the data indicates that a significant component of glutamate release is via Ca^{2+} dependant vesicular exocytosis.

Following this, an effort was made to deplete nerves of their vesicular glutamate stores using the same bafilomycin-a1 pre-treatment protocol as used with the neonatal RON (i.e. 120 minutes perfusion with bafilomycin-a1, including two brief exposures to 10mM KCl). The maximum peak concentration reached was slightly reduced to 19.85±3.75µM in the presence of bafilomycin-a1, but it was not statistically significant (*n*=6, p=0.49, Fig. 4.25a-b). However, I was not convinced that 10mM KCl was sufficient to promote sufficient vesicular turnover during the pre-treatment period. For this reason, a known effective concentration of K^+ was used; 50mM (see Chapter 3). However, again bafilomycin-a1 produced an insignificant

decrease in total glutamate release (Baf-a1: 24.85±6.94µM, *n*=6 *versus* Control: 31.73±8.14µM, *n*=5, p=0.37, Fig. 4.25c-d). The lack of a significant reduction in bafilomycin-a1 treated nerves is curious considering the removal of Ca^{2+} prevented a significant component of release.

A more direct way of examining vesicular fusion in myelinated WM is with the use of FM4-64. Coronal brain slices (400µM) including the corpus callosum were obtained from adult Thy-1/YFP^{+} mice. Slices were loaded with FM4-64 using an established 'high-K^{+}' loading protocol (see 'Materials and Methods'). As previously demonstrated, widespread FM4-64 loading was observed in YFP^{+} axons. Using two-photon confocal microscopy, FM-fluorescence was monitored for 30 minutes under control conditions (i.e. oxygenated aCSF). Over the course of 30 minutes, axonal FM-fluorescence decreased by 16.21±2.69% (*n*=23, Fig. 4.26), which may reflect a combination of spontaneous vesicular release and/or photo-bleaching due to relatively long periods of recording. However, the pronounced drop in FM-fluorescence was exacerbated following exposure to chemical ischemia (Fig. 4.27). Axonal FM-fluorescence became significantly reduced after 15 minutes of ischemia (p=0.02), decreasing by 27.33±2.0% after 25-30 minutes (*n*=35, p=0.0013, Fig. 4.28a-b). FM4-64 de-staining is indicative of vesicular docking occurring along the axon cylinder. As previously demonstrated in chapter 3, all YFP^{+} axons in the mouse CC are myelinated, with a mean diameter of 0.86±0.02µM (*n*=167), which is considerably higher than the largest diameter unmyelinated axon. As with K^{+}-evoked vesicular release, there was no evidence of localised de-staining along the axon cylinder, and therefore, the vast majority of vesicular fusion must occur underneath the myelin sheath, releasing into the peri-axonal space.

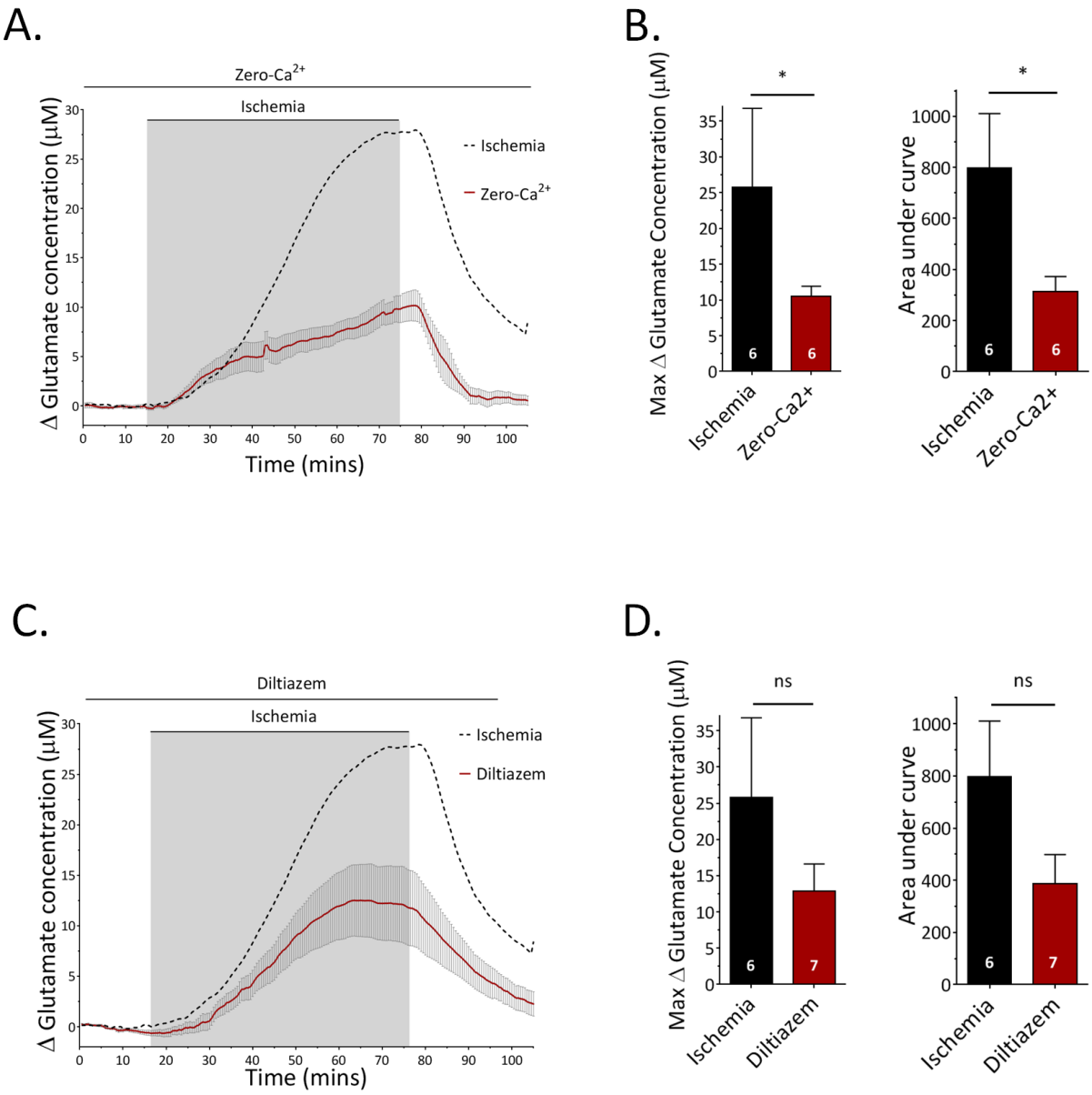

Fig. 4.24: Glutamate release is reduced under conditions aimed at preventing vesicular release.

a) Ischemia-induced glutamate release from adult RONs in a zero-Ca^{2+} aCSF solution. **b)** Histogram demonstrating the effect of zero-Ca^{2+} conditions on $[Glut]_e$ **c)** Ischemia-induced glutamate release in the presence of diltiazem. **d)** Histogram demonstrating the effect of diltiazem on $[Glut]_e$. ns $p>0.05$, *$p<0.05$.

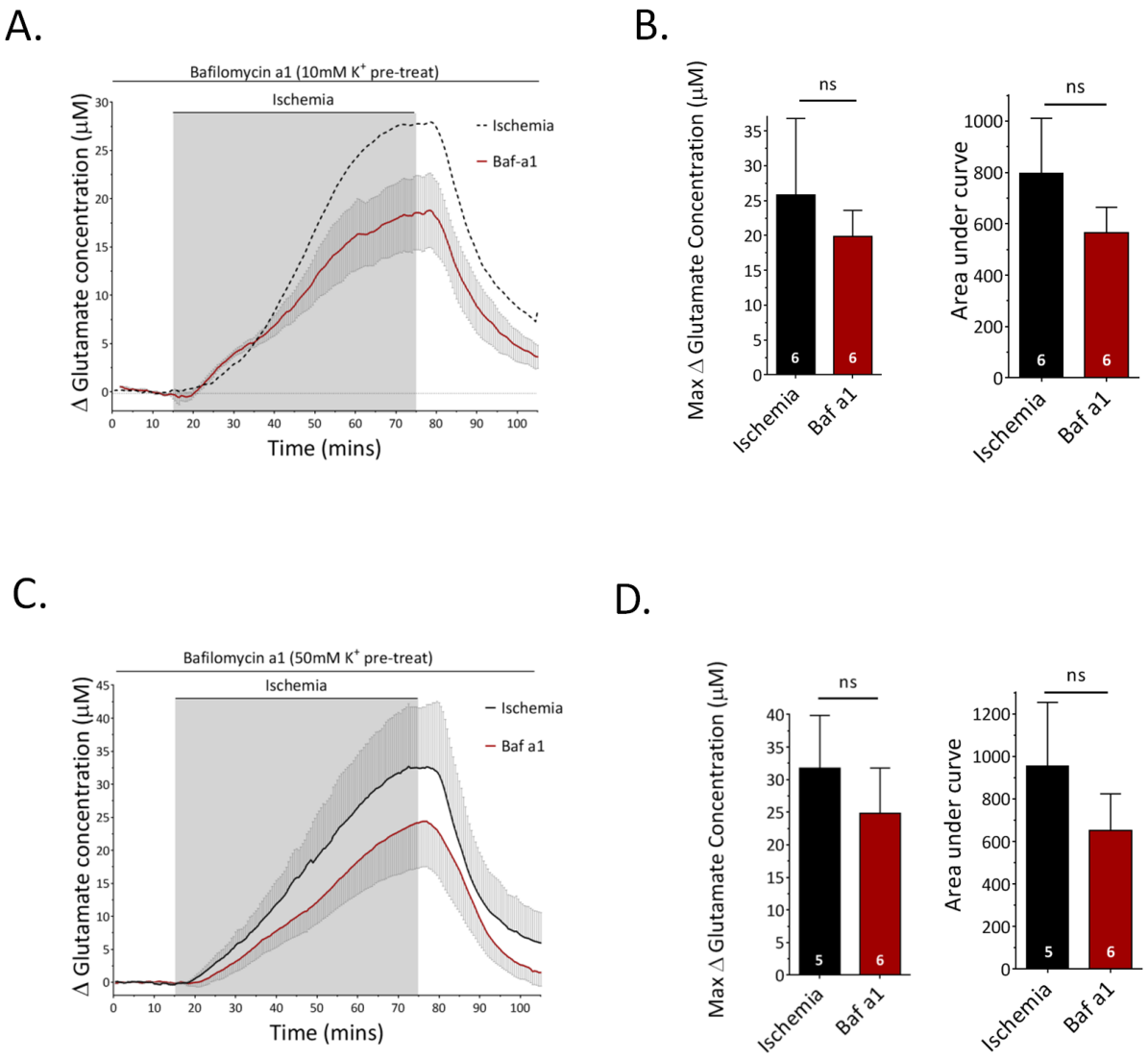

Fig. 4.25: Depleting nerves of their vesicular stores with bafilomycin-a1, does not significantly reduce glutamate release.

a) Ischemia-induced glutamate release in bafilomycin-a1 treated nerves (10mM KCl pre-treatment protocol). **b)** Histogram demonstrating the effect of bafilomycin-a1 on $[Glut]_e$. **c)** Ischemia-induced glutamate release in bafilomycin-a1 treated nerves (50mM KCl pre-treatment protocol). **d)** Histogram demonstrating the effect of bafilomycin-a1 on $[Glut]_e$. ns $p>0.05$.

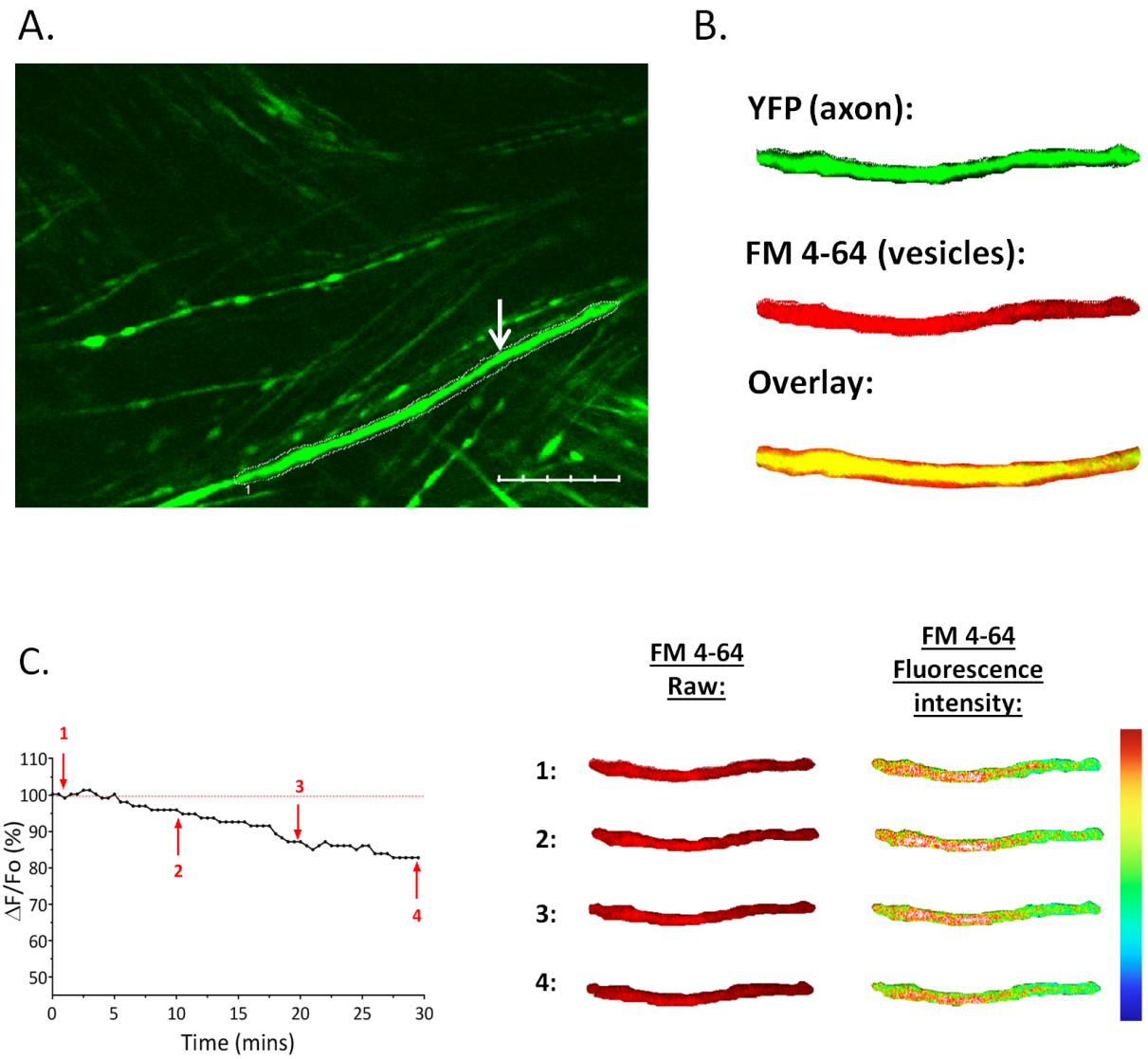

Fig. 4.26: FM4-64-loaded axons show a slight decrease in FM-fluorescence over 30 minutes in control aCSF.

a) Image of YFP+ axons in the mouse CC. An individual axon segment (indicated by a dotted boarder and arrow) was selected for analysis. **b)** Selected YFP+ axon segment is highly fluorescent with FM4-46 after loading protocol. **c)** Representative time-course of axonal FM fluorescence remains relatively stable under control conditions. Representative images at different time points are numbered 1-4 (1=1 minute, 2=10 minutes, 3=20 minutes, 4=30 minutes). Scale bar: 20um.

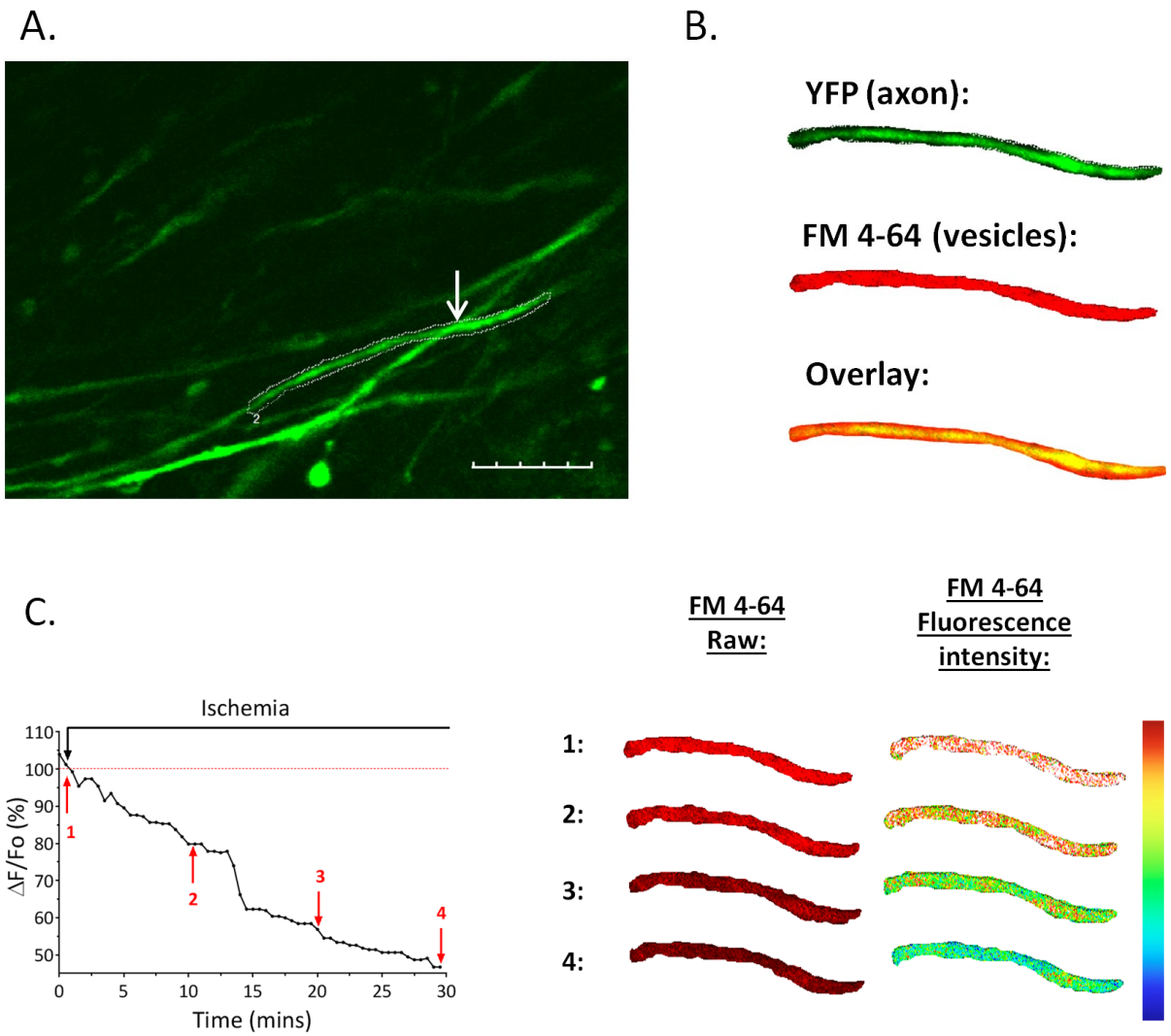

Fig. 4.27: FM4-64-loaded axons display a large drop in FM-fluorescence during 30 minutes of chemical ischemia.

a) Image of YFP+ axons in the mouse CC. An individual axon segment (indicated by a dotted boarder and arrow) was selected for analysis. **b)** Selected YFP+ axon segment is highly fluorescent with FM4-46 after loading protocol. **c)** Representative time-course of axonal FM fluorescence showing a decrease during chemical ischemia. Representative images at different time points are numbered 1-4 (1=1 minute, 2=10 minutes, 3=20 minutes, 4=30 minutes). Scale bar: 20um.

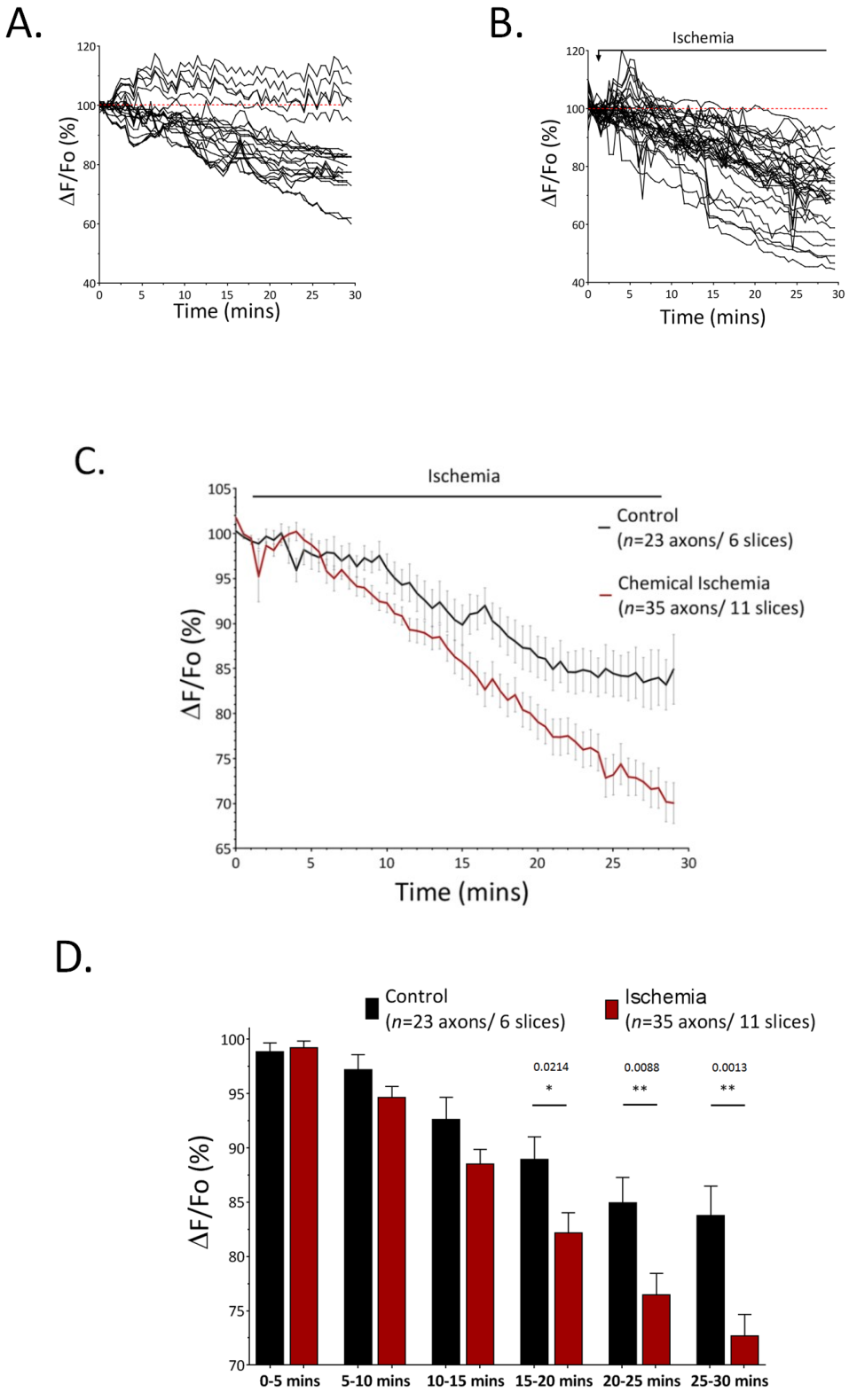

Fig. 4.28: FM4-64-loaded axons show a significant decrease in fluorescence during chemical ischemia.

a) Time-course of FM fluorescence from all individual axons under control conditions. **b)** Time-course of FM fluorescence from all individual axons during chemical ischemia. **c)** FM fluorescence time-course comparing chemical ischemia to control. **d)** Data summary under both conditions showing a significant drop in fluorescence after 15 minutes. * $p<0.05$, ** $p<0.001$.

4.3.4 Alternative release mechanisms do not contribute to elevated extracellular glutamate levels.

Next, I investigated alternative release mechanisms which could contribute to the rise in $[Glut]_e$. To exclude the possibility of the increased function of the glutamate-cystine antiporter, glutamate release was monitored in the presence of a known effective concentration of sulfasalazine (SAS, 250µM) (Soria, Pérez-Samartín et al. 2014), a non-substrate inhibitor of the glutamate-cystine antiporter. However, the application of SAS had no significant effect on total glutamate release during ischemia. The maximum peak concentration reached was not significantly different to control nerves, with concentrations reaching 18.14±2.32µM (*n*=6, p=0.98 *versus control; 27.98±6.8µM (n=7)*; Fig. 4.29a-b). It must be noted that $[Glut]_e$ appeared to plateau during the final 20 minutes of ischemia, indicative of a reduction in the rate of release during the later phase of ischemia.

I also tested the possibility of swelling-mediated release using furosemide (5mM), a NKCC inhibitor. However, ischemia-induced $[Glut]_e$ was not significantly different in the presence of furosemide, with concentrations reaching 31.18±3.80µM (*n*=4, p=0.93 *versus control; 27.98±6.8µM (n=7)*, Fig. 4.30c-d).

Together, this data indicates that like the P10 RON, excessive vesicular fusion contributes to the elevated extracellular glutamate levels recorded in the adult RON. However, the failure to completely abolish glutamate release under conditions aimed at preventing vesicular fusion (see Fig. 4.31) leave open the possibility that multiple mechanisms may collectively add to the rise in $[Glut]_e$. This would require further investigation which was beyond the scope of this project due to time constraints.

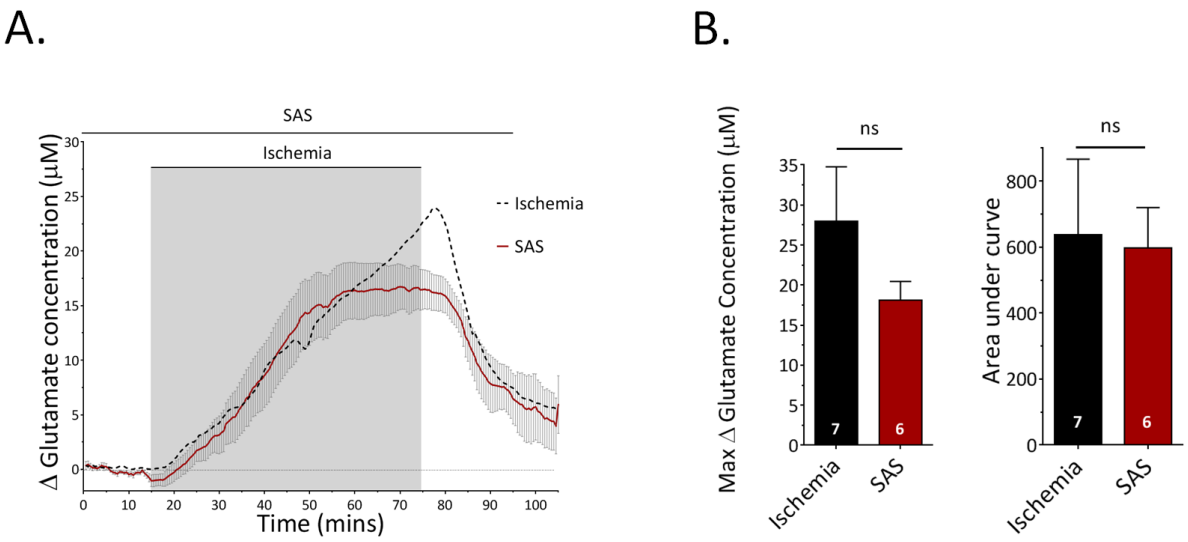

Fig. 4.29: Inhibition of the glutamate-cysteine antiporter with sulfasazine (SAS) does not significantly reduce the rise in extracellular glutamate.

a) Ischemia-induced glutamate release in the presence of sulfasazine (250μM). **b)** Histogram showing the effect of SAS on $[Glut]_e$. ns $p>0.05$.

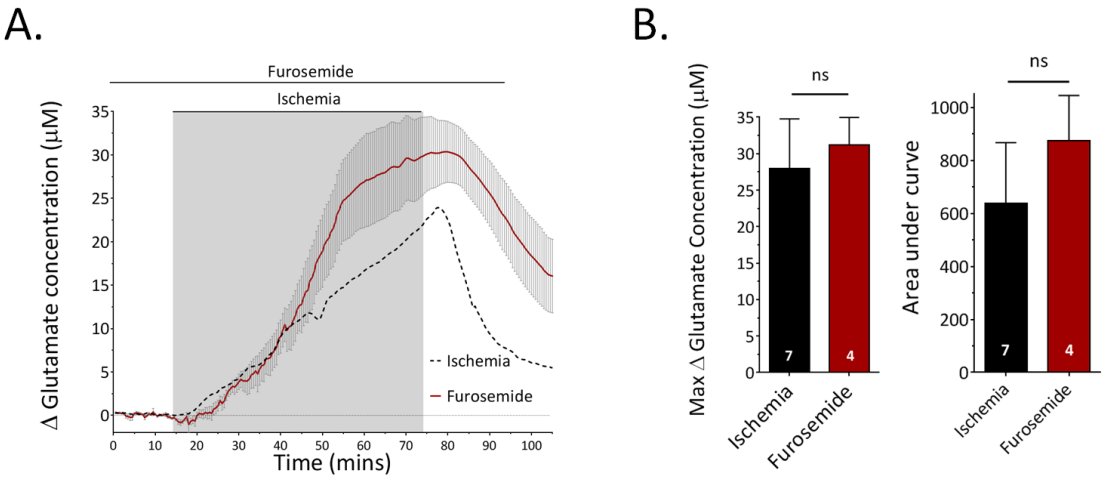

Fig. 4.30: Swelling-mediated glutamate release does not significantly contribute to the rise in extracellular glutamate.

a) Ischemia-induced glutamate release in the presence of furosemide (5mM). **b)** Histogram showing the effect of furosemide on $[Glut]_e$. ns $p>0.05$.

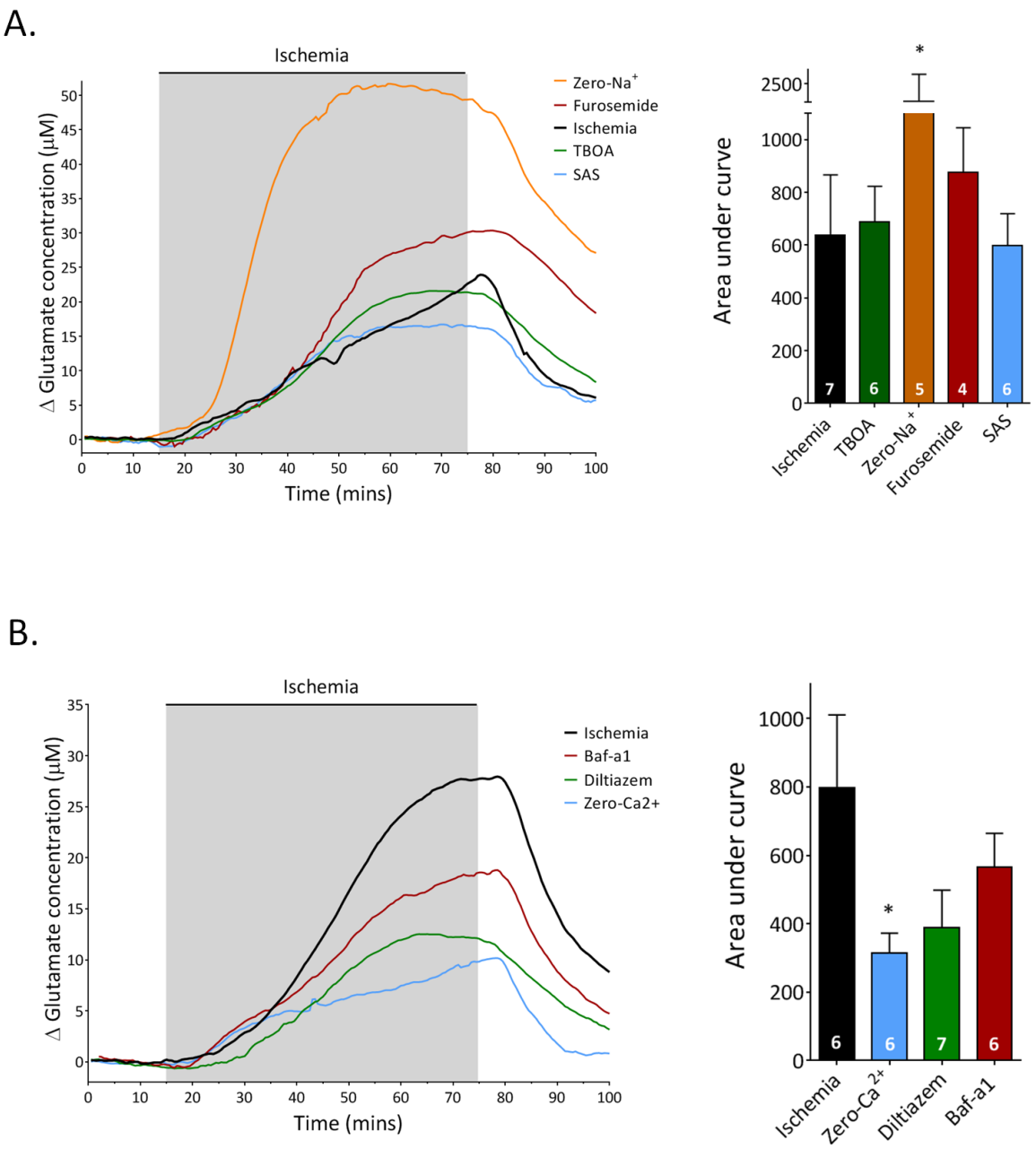

Fig. 4.31: Summary of ischemic glutamate release in the adult RON under a variety of conditions and pharmacological conditions

a) Glutamate release under conditions aimed at preventing EAAT reversal, swelling-mediated release and the glutamate/cysteine antiporter. **b)** Glutamate release under conditions aimed at preventing vesicular fusion. * $p<0.05$.

4.3: Discussion

4.3.1: Synopsis

The human brain is highly susceptible to prolonged periods of ischemia. Considering WM constitues approximately 50% of the adult human brain, it comes as no surprise that WM pathology is regularly observed following a variety of ischemic insults. Moreover, WM injury is of particular importance as the loss in axon function is fundamental to to the severe clinical impairments suffered by patients. Recent studies have demonstrated that excitotoxicty is a central injury mechansim underlying irreversible WM damage. As a result, glutamate release is a critical event in the pathophysiology of ischemic WM injury. In this chapter, I have established a glutamate release time-course in several WM tracts, and examined the the potential mechanims of ischemic glutamate release in developing and mature WM. I found that exposure to conditions which mimic ischemia led to a robust rise in $[Glut]_e$. Suprisingly, glutamate release was not via the reversal of glutamate transports. Similarly, release through hemichannels, the glutamate/cystine antiporter or volume regulated anion channels did not contribute to the rise in $[Glut]_e$. However, $[Glut]_e$ was significantly attenuated under conditions aimed at preventing vesicular fusion. Furthermore, depleting nerves of their vesicular glutamate stores improved functional recovery following oxygen-glucose deprivation. Together the data presented in this chapter demonstrates that excessive vesicular glutamate release during ischemia contributes to excitotoxic WM injury.

4.3.2: Ischemia evokes a rapid increase in extracellular glutamate in WM

Excitotoxicity is associated with a range of neurological disorders including Alzehimers', vascular dimentia, diabetic cognitive dysfunction and ischemia (Hynd, Scott et al. 2004, Baskys and Hou 2007, Tekkok, Ye et al. 2007, McCrimmon, Ryan et al. 2012). Techniques, such as microdialysis, have revealed that hypoxia/ischemia evokes a robust rise in extracellular glutamate in GM regions of the CNS (Benveniste, Drejer et al. 1984, Andiné, Sandberg et al. 1991, Cui, Zhang et al. 1999). While techniques such as high preformance liquid

chromatography (HPLC) have been used to detect glutamate fold-changes in the perfusate of isolated WM preparations (Ye, Wyeth et al. 2003, Tekkok, Ye et al. 2007, Yang, Hamner et al. 2014), the direct change in $[Glut]_e$ within WM has never been recorded. However, the recent development of enzymatic glutamate biosensors (sarissaprobes©), allows for real-time detection of glutamate concentrations within live tissue. Using glutamate biosensors, real-time changes in $[Glut]_e$ was recored from inside model WM tracts, the RON and CC.

As predicted, the resting $[Glut]_e$ in the ECS was in the low micromolar range. Considering experiments are conducted several hours after sensor insertion when $[Glut]_e$ has stabalised to a steady level, it is unlikely that these measurments reflect non-physiological elevations resulting from acute physical damage. With the exception of the adult RON, resting $[Glut]_e$ was between 1.3 and 4.5µM in all WM preparations. This is consistent with numerous studies which have recorded resting $[Glut]_e$ in the range of 1 and 5µM in various brain regions, in a variety of mammalian species (Moussawi, Riegel et al. 2011). This tonic pool of $[Glut]_e$ likely results from a balance of spontaneous vesicular glutamate release/release via glutamate-cystine antiporter and glutamate uptake via Na^+-dependent transporters (Baker, Xi et al. 2002, Moussawi, Riegel et al. 2011). As mentioned, glutamate transports (EAAT) are primarily responsible for the maintainence of low extracellular concentrations throughout the CNS. I found that inhibiting EAATs evokes a significant rise in resting $[Glut]_e$ in most WM tracts, with levels increasing by approximatly 25%. In support of Arranz *et al.* (2008) who demonstrated the expresssion of functional EAATs in WM, this suggests that EAATs maintain low glutamate concentrations in both developing and adult WM. Interestingly, the inhibition of EAATs did not elevate $[Glut]_e$ in the adult RON. Baltan *et al.* (2008) reported that there is a two-fold increase in GLT-1 protein expression in older WM. They also reported that this phenoenomon may be specific to WM as there was not detectable change in GLT-1 expression in the hippocampus. While the upregulation of EAAT expression was identified as a possible explanation for the enhanced release of glutamate during OGD (measured by HPLC) in this study, it also suggests that glutamate uptake may also be enhanced under physiological conditions. This may be releated to the heightened resting $[Glut]_e$ recorded in the adult RON (8.9µM; versus 1.4µM in the P10 RON), as more EAATs are required to regulate glutamate homeostasis. Alternatively, the heightened resting $[Glut]_e$ may be due to impaired EAAT transport in the adult RON. Nonetheless, glutamate transport in the adult RON was insensitive

to TBOA. However, TBOA did increase $[Glut]_e$ in the adult CC. Therefore, further experiments would be required to explain the ususal result in the adult RON.

Exposing nerves to ischemia evoked a striking increase in $[Glut]_e$ in both developing and mature WM tracts. Intriguingly, glutamate release occurred within minutes of ischemia, with $[Glut]_e$ typically increasing within the initial 5 minutes. The early onset of glutamate release was somewhat unexpected, as the aforementioned study by Baltan *et al.* (2008), found that glutamate levels began to increase after ~30 minutes in the MON (1 month old). However, it must be noted that HPLC measurments, as were used in this paper, are only detected once glutamate diffuses out from the ECS, through the outer membrane of the nerve and into the bath perfusate. Thus, biosensors will likely reflect a more accurate onset of glutamate release. In additon, it is likely that chemical ischemia depletes ATP levels much quicker than OGD. For example, my data demonstrates that nerve excitability is typically blocked within 30 minutes of chemical ischemia, whereas, 60 minutes OGD does not abolish CAP conduction (see Fig. 4.9 for comparision). Interestingly, the early initiation of glutamate release coincides with the early loss in nerve excitability during chemical-ischmia. This indicates that there is a readily releasable pool of intracellular glutamate within WM and that release is dependent on early events such as the initial loss in ionic homeostasis.

Following the onset of release, $[Glut]_e$ continued to increase throughout the duration of ischemia, demonstrating a contineous release of endogenous glutamate from WM cells, which subsequently accumulates in the ECS. $[Glut]_e$ increased at a steady rate throughout the entire 30-minute insult in the neonatal RON. Interestingly, increasing the duration of ischemia from 30 to 60 minutes with the adult RON, revealed a slight decrease in the rate of glutamate release during the later phase of ischemia in several nerves (6 out of 13). This might reflect the depletion of glutamate stores as energy deprivation persists or may be due to a second component of release mediated by an alternative release mechanism. Consistent with the depletion of glutamate stores, $[Glut]_e$ peaked after only 25-30 minutes in the adult MON, before gradually returning to baseline.

Ischemia produced a respective 5.6µM, 9.3 µM and 27µM $[Glut]_e$ increase in the neonatal RON, neonatal CC and adult RON glutamate levels, suggesting that ischemic glutamate release is a common feature thoughout WM and at different development stages. $[Glut]_e$ is

contineously washed away in the perfusing aCSF in our experimental set-up, and so it is reasonable to presume that $[Glut]_e$ accumulates *in vivo* producing much higher levels. Ischemia-induced changes in $[Glut]_e$ were comparible to levels recorded in several GM preparations (Wahl, Obrenovitch et al. 1994, Graf, Kumura et al. 2001). Upon the initiation of reperfusion, $[Glut]_e$ rapidly returned towards basline, which may reflect glutamate re-uptake as ionic gradients are re-established, or may be a result of glutamate wash-out into the bath perfusate. Nonetheless, exposure to ischemia evokes a early transient rise in WM $[Glut]_e$, likely responsible for the over-activation of iGluRs.

4.3.3: Reverse EAATs do not mediate ischemic glutamate release in WM

In 2000, two independent groups demonstrated that reverse EAATs are responsible for the majority of ischemic glutamate release in GM regions of the CNS (Jabaudon, Scanziani et al. 2000, Rossi, Oshima et al. 2000). Interestingly, several reports have since emerged that reverse transport also contributes to glutamate release in WM. As previously mentioned, the application of EAAT inhibitors improves functional recovery following ischemia/anoxia in isolated WM preparations (Li, Mealing et al. 1999, Tekkok, Ye et al. 2007). More recent work by Hamilton *et al.* reported that preloading brain slices with PDC reduced the ischemia-evoked inward current in oligodendrocytes by 68%, similar to the reduction observed in the presence of glutamate receptor antagonists NBQX and D-AP5 (Hamilton, Kolodziejczyk et al. 2016). Therefore, the established view is that glutamate release during ischemia is via the reversal of glutamate transporters.

However, despite the expression of functional EAATs in WM, blockers of EAATs (TBOA and zero-Na^+) did not prevent the ischemia-induced rise in $[Glut]_e$ in either the developing or adult RON. The lack of contribution from EAATs was surprising considering their reported involvement in alternative WM studies. One notable difference between my work and these previous reports is the model of ischemia used. While my study employs chemical ischemia, previous studies predominantly used OGD as a model of energy deprivation. Therefore, it is plausible that more severe ischemic insults, such as chemical-ischemia, may evoke release via alternative mechanisms. However, consistent with my $[Glut]_e$ experiments, I found no

significant improvement in post-OGD CAP recovery in the presence of TBOA. Alix and Fern (2009) also reported that zero-Na^+ conditions do not preserve either CAP amplitude or the ultrastructural integrity of P10 RONs exposed to 60 minutes OGD. In addition, previous studies used HPLC to show transport-mediated release in the ON. Changes in glutamate levels in the bath perfusate may reflect glutamate release from glial limitans and the pia matter surrounding the nerve. In contrast, my methodological approach directly measures glutamate levels in the extracellular space.

Curiously, glutamate release was exacerbated under zero-Na^+ conditions in the adult RON. Similarly, several other studies have reported an increase in OGD-induced neuronal damage in the presence of EAAT inhibitors (Fujimoto, Katsuki et al. 2004, Soria, Pérez-Samartín et al. 2014). A possible explanation for this is that EAATs contribute to the clearance of extracellular glutamate during ischemia (Namura, Maeno et al. 2002). However, I found that $[Glut]_e$ in the adult RON was unaffected in the presence of TBOA, which argues against this idea. An alternative explanation for this discrepancy is that the newly established transmembrane Na^+-gradient under zero-$[Na^+]_e$ conditions (ECS:0mM, intracellular:~10mM), may actually promote the reversal of EAATs. In fact, high cytosolic concentrations of Na^+ are known to promote reverse glutamate transport and excitotoxicity in rat hippocampal slices (Roettger and Lipton 1996, Raley-Susman, Kass et al. 2001). Nonetheless, together the data suggests that contrary to expectation, reverse glutamate transport does not mediate the ischemic rise in $[Glut]_e$ in WM. Accordingly, disrupted glutamate homeostasis must operate via an alternative mechanism(s).

4.3.4: Vesicular fusion contributes to ischemic glutamate release in WM

In the previous chapter I presented data which revealed the significance of vesicular glutamate release in WM. Moreover, the data demonstrates that exposing WM to 50mM K^+, a concentration that is comparable the level recorded during cerebral ischemia (Gido, Kristian et al. 1997), evokes a significant increase in $[Glut]_e$, a consequence of vesicular docking along WM axons. As mentioned, excessive vesicular fusion during ischemia is an early event in GM.

Káradóttir *et al.* (2005) also noted that when exposed to *in vitro* ischemia*,* the early inward current recorded in whole-cell clamped OPCs included an increase in the frequency of 'synaptic current-like' events.

Experiments under zero-Ca^{2+} conditions were carried out to determine whether the ischemic rise in $[Glut]_e$ was Ca^{2+}-dependent, as expected for vesicular exocytosis. $[Glut]_e$ in the pre-myelinated RON was dramatically attenuated when Ca^{2+} was omitted from perfusate. Interestingly, glutamate release was slightly lower when intracellular Ca^{2+} was also chelated with BAPTA-AM, yet there was no significant difference between experiments with or without BABPA-AM. Thus, my data does not resolve the precise source of intracellular Ca^{2+} required for vesicular fusion. $[Glut]_e$ was significantly reduced in the presence of either bafilomycin-a1 or rose bengal, inhibitors of vesicular glutamate loading. Together this indicates that vesicular glutamate release contributes to the accumulation of $[Glut]_e$ during ischemia. Consistent with these findings, post-OGD CAP amplitude was significantly higher in nerves which were treated with bafilomycin-a1, further demonstrating that vesicular glutamate release promotes irreversible WM injury in early myelinating WM.

The experiments carried out on the adult RON also suggest that vesicular fusion contributes to the rise in $[Glut]_e$ in fully myelinated WM. Similar to the P10 RON, $[Glut]_e$ was significantly reduced under zero-Ca^{2+} conditions in the adult RON, again suggesting that Ca^{2+} influx promotes vesicular fusion. Although statistical significance was not reached, blocking voltage-gated Ca^{2+} channels (VGCC) did appear to reduce glutamate release. In fact, there was no significant difference between zero-Ca^{2+} and VGCC blockade experiments. Although, the variability of glutamate changes in the adult RON during ischemia may have concealed a significant effect of VGCC blockade. However, since there was no significant reduction in the presence of VGCC blockers, it is possible that Ca^{2+} influx occurs through an alternative pathway, such as the Na^+/Ca^{2+} exchanger (or a combination of both). Nonetheless, a significant component of the high $[Glut]_e$ is released via a Ca^{2+}-dependent mechanism, as predicted from vesicular exocytosis.

Curiously, the application of bafilomyin-a1 did not significantly reduce the ischemia-evoked rise in glutamate in the adult RON. These findings provide an anomaly which is difficult to explain. There are several reasons as to why bafilomycin-a1 did not reduce $[Glut]_e$, as it did in

the pre-myelinated nerve. As discussed in the section 3.1.4, vesicular glutamate release plays a critical role in oligodendrocyte migration and maturation. Thus, it is plausible that vesicular fusion may be much more evident in early myelinating WM. However, recent studies (Micu, Plemel et al. 2016), experiments from the previous chapter and the fact that zero-Ca^{2+} reduced $[Glut]_e$ by approximately 60% (or ~15µm) indicate that adult WM also contains substantial vesicular pools. Another possibility to consider is incomplete myelin penetration. The principle difference between the P10 and adult RON is the presence of myelin sheath. Myelin sheath poses as a significant diffusion barrier and thus, may limit drug accessibility, reducing the concentration of the baf-a1 (Mr=622.83) which reaches axonal vesicles. Similarly, this may also work in reverse by confining internodal vesicular glutamate to the periaxonal space. In contrast, the P10 RON and CC are predominantly unmyelinated structures, where vesicular glutamate release along axons will diffuse directly into the ECS. However, the Ca^{2+}-dependent component of the elevated $[Glut]_e$ does not support this theory. Provided ischemia-evoked vesicular fusion is an early event (Katchman and Hershkowitz 1993, Marcoli, Bonfanti et al. 2004), it is probable that vesicular glutamate release accounts for a larger component of total $[Glut]_e$ during a shorter length of ischemia i.e. P10 nerves were exposed to 30 minutes of ischemia, while adult RONs were subject to 60 minutes. However, the profile of glutamate release in the adult RON indicates that bafilomycin-a does not delay the onset of glutamate release.

While the $[Glut]_e$ data demonstrates that vesicular fusion is a major component of ischemic glutamate release in the developing RON, it does not convincingly show that it is unequivocally involved in the adult RON. For this reason, FM4-64 was used to directly visualise vesicular fusion in myelinated axons during ischemia. Similar to my findings in the previous chapter, FM4-64 loaded, myelinated (YFP+) axons were evident throughout the adult mouse CC. Homogenous FM-dye de-staining along the axon was triggered by chemical ischemia, confirming that ischemia evokes vesicular fusion along myelinated axons.

While axonal vesicular fusion appears to be a major pathway of glutamate release in WM, it is highly unlikely that it operates in isolation. Experiments aimed at blocking vesicular exocytosis failed to completely abolish the ischemic rise in $[Glut]_e$. The inhibition of EAATs in 'vesicle-depleted nerves' (bafilomycin-a1 treated) failed to eliminate the residual rise in $[Glut]_e$. In addition, the inhibition of swelling-mediated release, hemi-channels or the

glutamate-cystine antiporter failed to reduce $[Glut]_e$ in both developing and mature WM tracts. However, due to the variability of glutamate changes, it may not be possible to uncover small decreases without repeating experiments on a high number of nerves. While my findings failed to reveal a second mechanism, I cannot conclusively exclude a potential role for these alternative pathways. Further experiments which combine the inhibition of vesicular release with alternative mechanisms would be required address this issue. Furthermore, alternative pathways are likely to operate during longer periods of ischemia, as vesicular pools are depleted. The data provided in this chapter does not challenge the idea that alternative release mechanisms may operate under ischemic conditions, but rather indicates that vesicular fusion is a significant mechanism of release.

In conclusion, I have demonstrated that ischemia evokes a robust rise in extracellular glutamate concentrations in two model WM tracts, the ON and CC. This build-up in glutamate is likely responsible for the glutamate receptor-mediated injury observed in a variety of WM studies. Surprisingly, I show for the first time that glutamate release was not via reverse EAATs, but rather via vesicular exocytosis in both unmyelinated and myelinated axons. This unexpected pathway of glutamate release contributes to irreversible injury in developing WM. Furthermore, the pattern of FM4-64 unloading (vesicular fusion) during ischemia indicates that the majority of vesicular fusion in myelinated axons occurs under the myelin sheath. Intriguingly, the internal surface of myelin expresses high levels of NMDA receptors (Micu, Jiang et al. 2006). Therefore, vesicular glutamate release into the periaxonal space may play an important role in acute myelin damage. This hypothesis will be investigated in the following chapter.

Chapter 5:

Excitotoxic Myelin Injury

5.1: Introduction

5.1.1: Current treatments and therapeutic strategies for dealing with ischemic stroke

Despite our current knowledge on the mechanisms which underlie irreversible neurological injury during ischemia, there is a distinct lack of effective therapeutic interventions. Ischemic stroke involves a variety of injury pathways including ionic imbalance, excitotoxicity, acidification, oxidative stress, apoptosis and inflammation. Furthermore, these events occur at different stages following the onset of ischemia. Due to the complex nature of ischemic cell death, single mechanistic treatments are often incapable of preventing widespread injury. In addition, the window of opportunity following the onset of ischemia is relatively short and as a result, many patients miss out on potential interventions. As mentioned in section 1.3.2, the incidence of stroke is continuously increasing due to an ageing population. In addition, recurrent strokes represent nearly a third of all stroke cases. Therefore, prophylactic treatments which elevate injury tolerance may prove to be invaluable in the treatment of acute ischemia. In addition, treatments which include a combination of therapeutic approaches, or procedures which target numerous injury pathways are more likely to improve clinical outcomes (George and Steinberg 2015).

5.1.1.1: Thrombolysis (t-PA) and Mechanical Thrombectomy

The primary objective following the onset of ischemia is the restoration of blood circulation. Currently, the only FDA approved pharmacological agent used in the treatment of acute stroke is thrombolytic tissue-plasminogen activator (t-PA). t-PA works by dissolving the clot (thrombolysis), which subsequently restores blood flow to the ischemic region. It is an endogenous serine protease found in endothelial cells which catalyses the conversion of plasminogen to its active form, plasmin (Nagai, Yamada et al. 2004). Plasmin's primary function is the lysis of blood clots (fibrinolysis). Meta-analysis of clinical trials have shown that vessel recanalization via t-PA is the most successful predictor of improved neurological outcomes in ischemic-stroke patients (Rha and Saver 2007). t-PA is known to improve clinical

outcomes in patients if administered intravenously within the initial 3 hours of a stroke (Disorders and Group 1995, Stankowski and Gupta 2011). Although t-PA is the gold standard in stroke treatment, the vast majority of stroke patients do not receive this treatment due to the narrow window of opportunity. It is estimated that only 2% of patients receive thrombolysis (Stankowski and Gupta 2011). In addition, t-PA exacerbates haemorrhagic stroke. In fact, in approximately 6% of patients, t-PA leads to an intracranial haemorrhage which can cause either serious disability or death in some cases (Stankowski and Gupta 2011). Therefore, patients must be examined (usually via MRI or ST scan) to determine whether the stroke is ischemic or haemorrhagic in nature. This takes time and thus, prolongs the period before a suitable treatment is administered. In addition, previous findings also indicate that t-PA administration may also promote excitotoxic damage due to its interactions with NR1 of the NMDA receptor (Liberatore, Samson et al. 2003). t-PA acts to restore the blood supply within the brain, however, it does not prevent cellular injury pathways during ischemia, nor does it prevent secondary injury associated with reperfusion.

While t-PA is effective in removing relatively small clots, it is regularly fails to degrade larger ones. After administrating t-PA, physicians can use neuro-imaging to determine whether t-PA administration was sufficient to dissolve the clot. If not, mechanical thrombectomy is typically the next step. Mechanical thrombectomy is an endovascular procedure in which large-vessel blood clots are physically removed via a stent retriever at the site of blockage within the brain. A stint retriever is a wire-caged device which is delivered via a catheter in the groin of the patient up to the blocked artery. It expands to stretch the walls of the blood vessel and subsequently captures the blood clot. This procedure can be done up to 8 hours following the onset of a stroke (Mordasini, Zubler et al. 2012).

5.1.1.2: Therapeutic Hypothermia

Alongside the restoration of blood flow, minimising damage to both grey and white matter regions is of upmost importance during ischemia. Mild brain hypothermia is currently being investigated as a neuroprotective strategy during acute stroke. Mild hypothermia (2-5°C decrease in the core body) is an established technique used to reduce metabolic activity and subsequently reduce the requirement for essential nutrients, such as oxygen and glucose. In

addition, several injury pathways involve the activation of numerous deleterious enzymes which are highly temperature dependant (Zhao, Steinberg et al. 2007). Similarly, therapeutic hypothermia decreases the production of excitatory neurotransmitters and free radical formation (Gibson and Andrews 2013). Current methods for the induction of hypothermia include the intravenous infusion of refrigerated NaCl (0.9%), vascular cooling catheters or by surface cooling via closed loop water-feedback systems such as cooling caps or heat exchange pads (Gibson and Andrews 2013). Recent studies have also investigated the effect of pharmacologically induced hypothermia using a neurotensin receptor 1 (NTR1) agonist, ABS201 (Choi, Hall et al. 2012). In a model of focal ischemia in mice, ABS201 reduced the core brain and body temperature by 2-5°C within 15-30 minutes, reduced the infarct volume by 30-40% and improved sensorimotor outcomes 21 days after the insult (Choi, Hall et al. 2012).

Mild hypothermia provides considerable protection in animal models of cerebral ischemia, capable of reducing the infarct volume by up to 40% (van der Worp, Sena et al. 2007). Lowering the temperature from 37 to 32/31°C dramatically improves post-OGD functional recovery in isolated WM preparations (Stys, Waxman et al. 1992, Baltan, Besancon et al. 2008). It is known to improve neurological outcomes in infants who suffer neonatal encephalopathy and in patients who suffer cardiac arrest (Bernard , Gray et al. 2002, Shankaran , Pappas et al. 2012). However, current methods of cooling are often impractical in intensive-care clinical situations. Furthermore, therapeutic hypothermia is closely associated with a number of adverse effects including hypothermia (Sydenham, Roberts et al. 2009), hypotension, hyperglycemia (Nielsen, Sunde et al. 2011) and shivering, which is known to increase metabolic oxygen demand (Gibson and Andrews 2013).

5.1.1.3: Cortical Stimulation

Cortical stimulation is a promising new technique aimed at reorganising neuronal circuits within the CNS to improve functional recovery following ischemia (George and Steinberg 2015). Functional recovery after stoke is closely associated with neuronal plasticity and rewiring of regions adjacent to the infarct core (Cheng, Wang et al. 2014). The remodelling of neuronal connections is facilitated by electrical signalling which is known to promote the release of a variety of trophic factors including brain-derived neurotropic factor (BDNF) and

neuregulin (Lundgaard, Luzhynskaya et al. 2013). As previously discussed, activity-dependent glutamate release promotes re-myelination and WM plasticity. Non-invasive techniques such as the application electrical fields via transcranial magnetic stimulation (TMS), transcranial direct current stimulation (tDCS) or optogenetics leads to improved functional improvements in animal models (Cheng, Wang et al. 2014, George and Steinberg 2015). Similarly, tDCS of the motor cortex significantly improves motor function (measured by Jebsen-Taylor Hand Function Test) in patients with chronic cerebral ischemia (Hummel, Celnik et al. 2005).

5.1.1.4: Stem Cell Therapy

Stem cell therapy is an exciting new frontier and has become an area of intense research for numerous pathological disorders. Stem cells are multipotent/pluripotent cells with the ability to develop into a variety of different cell types (George and Steinberg 2015). The exogenous application of transplanted stem cells to the damaged region following a stroke provides a direct method of cell replacement in the infarcted area. Stem cell therapy has shown promising results in animal models. For example, in a mouse model of hypoxia-ischemia, mesenchymal stem cells (MSCs) which were intranasally transplanted 10 days following the insult, dramatically decreased the degree of grey and white matter loss by 34% and 37%, respectively and significantly improved sensorimotor function (van Velthoven, Kavelaars et al. 2010). The acute delivery of stem cells following the onset of ischemia (within 48 hours) is capable of reducing the size of the lesion and also decreases the degree of cell death in the surrounding penumbra (Bliss, Andres et al. 2010). Although more research is required to fully understand the mechanisms of repair following neuronal loss, the production of trophic factors are known to stimulate several endogenous repair pathways (Hicks and Jolkkonen 2009, Bliss, Andres et al. 2010, van Velthoven, Kavelaars et al. 2010). Conversely, MSCs secrete a variety of neurotrophic factors which may enhance neurogenesis (Bang, Kim et al. 2016).

5.1.1.5: Pharmacological Neuroprotection

Unfortunately, there are currently no FDA-approved pharmacological agents for minimising brain injury during ischemia. Numerous neuroprotective drugs have shown promise in experimental animal models, with many demonstrating an ability to salvage ischemic tissue. Despite this, such compounds have failed in human clinical trials (Dirnagl, Iadecola et al. 1999). There are a number of reasons behind this disappointing outcome.

The response to pharmacological interventions is much more complex in humans. While the onset of ischemia/reperfusion is regularly defined in animal models, the onset of symptoms does not always coincide with the onset of ischemia in humans. As a result, drug administration can be delayed for several hours, which may lie outside the window of opportunity. In addition, unfavourable pharmacokinetic properties of compounds can lead to poor drug uptake, lack of efficacy and unacceptable side-effects (Dirnagl, Iadecola et al. 1999). For example, MK-801, an anti-excitotoxic agent, has proven to be highly protective in animal models, yet even low doses produces renal toxicity and other adverse effects in clinical trials. MK-801 is a broad-spectrum NMDA receptor antagonist which blocks all NMDA receptors. Consequently, MK-801 blocks critical physiological NMDA receptor signalling, which caused lapses into a coma in human trials (Lipton 2004). Considering the importance of NMDA receptor-mediated currents in WM alone (see section 3.1), the complete, unspecific inhibition of all NMDA receptors can hinder cell survival and therefore, must be avoided. In order to overcome this issue, compounds like memantine, which block excessive NMDA receptor activation without interfering with physiological functions, are currently being tested in the treatment of acute stroke. Memantine is clinically approved for the treatment of chronic neurodegenerative diseases such as Alzehimers'. Its rapid association-dissociation kinetics prevents the accumulation of the drug in the NMDA receptor channel, allowing for normal physiological transmission (Lipton 2004, Stys and Lipton 2007). Experimental work on cultured oligodendrocytes and the ON found that the application of clinically relevant concentrations of memantine significantly protects juvenile WM from irreversible ischemic injury (Bakiri, Hamilton et al. 2008).

However, one of the primary reasons for the failure of many neuroprotective compounds is thought to be due to the anatomical difference between the CNS of experimental animal

models (mainly rodents) and humans. As mentioned, WM constitutes approximately 14% of the rodent brain by volume, whereas the adult human brain occupies approximately 50%. Thus, nearly all pre-clinical studies have inadvertently focussed on protecting GM regions, while underestimating the involvement of WM damage during ischemia (Matute, Domercq et al. 2013). In addition, the traditional view that WM is less vulnerable to ischemia has hindered our understanding of WM injury pathways. Importantly, there are distinct differences between the injury mechanisms involved in GM and WM ischemia. Therefore, the development of effective treatments relies on the discovery of pharmacological compounds which can also preserve WM structures.

5.1.2: White Matter NMDA Receptors

NMDA receptors are ionotropic glutamate receptors. When compared to AMPA/kainate receptors, NMDA receptors have much slower gating kinetics and as a result, largely generate the latter component of EPSCs (Dingledine, Borges et al. 1999). NMDARs have received much attention in recent years due to their key involvement in modulating synaptic strength (plasticity), a feature which is closely related to their propensity to flux relatively large Ca^{2+} loads (Tong, Shepherd et al. 1995, Stys and Lipton 2007, Blanke and VanDongen 2009, Vyklicky, Korinek et al. 2014). NMDARs are highly permeable to Ca^{2+} ions showing a 10-fold selectivity for Ca^{2+} ions over Na^{+} (Mayer and Westbrook 1987, Stys and Lipton 2007). Consequently, cells which express functional NMDARs are particularly susceptible to excitotoxic damage. NMDARs have long been implicated in a variety of neurological disorders including ischemia (Ogden and Traynelis 2011). Thus, there is a high demand for effective NMDAR antagonists which can block excessive receptor activation, yet do not interfere with physiological synaptic transmission.

5.1.2.1: Structure

NMDA receptors are tetrameric ion channels which incorporate subunits from three distinct families; NR1, NR2 and NR3. The NR1 subunit has 8 different splice variants which originate

from a single gene (Zukin and Bennett 1995, Jin and Woodward 2006). In contrast, NR2 and NR3 are encoded by 4 and 2 genes, respectively (Vyklicky, Korinek et al. 2014). Functional receptors require the expression of two mandatory glycine-binding NR1 subunits, in combination with two NR2(A-D) and/or NR3(A-B) subunits (Vyklicky, Korinek et al. 2014). The composition of NR2(A-D) subtypes incorporated in the receptor strongly dictates its functional properties (Cull-Candy, Brickley et al. 2001). However, functional NR2-lacking NMDA receptors are also evident in WM (Piña-Crespo, Talantova et al. 2010).

All subunits are structurally homologous, expressing an extracellular amino-terminal domain, an extracellular ligand binding domain, a transmembrane domain comprised of three transmembrane helices plus a re-entrant loop, and a cytoplasmic C-terminus (Paoletti and Neyton 2007, Vyklicky, Korinek et al. 2014). Activation of conventional NR1/NR2 receptors requires the simultaneous binding of glutamate on each NR2 subunits and glycine (co-agonist) on each NR1 subunit (Kleckner and Dingledine 1988, Clements and Westbrook 1991). Receptor activation induces a conformational change, leading to ion channel opening and a subsequent influx of a range of cations, particularly Na^+ and Ca^{2+}.

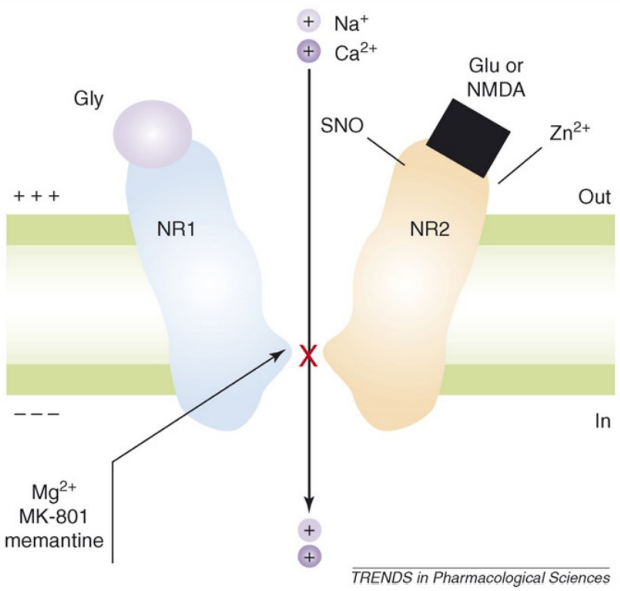

Fig. 5.1: Schematic representation of the NMDA receptor.

The image shows a side-profile of a conventional NMDAR incorporating the 'glycine-binding' NR1 and 'glutamate/NMDA-binding' NR2 subunits. The model illustrates the binding sites of several modulators including Mg^{2+}, MK-801, memantine, Zn^{2+}, sulfhydryl nitric oxide (SNO), glycine, glutamate and NMDA. Taken from (Stys and Lipton 2007).

WM NMDA receptors have a unique subunit composition. There are several reports that oligodendrocyte and myelinic NMDA receptors incorporate the NR1, NR2C, NR2D and/or NR3A subunits (Káradóttir, Cavelier et al. 2005, Salter and Fern 2005, Micu, Jiang et al. 2006, Micu, Plemel et al. 2016). The NMDA-mediated rise in myelinic Ca^{2+} during chemical ischemia is insensitive to specific blockers of NR2A and -2B blockers (Micu, Jiang et al. 2006). Similarly, NMDA-mediated currents in developing oligodendrocytes are unaffected by either ifenprodil, which inhibits NR2B-containing receptors, or by pregnenolone sulphate, which potentiates NR2A and -2B receptors (Káradóttir, Cavelier et al. 2005). On the other hand, high levels NR2C and NR3 subunit expression is evident on the myelinating processes of developing and mature oligodendrocytes (Káradóttir, Cavelier et al. 2005, Salter and Fern 2005). Genetic ablation of either the NR2D or NR3A subunits, dramatically reduced activity evoked increases in myelinic Ca^{2+} levels (Micu, Plemel et al. 2016). Interestingly, NR3 subunit expression can exist both with and without NR2 subunits (Stys and Lipton 2007, Vyklicky, Korinek et al. 2014). NR1/NR3 form 'glycine only' receptors as they are gated by glycine alone and do not require glutamate for activation (Stys and Lipton 2007, Piña-Crespo, Talantova et al. 2010). Furthermore, functional 'glycine only' NMDA receptors are present in CNS myelin (Piña-Crespo, Talantova et al. 2010).

As previously mentioned, WM NMDA receptors are approximately 10 times less sensitive to Mg^{2+} blockade, when compared to conventional neuronal NMDA receptors (Káradóttir, Cavelier et al. 2005). Receptors expressing NR2C/D and/or NR3 subunits are relatively resistant to Mg^{2+} block, but are less permeable to Ca^{2+} ions (Sasaki, Rothe et al. 2002, Stys and Lipton 2007). Thus, WM NMDA receptor activation may occur in the absence of strong membrane depolarisation (typically required to relieve the Mg^{2+} block).

5.1.2.2: Modulation

Given the Ca^{2+} permeability of NMDARs, receptor activation is highly controlled. NMDARs express several modulatory sites for endogenous ligands. NMDAR activation requires the simultaneous binding of two molecules of a co-agonist. Glycine, an endogenous amino acid, is the main co-agonist at extrasynaptic NMDA receptors (Papouin, Ladepeche et al. 2012). However, a variety of alternative molecules (e.g. serine and alanine) can also activate

receptors as co-agoinsts (Vyklicky, Korinek et al. 2014). Similarly, NMDAR activation is voltage-dependent. At resting membrane potential, ionic flux through NMDA receptors is physically blocked by extracellular Mg^{2+} ions. While physiological concentrations of extracellular Mg^{2+} are ~2mM, the intracellular concentrations of such ions is in the micro-molar range. Thus, at a negative resting membrane potential, an inward flux of Mg^{2+} ions prevails and subsequently binds to a Mg^{2+}-binding site located within the receptor pore. (Note; it has been reported that intracellular Mg^{2+} ions are also capable of blocking current flow (Johnson and Ascher 1990)). However, this block is rapidly relieved following membrane depolarisation (Kampa, Clements et al. 2004). AMPA/kainate receptor-mediated depolarisation promotes the removal of the Mg^{2+} blockade by a process of electrostatic repulsion (Qian and Johnson 2002, Paoletti and Neyton 2007, Blanke and VanDongen 2009). Endogenous Zn^{2+} is another non-competitive antagonist of NMDA receptors. Zn^{2+} selectively inhibits NR2A expressing receptors and does not operate in a voltage dependant manner (Westbrook and Mayer 1987, Paoletti and Neyton 2007). In addition, NMDA receptors are also strongly modulated by extracellular pH (Traynelis and Cull-Candy 1990). The receptors are selectively inhibited by H^+ ions and thus display a higher degree of inhibition in acidic environments. The IC_{50} for H^+ ions resides close to a physiological pH of 7.4. Therefore, under control conditions, receptors are not fully activated (Traynelis and Cull-Candy 1990). Furthermore, NMDA receptors desensitize in the sustained presence of glutamate, decreasing current flow over time (Nahum-Levy, Lipinski et al. 2001). This includes a Ca^{2+}-dependant form of desensitization where increasing concentrations of intracellular Ca^{2+} decreases receptor activity via a negative feedback loop (Rosenmund, Feltz et al. 1995).

Following the discovery of distinct NMDA receptor subunits, a variety of sub-unit selective compounds have become available. First generation NMDAR antagonists (e.g. MK801) failed to discriminate between different subunits. The development of tolerable sub-unit selective antagonists would permit the regulation of receptor inhibition in a region-specific manner (Ogden and Traynelis 2011). Thus, subunit-selective antagonists pose as a promising therapeutic agent to overcome the unselective inhibition of all NMDA receptors and thus, minimise the unacceptable side-effects. Unfortunately, there are no truly selective NR3 selective antagonists available at the moment. However, a range of NR2 sub-unit selective

antagonists are. The regional diversity of NR2 (A-D) subunits throughout the CNS may aid in the development of acceptable neuroprotective agents.

5.1.3: Ischemic Myelin Damage:

Myelin can protect underlying axons in several ways. As discussed in chapter 3, myelin provides metabolic support to actively firing axons. In addition, myelin acts as a protective cushion which can protect axons from physical trauma (Reeves, Doperalski et al. 2014). Paranodal myelin loops form a tight junction with the axonal membrane, forming a insulating seal around the axon cylinder. Although there are narrow gaps which separate the myelin and the axon at the paranodal junction flanking each node (~2-4nm) (Mierzwa, Shroff et al. 2010), the insulating myelin sheath forms a diffusional barrier between the axon and the extracellular space (Velumian and Samoilova 2014). Therefore, myelin can shield the axolemma from potentially harmful substances in the extracellular milieu (Reeves, Doperalski et al. 2014). In theory, this can also exacerbate myelin injury under pathological conditions. The tight axo-myelinic junction leaves the periaxonal space particularly susceptible to the accumulation of potentially toxic substances. For example, K^+ released from under-laying axons during electrical stimulation is known to accumulate in in the periaxonal space (David, Barrett et al. 1993, Brazhe, Maksimov et al. 2011). This could potentially promote the degradation of myelin sheath under pathological conditions such as ischemia.

Myelin sheath is highly susceptible to ischemic injury. Myelin degradation and decompaction occurs rapidly following the onset of ischemia, typically within the initial 30 minutes. For example, adult SD rats subject to four-vessel occlusion display early demyelination and a drop in MBP levels (Chen, Yi et al. 2013). Similarly, Walker *et al.* also found a dramatic decrease in MBP staining following transient global ischemia (bilateral common carotid occlusion) in adult mice (Walker and Rosenberg 2010). Ultrastructural analysis of the adult rat cerebellum and ON has revealed that ischemia leads to the focal splitting, loosening and separation of myelin lamella (Micu, Jiang et al. 2006, Hamilton, Kolodziejczyk et al. 2016).

Myelin damage is fundamental to the functional loss WM experiences in a number of disease states including multiple sclerosis (MS), traumatic brain injury (TBI), stroke and cerebral palsy

(Fern, Matute et al. 2014, Mierzwa, Marion et al. 2015, Macrez, Stys et al. 2016, Saab, Tzvetavona et al. 2016). As previously mentioned, $NaV_{1.2}$ expression along unmyelinated axons facilitates AP conduction prior to the initiation of myelination. However, during myelination, $NaV_{1.2}$ expression is replaced by clusters of $NaV_{1.6}$ at the node of Ranvier in order to facilitate saltatory conduction in myelinated axons. Acutely demyelinated axons lack the insulating properties of myelin sheath. As a result, demyelination increases membrane capacitance and decreases membrane resistance. Therefore, in the absence of intact myelin, clustered Na^+ influx at the node is typically incapable of depolarising the newly demyelinated axon segment. Although, $NaV_{1.2}$ expression may persist in myelinated axons, they are unable to support AP conduction following demyelination (Smith 1994, Debanne, Campanac et al. 2011). Therefore, axons regularly exhibit complete conduction block following myelin breakdown (Smith 1994).

5.1.4: NMDA receptor involvement in myelin damage?

While the decompaction and breakdown of internodal myelin is a major cause of WM dysfunction, the mechanism(s) of myelin injury during ischemia is a highly debated topic at the moment. The established view is that the rise in $[Glut]_e$ is responsible for the over-activation of myelinic NMDA receptors, which facilitates the excessive influx of Ca^{2+} ions. Although myelin is electrically silent (Saab, Tzvetavona et al. 2016), several studies have shown that myelin disruption is a Ca^{2+}-dependent process. The activation of Ca^{2+}-dependent enzymes, such as calpain, is recognised as a trigger for myelin breakdown during ischemia (Lankiewicz, Marc Luetjens et al. 2000). Early studies by Li and Stys (2000) found that incubating dorsal column WM with glutamate (1mM for 3hours) led to severe myelin damage, characterised by the degeneration of MBP (Li and Stys 2000). The expression of NMDA receptor subunits throughout compact myelin, combined with their ability to permit Ca^{2+} influx, leaves myelin susceptible to excitotoxic injury under ischemic conditions (Káradóttir, Cavelier et al. 2005, Micu, Jiang et al. 2006, Micu, Plemel et al. 2016). NMDA-receptor activation is known to mediate a direct rise in myelinic Ca^{2+}, which promotes the pathological loosening and vacuolation of myelin sheath during metabolic inhibition (Micu, Jiang et al. 2006, Pina-Crespo, Talantova et al. 2010).

Despite evidence of NMDAR-mediated myelin breakdown during ischemia and the expression of functional NMDA receptor subunits in myelin (Karadottir, Cavelier et al. 2005, Micu, Jiang et al. 2006, Pina-Crespo, Talantova et al. 2010, Micu, Plemel et al. 2016), there is currently no evidence demonstrating functional protection of fully-myelinated WM tracts following the application NMDAR antagonists. As outlined in section 4.1.1.3, NMDAR blockade improves post-OGD functional recovery in the pre-myelinated and early-myelinating RON (P0-P28) (Bakiri, Hamilton et al. 2008, Alix and Fern 2009, Huria, Beeraka et al. 2015). However, this is closely associated with the direct protection of small diameter pre-myelinated axons. While non-NMDAR antagonists are known to preserve CAP conduction in fully-myelinated WM following ischemia (Li, Mealing et al. 1999, Kanellopoulos, Xu et al. 2000, Tekkök and Goldberg 2001, Tekkok, Ye et al. 2007, Baltan, Besancon et al. 2008), numerous studies have found no significant functional protection in the presence of NMDAR antagonists (Yam, Dunn et al. 2000, Tekkok, Ye et al. 2007, Baltan 2016). For example, treating adult MONs with the broad-spectrum AMPA/kainate receptor antagonists, NBQX and CNQX, dramatically improves post-OGD CAP recovery by 45.3% and 42.8%, respectively (Tekkök, Ye et al. 2007). However, the same study found no significant improvement following treatment with NMDAR antagonists, MK-801, 7-CKA and DL-AP7. In fact, NMDAR inhibition, with 7-CKA, is reported to hinder post-OGD functional recovery in the adult MON (Baltan 2016).

As a result, the involvement of ischemic NMDA receptor activation in fully-myelinated WM tracts is controversial. Several reports have challenged the idea. Recently, Hamilton *et al.* (2016) published findings which demonstrate that current flow through NMDA receptors only accounts for a small component of the total inward current recorded from whole-cell clamped, mature cerebellar oligodendrocytes during ischemia (Hamilton, Kolodziejczyk et al. 2016). Interestingly, they found the application of NMDA did not lead to an elevation in $[Ca^{2+}]_i$ levels in either the soma or myelinating processes of mature oligodendrocytes. Instead, approximately 70% of the ischemia evoked rise in $[Ca^{2+}]_i$ was via TRP-A1 channels, which are activated by elevated $[H^+]_i$. While Hamilton *et al.* relied on live imaging from the cytoplasmic domain of oligodendrocytes, it must be noted that this region is distinct from the myelin sheath. Yang *et al.* (2014) proposed a plausible explanation as to why NMDA receptors are not involved in WM ischemia. The proton binding site on NMDA receptors leave it particularly sensitive to changes in extracellular pH. They suggested that the drop in pH during ischemia

(acidosis) blocks NMDAR-mediated ion fluxes. Interestingly, they found that NMDAR blockade prevents the morphological disruption to myelin and significantly preserves CAP area following an alternative form of energy deprivation, algycemia. They noted that unlike ischemia, aglycemia leads to an alkaline shift in pH and a decrease in $[Glut]_e$, as glutamate is metabolised in a desperate effort to generate ATP. In contrast, elevated intracellular oxaloacetate levels promote an increase in extracellular levels of aspartate, an alternative NMDA receptor agonist (Yang, Hamner et al. 2014).

This raises the question as to whether NMDAR activation actually promotes myelin breakdown, and if so, why have many studies found that NMDAR blockade does not improve functional recovery following ischemia.

5.1.5: Objective

Evidence suggests that NMDAR expression moves from the oligodendrocyte to myelin during development, with a notably high expression of NMDAR sub-units on the inner loops of myelin which face the axolemma. The previous chapter demonstrated internodal vesicular glutamate release along myelinated axons. It is therefore reasonable to presume that axonal vesicular release under ischemic conditions will empty directly into the tight peri-axonal space between the internal myelin surface and the axolemma (20nm).

Thus, the overall aim of this chapter is to examine the significance of excitotoxic myelin injury during ischemia. More specifically, I aim to resolve the controversy regarding the involvement of myelinic NMDA receptors. In addition, I hope to test the effect of a variety of sub-unit selective NMDAR antagonists with high clinical potential.

5.2: Results

5.2.1: OGD-induced injury in the developing rat ON and CC

Action potential failure underlies a variety of functional deficits in pre-term infants who suffer neonatal stroke. To access the effect of ischemia on developing WM, CAPs were recorded from the P10 rat ON and CC. WM tracts were subject to 60-minutes OGD (oxygen-glucose deprivation), followed by 60-90 minutes reperfusion. RON CAP recordings remained stable under control conditions for 135-minutes, showing no decrease in CAP amplitude (105.60±3.48%, *n*=10, Fig. 5.2a-c). In contrast, withdrawal of O_2 and glucose led to a gradual decline in CAP amplitude over the course of 60 minutes, reaching 8.03±1.15% (*n*=18) before reperfusion. CAP amplitude only partially recovered following 60-minutes reperfusion, reaching 47.04±4.58% (*n*=18) of the initial, pre-OGD amplitude ($p<0.0001$, Fig. 5.2a-c).

In addition to irreversible functional injury, structural axonal damage was also observed following OGD. RONs were collected after control and OGD experiments. In order to examine axon integrity, immunohistochemistry (IHC) was performed on RON sections using the axonal maker, NF-70. Confocal imaging of NF-staining revealed severely disrupted axon cylinders following OGD, characterised by axonal fragmentation and disorientation (Fig. 5.3b). In contrast, time-matched controls show little to no evidence of axon disruption (Fig. 5.3a). NF-70 staining was quantified by measuring fluorescence intensity using Image-J software. Similar to CAP recordings, NF-70 reactivity in OGD-exposed nerves was significantly attenuated when compared to control nerves (OGD pixel intensity was 38.75±7.66% lower than control) ($p=0.01$, Fig. 5.3d).

In an effort to access and compare the effect of OGD on the neonatal CC, CAP recordings from the 'whole CC' were carried out using an identical technique to that employed with the RON (Li, Velumian et al. 2016). The CC was dissected out from a 400µm thick coronal brain slice (see 'Materials and Methods' for details) and each end was gently nudged into the barrel of a glass electrode. While the overall amplitude recorded from the CC was generally smaller than the RON (presumably due to an imperfect, looser fit inside the barrel of the electrode which will decrease external resistance (R_o) (Stys, Ransom et al. 1991)), the biphasic CAP

shape remained. Under control conditions, CAP amplitude remained stable for 165 minutes (100.60±10.24%, *n*=3, Fig. 5.4). However, exposure to OGD resulted in a progressive decline in CAP amplitude to 0.46±0.34% (*n*=9) after 60 minutes. Following the restoration of normoxic conditions, CAP amplitude slowly recovered to 41.04±8.70% of its initial size after 90 minutes (*n*=9, p=0.0046, Fig. 5.4). When compared to time-matched OGD experiments on the RON, there was no significant difference in CAP recovery after 90 minutes (versus RON: 36.13±5.50% (*n*=8), p=0.67, Fig. 5.5a,c). However, the rate of CAP recovery following re-introduction of O_2 and glucose was significantly slower in the CC (p=0.029, Fig. 5.5a-b). This is the first direct comparison between two distinct developing WM tracts.

Given that iGluR activation is known to mediate a large degree of irreversible functional damage in the P10 RON (Alix and Fern 2009), I decided to investigate the contribution of iGluR-mediated excitotoxic injury in the P10 CC. Replicating a known effective protocol (Alix and Fern 2009), the isolated CC was perfused with a combination of NBQX (20µM, AMPA/kainate receptor antagonist) and MK801 (10µM, NMDA receptor antagonist) for 20 minutes before, during and for 40 minutes after OGD. However, the simultaneous blockade of AMPA/kainate and NMDA receptors did not improve CAP recovery to a level of significance in the CC (52.78±11.93%, *n*=9, p>0.05, Fig. 5.6).

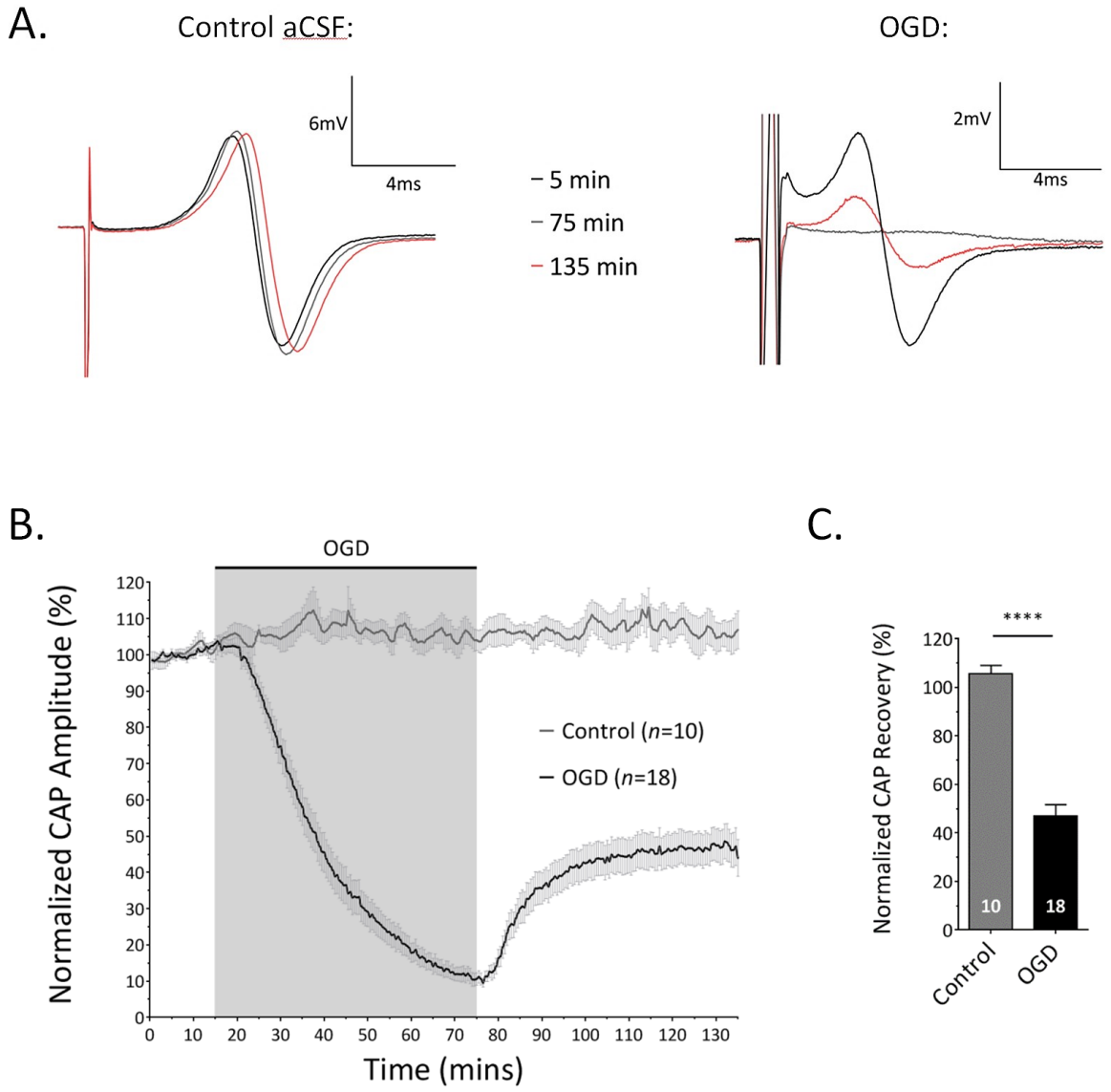

Fig. 5.2: Ischemia-induced functional injury in the early myelinating (P10) RON.

a) Representative biphasic CAP traces recorded under control conditions and during exposure to 60 minutes of OGD. (*For all remaining representative CAP traces, the time points correspond to the CAP time-course below (B); black = pre-OGD, grey = 60 minutes OGD and red = 60-90 minutes reperfusion).* **b)** CAP time-course under control conditions and for OGD experiments. Note the reversible drop in CAP amplitude during OGD, followed by a partial recovery during reperfusion. **c)** Histogram comparing CAP amplitude recovery after OGD against time-matched control experiments. ****p<0.0001.

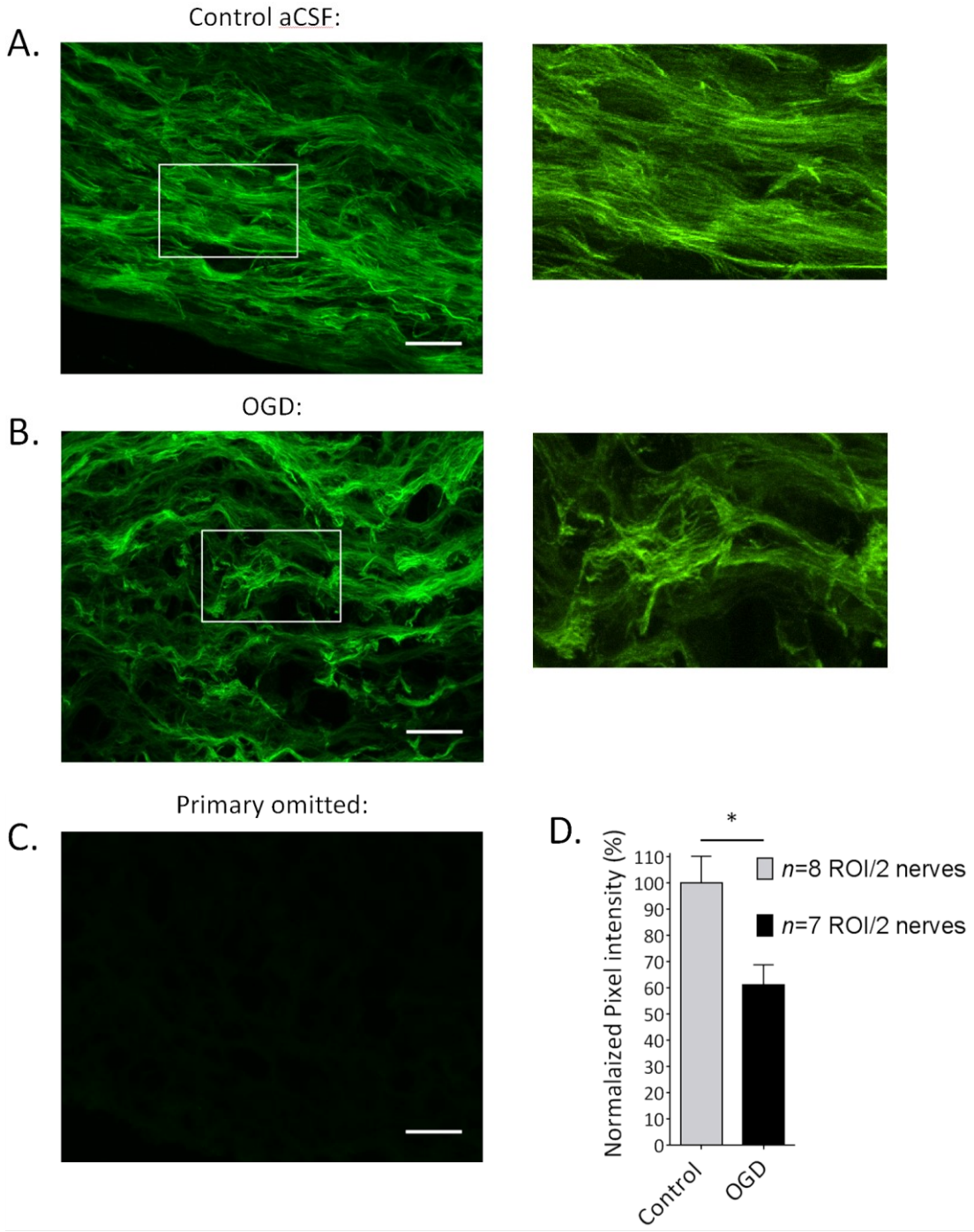

Fig. 5.3: Ischemia-induced disruption of axon structural integrity in the early myelinating (P10) RON.

a) Representative image of neurofilament-70 (NF-70) immunofluoresence in fixed P10 RON following a control experiment. Inset shows an example of NF-70 staining at a higher gain. Note the continuous unidirectional pattern of axon cylinders. **b)** Representative image of NF-70 immunofluoresence in fixed P10 RON following 60 minutes of OGD and 60 minutes reperfusion. Inset shows an example of NF-70 staining at a higher gain. Note the disrupted pattern of staining characterised by disorientated axon cylinders and the loss of NF-70 fluorescence in several regions. **c)** No immunoreactivity is observed when NF-70 is omitted. **d)** Histogram comparing the relative NF-70 immunofluoresence intensity between control and OGD nerves. Note the drop in fluorescence following OGD. *$p<0.05$, scale bar = 20µm.

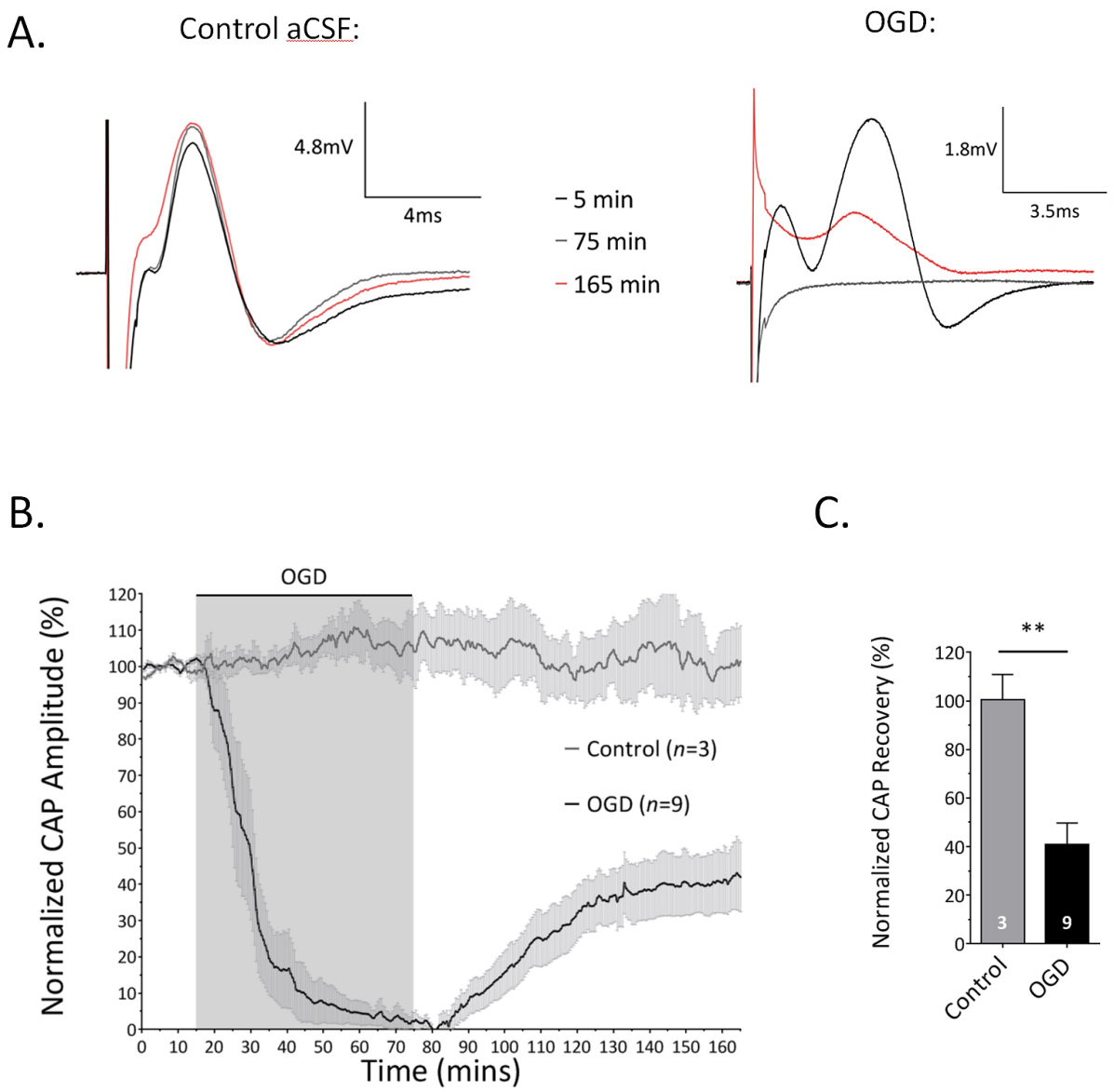

Fig. 5.4: Ischemia-induced functional injury in the early myelinating (P10) rat CC.

a) Representative biphasic CAP traces recorded under control conditions and during exposure to 60 minutes of OGD. **b)** CAP time-course under control conditions and for OGD experiments. Note the reversible drop in CAP amplitude during OGD, followed by a partial recovery during reperfusion. **c)** Histogram comparing CAP amplitude recovery after OGD against time-matched control experiments. **p<0.01.

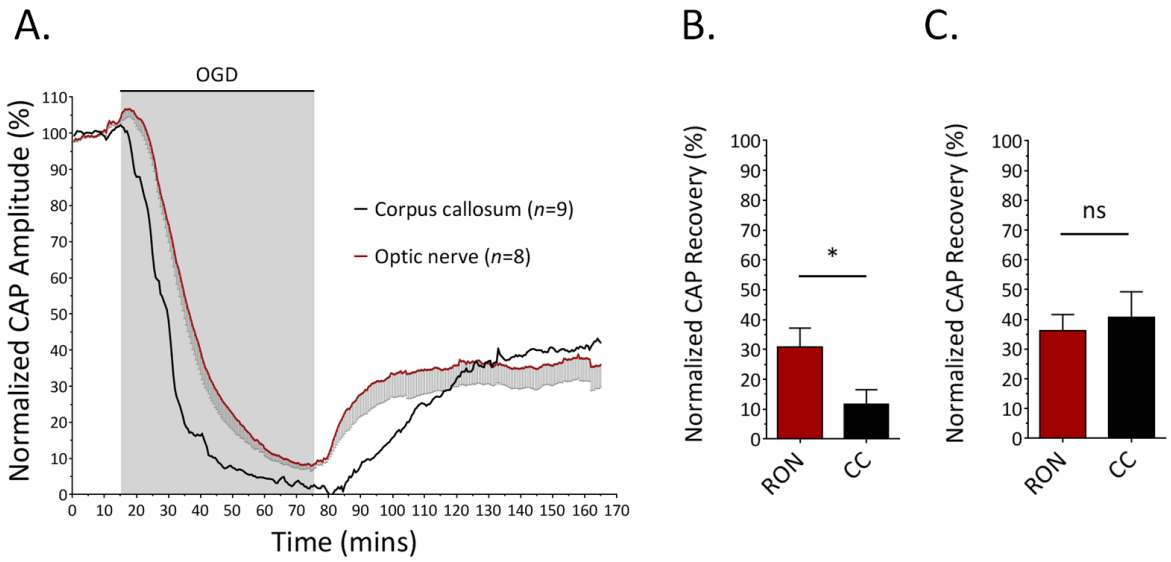

Fig. 5.5: The P10 RON and CC display a similar degree of sensitivity to OGD.

a) Overlay of the mean CAP time-course recorded from the CC and time-matched RON experiments. Note how CAP recovery after OGD is slower in the CC, yet the overall recovery is near identical. **b)** Histogram comparing CAP amplitude after 20 minutes of reperfusion. **c)** Histogram comparing CAP amplitude after 90 minutes reperfusion. ns $p>0.05$, *$p<0.05$.

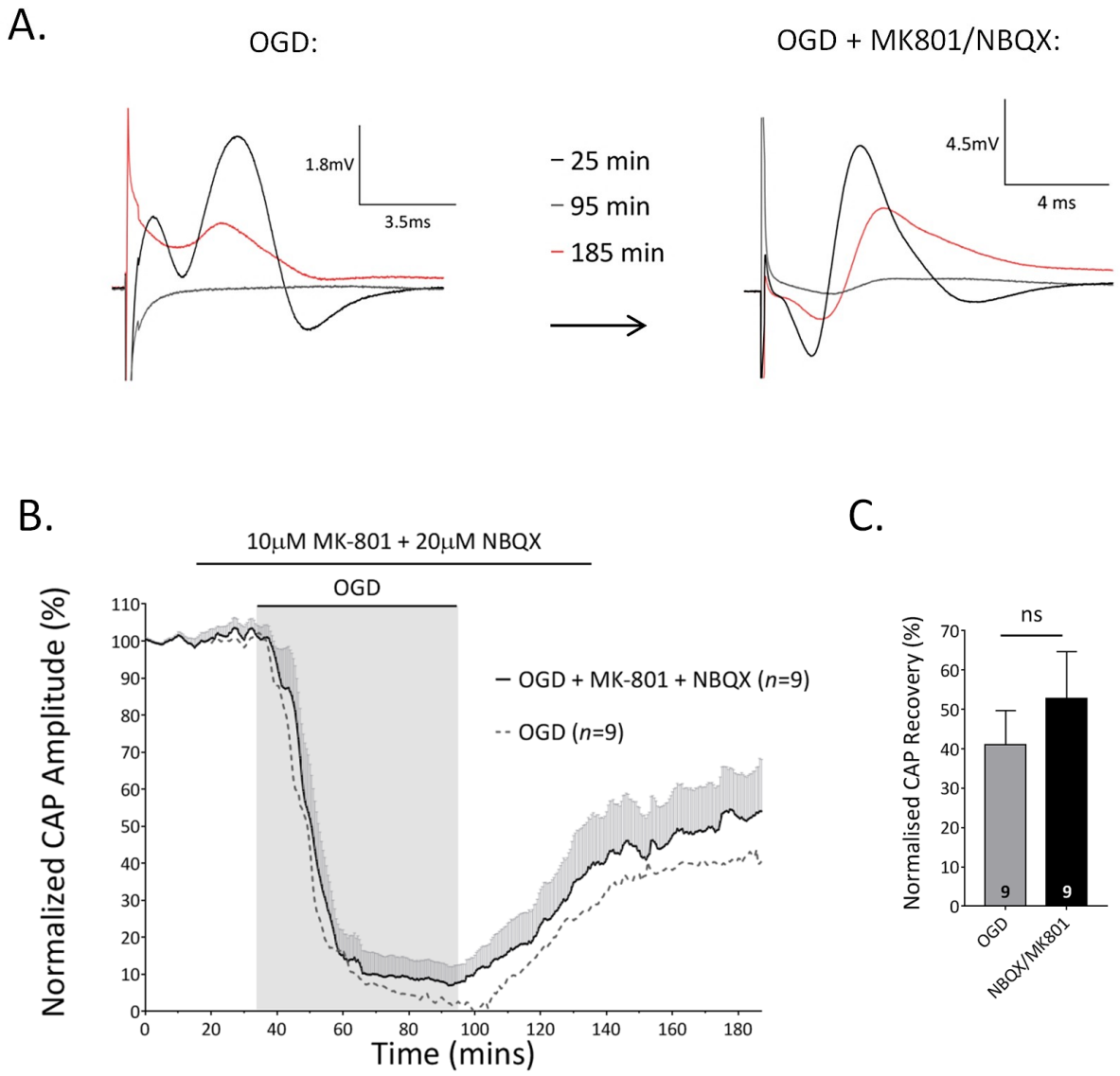

Fig. 5.6: Blockade of ionotropic glutamate receptors does not significantly reduce OGD-induced injury in the P10 CC.

a) Representative CAP trace in the presence of AMPA/kainate receptor blocker, NBQX and NMDA receptor blocker, MK-801. **b)** CAP time-course in the presence of iGluR antagonists. The dotted trace represents the mean CAP time-course in OGD experiments without drug. **c)** Histogram showing the effect of NBQX and MK-801 on functional recovery post-OGD. ns $p>0.05$.

5.2.2 OGD-induced injury in the adult RON

In adults, approximately 95% of strokes affect WM (Wang, Liu et al. 2016). Unlike the neonatal RON, the CAP waveform recorded from the adult RON is typically triphasic in shape (see Fig. 5.7a for example). Therefore, the rectified area under the curve was recorded as a quantitative measure of axonal function. Under control conditions, CAP area showed no attenuation over a 165-minute period, slightly increasing by 13.90±6.72% of initial control area (*n*=4, Fig. 5.7c-e). In contrast, exposure to OGD led to a rapid drop in CAP area, followed by a complete block in AP conduction. Once CAP failure initiated, all three peaks initially fell in unison (Fig 5.7e). However, the first peak was typically the final peak to completely block out. CAP area was reduced to 50% of initial control recordings within 4.19±0.52 minutes of OGD (*n*=13). The mean CAP area after 60-minutes of OGD, followed by 90-minutes reperfusion, was irreversibly reduced to 15.12±1.71% of its original pre-OGD size (*n*=13, $p<0.0001$, Fig. 5.7a-e). CAP recovery typically stabilised within 37.81±4.10 minutes following the re-introduction of O_2 and glucose.

Following ON isolation, nerves were typically allowed to rest in the perfusion chamber under control conditions for 60 minutes before OGD was initiated. However, some experiments later in this chapter will require long drug pre-treatment periods of 2 hours. To investigate whether a longer resting period has any effect on OGD-sensitivity, several nerves were allowed to rest for 3 hours (i.e. 2 additional hours) in the chamber before exposure to OGD. However, there was no significant difference between the two groups (1 hour rest: 15.97±2.28% (*n*=9) *versus* 3 hour rest; 13.11±2.31% (*n*=4), p=0.47, Fig. 5.7a). For this reason, the data was pooled together.

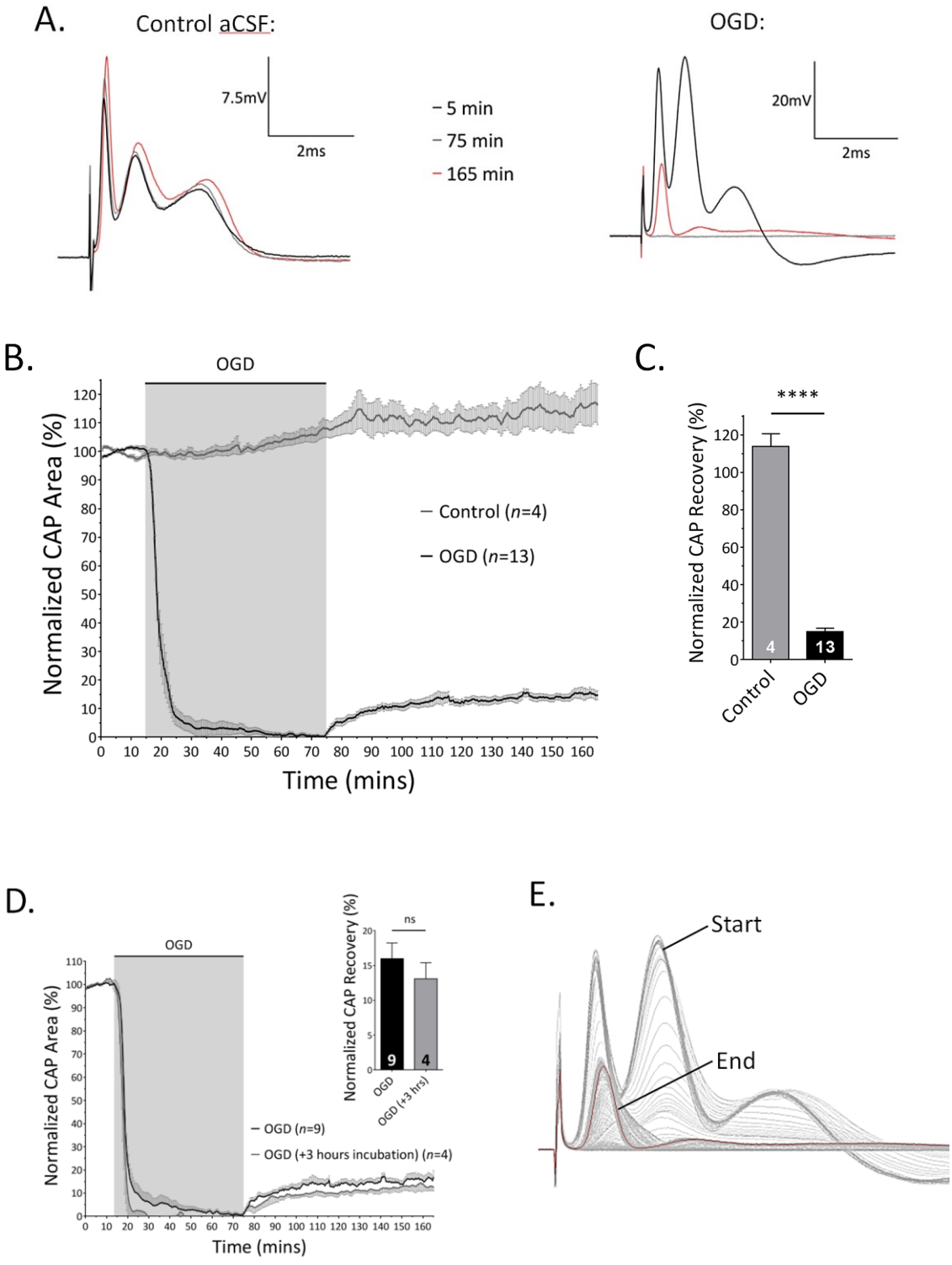

Fig. 5.7: Ischemia-induced functional injury in the fully-myelinated, adult RON.

a) Representative triphasic CAP traces recorded under control conditions and during exposure to 60 minutes of OGD. **b)** CAP time-course under control conditions and for OGD experiments. Note the rapid drop in CAP area upon exposure to OGD, followed by low recovery during reperfusion. **c)** Histogram comparing CAP recovery after OGD against time-matched control experiments. **d)** CAP time-course for OGD experiments in which nerves were allowed to stabilise for either 1 or 3 hours in the perfusion chamber before recording. Inset; histogram comparing CAP recovery post-OGD. **e)** A single representative CAP trace showing the pattern of CAP decline during OGD (grey). ns $p>0.05$, ****$p<0.0001$.

5.2.3 AMPA/kainate receptor-mediated injury

The adult RON is a well-established model WM tract and therefore, the injury mechanisms involved in WM anoxia/ischemia are relatively well-characterised (Stys 1998, Stys 2005). AMPA/kainate receptors are reported to mediate excitotoxic damage in adult WM by acting on the oligodendrocyte cell body (Li and Stys 2000, Tekkok and Goldberg 2001, McCarran and Goldberg 2007, Tekkok, Ye et al. 2007, Baltan, Besancon et al. 2008). In an effort to confirm the involvement of AMPA/kainate receptors in ischemic WM injury, experiments were performed in the presence of an known effective concentration of the broad-spectrum AMPA/kainate receptor antagonist, NBQX (20μM) (Alix and Fern 2009).

Initially, RONs were perfused with NBQX under control conditions. Perfusion with NBQX had no effect on CAP area over a 120 minute recording period. Furthermore, there was no significant difference between NBQX-treated nerves after 50 minutes wash-out, when compared to time-matched controls (NBQX: 98.94±8.54% (*n*=3), versus 113.90±6.72% (*n*=4), p=0.164, Fig. 5.8). This data demonstrates that NBQX exerts no toxic effects under control conditions. When nerves were exposed to OGD in the presence of NBQX (20 minutes before, during and 40 minutes after OGD), CAP recovery was significantly higher than experiments without the drug, reaching 35.55±7.98% after 90 minutes reperfusion (*n*=4, p=0.027, Fig. 5.9a-c), confirming the involvement of AMPA/kainate receptor activation during ischemia.

Next, I investigated whether the anti-excitotoxic effect of NBQX is dependent on its lipid permeability. NBQX has a lipid partition co-efficient of 1.4 (logP) at 7.0pH. In contrast, a disodium derivative of the drug, NBQX-disodium salt (NBQX-Na), is much more lipophobic, with a lipid partition co-efficient of 0.17 (logP) at 7.0pH. To test whether a difference in lipophilicity affects CAP recovery, experiments were repeated using NBQX-Na (20μM). Despite the difference in lipid partitioning, there was no significant difference between the two species of NBQX, with CAP recovery reaching 27.67±4.00% (*n*=4, p=0.41, Fig. 5.9a-b). This is consistent with reports that AMPA/kainate receptors are located on the oligodendrocyte body, not in myelin. The results from both species of NBQX were pooled, giving an overall CAP recovery of 31.61±4.39 (*n*=8, p=0.015, Fig. 5.9d-e).

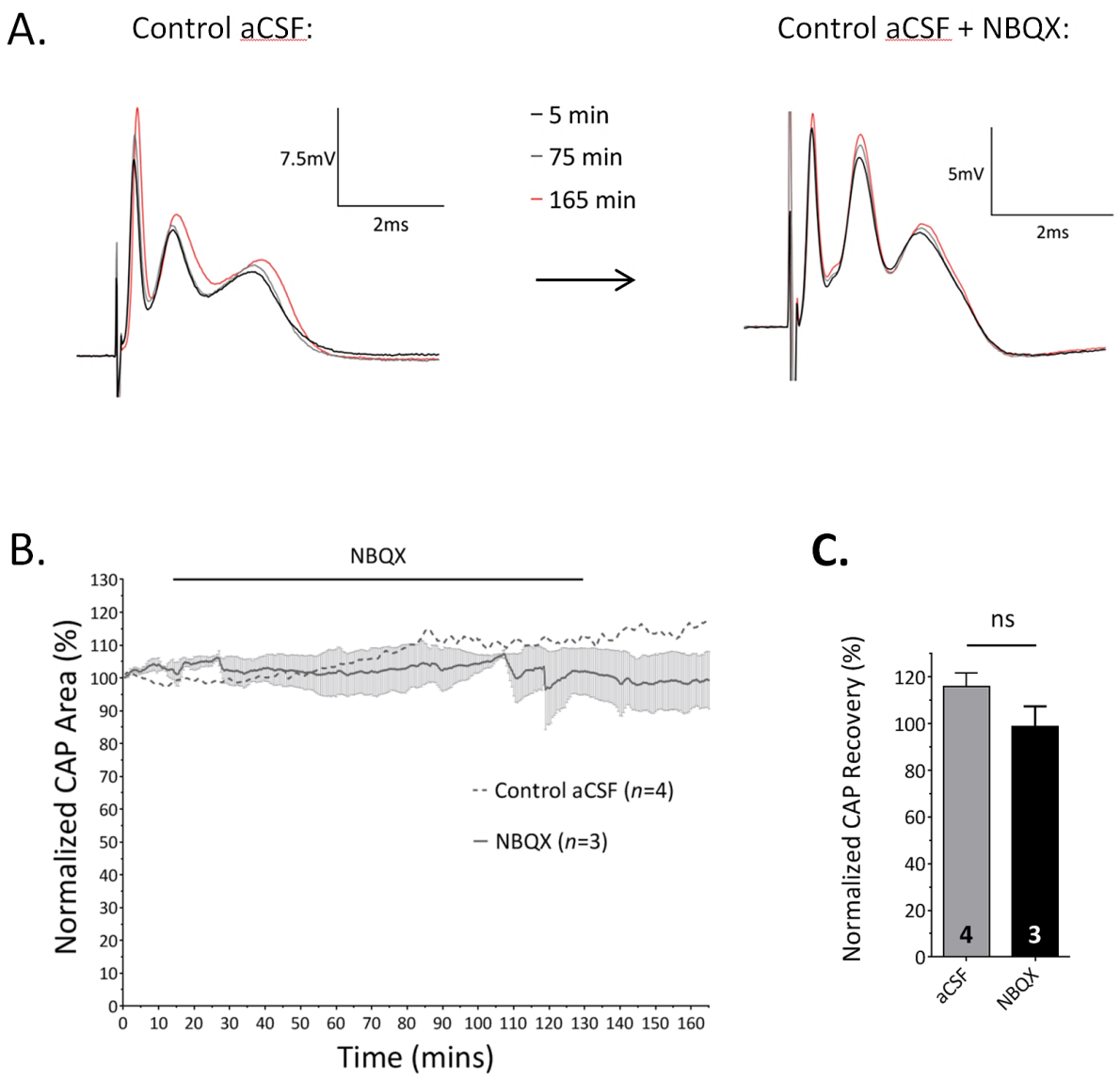

Fig. 5.8: Blockade of AMPA/kainate receptors under control conditions does not adversely affect CAP conduction.

a) Representative CAP trace in the presence of NBQX under normxic conditions in control aCSF. **b)** CAP time-course under control conditions including a 120-minute exposure to NBQX. **c)** Histogram showing the effect of NBQX on CAP area after 120 minutes exposure followed by 30 minutes wash-out. ns p>0.05.

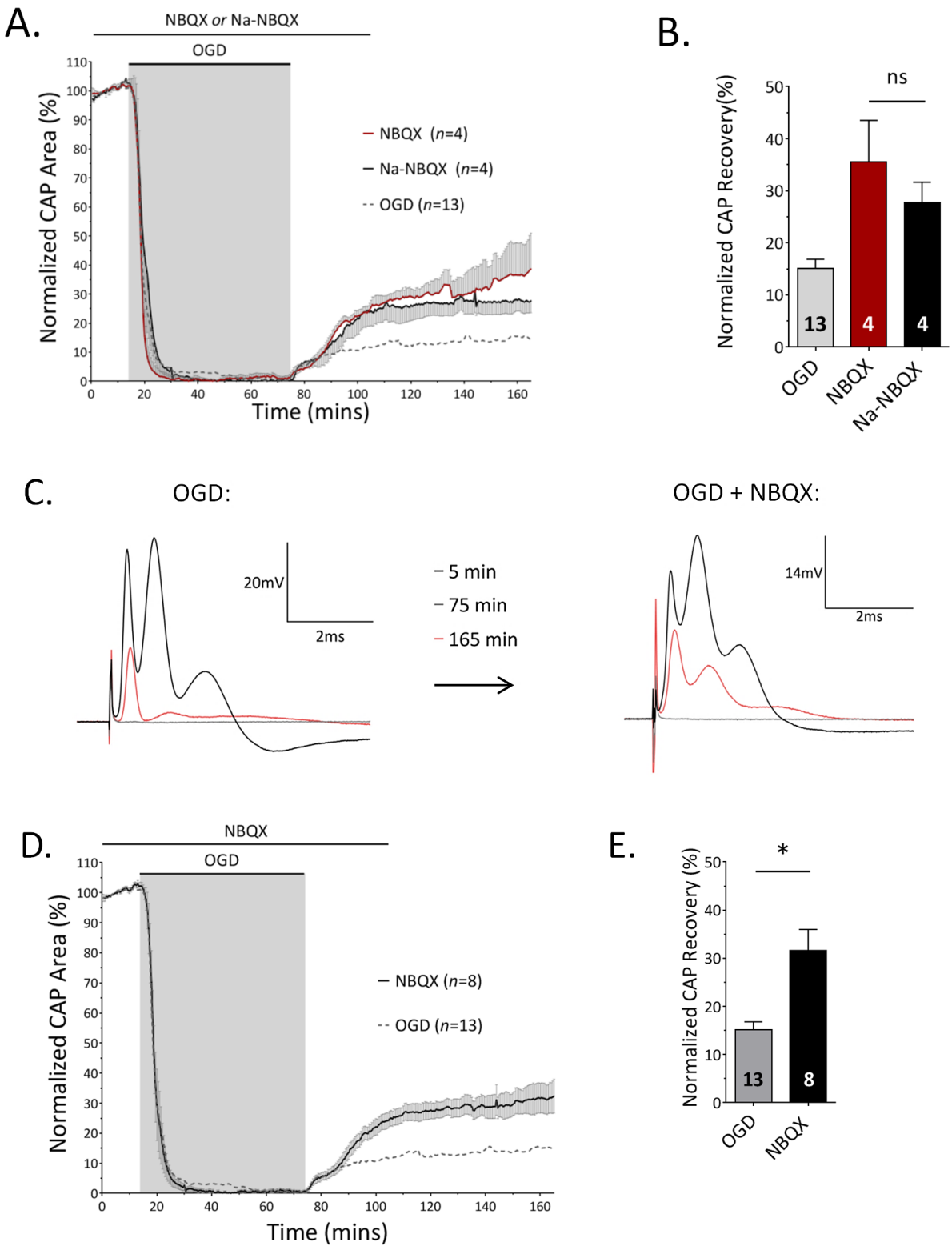

Fig. 5.9: Blockade of AMPA/kainate receptors improves functional recovery following OGD.

a) CAP time-course in the presence of either a lipid-soluble species of NBQX or a water-soluble species (Na-NBQX). Note; both AMPA/kainate receptor antagonists have a similar protective effect. **b)** Histogram comparing post-OGD CAP recovery in the presence of two NBQX species. **c)** Representative CAP trace in the presence of NBQX. **d)** CAP time-course in the presence of NBQX (pooled data). **e)** Histogram showing the effect of NBQX on functional recovery post-OGD (pooled data). ns $p>0.05$, * $p<0.05$.

5.2.4 Myelinic NMDA-receptor involvement in ischemic WM injury

Although adult WM expresses both AMPA/kainate and NMDA receptors, only AMPA/kainate receptors are thought to contribute to irreversible functional injury. Numerous studies have tested the effect of NMDA receptor inhibition during ischemia, but many have failed to find any significant improvement in functional recovery in mature myelinated WM (Li and Stys 2000, Tekkok, Ye et al. 2007, Baltan 2009). This is somewhat surprising considering they are reportedly involved in mediating functional damage in pre-myelinated WM, injury to developing oligodendrocyte process and myelin sheath disruption during modelled ischemia (Káradóttir, Cavelier et al. 2005, Salter and Fern 2005, Micu, Jiang et al. 2006, Alix and Fern 2009, Huria, Beeraka et al. 2015). Therefore, I aimed to further investigate the role of NMDA receptor activation during ischemia.

To start the investigation, I initially examined CAP recovery in the presence of MK-801 (10μM), a broad-spectrum NMDAR antagonist. Following a previous protocol (Alix and Fern 2009, Baltan 2009), RONs were perfused with MK-801 for 20 minutes before, during and 40 minutes after OGD. While MK-801 did appear to have a mild protective tendency using this protocol, it did not significantly improve CAP recovery (25.94±6.31, *n*=3, p=0.72, Fig. 5.10). Experiments were repeated using 50μM MK-801. However, again this did not improve CAP recovery to a level of significance (30.58±4.87, *n*=4, p=0.27, Fig. 5.10). Consistent with previous findings, we found no significant protection using this protocol with either 10 or 50μM MK-801. However, it did appear to partially preserve CAP area which inspired further examination.

Unlike AMPA/kainate receptors, which are located on the oligodendrocyte cell body, NMDA receptors are primarily expressed on the myelinating processes of oligodendrocytes (Káradóttir, Cavelier et al. 2005, Salter and Fern 2005) and within compact myelin sheath (Micu, Jiang et al. 2006, Micu, Plemel et al. 2016). Results from the previous chapter indicate that the peri-axonal space may be a significant site of excitotoxic injury during ischemia. Drug penetration through the myelin sheath is relatively slow and therefore, the interaction of MK-801 with NMDA receptors may be limited if the pre-treatment exposure time is short (i.e. 20 minutes). To access whether incomplete drug penetration was a limiting factor, we increased the length of the MK-801 pre-treatment period. RONs were perfused with MK-801 (50μM) for 90 minutes before, during and 40 minutes after O_2-glucose withdrawal. Curiously, this pre-

treatment protocol significantly improved post-OGD CAP recovery to 43.91±10.40% (*n*=4, p=0.002, Fig. 5.11b-d). Moreover, further increasing the length of drug pre-treatment to 120 minutes dramatically improved CAP recovery, with CAP area reaching 62.02±4.80% after reperfusion (*n*=6, p<0.0001, Fig. 5.11a-d). This translates to a 410% improvement in functional recovery. A longer pre-treatment period of 165 minutes failed to confer additional protection (56.31±11.24%, *n*=4, p<0.0001, Fig. 5.11b-d). Thus, MK801-mediated protection increased with pre-treatment time up to 120 minutes, where it was maximally protective (Fig.5.11d). The data supports the hypothesis that drug penetration into myelin is a slow process. For all remaining experiments requiring the use of NMDA receptor modulators, 120 minute pre-treatment periods were used.

In order to confirm that MK801 does not have any potentially interfering effect on CAP shape/area, CAP area was monitored under control conditions during exposure to MK-801 (50µM). Following a 120-minute pre-treatment period, CAP area was recorded for 125 minutes in the continued presence of MK-801, followed by a 40 minute wash-out period. MK-801 had no significant effect on CAP area under normoxic conditions (108.10±2.46%, *n*=3, (versus control; 113.90±6.72% (*n*=4)), p=0.39, Fig. 5.12).

Considering NBQX also provided a significant degree of functional protection, experiments were performed in the presence of both MK-801 (50µM) and NBQX (20µM). RONs were pre-treated with MK-801 for 120 minutes and NBQX for 20 minutes. The co-application of both antagonists resulted in a CAP recovery of 55.87±3.94 (*n*=4, p<0.0001). However, this was not significantly different to experiments with MK-801 alone, demonstrating that NBQX provides no additional protection (p=0.32, Fig. 5.13).

ICH was also performed to access the axonal integrity of MK-801 treated nerves (120 minute pre-treatment protocol). Nerves were collected following control, OGD and MK-801 experiments and post-fixed RON sections were stained with the axonal marker, NF-200. When compared to control slices (*n*=3), OGD-exposed nerves (*n*=4) were clearly disrupted, displaying a marked decrease in NF-200 fluorescence, axonal fragmentation and multiple regions of NF+ aggregations (see Fig. 5.14a-b). Interestingly, while MK-801 treated nerves (*n*=4 nerves) did appear to have numerous intact axons and much less NF+ aggregations, NF staining was still notably disrupted. Normalising NF-fluorescence data to OGD experiments

revealed that there was no significant improvement in NF-fluorescence intensity when nerves were treated with MK-801 (p=0.25, Fig. 5.14b). This is surprising considering NMDAR blockade preserves AP conduction.

Next, myelin structural integrity was examined using the fluorescent myelin stain, fluromyelin red. When compared to control nerves (*n*=3), OGD caused a dramatic decrease in fluorescence intensity, accompanied by distinct regions of myelin breakdown (*n*=3). In contrast, MK-801 treated nerves (*n*=3) retained a high degree of fluorescence which was not significantly different to control nerves (p=0.0635). MK-801 treatment prevented the formation of regions of myelin breakdown during OGD, significantly improving fluoromyelin reactivity (p=0.005, Fig. 5.15). Together, this data suggests that NMDA receptor block prevents myelin breakdown down during ischemia, which preserves AP conduction.

A recent study by Hamilton *et al.* (2016), reported that the toxic Ca^{2+} rise in myelin during ischemia, is a result of elevated $[K^+]_e$ which indirectly gates Ca^{2+}-permeable TRP-A1 channels, expressed on the myelinating oligodendrocyte process. Furthermore, they suggest that the rise in $[K^+]_e$ is primarily a result of NMDA receptor-mediated depolarisation. This raised the question of whether the functional and structural protection observed in the presence of MK-801 (Fig. 5.11 and Fig. 5.15), is a consequence of reduced TRP-A1 channel activity. To access the possible involvement of TRP-A1 channels, I examined CAP recovery in the presence of A-967079, a selective TRP-A1 receptor antagonist (Hamilton, Kolodziejczyk et al. 2016). To ensure sufficient penetration through the myelin sheath, adult RONs were pre-treated with TRP-A1 (10µM) for 120 minutes before exposure to OGD. However, A-967079 did not significantly improve functional recovery, with post-OGD CAP area reaching 24.35±6.61 (*n*=6, p=0.69, Fig. 5.16). This suggests the activation of myelinic NMDA receptors during ischemia, is directly responsible for the pathological disruption of myelin sheath.

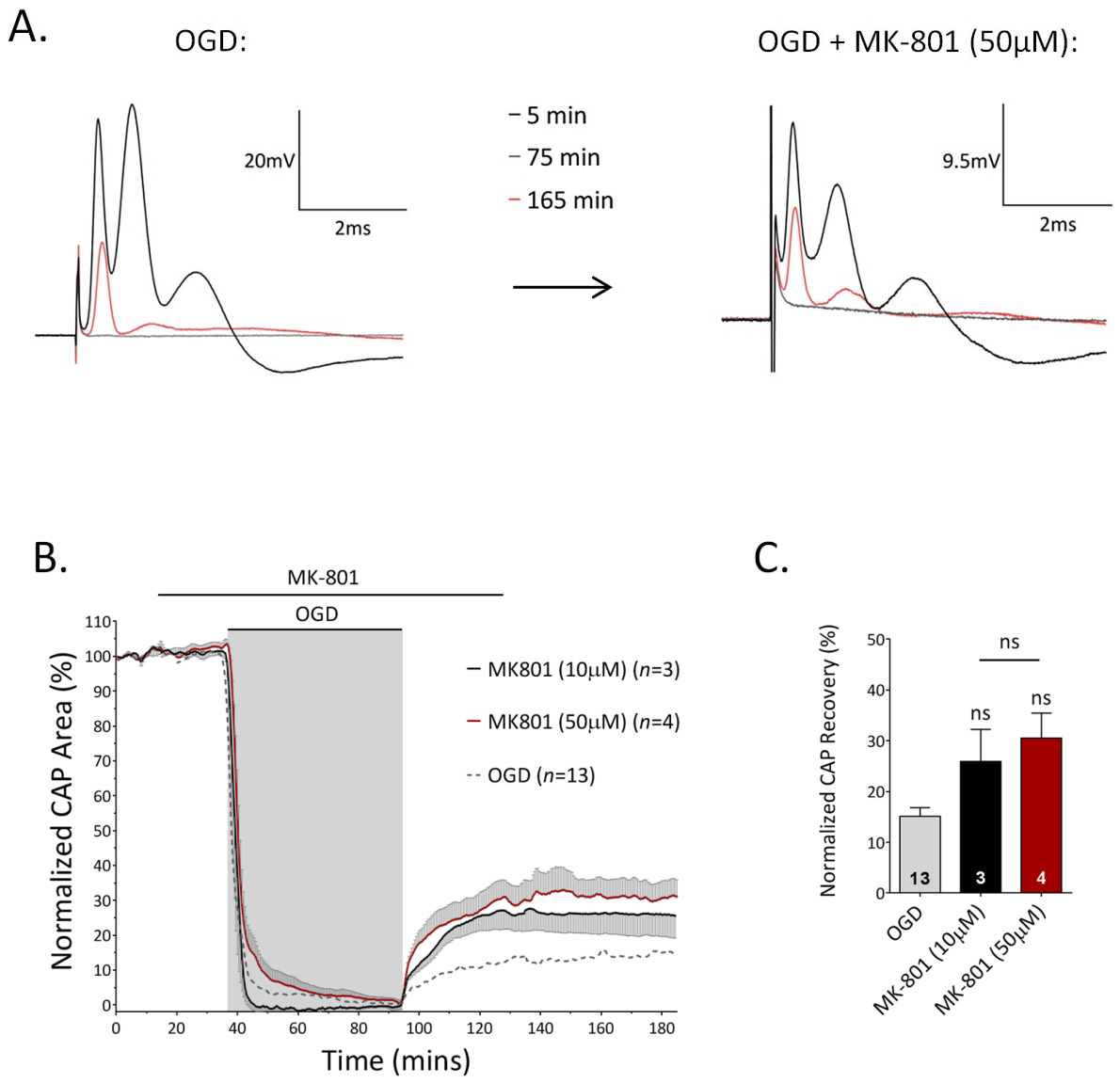

Fig. 5.10: A short pre-treatment period of NMDA receptor blockade does not significantly improve functional recovery following OGD.

a) Representative CAP trace in the presence of NMDA receptor blocker, MK-801. **b)** CAP time-course in the presence either 10 or 50µM MK-801, including a 20 minute pre-treatment period. **c)** Histogram comparing CAP recovery in the presence of MK-801. Note; both concentrations of MK-801 do not significantly improve post-OGD recovery using this protocol. ns $p>0.05$.

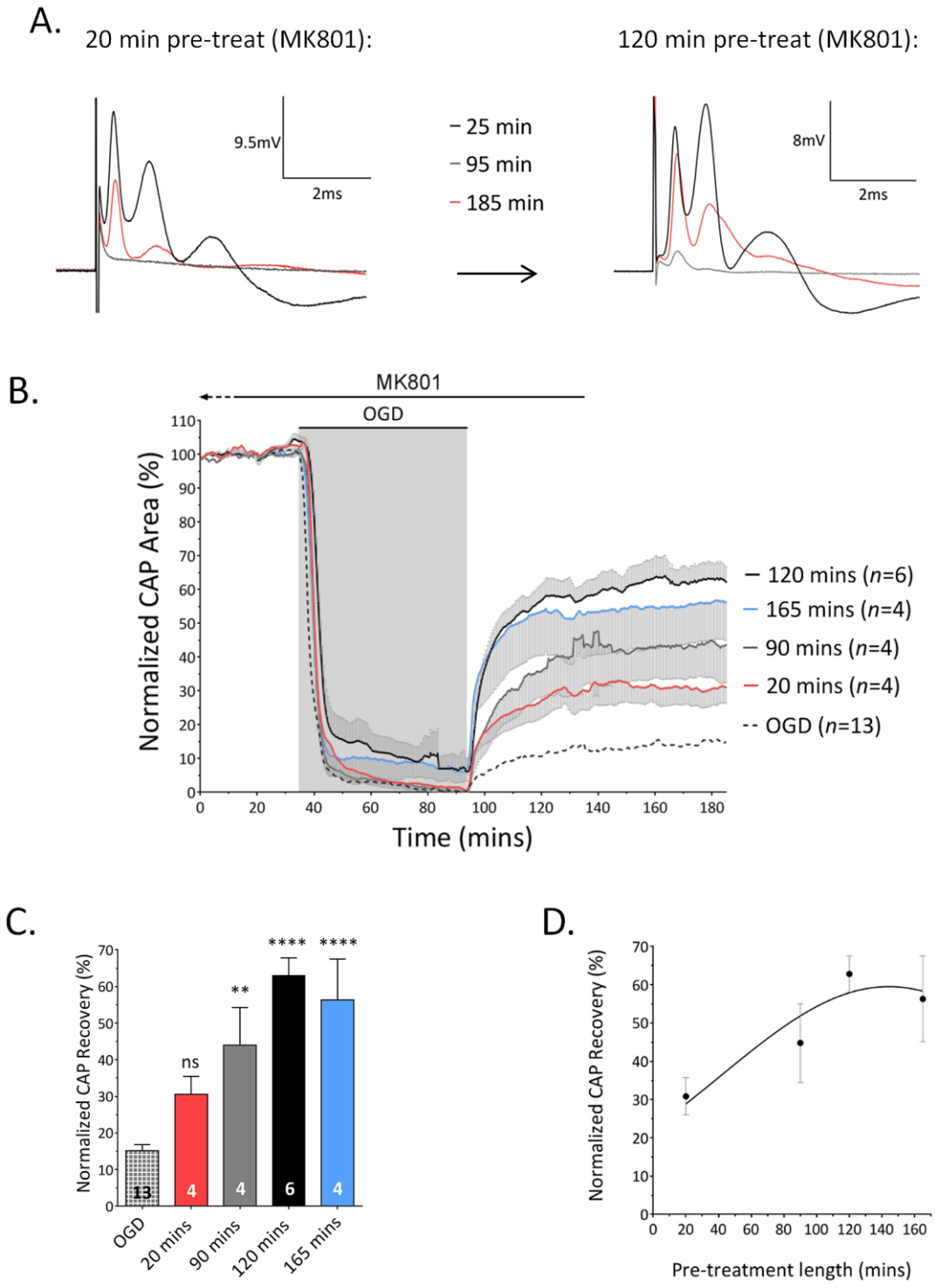

Fig. 5.11: NMDA receptor blockade elevates functional recovery following long pre-treatment periods.

a) Representative CAP trace in the presence of MK-801 following a 120 minute pre-treatment period before OGD. **b)** CAP time-course following different periods of MK-801 pre-treatment. Note how increasing the pre-treatment length improved functional recovery following OGD. **c)** Histogram comparing CAP recovery between a range of MK-801 pre-treatment periods. **d)** Data summary. ns $p>0.05$, **$p<0.01$, ****$p<0.0001$.

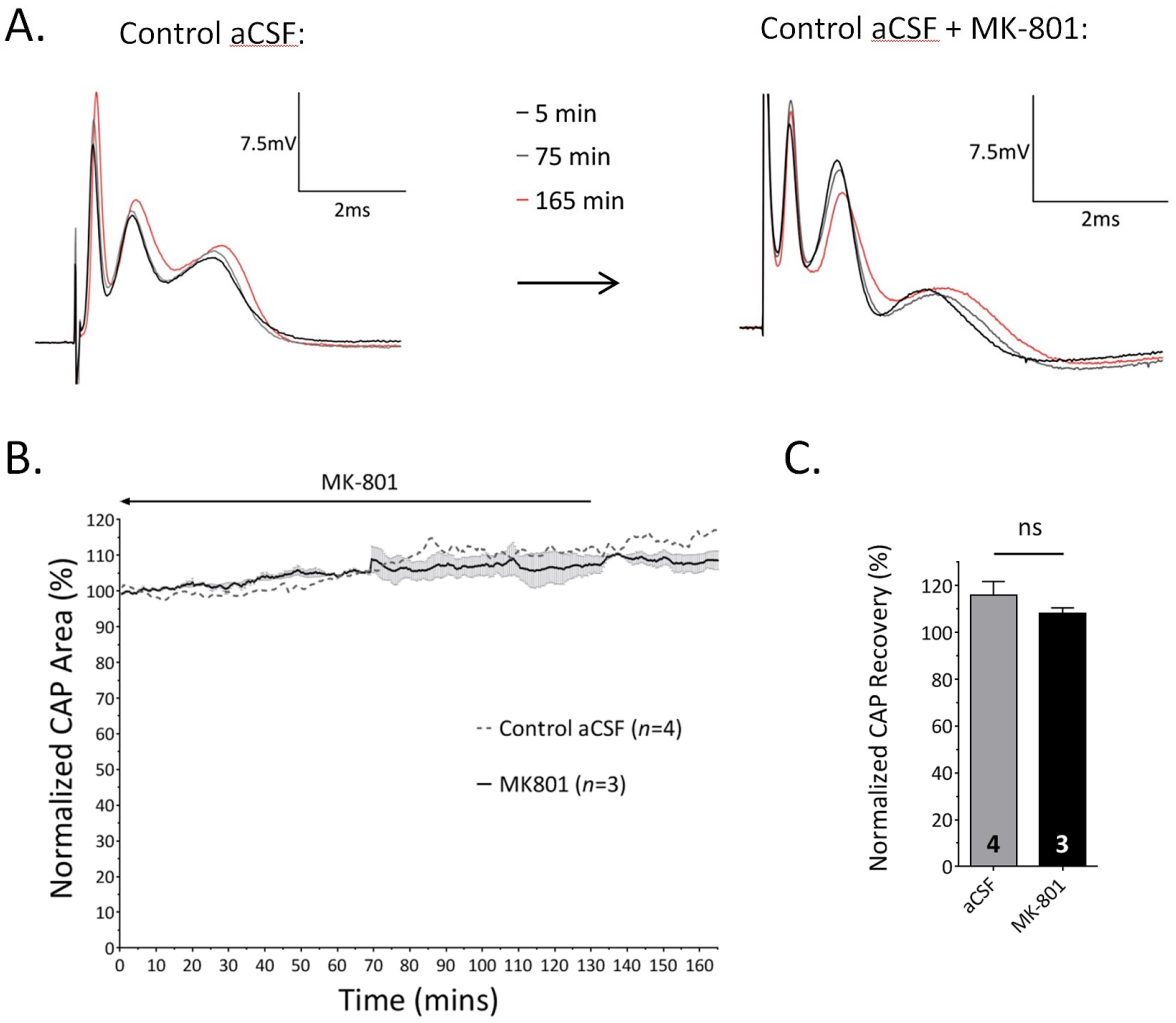

Fig. 5.12: Blockade of NMDA receptors under control conditions does not adversely affect CAP conduction.

a) Representative CAP trace in the presence of MK-801 under normxic conditions in control aCSF. **b)** CAP time-course under control conditions including a 120-minute exposure to MK-801. Note; before recording was initiated, nerves were also pre-treated with MK-801 for 120 minutes (total exposure to MK-801=240 minutes). **c)** Histogram showing the effect of MK-801 on CAP area after 120 minutes exposure followed by 45 minutes wash-out. ns $p>0.05$.

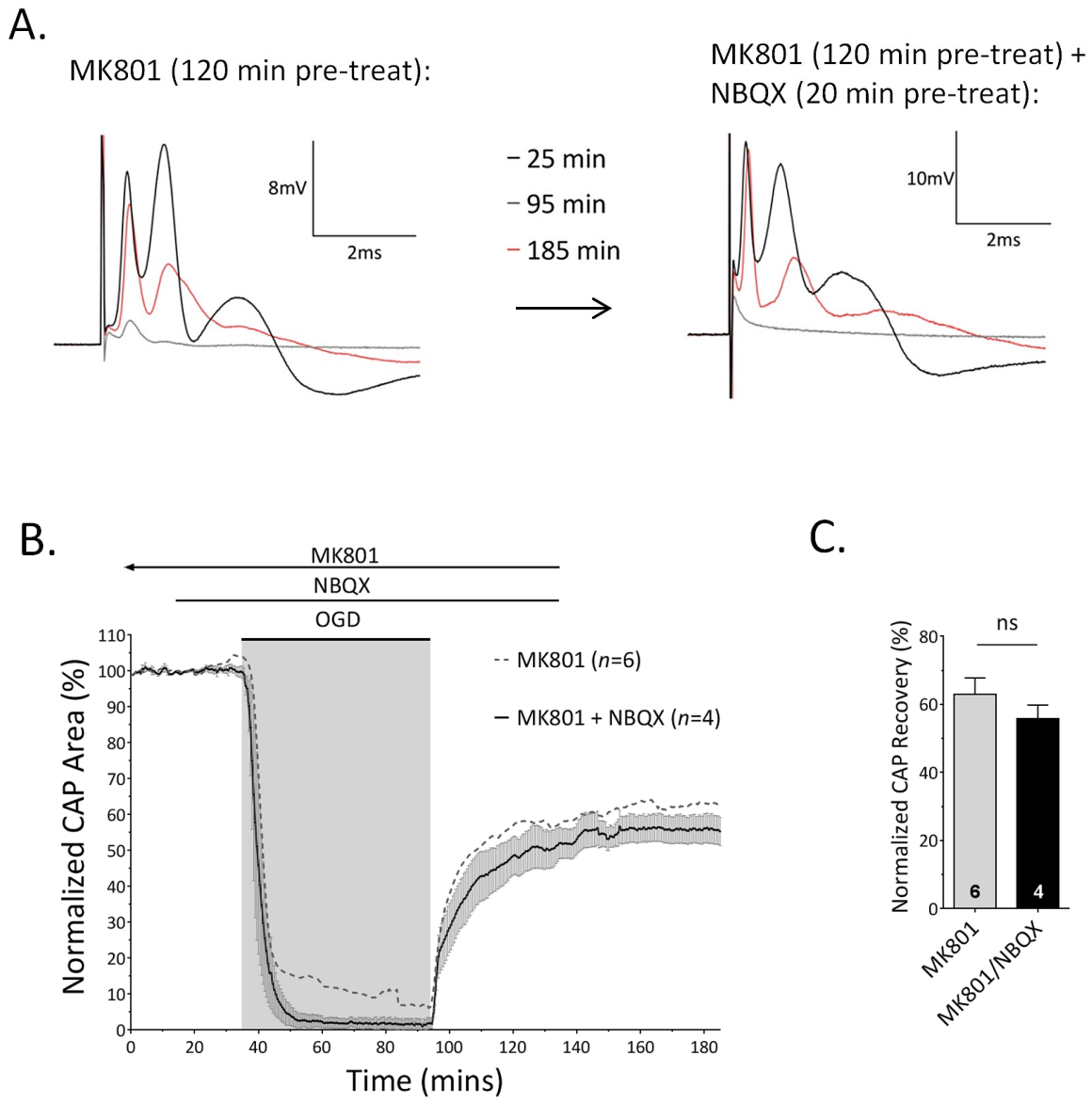

Fig. 5.13: The combined block of NMDA and AMPA/kainate receptors does not provide additional protection when compared to MK-801 alone.

a) Representative CAP trace in the presence of MK-801 and NBQX. **b)** CAP time-course following a 120 minute pre-treatment period with MK-801 and a 20 minute pre-treatment with NBQX. Note the high degree of functional recovery post-OGD. However, MK-801 mediated protection is not potentiated by NBQX. **c)** Histogram comparing CAP recovery in MK-801 treated nerve, with and without NBQX. ns $p>0.05$.

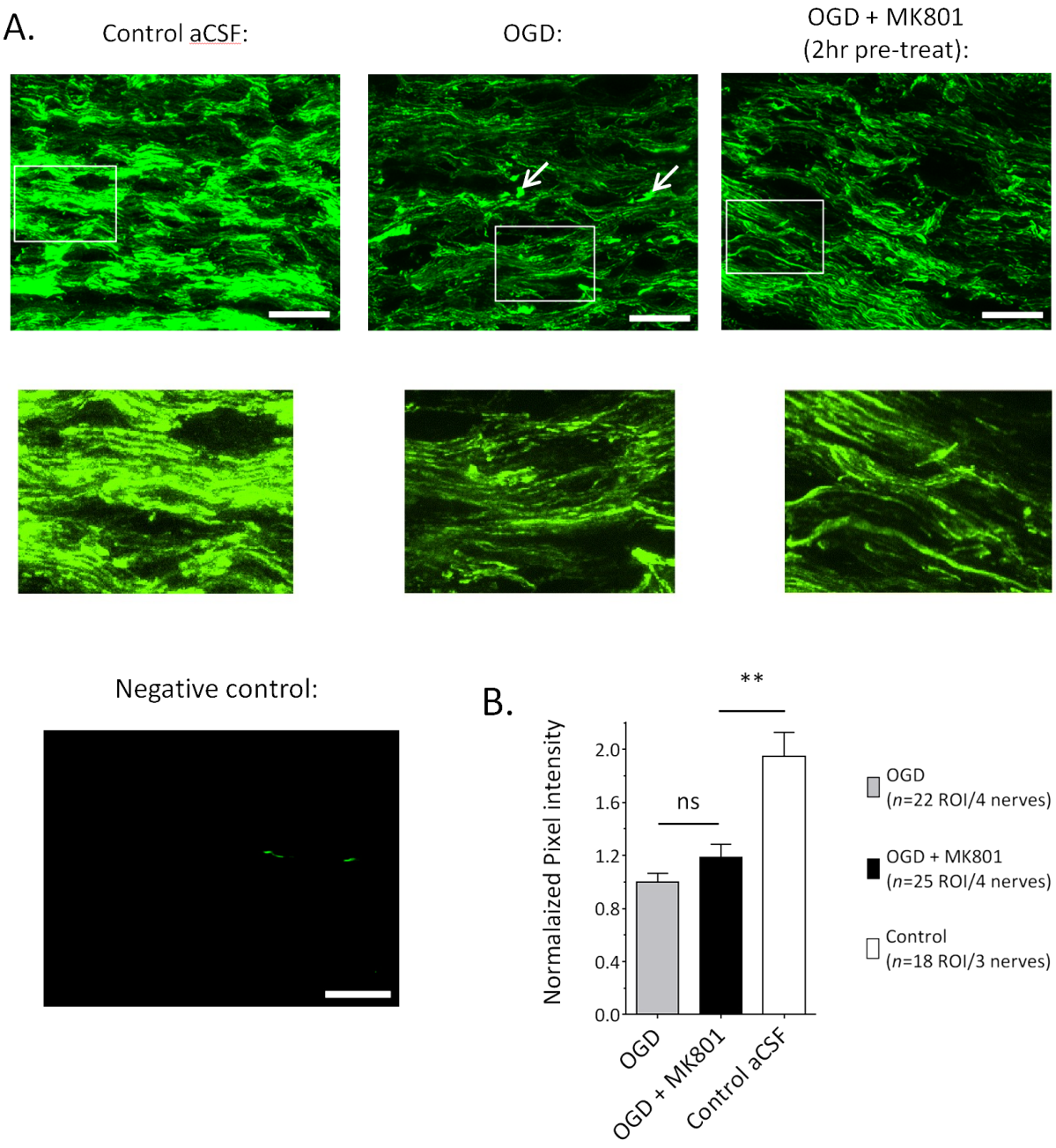

Fig. 5.14: NMDA receptor blockade does not preserve axon structural integrity during OGD.

a) Representative images of neurofilament-200 (NF-200) immunofluorescence in fixed adult RONs following a number of treatments. Note the formation of NF-200 aggregations (see arrows) and overall drop in staining intensity between control and OGD experiments. Surprisingly, NF-200 staining intensity did not improve following experiments with MK-801. Inset shows an example of staining at a higher gain. No immunoreactivity is observed when NF-200 is omitted. **b)** Histogram comparing the relative NF-200 immunofluoresence intensity between all treatments. ns $p>0.05$, ** $p<0.01$, scale bar = 20µm.

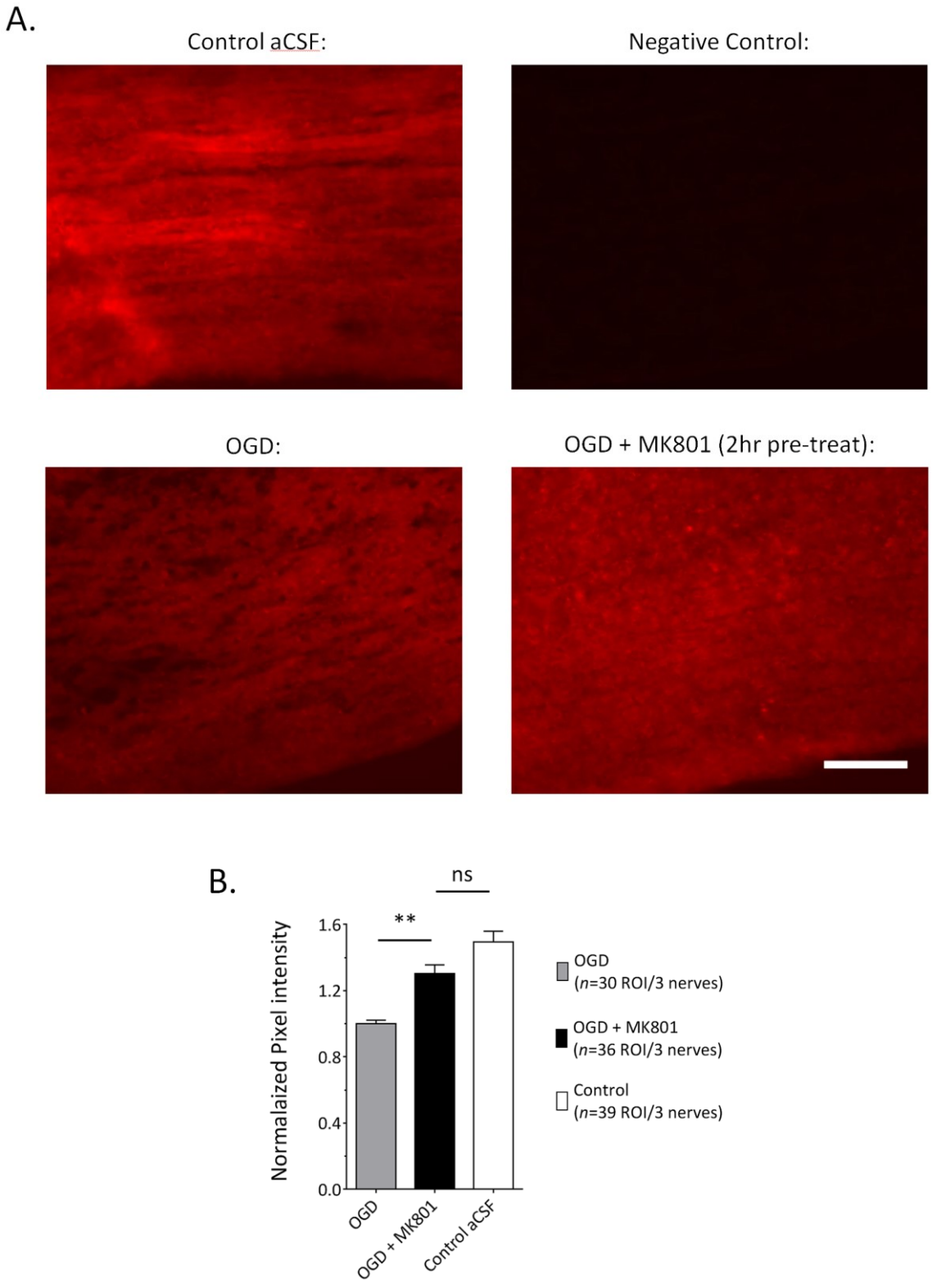

Fig. 5.15: NMDA receptor blockade prevents OGD-induced myelin disruption.

a) Representative images of fluromyelin staining in fixed adult RONs following a number of treatments. Overall fluorescence intensity is reduced following OGD. In addition, numerous regions display a complete loss in fluorescence. MK-801 treatment restored fluorescence intensity. No auto-fluorescence is observed when fluromyelin is omitted. **b)** Histogram comparing the relative fluorescence intensity between all treatments. ns $p>0.05$, ** $p<0.01$, scale bar = 100µm.

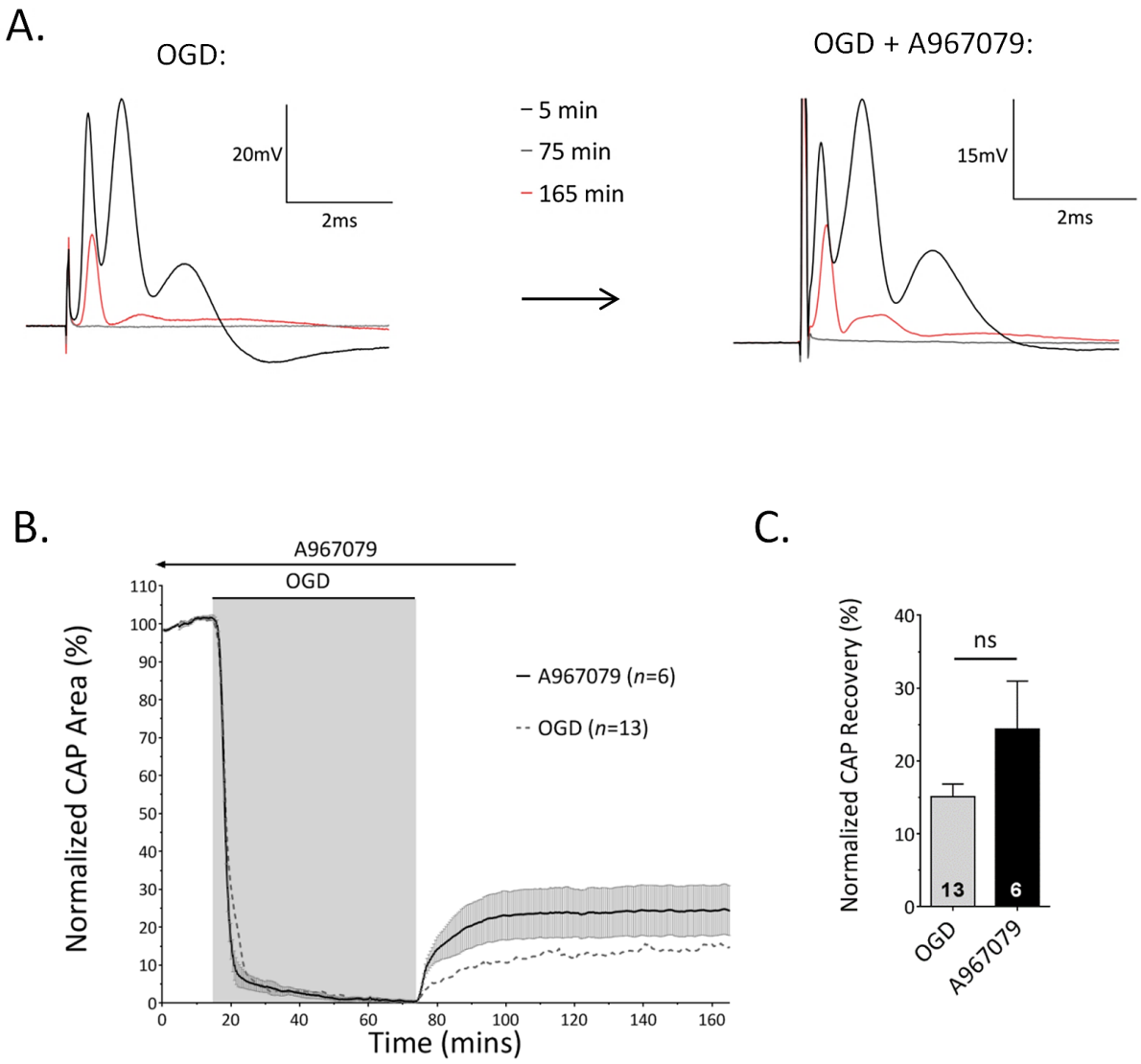

Fig. 5.16: Blockade of TRP-A1 channels does not improve recovery following OGD.

a) Representative CAP trace in the presence of a selective TRP-A1 channel blocker, A967079. **b)** CAP time-course in the presence of A967079. Note; nerves were pre-treated with A967079 for 120 minutes before exposure to OGD. **c)** Histogram demonstrating the lack of protection with A967079. ns p>0.05.

5.2.4 NR2C/D incorporating NMDA-receptors mediate ischemic myelin injury

As discussed, NMDA receptors express different combinations of sub-units which strongly affect their physiological and pharmacological properties (Hollmann and Heinemann 1994, Parsons, Danysz et al. 1998). Previous studies have reported that myelinic NMDA receptors are composed of the obligatory NR1 subunit, and a combination of NR2C, NR2D and/or NR3 subunits (Káradóttir, Cavelier et al. 2005, Salter and Fern 2005, Micu, Jiang et al. 2006, Piña-Crespo, Talantova et al. 2010). Interestingly, NR2C/D incorporating NMDA receptors are only weakly blocked by Mg^{2+}, and considered to be more sensitive to glutamate and glycine (Parsons, Danysz et al. 1998, Káradóttir, Cavelier et al. 2005, Micu, Jiang et al. 2006, Mosley, Acker et al. 2010).

CIQ is a highly selective potentiator of NR2C/D subunit-containing receptors, which increase the frequency of channel opening without altering the EC_{50} value for glutamate (Mullasseril, Hansen et al. 2010). To test whether the enhanced activation of NR2C/D-expressing NMDA receptors is toxic under control conditions, nerves were perfused with CIQ (20μM) for 120 minutes. However, exposure to CIQ had no significant effect on CAP area during this period (106.50±3.60%, *n*=3, p=0.11, Fig. 5.17a, note; recording was initiated after a 120 minute pre-treatment with CIQ). Furthermore, exposure to OGD in the presence of CIQ, did not potentiate injury, with CAP area recovering to 18.28±8.61% (*n*=4), not significantly different to control OGD nerves (p=0.988, Fig. 5.17b-d). It is worth noting that although statistical significance was not achieved, AP conduction tended to block out at a quicker rate in the presence of CIQ (p=0.18).

The endogenous neurosteroid, pregn*e*nolone sulphate, strongly potentiates currents with NR2A/B-expressing NMDA receptors, having minimal effect on NR2C/D-expressing receptors (Káradóttir, Cavelier et al. 2005). In contrast, pregn*a*nolone sulphate is a negative modulator of all NR2 receptor subunits, but is 4 times more potent at receptors expressing NR2C/D subunits (Malayev, Gibbs et al. 2002). Curiously, perfusion with pregn*a*nolone hemisuccinate (3α5βHS; 100μM, (Weaver, Marek et al. 1997)), a synthetic analogue of the sulphated species, (for 120 minutes before, during and 40 minutes after OGD) had no significant effect on CAP recovery after 60 minutes OGD (17.32±5.02%, *n*=4, p=0.99, Fig. 5.18). This result is unlikely to

be due to any toxic effect of 3α5βHS as exposure under normoxic conditions did not appear to reduce CAP area (*n*=1, Fig. 5.18). Interestingly, previous studies show that 3α5βHS was only responsible for a maximal 20-47% reduction in NMDA-mediated currents in neuronal cultures (Weaver, Marek et al. 1997). Therefore, it is possible that 3α5βHS does not exert a strong enough inhibition of NMDA receptors to confer protection.

To further test the involvement of NR2C/D containing receptors, experiments were repeated using a more potent NMDAR antagonist, PPDA. PPDA preferentially binds to NR2C/D-containing receptors, displaying a 3 to 5 fold increase in affinity over NR2A/B-containing receptors (Feng, Tse et al. 2004). The application of PPDA (20μM) significantly improved post-OGD recovery to 42.08±8.86% (*n*=5, p=0.0022, Fig. 5.19). Next, to test whether the accumulation of low concentrations of PPDA is sufficient to confer protection, experiments were repeated using 1μM PPDA. However, this protocol did not provide any significant protection following OGD (13.49±4.00%, *n*=3, p=0.99, Fig. 5.19b-c). Longer pre-treatment times with 1μM were not tested as this would presumably push the limits of nerve viability in the recording chamber.

QNZ-46, an allosteric modulator of NMDA receptors, is currently the most selective inhibitor of NR2C/D-containing receptors, displaying a 50-fold selectivity over NR2A/B-containing receptors (Mosley, Acker et al. 2010). Furthermore, QNZ-46 inhibits in an activity-dependant manner (Hansen and Traynelis 2011). To test whether QNZ-46 is capable of preserving WM function following ischemia, CAP area was recorded in the presence of QNZ-46. Due to poor aqueous solubility at 100μM and 70μM, 50μM QNZ-46 was used during experiments. QNZ-46 led to a significant increase in CAP recovery following OGD (43.44±4.50%, *n*=5, p=0.0013, Fig. 5.20). However, due to its poor aqueous solubility, we may be under-estimating its protective effect (Mosley, Acker et al. 2010). Experiments were repeated using 1μM QNZ-46, but similar to PPDA, low concentrations had no significant effect on CAP recovery (15.87±2.32%, *n*=3, p=0.99, Fig. 5.20).

To examine myelin disruption during OGD, dual live-imaging of myelin (fluromyelin) and the cytoplasmic compartment of oligodendrocytes (using PLP-GFP mice) was monitored via spinning disk confocal microscopy. Examination of MONs revealed that myelin and oligodendrocyte processes are two distinct regions (Fig. 5.21a, see arrows). Thus, any

structural or morphological changes in fluorescent oligodendrocyte processes will not reflect myelin damage. Consistent with previous ultrastructural studies (Micu, Jiang et al. 2006, Hamilton, Kolodziejczyk et al. 2016), myelin decompaction was evident after 60 minutes of OGD, with myelin diameter increasing from 0.67±0.004µm (*n*=967 myelin strands/13 MONs) to 0.86±0.01µm (*n*=318 myelin strands/5 MONs, Fig.5.21b-d, p=0.0003). This was accompanied by oligodendrocyte somata swelling and the disruption of cell processes (oligodendrocyte injury was not quantified). Consistent with previous CAP recordings (see Fig. 5.16), the TRP-A1 channel blocker, A-967079, had no effect on myelin injury, with myelin diameter increasing to 0.92±0.01µm after 60 minutes OGD (n=205 myelin strands/4 MONs, Fig5.21c-d, p<0.0001). In contrast, myelin decompaction was largly prevented in the presence of QNZ-46 (120-minute pre-treatment protocol). In QNZ-46 treated nerves, myelin diameter increased to 0.75±0.01µm following OGD, a significant reduction when compared to untreated nerves (*n*=216 myelin strands/4 MONs, p=0.02, Fig. 5.21c-d). This supports my previous findings that NMDAR activation mediates myelin breakdown. In contrast, oligodendrocyte cell injury appeared to be unaffected by QNZ-46, indicating that oligodendrocyte injury operates via an alternative mechanism, likely AMPA/kainate or TRP-A1 receptor mediated (Tekkok and Goldberg 2001, Hamilton, Kolodziejczyk et al. 2016).

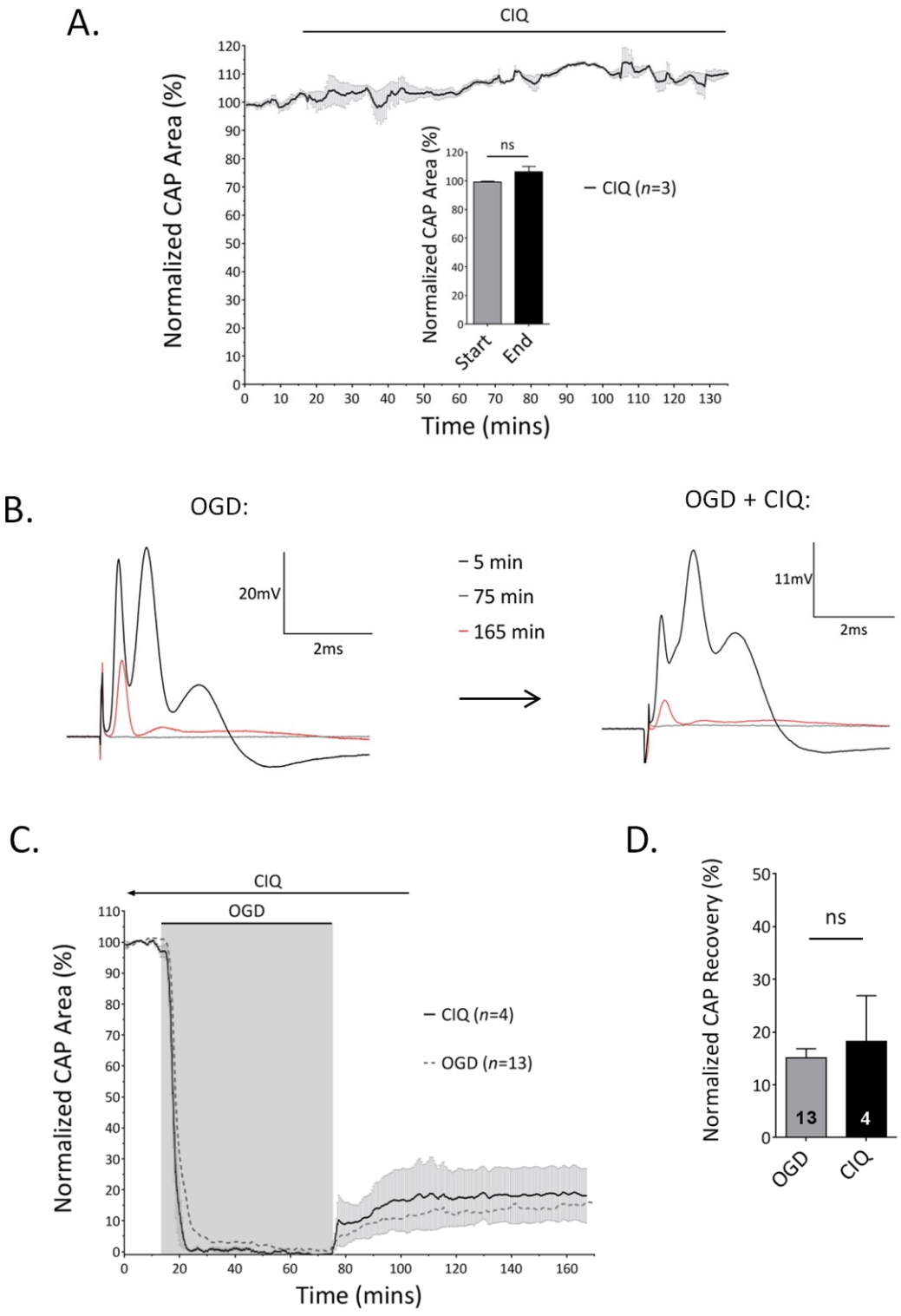

Fig. 5.17: Potentiation of NR2C/D-containing NMDA receptors does not affect CAP conduction.

a) CAP time-course under control conditions including a 120 minute exposure to a NR2C/D-containing NMDA receptor potentiator, CIQ. Inset; histogram comparing CAP area after 120 minutes perfusion with CIQ to initial starting CAP area in the absence of the drug. Note; CIQ has no effect on CAP area under control conditions. **b)** Representative CAP trace in the presence of CIQ for an OGD experiment. **c)** CAP time-course in the presence of CIQ. Note; nerves were pre-treated with CIQ for 120 minutes before exposure to OGD. CIQ does not exacerbate post-OGD recovery. **d)** Histogram comparing post-OGD recovery in the presence of CIQ to time-matched controls. ns $p>0.05$.

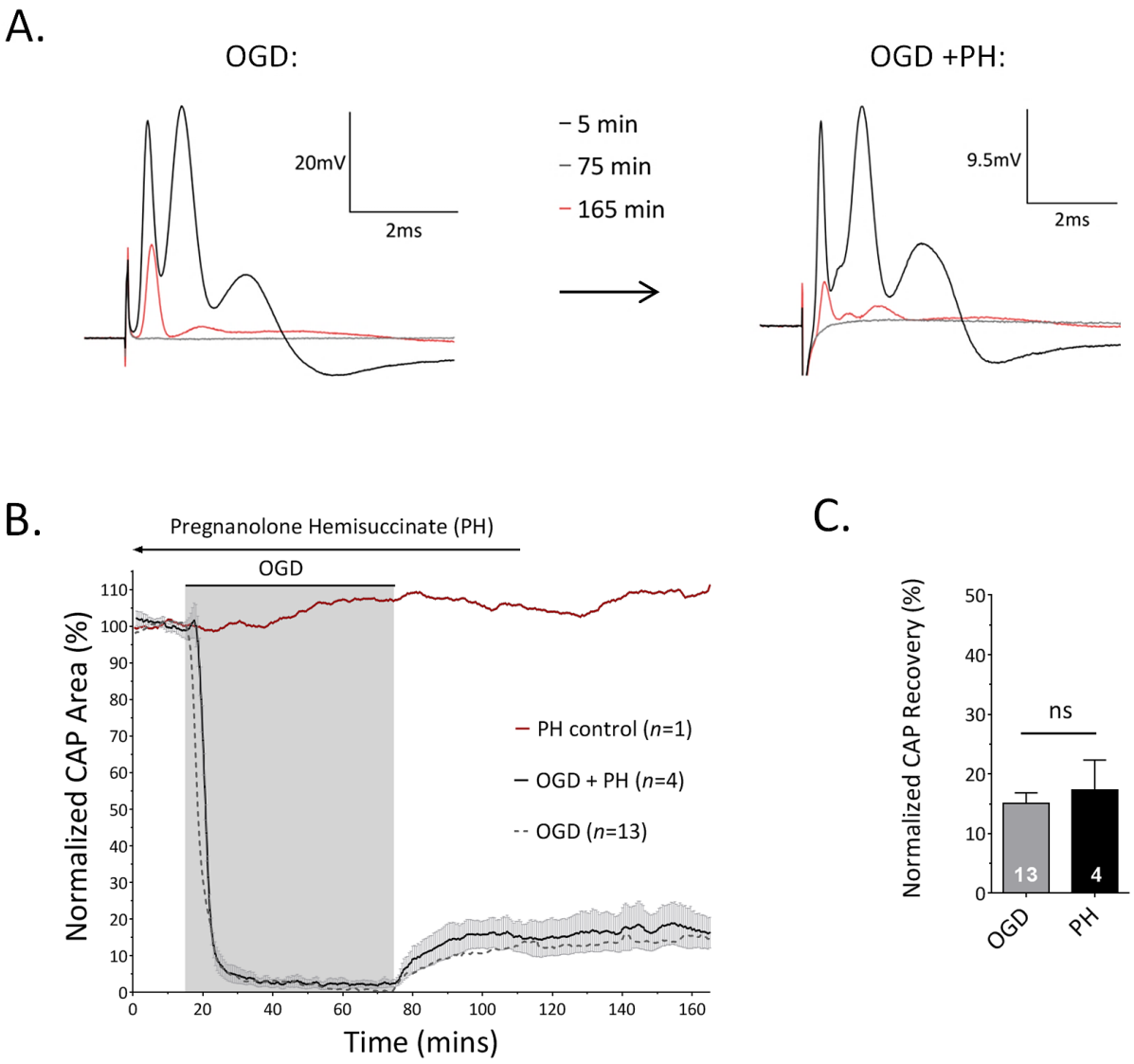

Fig. 5.18: Inhibition NMDA receptors with the neurosteroid, pregnanolone hemisuccinate, does not improve post-OGD functional recovery.

a) Representative CAP trace in the presence of a negative modulator of NMDA receptors, pregnanolone hemisuccinate (PH). **b)** CAP time-course in the presence of PH. Note; nerves were pre-treated with PH for 120 minutes before exposure to OGD. PH does not affect CAP conduction under control conditions. However, it does not protect during OGD. **c)** Histogram comparing post-OGD recovery in PH to time-matched controls. ns p>0.05.

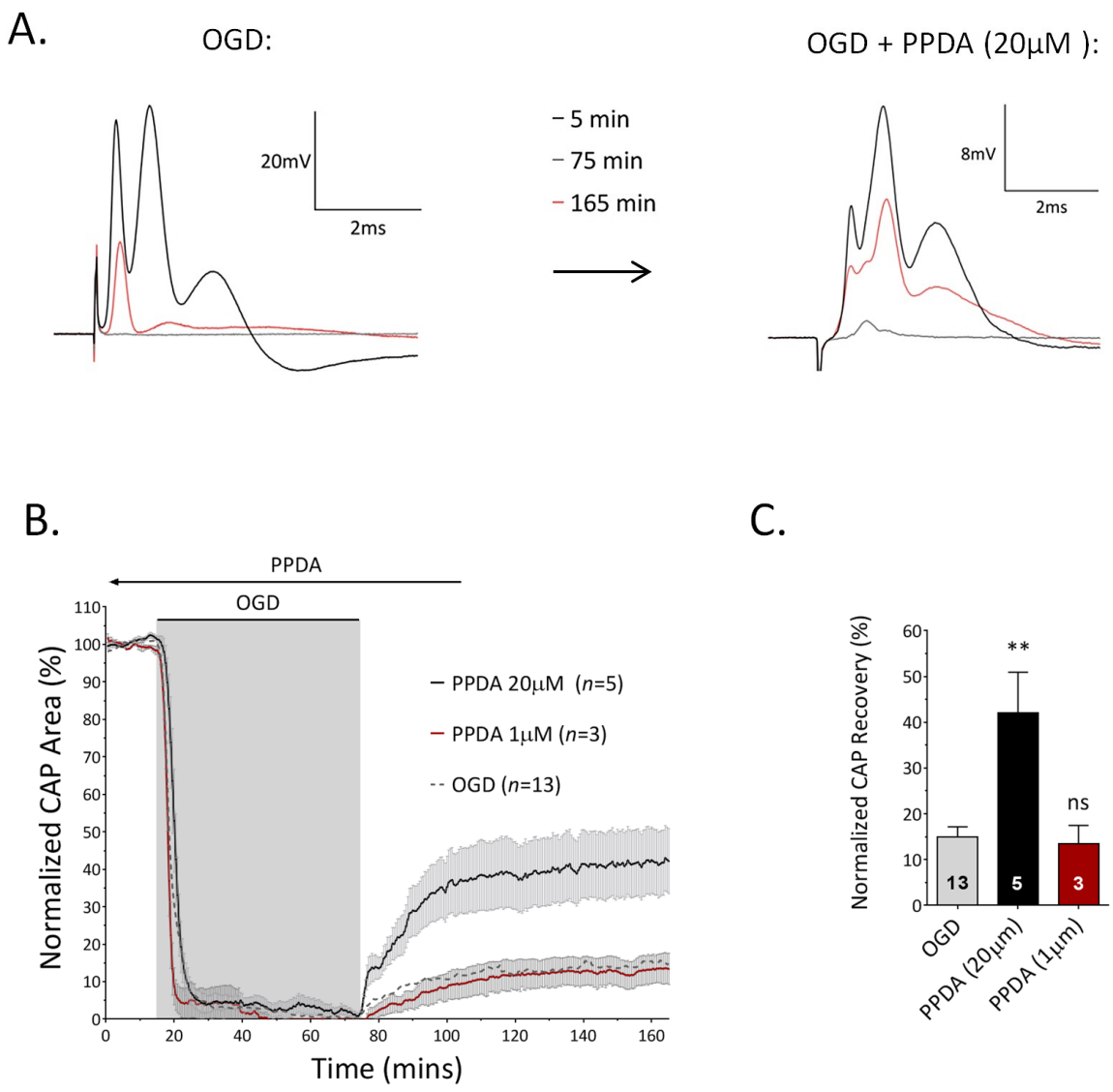

Fig. 5.19: PPDA, a selective inhibitor of NR2C/D-containing NMDA receptors, improves functional recovery following OGD.

a) Representative CAP trace in the presence of a negative modulator of NR2C/D-containing NMDA receptors, PPDA. **b)** CAP time-course in the presence of two different concentrations of PPDA. Note; nerves were pre-treated with PPDA for 120 minutes before exposure to OGD. 20µM PPDA dramatically increased CAP area after OGD, while 1µM PPDA failed to preserve CAP conduction. **c)** Histogram comparing post-OGD recovery in in the presence of PPDA to time-matched controls. ns $p>0.05$, ** $p<0.01$.

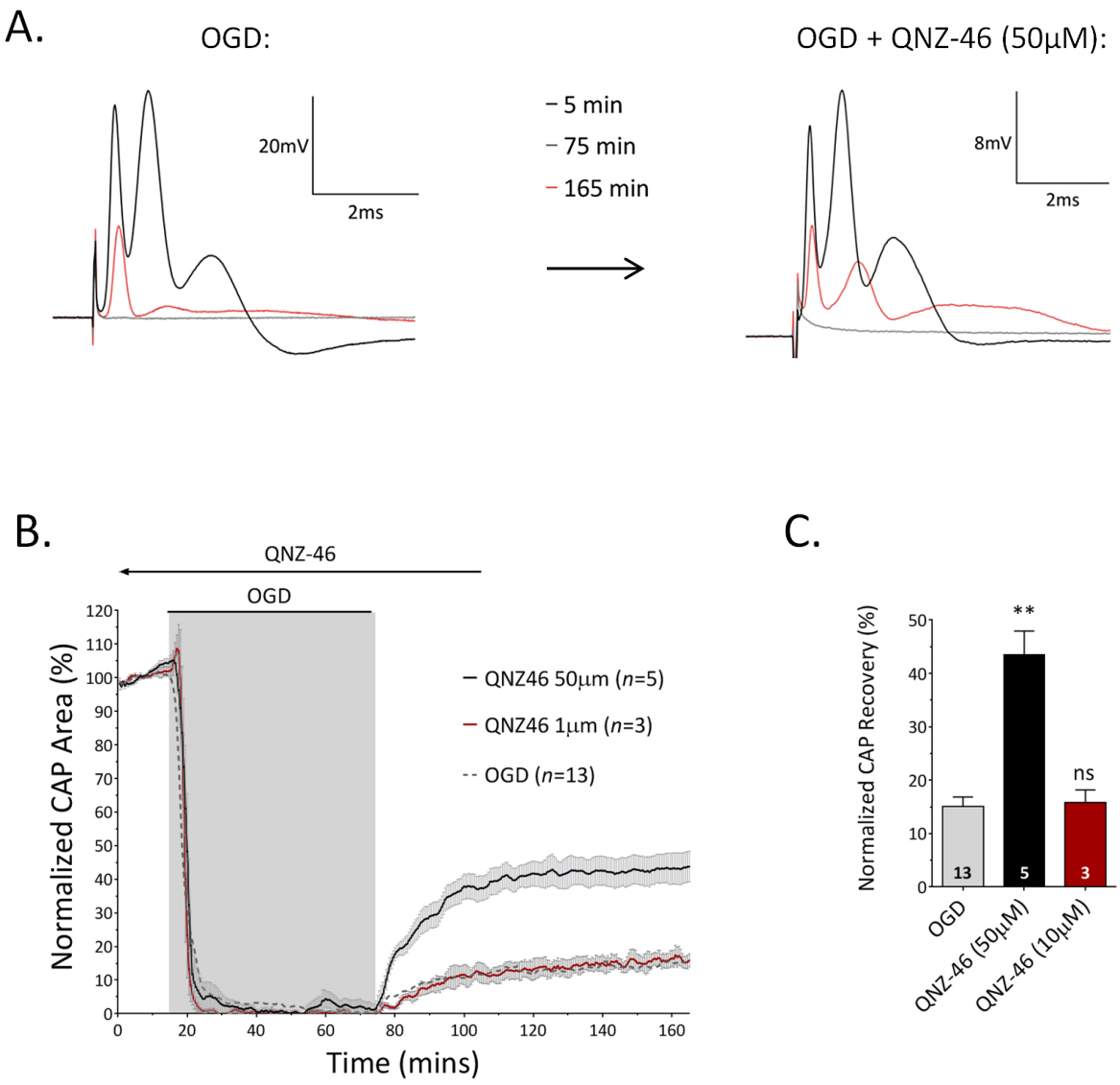

Fig. 5.20: QNZ-46, a selective inhibitor of NR2C/D-containing NMDA receptors, improves functional recovery following OGD.

a) Representative CAP trace in the presence of a negative modulator of NR2C/D-containing NMDA receptors, QNZ-46. **b)** CAP time-course in the presence of two different concentrations of QNZ-46. Note; nerves were pre-treated with QNZ-46 for 120 minutes before exposure to OGD. 50µM PPDA dramatically increased CAP area after OGD, while 1µM QNZ-46 failed to preserve CAP conduction. **c)** Histogram comparing post-OGD recovery in in the presence of QNZ-46 to time-matched controls. ns $p>0.05$, **$p<0.01$.

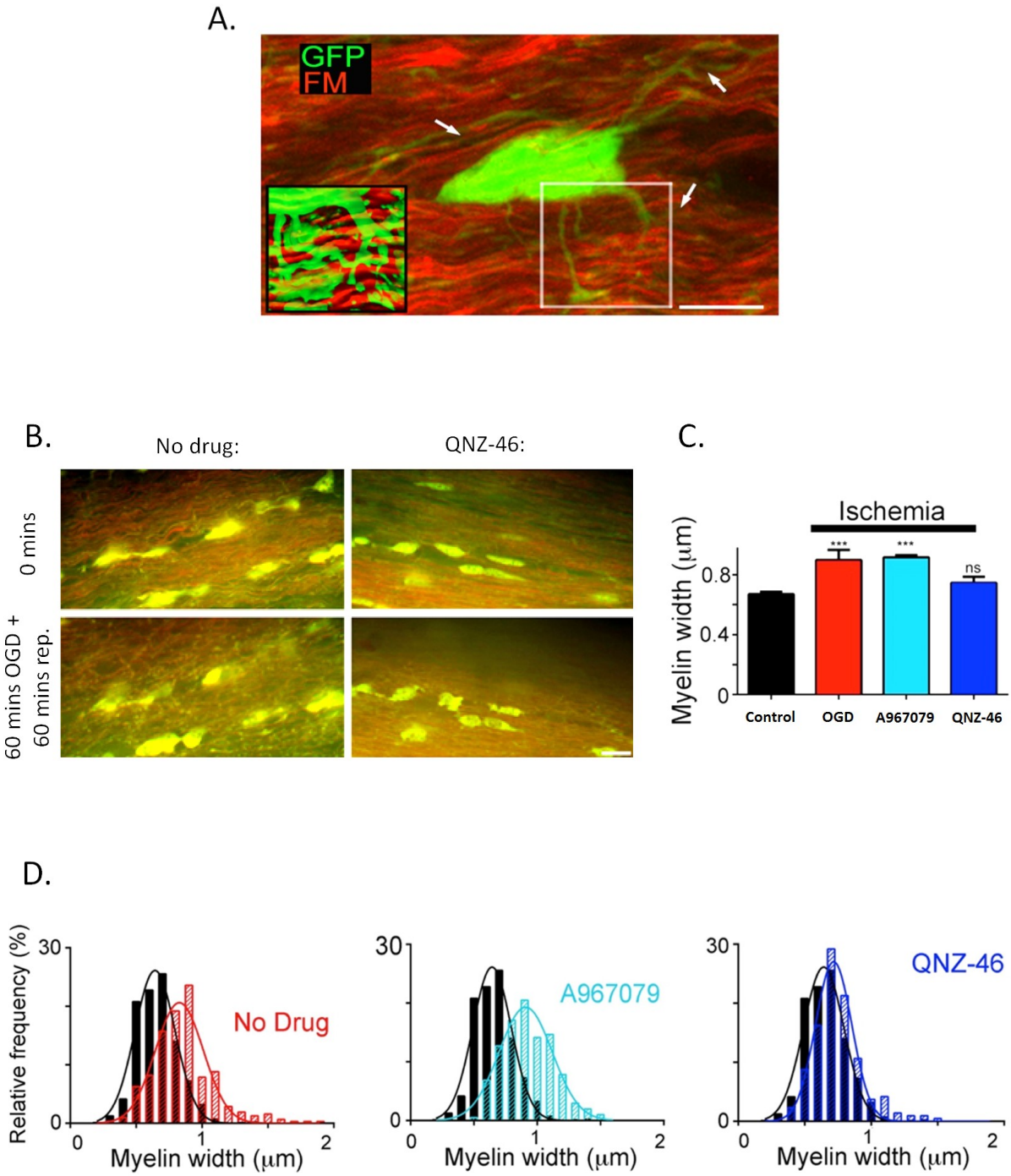

Fig. 5.21: QNZ-46 prevents myelin decompaction during OGD.

a) Oligodendrocyte cytoplasmic domain (PLP-GFP mouse; green) is distinct from myelin sheath (fluromyelin; red). See arrows. Inset shows an example of a stacked image of GFP-fluromyelin at a higher gain. **b**) Representative images of myelin and oligodendrocytes in live adult MONs, before and after 60 minutes of OGD followed by 60 minutes reperfusion (rep.). Note; QNZ-46 prevents myelin damage, but does not preserve oligodendrocytes. Nerves were pre-treated with QNZ-46 for 120 minutes before exposure to OGD. **c)** Histogram comparing myelin diameter before and after OGD. 60 minutes of OGD increases myelin sheath diameter. QNZ-46 prevents myelin decompaction during OGD, but A967079 (TRP-A1 channel blocker) does not. **d)** Frequency distribution curve demonstrating how the OGD-evoked increase in myelin diameter is prevented by QNZ-46, not by A-967079. *p<0.05, **p<0.01. Scale bar= 10µm.

5.2.5 QNZ-46 accumulation in myelin

QNZ-46 is a derivative of 4-oxo-3(4*H*)quinazolinyl, containing the trans-stilbene pharmacophore (Mosley, Acker et al. 2010). It also contains the quinazolinone backbone which is known to exhibit strong fluorescence (Naleway, Fox et al. 1994) (see Fig. 2.11). Together, this gives QNZ-46 the structural properties of a fluorescent myelin stain. The fluorescent properties of QNZ-46 were confirmed with a lambda scan, which revealed a peak emission of 450nm (blue) in a lipid environment (excitation at 405nm) (see Fig. 2.11 in chapter 2).

This is highly advantageous as it allows for drug uptake to be monitored in real-time. Adult RONs were perfused with QNZ-46 (50µM) for a total of 120 minutes, followed by a 60 minute wash-out period. Nerves were transferred and imaged (in QNZ46-free aCSF) using a fluorescent microscope at various time-points through-out. Perfusion with the drug, led to a progressive increase in QNZ-46 relative-emission throughout the 120 minute treatment period, increasing by 152.40±18.03% (*n*=4, Fig. 5.22). Consistent with previous results, the data suggests that QNZ-46 slowly accumulates in myelin over time. Interestingly, QNZ-46 fluorescence remained high following 60 minutes wash-out in control aCSF. There was no significant difference in QNZ-46 emission after wash-out when compared to the maximum emission during perfusion with the drug (120mins QNZ-46 *versus* 60 minutes wash-out, p=0.33), indicating that QNZ-46 partitions into the myelin sheath and is retained during wash-out.

To confirm the selective localisation of QNZ-46 in myelin, coronal rat brain slices were incubated (5°C) in QNZ-46 (50µM) and fluromyelin (1:20) for 120 minutes. Slices were subsequently transferred to a control aCSF solution (QNZ-56/fluromyelin- free) and imaged using laser scanning confocal microscopy. Consistent with our hypothesis, QNZ-46 fluorescence localised in myelinated WM (corpus callosum) and was largely absent from neighbouring GM regions (Fig. 5.23a-b). Note the WM-GM boarder in Fig. 5.23b. High magnification images revealed vital QNZ-46 fluorescence in myelin-axon profiles, which co-localised with the established myelin stain, fluromyelin (red) (Fig. 5.23c).

A.

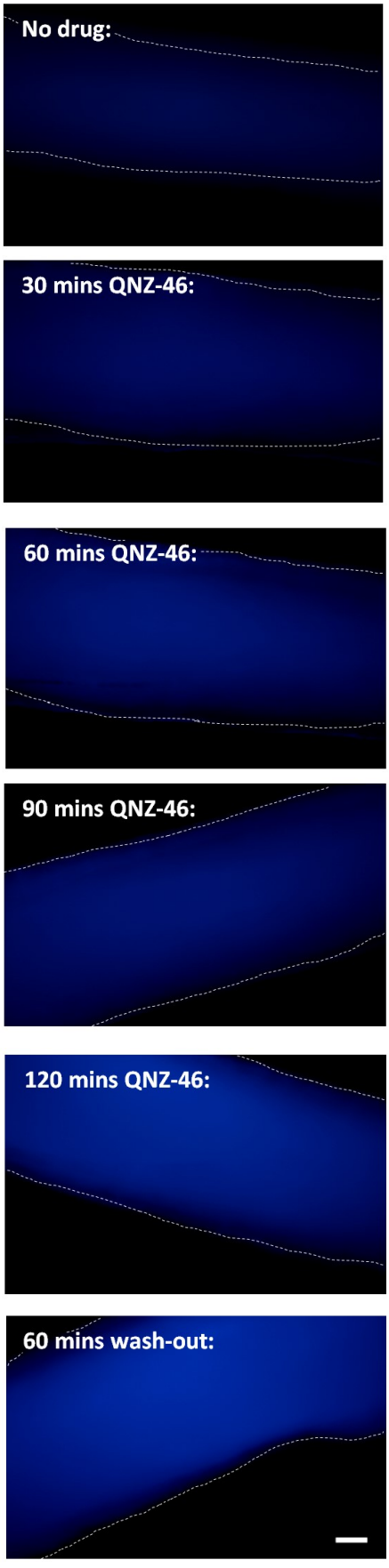

B.

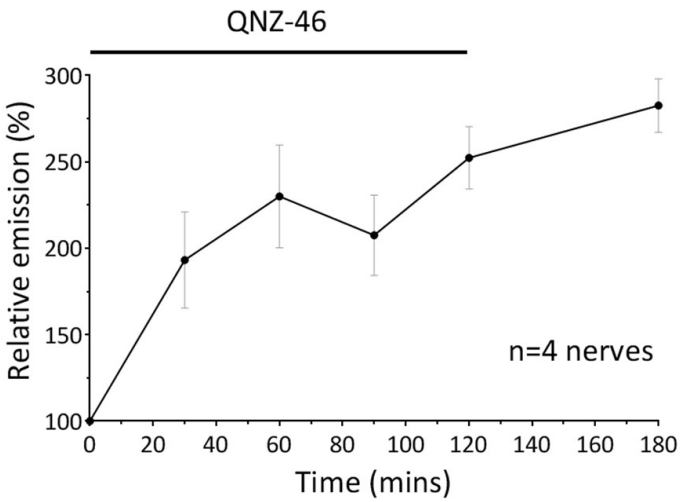

Fig. 5.22: QNZ-46 accumulates in the adult RON and is retained following wash-out.

a) Representative live-images of QNZ-46 emission in the adult RON during perfusion with the drug for 120 minutes. White dotted line outlines the RON. QNZ-46 fluorescence intensity gradually increases over time and remains high following 60 minutes wash-out. **b)** Plot of relative QNZ-46 emission against time. Scale bar= 100µm.

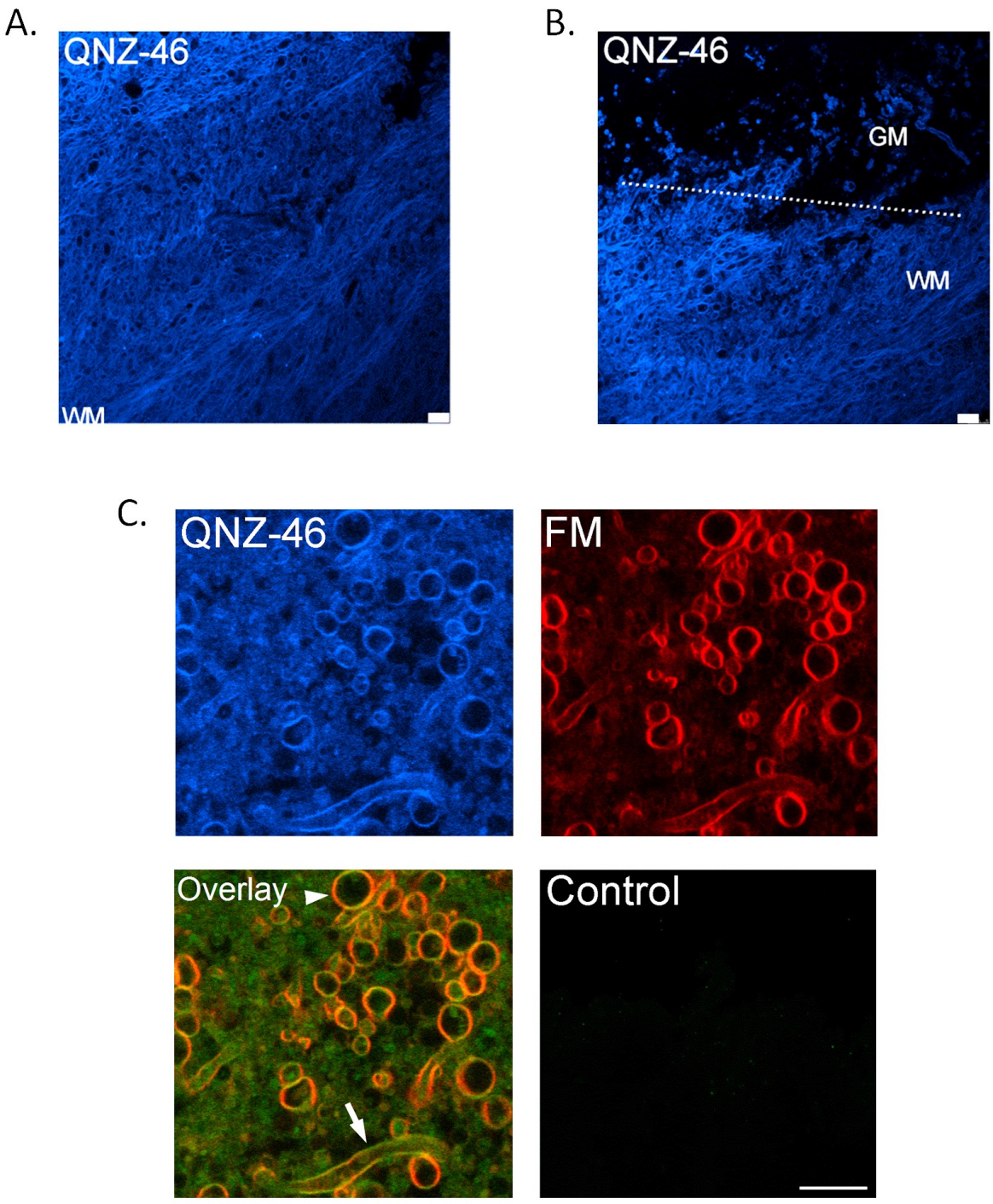

Fig. 5.23: QNZ-46 selectively accumulates in myelin sheath.

a) Sample live-images of QNZ-46 emission (blue) in the adult rat CC and **b)** at the WM-GM border. Note; adult rat coronal brain slices were pre-incubated with QNZ-46 for 120 minutes. QNZ-46 fluorescence is high in WM regions, but absent in neighbouring GM. **c)** Sample image of vital QNZ-46/fluromyelin (FM; red) co-staining of myelinated axon profiles in the adult CC. QNZ-46 emission is high in myelin profiles. Merged image is recoloured for clarity. Scale bar= 5µm.

5.2.6 QNZ-46 acts as a persistent myelin shield and crosses the BBB *in vivo*

The accumulation and subsequent retention of QNZ-46 in myelin may provide sufficient protection following its removal from the extracellular space. To test this hypothesis, RONs were pre-treated with QNZ-46 for 60 minutes, followed by a 60 minute wash-out period (in control aCSF) before exposure to OGD (see Fig. 5.24a). This pre-treatment protocol led to a significant improvement in CAP recovery, with CAP area reaching 33.26±4.62% following the re-introduction of oxygen and glucose (*n*=6, p=0.047, Fig. 5.24b-d). In contrast, replicating this protocol with NBQX (20µM), had no significant protective effect, with CAP area recovering to 22.84±6.83% (*n*=4, p=0.83, Fig. 5.25), consistent with the expression of AMPA/kainate receptors on the oligodendrocyte cell body. Not only does this data complement our findings that QNZ-46 accumulates in myelin, but more importantly, it is the first drug to persistently provide protection in the CNS even when the drug is removed from the extracellular space.

Drug permeability through the blood brain barrier (BBB) is one of the most important limiting factors in the development of pharmacological neurotherapeutics (Pardridge 2001, Pardridge 2005). A recent study found that a similar compound (UBP141) effectively crossed the BBB following intraperitoneal (i.p.) injection in mice (Lozovaya, Gataullina et al. 2014). Therefore, we sought to determine whether QNZ-46 crosses the BBB *in vivo*. Assuming a total circulating blood volume of approximately 1170µl in an average 20g mouse, *in silico* modelling predicts an estimated concentration of ~50µM in the brain following a 200µl i.p. injection of QNZ-46 (20mg/kg^{-1}). In an effort to prevent crystallisation, QNZ-46 injections were dissolved in 50/50 DMSO/20mM β-cyclodextrin and required gentle heating. C57Bl/6 wild-type mice were i.p. injected with either QNZ-46 or a vehicle 4 hours prior to animal sacrifice. Tissue was dissected into QNZ-46-free aCSF. QNZ-46 distribution was initially examined in coronal brain slices. Interestingly, vital QNZ-46 fluorescence displayed a similar distribution to that observed in the rat brain slices following bath loading (Fig. 5.26). QNZ-46 selectively localised in myelinated WM regions and was essentially absent from GM. Furthermore, QNZ-46 co-localised with fluromyelin (following a brief incubation at 5°C for 30 minutes, Fig. 5.26). Again, this demonstrates myelin retention, but also provides direct evidence of BBB penetration.

QNZ-46 fluorescence was also observed in myelin strands within the MON following i.p. injection (Fig. 5.27a). CAPs were recorded from the ON of i.p. injected mice to access whether QNZ-46 accumulation is sufficient to confer protection. ONs from either vehicle control or QNZ-46 injected mice were dissected into and subsequently perfused with drug-free aCSF for 60 minutes before O_2-glucose withdrawal. CAP area recovered to 6.79±1.92% (*n*=4) in vehicle-control injected mice. However, CAP recovery was significantly higher in QNZ-46 injected mice, with post-OGD CAP area increasing to 18.91±5.63% (*n*=5, p=0.048, Fig. 5.27b-d). The protective effect was not potentiated when QNZ-46 was added to the perfusing aCSF solution (17.00±2.97, *n*=4, Fig. 5.27c-d).

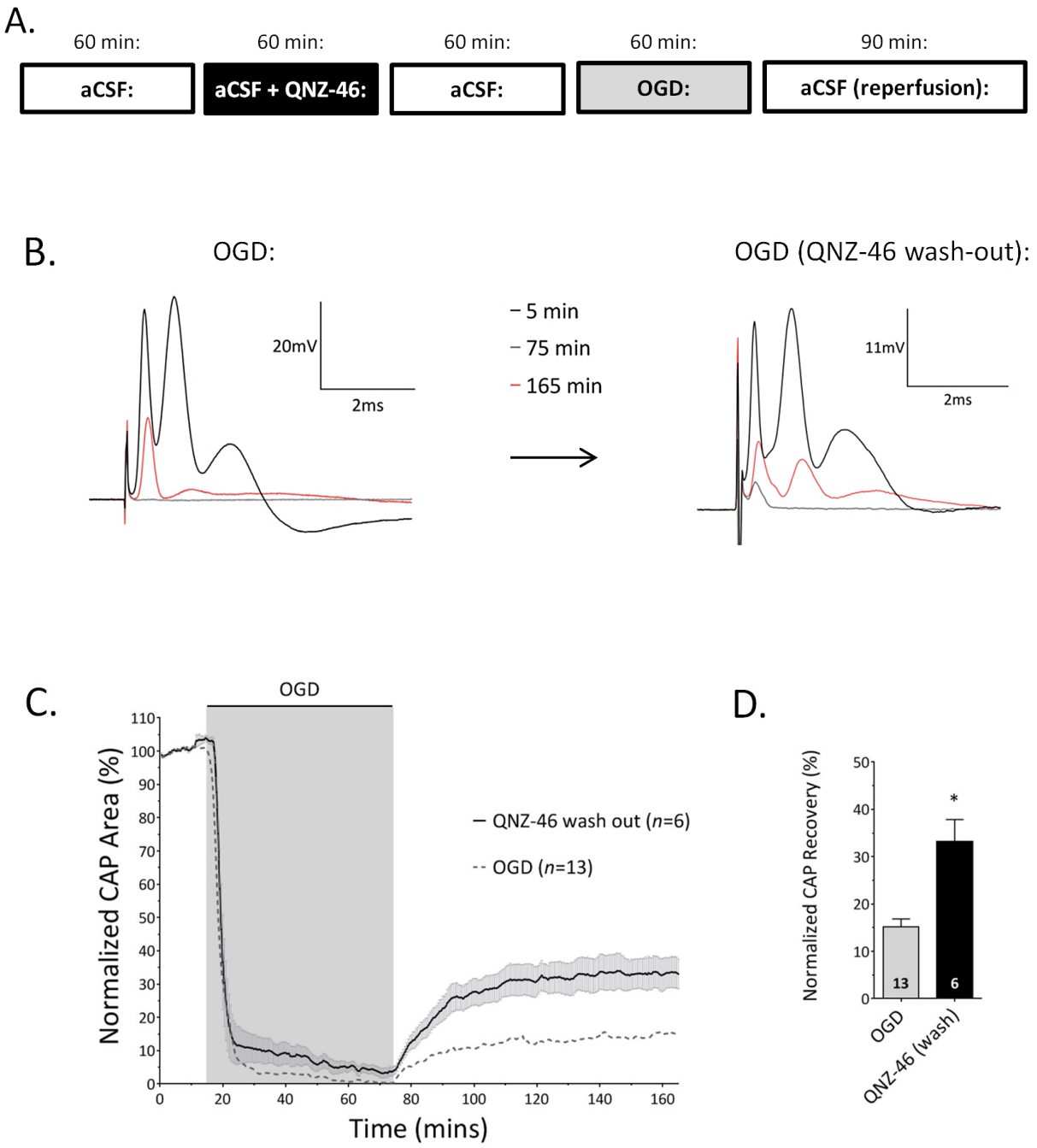

Fig. 5.24: QNZ-46 provides persistent protection following wash-out.

a) Schematic diagram of the QNZ-46 wash-off protocol. **b)** Representative CAP trace after QNZ-46 wash-out. **c)** CAP time-course following QNZ-46 wash-off protocol. Post-OGD CAP area is elevated following treatment with QNZ-46. **d)** Histogram comparing post-OGD recovery after QNZ-46 wash-off treatment to time-matched controls. *p<0.05.

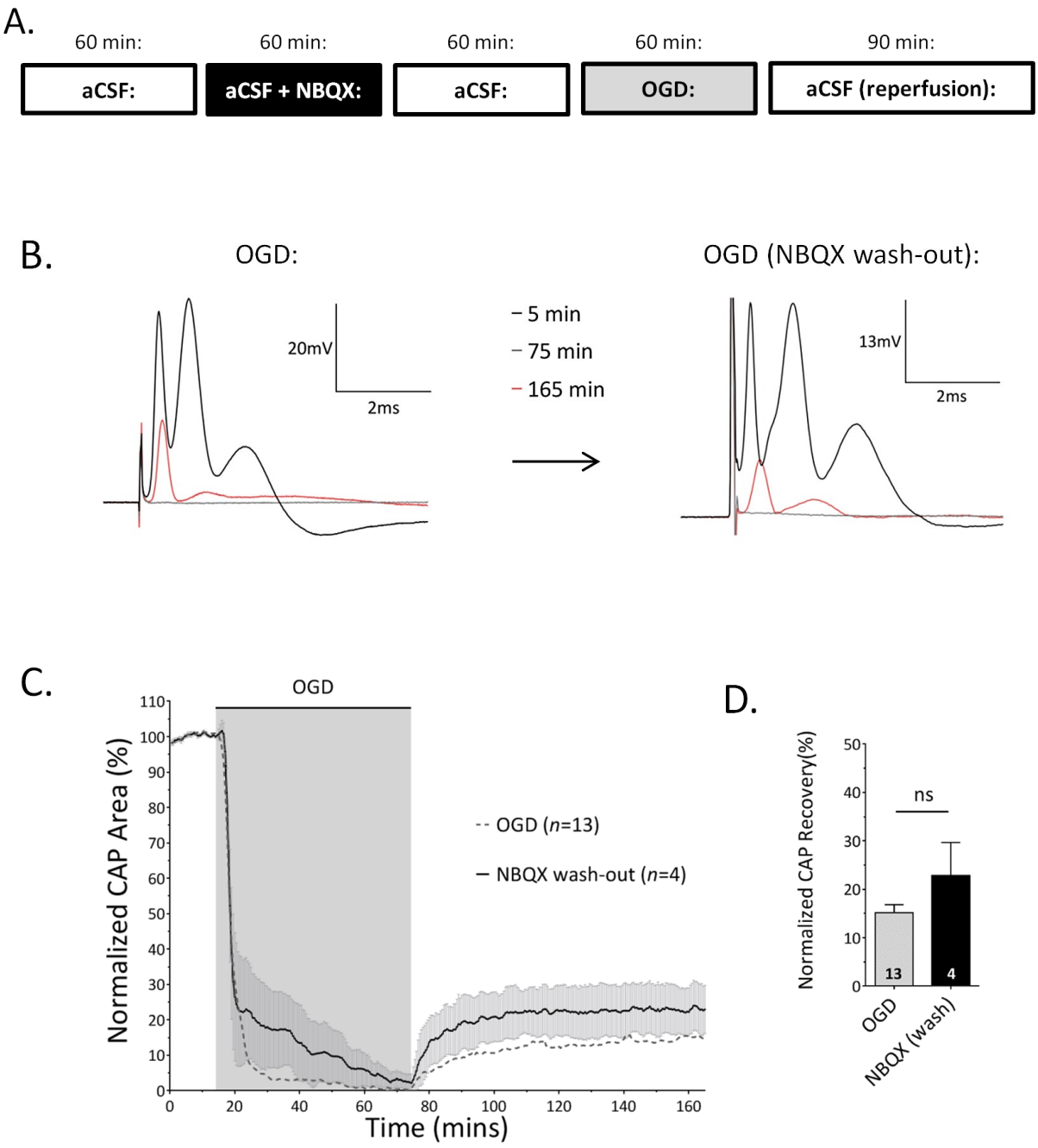

Fig. 5.25: NBQX does not improve post-OGD functional recovery following wash-out.

a) Schematic diagram of the NBQX wash-off protocol. **b)** Representative CAP trace after NBQX wash-out. **c)** CAP time-course following NBQX wash-off protocol. Note; NBQX wash-off does not elevated post-OGD CAP area. **d)** Histogram comparing post-OGD recovery after NBQX wash-off treatment to time-matched controls. ns $p>0.05$.

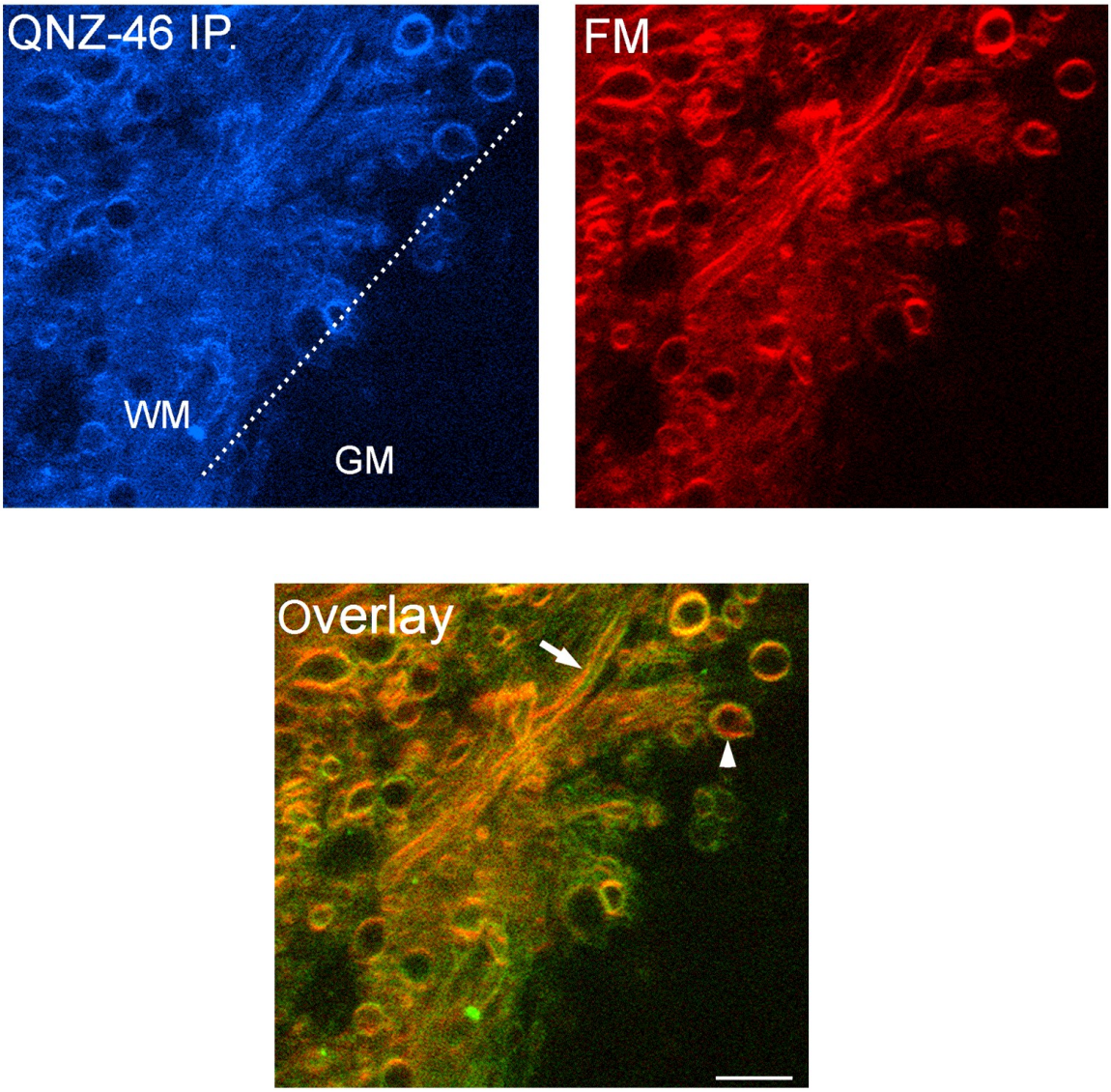

Fig. 5.26: QNZ-46 crosses the BBB and accumulates in central WM following I.P. injection in adult mice.

a) Sample image of QNZ-46 emission (blue) in an adult mouse brain slice after an I.P. injection. Note the WM-GM border demonstrating QNZ-46 fluorescence in myelinated WM regions. QNZ-46 selectively localises in myelin sheath (FM; fluromyelin; red). See arrows. Merged image is recoloured for clarity. Scale bar= 5µm.

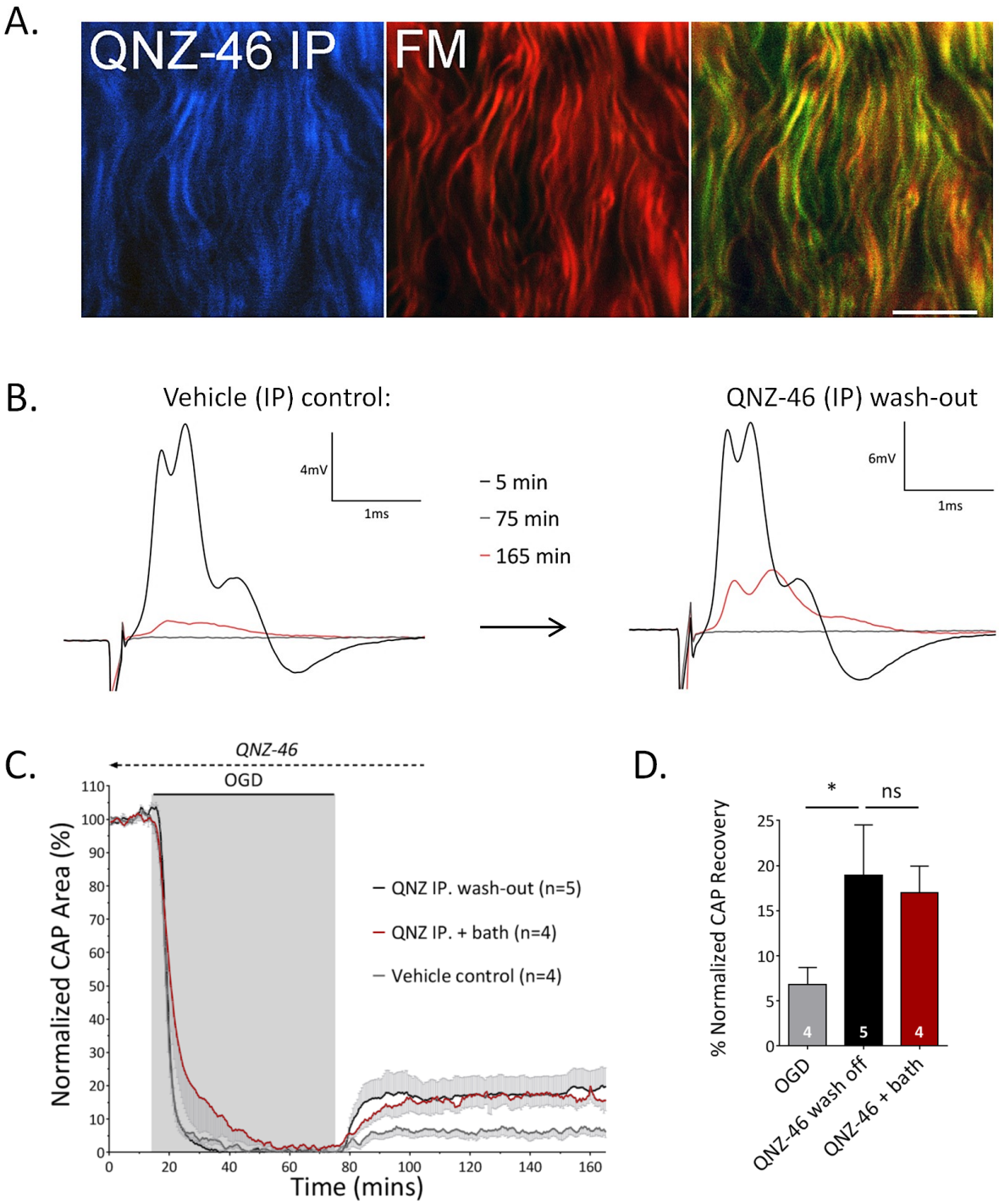

Fig. 5.27: I.P. injected QNZ-46 accumulates in ON myelin and improves functional recovery after OGD.

a) Sample image of QNZ-46 emission (blue) in MON myelin profiles (FM; fluromyelin; red) following I.P. injection. Merged image is recoloured for clarity. **b)** Representative CAP trace recorded from vehicle and QNZ-46 injected adult MONs. **c)** CAP time-course of I.P. injected mice with either vehicle or QNZ-46. QNZ-46 improves post-OGD CAP recovery (black), but protection is not potentiated when QNZ-46 is included in the bath during OGD (red). **d)** Histogram showing the effect of QNZ-46 injection on functional recovery. ns $p>0.05$, * $p<0.05$. Scale bar= 5µm.

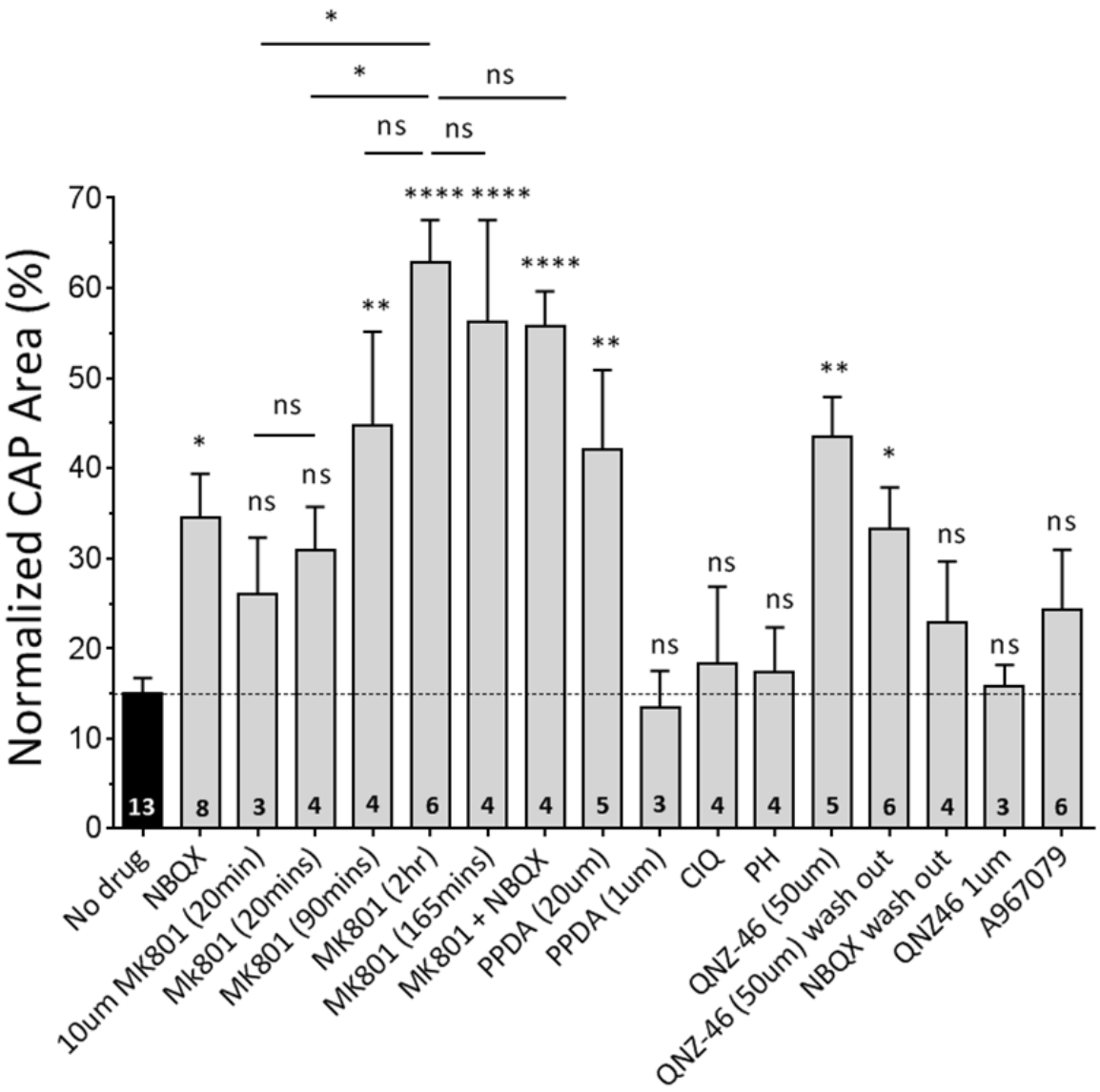

Fig. 5.28: Adult RON data summary.

Functional recovery after 60 minutes of OGD following a variety of pharmacological treatments. NMDA receptor antagonists significantly preserve CAP area after OGD. ns $p>0.05$, * $p<0.05$, ** $p<0.01$, **** $p<0.0001$.

5.3: Discussion

5.3.1: Synopsis

Excitotoxicty may be the single most important mechanism underlying ischemic WM damage. A common feature of WM ischemia is rapid myelin disruption which ultimately leads to action potential failure and functional deficits in patients. Results from the previous chapters indicate that the periaxonal space between the axon and inner layers of myelin sheath may be a significant site of excitotoxic injury. However, the exact mechanism(s) of ischemic myelin disruption is controversial. In this chapter, I show that the cytotoxic activation of NR2C/D-containing myelinic NMDA receptors mediates the structural and functional injury of myelinated WM. Resolving prior conflicting results; the data also demonstrates that drug penetration through the myelin sheath is slow and thus, requires relatively long pre-treatment periods. Furthermore, TRP-A1 antagonists do not confer functional protection.

I have also identified a highly-selective, allosteric inhibitor of myelinic NR2C/D-containing NMDA receptors, QNZ-46. QNZ-46 has the characteristics of a fluorescent myelin stain which revealed its selective accumulation and retention in myelin over time. Furthermore, the systemic injection of QNZ-46 elevates the injury tolerance of WM, even when the drug is removed from the extracellular space. QNZ-46 is the first drug to exhibit persistent CNS protection. This feature combined with its ability to cross the BBB and its high selectivity for NR2C/D expressing receptors suggest that QNZ-46 may have significant clinical implications, not only for stroke patients, but also for a range of neurological disorders which involve myelin breakdown.

5.3.2: OGD-induced injury in early myelinating WM

Developing WM injury is the most common neuropathological correlate associated with the incurable condition, cerebral palsy. The neonatal rat ON and CC are regularly used to study ischemic injury in developing WM tracts (Follett, Rosenberg et al. 2000, Alix and Fern 2009). There is evidence to suggest that regional differences in sensitivity exist between different

regions of the CNS (Tekkok and Ransom 2004, Tekkok, Ye et al. 2007). Using a combination of electrophysiological and immunohistochemical techniques, a direct comparison was made between the two early myelinating WM tracts. In agreement with previous studies, 1 hour of OGD produced an irreversible decrease in CAP amplitude in the P10 RON (Alix and Fern 2009). In addition, disrupted axon structural integrity was also observed demonstrating that a relatively brief period of acute ischemia leads to both structural and functional injury. Thanks to the development of a novel technique which allows the recording of CAPs from the 'whole' CC (Li, Velumian et al. 2016), OGD-sensitivity in the P10 CC was also examined. Interestingly, CC excitability fell more rapidly during ischemia. Although CAP recovery following OGD was delayed in the CC, there was no significant difference in total functional recovery after 90 minutes reperfusion, indicating that both WM tracts have a similar degree of sensitivity to ischemia. Tekkok and Ransom (2004) reported that the adult MON and CC react similarly to anoxia, with 120 minutes of anoxia producing an identical degree of irreversible injury. Consistent with these findings, my data demonstrates that developing WM tracts also display a remarkably similar response to energy deprivation. Further experiments are required to determine whether all WM tracts in the brain are equally sensitive to ischemia.

As mentioned, previous studies have shown that the over-activation of iGluRs mediates a large component of irreversible functional injury in the P10 RON (Alix and Fern 2009, Alix, Zammit et al. 2012). I investigated whether excitotoxicity also contributes to injury in the P10 CC. While the application of iGluR antagonists did appear to have a protective tendency, there was no significant improvement in functional recovery following OGD. This suggests that the injury mechanisms which operate in the CC are different to the RON. However, the high degree of variability in CAP recordings using this adapted methodological approach may have concealed the protective effect of such antagonists. This may be, in part, due to the varying distance between the mouth of the recording and stimulating electrode. For several experiments, a short recording distance between electrodes (1-2mm) was required to produce sufficiently large CAPs. This short conduction distance will inevitably expose only a short fragment of the tract to true OGD (since both electrodes are filled with control aCSF). Thus, this is likely to contribute to the varying degree of post-OGD recovery. Further experiments are required to conclusively determine whether excitotoxicity contributes to irreversible injury in the CC.

5.3.3: Excitotoxic injury in myelinated WM

In agreement with previous studies, NBQX partially preserved WM function following ischemia (Tekkok and Goldberg 2001, McCarran and Goldberg 2007, Tekkok, Ye et al. 2007). This confirms that AMPA/kainate receptor activation contributes to excitotoxic WM injury in adult WM. Interestingly, a water-soluble derivative of NBQX, disodium-NBQX (Na-NBQX), was equally protective. In general, lipid membranes are permeable to liposoluble or non-polar compounds, such as NBQX. The similar degree of protection provided by both species of the drug suggests that liposolubility does not affect the actions of AMPA/kainate receptor antagonists. This is consistent with the expression of AMPA/kainate receptors on the surface of oligodendrocytes, not within compact myelin.

NMDA receptor activation is reportedly involved in the ischemic breakdown of myelin. Yet surprisingly, there are no reports in the literature of NMDA-mediated functional injury in fully-myelinated WM tracts. Consistent with these findings, short pre-treatment periods with an established NMDA-receptor antagonist (MK-801) failed to significantly preserve nerve function from ischemic injury. However, due to the expression of functional NMDA receptors within myelin, particularly along inner surface of myelin sheath, we reasoned that drug penetration into the periaxonal space may be slow. There are two potential routes by which NMDA receptor antagonists can access the periaxonal space. Firstly, the paranodal junction (PNJ) flanking each node is separated from the underlying axon by a narrow space of approximately 2-4nm (Rosenbluth 2009). This tight space is suggested to provide a route by which juxtaparanodal K^+ channels can influence nodal activity, potentially regulating AP conduction (Rosenbluth 2009). Mierzwa *et al.* (2010) demonstrated that water-soluble, fluorescent dextran tracers (3 and 70kDa in size) are capable of penetrating the PNJ into the periaxonal space, diffusing symmetrically on both sides of the node of Ranvier. Both 3 and 70kDa tracers were able to penetrate live and fixed nerves indicating that transport is via passive diffusion. However, the diffusion distance travelled in live nerves was only 4.4µm over a period of 135 minutes. Alternatively, lipid soluble compounds can directly penetrate through the myelin sheath. A previous study has shown that the association of MK-801 with an intact biological membrane (synaptoneurosome) takes less than 5 minutes (Moring, Niego et al. 1994). Similarly, dissociation from the membrane takes approximately 10 minutes. The

fast kinetics of the association/disassociation time constants is consistent with the quick onset and short acting nature of MK-801 *in vivo* (Vezzani, Serafini et al. 1989, Moring, Niego et al. 1994, Yang, Ren et al. 2016). However, myelin sheath is made up of multiple wraps of myelin (up to 14 layers in larger axons) which may significantly hinder the rate of drug penetration. Early studies found that C^{14} labelled compounds like phenobarbital (an anti-epileptic drug) penetrate cerebral GM much more rapidly than WM regions in the adult cat (Roth and Barlow 1961). In contrast, WM is more readily penetrated in new-born kittens, which was due to the incomplete formation of myelin. Together, this suggests that myelin forms a significant barrier which reduces the rate of drug penetration, and thus, is comparable to the blood brain barrier.

In order to facilitate sufficient drug penetration either through the PNJ or directly through the multi-layered myelin sheath, nerves were pre-treated with MK-801 for long periods. Intriguingly, increasing the duration of drug exposure dramatically increased functional recovery following ischemia. Maximum protection of >400% was observed following 120 minutes pre-treatment the drug. This is consistent with the expression of NMDARs throughout compact myelin and that receptor activation during ischemia mediates ischemic myelin damage (Káradóttir, Cavelier et al. 2005, Micu, Jiang et al. 2006). Furthermore, it suggests that previous studies may have underestimated the involvement of NMDA receptor activation due incomplete drug penetration through the myelin sheath. Considering the average length of the MON internode is 134µm (Butt, Colquhoun et al. 1994) and that dextran traces diffuse only 4.44µm away from the node in 135 minutes (Mierzwa, Shroff et al. 2010), it is unlikely that drug diffusion through the PNJ accounts for such outstanding protection. Although MK-801 is much smaller (Mr=337) than the tracers used in that study, it is a positively charged molecule which will significantly hinder diffusion through the PNJ. Nonetheless, drug penetration through the multi-layered myelin sheath is likely the primary route of MK801 diffusion. Interestingly, simultaneous AMPA/kainate receptor blockade in the presence of MK-801 provided no additional protection during OGD, suggesting that preserving the oligodendrocyte-myelin unit is as equally protective as preventing myelin damage alone. Thus, this may be the maximum protection provided by iGluR antagonists.

In agreement with previous reports, myelin degeneration was observed following OGD. However, myelin disruption was prevented in the presence of NMDA receptor blockers

(MK801; long pre-treatment), demonstrating that NMDAR activation during ischemia promotes myelin damage and that myelin preservation is sufficient to maintain functional WM. Interestingly, NMDAR blockade did not significantly preserve underlying axon integrity following OGD. Considering MK801 significantly improves AP conduction post-OGD, it is hard to believe that NMDAR blockade does not preserve axon structure. Changes in absolute NF200 fluorescence intensity may not be sufficient to accurately access structural changes in individual axons. As mentioned, MK801 treated nerves did appear to display a higher number of intact axon cylinders. An axon scoring system may provide a more comprehensive assessment of drug efficacy.

Contrary to Hamilton *et al.* (2016), who found that Ca^{2+}-permeable TRP channels mediate myelin disruption in cerebellar WM, the selective inhibition of TRP-A1 channels did not significantly improve functional recovery after OGD. Moreover, it did not prevent myelin decompaction in the adult MON. However, this study and others, often rely on either live-imaging or patch-clamp recordings from oligodendrocyte processes (Káradóttir, Cavelier et al. 2005, Hamilton, Kolodziejczyk et al. 2016). Dual imaging of myelin and the cytoplasmic domain of oligodendrocyte processes in the MON revealed that they are in fact, two distinct compartments. As a result, it is possible that the injury mechanisms which mediate ischemic myelin damage and oligodendrocyte injury are also distinct.

5.3.4: NR2C/D-containing NMDA receptors mediate ischemic myelin damage

Sub-unit selective antagonists of NMDA receptors have high clinical potential. As previously discussed, WM NMDA receptors have an unusual subunit composition, including NR2C/D and/or NR3A/B subunits. Curiously, a novel synthetic analogue of pregnanolone succinate (3α5βHS), a negative modulator of all NMDA receptor subunits, failed to preserve nerve function following OGD. However, work by Malayev *et al.* (2002) demonstrated that although pregnanolone succinate decreases the efficiency of NMDA activation, it does not completely inhibit NMDA mediated currents. Thus, it is possible that partial NMDA blockade is incapable of preventing myelin injury. In addition, CIQ, a positive modulator of NR2C/2D-expressing

receptors, failed to potentiate injury. With that said, CIQ operates by increasing the frequency of channel opening, which demonstrates that myelinic NMDA receptors are already maximally activated during ischemia. Consistent with the reported expression of NR2C/2D subunits in myelin, potent antagonists of NR2C/2D-expressing NMDA receptors, PPDA and QNZ-46, dramatically improved functional recovery following OGD, increasing CAP area to a surprisingly similar level, 42 and 43%, respectively. This translates to a ~240% improvement in functional recovery. Notably, this is considerably lower than the protection provided by the broad-spectrum NMDA antagonist, MK-801 (63%). Functional NR1/3-expressing NMDA receptors, which lack the NR2 subuint, are also expressed in ON myelin (Piña-Crespo, Talantova et al. 2010). NR1/3 receptors mediate a rise in Ca^{2+} myelin in response to NMDA receptor co-agonists, including glycine and D-serine (Piña-Crespo, Talantova et al. 2010). Moreover, they are insensitive to D-AP5, a glutamate site antagonist of NR2-expressing receptors (Piña-Crespo, Talantova et al. 2010). Therefore, NMDA mediated injury in myelin may arise from the over-activation of a combination of NMDA sub-types, including NR2C/D and NR3 subunits. Although selective antagonists of NR3A/B-containing receptors are not currently available, it would be interesting to test whether a combined block of both sub-types would provide a similar degree of protection as broad-spectrum NMDA antagonists, such as MK801.

The K_i values (inhibition constant) for PPDA are 0.55, 0.31, 0.125 and 0.096µM for 2A, B, C and D-containing receptors, respectively (Feng, Tse et al. 2004). Thus, PPDA displays a ~3-5 fold preference for NR2C/2D-containing receptors. However, QNZ-46 has IC_{50} values of >300, 229, 6 and 3µM for 2A, B, C and D-containing receptors, respectively (Mosley, Acker et al. 2010), and therefore, displays a ~50-fold preference for NR2C/2D-containing receptors. QNZ-46 is a member of a novel class of non-competitive antagonists which operates by a unique mechanism (Hansen and Traynelis 2011). QNZ-46 inhibition of NMDA receptors is use-dependent, requiring the simultaneous binding of glutamate to the NR2 sub-unit. Hansen and Traynelis (2011) presented a model for the predicted mechanism of NMDAR inhibition by QNZ-46. The binding of glutamate to the NR2 subunit induces a conformational change which either enhances the availability of the QNZ-46 binding site, or changes the binding-site to a higher affinity conformation (see Fig. 5.29). The occupation of QNZ-46 increases the activation

energy required for the conformational change of each receptor subunit, and therefore, prevents the opening of the channel (Hansen and Traynelis 2011).

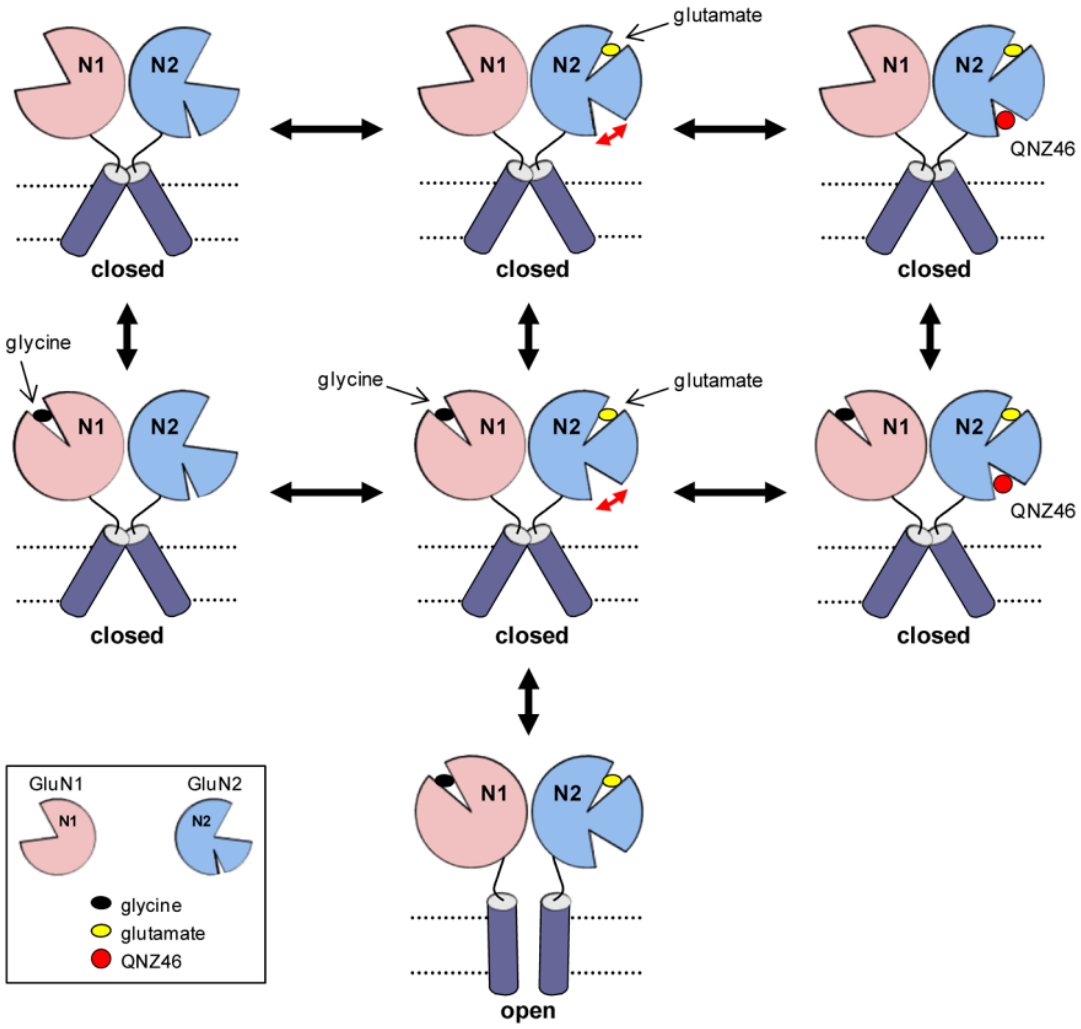

Fig. 5.29: **Predicted hypothesis of QNZ-46 inhibition of NR2C/D-containing receptors.** Taken from (Hansen and Traynelis 2011).

The sub-unit selectivity and use-dependent nature of QNZ-46 represents a potentially powerful therapeutic advantage, capable of overcoming the side-effects associated with many non-selective antagonists. Live-imaging of myelin in PLP-GFAP adult mice revealed that treatment with QNZ-46 prevents the ischemia-induced decompaction of myelin sheath. This

indicates that the over-activation of NR2C/D-containing NMDA receptors mediates myelin breakdown during ischemia. As predicted, it did not appear to prevent the swelling and fragmentation of oligodendrocyte cell processes or soma, further indicating that injury occurs through distinct mechanisms.

As discussed, QNZ-46 has the lipophilicity of a fluorescent myelin stain due to the trans-stilbene pharmacophore and quinazolinone backbone (Wang, Popescu et al. 2010). The fluorescent properties of the drug were used to confirm the slow penetration of QNZ-46 into myelin over a 2 hour period. This is in agreement with the long pre-treatment time required for MK-801 to provide significant functional protection. Curiously, QNZ-46 emission remained high during wash-out, indicating that it accumulates in myelin over time and is retained following wash-out. Similarly, the localisation of QNZ-46 in myelin axon profiles and its absence from neighbouring GM regions further support the idea that QNZ-46 partitioning through myelin sheath is a slow process, but it also suggests that its retention during wash-out may provide persistent protection. 60 minutes of treatment with QNZ-46 followed by 60 minutes wash-out, significantly elevated functional recovery in the adult RON. This continued protection in the absence of the drug suggests that trapping of QNZ-46 in myelin sheath and integration with NMDA receptors, provides persistent functional protection over relatively long periods. Thus, myelin acts as a reservoir for NMDA-antagonists such as MK-801 and QNZ-46. Consistent with the expression of AMPA/kainate receptors on oligodendrocyte cell bodies (Tekkok and Goldberg 2001, Salter and Fern 2005), and their absence in myelin, an identical protocol using NBQX did not preserve functional recovery.

The BBB poses as a significant obstacle in the delivery of many drugs to the CNS. There are a number of transport mechanisms by which compounds can cross the BBB, including endocytosis, and active transports. However, transmembrane diffusion is the most common mechanism. Conversely, lipid solubility and molecular weight are important factors in BBB permeability (Banks 2009). A substantial fraction of molecules with a lipid/water partition coefficient greater than 0.03 readily penetrate the BBB (Oldendorf 1974). However, compounds which greatly surpass this lipid solubility can accumulate in the BBB and are subsequently sequestered by the capillary bed (Banks 2009). Similarly, high lipid solubility favours the accumulation of drugs in peripheral tissue, and thus, decreases the concentration of the drug which reaches the BBB. Therefore, the development of effective neuroprotective

agents must find a balance between sufficient solubility to permeate the BBB, yet not to the extent that decreases the availability of the drug presented at the BBB (Banks 2009). Another important factor in BBB permeability is molecular weight. However, relatively large compounds (over 600Da) are known to penetrate the BBB (Banks 2009). In fact, cytokine-induced neutrophil chemoattractant-1 (CINC1), a chemokine with a molecular weight of 7,800Da, completely crosses the BBB following i.v. bolus injection (Pan and Kastin 2001). While QNZ-46 has a relatively low molecular weight of 443.41 (Tocris), its lipophilicity and accumulation in myelin raise the question of whether QNZ-46 crosses the BBB. Adult mice which were I.P. injected with QNZ-46 displayed widespread emission throughout WM regions of the CNS, including the corpus callosum and ON. This demonstrates that QNZ-46 readily crosses the BBB and selectively accumulates in myelin sheath. Furthermore, functional recovery was significantly elevated in I.P. injected mice, suggesting that the incorporation of QNZ-46 in myelin acts as a protective myelin shield. The lack of additional protection observed in I.P. injected mice which were also perfused with the drug following nerve dissection, suggests that myelin trapping following systemic QNZ-46 pre-treatment results in maximal protection. Thus, QNZ-46 elevates the injury tolerance of WM, even when the drug is removed from the extracellular space. The persistent protection provided by QNZ-46 has high clinical potential for patients who are at high risk of stroke, particularly those who are susceptible to recurrent stoke. In addition, QNZ-46 may prove to be beneficial in a range of pathological disorders which display myelin degradation, including multiple sclerosis.

To summarise, I examined the involvement of myelinic NMDA receptors in ischemic WM injury. NMDA receptor antagonists provided exceptional protection when applied for sufficient time to penetrate myelin sheath. My results also show that NR2C/D-containing receptors mediate the ischemic decompaction of myelin. QNZ-46, a fluorescent NR2C/D NMDA receptor antagonist, elevates injury tolerance in myelinated WM tracts and provides persistent protection over time.

Chapter 6:

Final Discussion and Conclusion

The goal of this thesis is to determine the mechanisms of glutamate release in central WM and to test the hypothesis that myelinic NMDA receptor activation mediates ischemic myelin injury. In this chapter, I will give a brief review of my findings, explain the proposed model of ischemic myelin injury and discuss the possible implications of the data on QNZ-46.

6.1: Overview

In chapter 3, I investigated the significance of vesicular glutamate release in adult WM. I showed that widespread depolarisation evokes a sharp rise in $[Glut]_e$ in the adult corpus callosum. Interestingly, the time-course and amplitude of glutamate release was independent of glutamate transporter activity, but was dramatically reduced by inhibition of vesicular glutamate loading. Similarity, depolarisation evoked rapid de-staining of the vesicular probe, FM4-64. Consistent with previous findings, this suggests that vesicular neurotransmitter exocytosis is evident within mature WM. However, this is the first direct evidence that vesicular glutamate release in WM can significantly elevate extracellular concentrations. In addition, I demonstrate the surprising extent of vesicular fusion along myelinated axons when compared to their companion astrocytes. Curiously, WM astrocytes show no evidence of vesicular docking suggesting that the robust rise in extracellular glutamate originates from axons. This is the first direct comparison of vesicular docking within different cellular compartments in mature WM. Considering there was no evidence of localised vesicular fusion at discrete sites along myelinated axons, vesicular glutamate release must occur underneath myelin sheath, elevating glutamate concentrations in the periaxonal space. These findings support the existence of an axo-myelin synapse in WM, providing a mechanism by which axons can signal to overlaying myelin. This novel synapse could represent an important physiological mechanism by which axonal activity regulates a variety of physiological functions including AP conduction velocity, myelin structure and/or metabolic support. Recent work by Micu *et al.* (2016) provides evidence that AP conduction induces a bafilomycin-a1 sensitive rise in myelinic Ca^{2+}. Although electrical stimulation interfered with microelectrode biosensor recordings in my experiments, it would be interesting to test whether electrical activity evokes vesicular fusion in myelinated axons *in situ*. A possible way

of achieving this could be via monitoring axonal FM4-64 fluorescence in YFP+ axons following electrical stimulation.

In chapter 4, I monitored $[Glut]_e$ under acute ischemic conditions and examined the potential mechanisms of ischemic glutamate release. I provide the first direct measurement of resting $[Glut]_e$ in several WM tracts, demonstrating that physiological concentrations are in the low micromolar range. Furthermore, I show that functional glutamate transports maintain low $[Glut]_e$ in most WM tracts. Following the onset of ischemia, $[Glut]_e$ increased within a matter of minutes and continued to do so throughout the duration of ischemia (with the exception of the adult MON). Pharmacological inhibition of a variety of potential release pathways, including glutamate transporters, VRACs, hemi-channels and the glutamate-cystine antiporter, failed to significantly reduced the rise in $[Glut]_e$. A number of conditions and treatments aimed at preventing vesicular fusion dramatically reduced overall glutamate release. In addition, depleting WM tracts of their vesicular glutamate stores significantly elevated functional recovery following OGD. Similar to results in chapter 3, ischemia-evoked vesicular fusion occurred along the internode of myelinated axons. Together, the findings in this chapter provide a novel pathway of ischemia-induced glutamate release in WM. In addition, the data also indicates that the axo-myelin synapse may be a significant site of excitotoxic WM injury during energy deprivation.

Following on from my findings in chapter 4, I examined the mechanism of ischemic myelin injury in chapter 5. I found that NMDA receptor-mediated injury in myelinated WM mediates a large component of irreversible functional injury. Resolving prior controversies, NMDA receptor blockade was only protective when antagonists were applied for long pre-treatment periods, providing sufficient time to penetrate the myelin sheath. Interestingly, I provide evidence that the gating of myelinic NMDA receptors during ischemia promotes myelin degradation and decompaction. In contrast, selective inhibitors of TRP-A1 channels did not preserve CAP area or prevent structural myelin damage during OGD. Negative modulators of NR2C/D-containing NMDA receptors dramatically improved functional recovery, consistent with the expression of NR2C and 2D subunits within compact myelin. Finally, I identified a highly selective NR2C/D-containing NMDA antagonist (QNZ-46) that also acts as a fluorescent myelin stain. QNZ-46 slowly accumulates in myelin over time, prevents myelin decompaction and elevates functional recovery following OGD. Interestingly, QNZ-46 is retained in myelin

following wash-out and provides persistent protection following the removal of the drug from the extracellular space. QNZ-46 selectively accumulates in myelinated central WM following systemic administration, providing direct evidence of BBB penetration and myelin retention. In addition, IP injected mice display an elevated injury tolerance during OGD, suggesting that QNZ-46 has exceptional clinical potential, not only for those at high risk of stroke, but also for a range of neurological disorders which involve myelin damage.

6.2: A novel pathway of ischemic myelin injury

The data presented in this thesis provides evidence of a novel pathway of myelin injury during ischemia. I found that vesicular exocytosis contributes to the ischemia-induced rise in $[Glut]_e$. While the rise in $[Glut]_e$ may originate from unmyelinated axons which are directly exposed to the ECS, the data also provides evidence of vesicular fusion along myelinated axons i.e. at the axo-myelin synapse. In addition, the results presented in chapter 5 indicate that acute myelin injury during ischemia is primarily a result of the over-activation of NR2C/D containing NMDA receptors within myelin sheath. Together these findings suggest that ischemia initiates an unexpected cascade of events which ultimately leads to myelin disruption and AP failure.

Under physiological conditions, myelinic NMDA receptors respond to activity-dependant vesicular glutamate release from axons. NMDA receptor activation leads to a rise in myelinic Ca^{2+} levels which may regulate a number of essential physiological processes (Fruhbeis, Frohlich et al. 2013, Micu, Plemel et al. 2016, Saab, Tzvetavona et al. 2016). $[Glut]_e$ is maintained in the low micromolar range due to the activity of glutamate transporters. However, under ischemic conditions, cellular ATP levels rapidly decline leading to ischemic depolarisation throughout WM. An early rise in axonal Ca^{2+} promotes the excessive fusion of glutamatergic vesicles with the internodal axolemma of myelinated (and unmyelinated) axons. This rapidly elevates glutamate concentrations in the confined periaxonal space separating the axolemma and inner loops of myelin. In turn, the accumulation of periaxonal glutamate activates a high density of functional NMDA receptors expressed in the overlaying myelin sheath. The over-activation of myelinic NMDA receptors during ischemia promotes the decompaction and degradation of myelin, an event which ultimately leads to a failure in

saltatory AP conduction. Notably, it is the irreversible loss in nerve excitability which underlies a range of functional deficits observed in patients who experience severe ischemia. This surprising injury pathway is distinct from the mechanisms which mediate injury to the cytoplasmic processes and soma of oligodendrocytes, which likely involve the activation of TRP-A1 and non-NMDA receptors, respectively (Tekkok and Goldberg 2001, Hamilton, Kolodziejczyk et al. 2016).

The pathway elucidated here presents myelinic NMDA receptors as an attractive therapeutic target in the treatment of ischemic WM injury. The sub-unit selective NMDA receptor antagonist, QNZ-46, penetrates myelin and is retained in myelinated WM regions of the CNS following systemic injection of the drug. The incorporation of QNZ-46 in central myelin selectively inhibits myelinic NMDA receptor activation in a use-dependent manner, which prevents the over-activation of NMDA receptors during ischemia. As a result, QNZ-46 preserves myelin structure, which ultimately improves functional recovery (see fig 6.1).

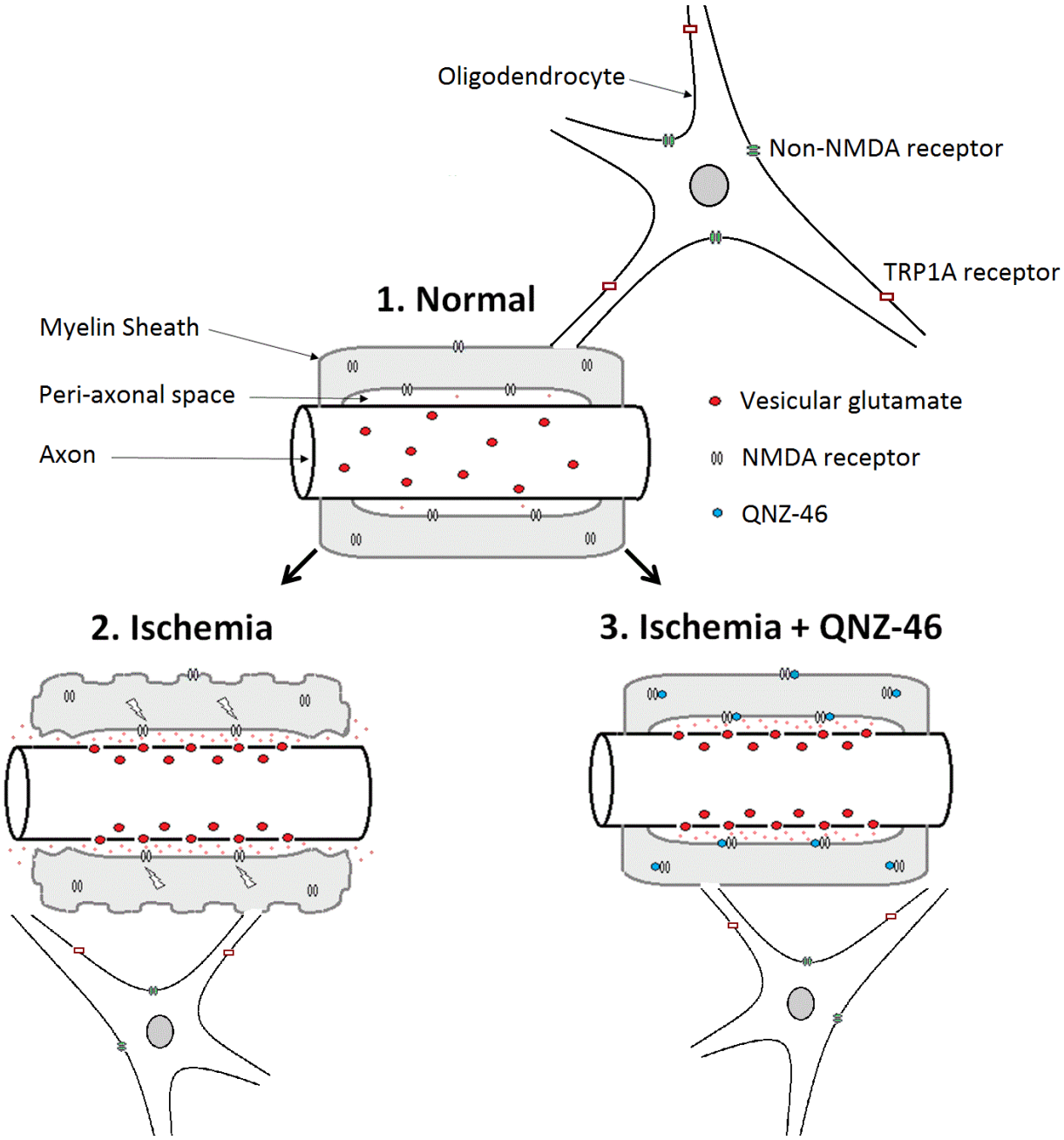

Fig. 6.1: Schematic depiction of the proposed model of ischemic myelin injury. Compact myelin contains a high density of functional NR2C/D-containing NMDA receptors which are expressed throughout the myelin sheath. The underlying axon contains a number of glutamatergic vesicles. The axon and inner loops of myelin are separated by a confined region known as the peri-axonal space. Non-NMDA receptors are located on the oligodendrocyte cell soma, while TRP-A1 receptors are found on the cytoplasmic domain of the oligodendrocyte processes. (1) Under physiological conditions, $[Glut]_e$ are kept low. (2) Under ischemic conditions, glutamatergic vesicles fuse with the axolemma, releasing glutamate into the confined peri-axonal space. The accumulation of glutamate within the peri-axonal space over-activates myelinic NMDA receptors, which leads to myelin injury. (3) Treating nerves with QNZ-46 prevents the sustained activation of myelinic NMDA receptors, which subsequently prevents the excitotoxic degradation of myelin during ischemia.

6.3: Implications of QNZ-46

NMDA receptor-mediated excitotoxity is implicated in a variety of neurological disorders including ischemia, Alzehimers' disease, Parkinsons' disease, chronic pain and multiple sclerosis (MS) (Cull-Candy, Brickley et al. 2001). Myelin-specific NMDA receptors provide a novel therapeutic target for a number of neurological disorders which affect myelin. QNZ-46 in particular, displays a number of desirable characteristics associated with tolerable clinical neuroprotective agents. These features include brain accessibility, sub-unit selectivity, drugability and use-dependence. Thus, a relative sparing of physiological NMDA receptor activation is predicted which may overcome a variety of adverse effects. In addition, myelin accumulation and retention provide a suitable mechanism by which QNZ-46 provides persistent protect following the removal of the drug from the extracellular space, the first known drug to exhibit this unique characteristic. This may prove to be a major development in the treatment of chronic neurological disorders, such as neurodegenerative diseases and multiple sclerosis (MS). Similarly, it may elevate the injury tolerance of those who are at high risk of stroke, or susceptible to recurrent stroke.

In vivo administration of an effective concentration of QNZ-46 in mice showed no evidence of acute adverse effects or behavioural alterations. While further investigations into the tolerability of QNZ-46 are required, initial findings suggest that its translational potential is exceptional. Considering the complexity of ischemic brain injury, it is unlikely that QNZ-46 alone will provide a dramatic degree of protection clinically. However, the application of QNZ-46 in conjunction with alternative pharmacological compounds targeting alternative cellular compartments (e.g. AMPA/kainate receptor inhibitors, TRP-A1 channel blockers, NCX inhibitors) may prove to be highly protective. QNZ-46 may represent a novel class of pharmacological inhibitors capable of providing persistent neurological protection.

6.4: Concluding remarks

The overall motivation behind this thesis is to contribute to a better understanding of the injury mechanisms involved in irreversible WM damage. The work presented here provides evidence of a novel injury pathway which is responsible for ischemic myelin disruption and irreversible functional injury. This discovery not only challenges the involvement of reverse glutamate transporters, but also raises the question of whether the axonal vesicular release injury pathway is also implicated in alternative neurological disorders. In addition, it supports recent reports of the axo-myelinic synapse which may play an important role in a number of physiological processes in central WM. Results on QNZ-46 provide an exciting new opportunity for further experiments into the actions, potential adverse effects and efficacy of the drug. Together, these findings will hopefully pave the way for further research and contribute to the development of effective clinical interventions.

Bibliography:

AGRAWAL, S. K., E. THERIAULT and M. G. FEHLINGS (1998). "Role of group I metabotropic glutamate receptors in traumatic spinal cord white matter injury." Journal of neurotrauma **15**(11): 929-941.

al-Baldawi, N. F. and R. F. Abercrombie (1995). "Calcium diffusion coefficient in Myxicola axoplasm." Cell Calcium **17**(6): 422-430.

Alberdi, E., A. Ruiz and C. Matute (2014). Calcium Dyshomeostasis in White Matter Injury. White Matter Injury in Stroke and CNS Disease. S. Baltan, S. T. Carmichael, C. Matute, G. Xi and J. H. Zhang. New York, NY, Springer New York**:** 433-460.

Alix, J. J., A. C. Dolphin and R. Fern (2008). "Vesicular apparatus, including functional calcium channels, are present in developing rodent optic nerve axons and are required for normal node of Ranvier formation." J Physiol **586**(17): 4069-4089.

Alix, J. J. and A. M. Domingues (2011). "White matter synapses: form, function, and dysfunction." Neurology **76**(4): 397-404.

Alix, J. J. and R. Fern (2009). "Glutamate receptor-mediated ischemic injury of premyelinated central axons." Ann Neurol **66**(5): 682-693.

Alix, J. J. and R. Fern (2009). "Glutamate receptor ‐ mediated ischemic injury of premyelinated central axons." Annals of neurology **66**(5): 682-693.

Alix, J. J., C. Zammit, A. Riddle, C. K. Meshul, S. A. Back, M. Valentino and R. Fern (2012). "Central axons preparing to myelinate are highly sensitivity to ischemic injury." Annals of neurology **72**(6): 936-951.

Alix, J. J. P. (2006). "The pathophysiology of ischemic injury to developing white matter." McGill Journal of Medicine : MJM **9**(2): 134-140.

Alix, J. J. P., A. C. Dolphin and R. Fern (2008). "Vesicular apparatus, including functional calcium channels, are present in developing rodent optic nerve axons and are required for normal node of Ranvier formation." The Journal of Physiology **586**(17): 4069-4089.

Alix, J. J. P., A. C. Dolphin and R. Fern (2008). "Vesicular apparatus, including functional calcium channels, are present in developing rodent optic nerve axons and are required for normal node of Ranvier formation." J Physiol **586**(Pt 17): 4069-4089.

Alix, J. J. P., C. Zammit, A. Riddle, C. K. Meshul, S. A. Back, M. Valentino and R. Fern (2012). "Central axons preparing to myelinate are highly sensitivity to ischemic injury." Annals of neurology **72**(6): 936-951.

Allen, N. J. and B. A. Barres (2009). "Neuroscience: Glia [mdash] more than just brain glue." Nature **457**(7230): 675-677.

Allen, N. J., R. Káradóttir and D. Attwell (2005). "A Preferential Role for Glycolysis in Preventing the Anoxic Depolarization of Rat Hippocampal Area CA1 Pyramidal Cells." The Journal of Neuroscience **25**(4): 848-859.

Amara, S. G. and A. C. K. Fontana (2002). "Excitatory amino acid transporters: keeping up with glutamate." Neurochemistry International **41**(5): 313-318.

Anderson, C. M. and R. A. Swanson (2000). "Astrocyte glutamate transport: Review of properties, regulation, and physiological functions." Glia **32**(1): 1-14.

Andiné, P., M. Sandberg, R. Bågenholm, A. Lehmann and H. Hagberg (1991). "Intra- and extracellular changes of amino acids in the cerebral cortex of the neonatal rat during hypoxic-ischemia." Developmental Brain Research **64**(1–2): 115-120.

Andiné, P., M. Sandberg, R. Bågenholm, A. Lehmann and H. Hagberg (1991). "Intra-and extracellular changes of amino acids in the cerebral cortex of the neonatal rat during hypoxic-ischemia." Developmental brain research **64**(1): 115-120.

Arranz, A. M., A. Hussein, J. J. Alix, F. Perez-Cerda, N. Allcock, C. Matute and R. Fern (2008). "Functional glutamate transport in rodent optic nerve axons and glia." Glia **56**(12): 1353-1367.

Arranz, A. M., A. Hussein, J. J. P. Alix, F. Pérez-Cerdá, N. Allcock, C. Matute and R. Fern (2008). "Functional glutamate transport in rodent optic nerve axons and glia." Glia **56**(12): 1353-1367.
Attwell, D. and S. B. Laughlin (2001). "An energy budget for signaling in the grey matter of the brain." J Cereb Blood Flow Metab **21**(10): 1133-1145.
Back, S. A. (2014). "Cerebral white and gray matter injury in newborns: new insights into pathophysiology and management." Clin Perinatol **41**(1): 1-24.
Back, S. A. (2014). "Cerebral White and Gray Matter Injury in Newborns: New Insights into Pathophysiology and Management." Clinics in Perinatology **41**(1): 1-24.
Back, S. A., A. Craig, R. J. Kayton, N. L. Luo, C. K. Meshul, N. Allcock and R. Fern (2007). "Hypoxia–ischemia preferentially triggers glutamate depletion from oligodendroglia and axons in perinatal cerebral white matter." Journal of Cerebral Blood Flow & Metabolism **27**(2): 334-347.
Back, S. A., B. H. Han, N. L. Luo, C. A. Chricton, S. Xanthoudakis, J. Tam, K. L. Arvin and D. M. Holtzman (2002). "Selective Vulnerability of Late Oligodendrocyte Progenitors to Hypoxia–Ischemia." The Journal of Neuroscience **22**(2): 455-463.
Back, S. A. and P. A. Rosenberg (2014). "Pathophysiology of glia in perinatal white matter injury." Glia **31**(10): 22658.
Baker, D. A., Z. X. Xi, H. Shen, C. J. Swanson and P. W. Kalivas (2002). "The origin and neuronal function of in vivo nonsynaptic glutamate." J Neurosci **22**(20): 9134-9141.
Bakiri, Y., V. Burzomato, G. Frugier, N. B. Hamilton, R. Karadottir and D. Attwell (2009). "Glutamatergic signaling in the brain's white matter." Neuroscience **158**(1): 266-274.
Bakiri, Y., N. B. Hamilton, R. Karadottir and D. Attwell (2008). "Testing NMDA receptor block as a therapeutic strategy for reducing ischaemic damage to CNS white matter." Glia **56**(2): 233-240.
Balice-Gordon, R. J., L. J. Bone and S. S. Scherer (1998). "Functional gap junctions in the schwann cell myelin sheath." J Cell Biol **142**(4): 1095-1104.
Baltan, S. (2009). "Ischemic injury to white matter: an age-dependent process." The Neuroscientist **15**(2): 126-133.
Baltan, S. (2016). "Age-specific localization of NMDA receptors on oligodendrocytes dictates axon function recovery after ischemia." Neuropharmacology **110**(Pt B): 626-632.
Baltan, S., E. F. Besancon, B. Mbow, Z. Ye, M. A. Hamner and B. R. Ransom (2008). "White matter vulnerability to ischemic injury increases with age because of enhanced excitotoxicity." The Journal of Neuroscience **28**(6): 1479-1489.
Baltan, S., S. T. Carmichael, C. Matute, G. Xi and J. H. Zhang (2014). White matter injury in stroke and CNS disease, Springer.
Bang, O. Y., E. H. Kim, J. M. Cha and G. J. Moon (2016). "Adult Stem Cell Therapy for Stroke: Challenges and Progress." J Stroke **18**(3): 256-266.
Banker, B. Q. and J. C. Larroche (1962). "Periventricular leukomalacia of infancy. A form of neonatal anoxic encephalopathy." Arch Neurol **7**: 386-410.
Banks, W. A. (2009). "Characteristics of compounds that cross the blood-brain barrier." BMC Neurology **9**(Suppl 1): S3-S3.
Barnett, M. W. and P. M. Larkman (2007). "The action potential." Pract Neurol **7**(3): 192-197.
Barnett, M. W. and P. M. Larkman (2007). "The action potential." Practical neurology **7**(3): 192-197.
Barres, B. A. and M. C. Raff (1994). "Control of oligodendrocyte number in the developing rat optic nerve." Neuron **12**(5): 935-942.
Baskys, A., I. Bayazitov, L. Fang, M. Blaabjerg, F. R. Poulsen and J. Zimmer (2005). "Group I metabotropic glutamate receptors reduce excitotoxic injury and may facilitate neurogenesis." Neuropharmacology **49 Suppl 1**: 146-156.
Baskys, A. and A. C. Hou (2007). "Vascular dementia: Pharmacological treatment approaches and perspectives." Clinical Interventions in Aging **2**(3): 327-335.
Baud, O., R. F. Haynes, H. Wang, R. D. Folkerth, J. Li, J. J. Volpe and P. A. Rosenberg (2004). "Developmental up-regulation of MnSOD in rat oligodendrocytes confers protection against oxidative injury." Eur J Neurosci **20**(1): 29-40.

Bazargani, N. and D. Attwell (2016). "Astrocyte calcium signaling: the third wave." Nat Neurosci **19**(2): 182-189.
Beiu, V., B. A. M. Madappuram, P. M. Kelly and L. J. McDaid (2011). On Two-Layer Brain-Inspired Hierarchical Topologies – A Rent's Rule Approach –. Transactions on High-Performance Embedded Architectures and Compilers IV. P. Stenström. Berlin, Heidelberg, Springer Berlin Heidelberg**:** 311-333.
Belhage, B., G. H. Hansen and A. Schousboe (1993). "Depolarization by K+ and glutamate activates different neurotransmitter release mechanisms in gabaergic neurons: Vesicular versus non-vesicular release of GABA." Neuroscience **54**(4): 1019-1034.
Benveniste, H., J. Drejer, A. Schousboe and N. H. Diemer (1984). "Elevation of the extracellular concentrations of glutamate and aspartate in rat hippocampus during transient cerebral ischemia monitored by intracerebral microdialysis." J Neurochem **43**(5): 1369-1374.
Bergles, D. E., J. D. Roberts, P. Somogyi and C. E. Jahr (2000). "Glutamatergic synapses on oligodendrocyte precursor cells in the hippocampus." Nature **405**(6783): 187-191.
Bernard , S. A., T. W. Gray , M. D. Buist , B. M. Jones , W. Silvester , G. Gutteridge and K. Smith (2002). "Treatment of Comatose Survivors of Out-of-Hospital Cardiac Arrest with Induced Hypothermia." New England Journal of Medicine **346**(8): 557-563.
Beyenbach, K. W. and H. Wieczorek (2006). "The V-type H+ ATPase: molecular structure and function, physiological roles and regulation." J Exp Biol **209**(Pt 4): 577-589.
Bezzi, P., G. Carmignoto, L. Pasti, S. Vesce, D. Rossi, B. L. Rizzini, T. Pozzan and A. Volterra (1998). "Prostaglandins stimulate calcium-dependent glutamate release in astrocytes." Nature **391**(6664): 281-285.
Bezzi, P., V. Gundersen, J. L. Galbete, G. Seifert, C. Steinhauser, E. Pilati and A. Volterra (2004). "Astrocytes contain a vesicular compartment that is competent for regulated exocytosis of glutamate." Nat Neurosci **7**(6): 613-620.
Binamé, F., D. Sakry, L. Dimou, V. Jolivel and J. Trotter (2013). "NG2 Regulates Directional Migration of Oligodendrocyte Precursor Cells via Rho GTPases and Polarity Complex Proteins." The Journal of Neuroscience **33**(26): 10858-10874.
Blandini, F., R. H. P. Porter and J. T. Greenamyre (1996). "Glutamate and Parkinson's disease." Molecular Neurobiology **12**(1): 73-94.
Blanke, M. L. and A. M. VanDongen (2009). "Activation mechanisms of the NMDA receptor."
Blaurock, A. E. (1981). "The spaces between membrane bilayers within PNS myelin as characterized by X-ray diffraction." Brain Res **210**(1-2): 383-387.
Bliss, T. M., R. H. Andres and G. K. Steinberg (2010). "Optimizing the Success of Cell Transplantation Therapy for Stroke." Neurobiology of disease **37**(2): 275.
Bradl, M. and H. Lassmann (2010). "Oligodendrocytes: biology and pathology." Acta Neuropathologica **119**(1): 37-53.
Brazhe, A. R., G. V. Maksimov, E. Mosekilde and O. V. Sosnovtseva (2011). "Excitation block in a nerve fibre model owing to potassium-dependent changes in myelin resistance." Interface Focus **1**(1): 86-100.
Bridges, R. J. and C. S. Esslinger (2005). "The excitatory amino acid transporters: Pharmacological insights on substrate and inhibitor specificity of the EAAT subtypes." Pharmacology & Therapeutics **107**(3): 271-285.
Bridges, R. J., N. R. Natale and S. A. Patel (2012). "System x(c)(-) cystine/glutamate antiporter: an update on molecular pharmacology and roles within the CNS." British Journal of Pharmacology **165**(1): 20-34.
Brown, A. M., R. E. Westenbroek, W. A. Catterall and B. R. Ransom (2001). "Axonal L-type Ca2+ channels and anoxic injury in rat CNS white matter." Journal of neurophysiology **85**(2): 900-911.
Brown, A. M., R. E. Westenbroek, W. A. Catterall and B. R. Ransom (2001). "Axonal L-type Ca2+ channels and anoxic injury in rat CNS white matter." J Neurophysiol **85**(2): 900-911.
Bruno, V., A. Copani, G. Battaglia, R. Raffaele, H. Shinozaki and F. Nicoletti (1994). "Protective effect of the metabotropic glutamate receptor agonist, DCG-IV, against excitotoxic neuronal death." European Journal of Pharmacology **256**(1): 109-112.

Burger, P. M., E. Mehl, P. L. Cameron, P. R. Maycox, M. Baumert, F. Lottspeich, P. De Camilli and R. Jahn (1989). "Synaptic vesicles immunoisolated from rat cerebral cortex contain high levels of glutamate." Neuron **3**(6): 715-720.
Butt, A. M., K. Colquhoun, M. Tutton and M. Berry (1994). "Three-dimensional morphology of astrocytes and oligodendrocytes in the intact mouse optic nerve." J Neurocytol **23**(8): 469-485.
Butt, A. M., A. Duncan, M. F. Hornby, S. L. Kirvell, A. Hunter, J. M. Levine and M. Berry (1999). "Cells expressing the NG2 antigen contact nodes of Ranvier in adult CNS white matter." Glia **26**(1): 84-91.
Butt, A. M., M. Pugh, P. Hubbard and G. James (2004). "Functions of optic nerve glia: axoglial signalling in physiology and pathology." Eye (Lond) **18**(11): 1110-1121.
Butt, A. M. and B. R. Ransom (1993). "Morphology of astrocytes and oligodendrocytes during development in the intact rat optic nerve." J Comp Neurol **338**(1): 141-158.
C. Raff, M. and R. H. Miller (1984). "Glial cell development in the rat optic nerve." Trends in Neurosciences **7**(12): 469-472.
Cavaliere, F., O. Urra, E. Alberdi and C. Matute (2012). "Oligodendrocyte differentiation from adult multipotent stem cells is modulated by glutamate." Cell Death Dis **3**: e268.
Cavelier, P. and D. Attwell (2005). "Tonic release of glutamate by a DIDS-sensitive mechanism in rat hippocampal slices." J Physiol **564**(Pt 2): 397-410.
Cavelier, P. and D. Attwell (2007). "Neurotransmitter depletion by bafilomycin is promoted by vesicle turnover." Neurosci Lett **412**(2): 95-100.
Chaudhry, F. A., K. P. Lehre, M. van Lookeren Campagne, O. P. Ottersen, N. C. Danbolt and J. Storm-Mathisen (1995). "Glutamate transporters in glial plasma membranes: highly differentiated localizations revealed by quantitative ultrastructural immunocytochemistry." Neuron **15**(3): 711-720.
Chen, Y. and R. A. Swanson (2003). "Astrocytes and brain injury." Journal of Cerebral Blood Flow & Metabolism **23**(2): 137-149.
Chen, Y., Q. Yi, G. Liu, X. Shen, L. Xuan and Y. Tian (2013). "Cerebral white matter injury and damage to myelin sheath following whole-brain ischemia." Brain Research **1495**: 11-17.
Cheng, M. Y., E. H. Wang, W. J. Woodson, S. Wang, G. Sun, A. G. Lee, A. Arac, L. E. Fenno, K. Deisseroth and G. K. Steinberg (2014). "Optogenetic neuronal stimulation promotes functional recovery after stroke." Proceedings of the National Academy of Sciences **111**(35): 12913-12918.
Chevalier-Larsen, E. and E. L. F. Holzbaur (2006). "Axonal transport and neurodegenerative disease." Biochimica et Biophysica Acta (BBA) - Molecular Basis of Disease **1762**(11–12): 1094-1108.
Choi, D. W. (1985). "Glutamate neurotoxicity in cortical cell culture is calcium dependent." Neuroscience Letters **58**(3): 293-297.
Choi, D. W. (1987). "Ionic dependence of glutamate neurotoxicity." J Neurosci **7**(2): 369-379.
Choi, D. W. and S. M. Rothman (1990). "The role of glutamate neurotoxicity in hypoxic-ischemic neuronal death." Annual review of neuroscience **13**(1): 171-182.
Choi, K. E., C. L. Hall, J. M. Sun, L. Wei, O. Mohamad, T. A. Dix and S. P. Yu (2012). "A novel stroke therapy of pharmacologically induced hypothermia after focal cerebral ischemia in mice." FASEB J **26**(7): 2799-2810.
Clements, J. D. and G. L. Westbrook (1991). "Activation kinetics reveal the number of glutamate and glycine binding sites on the N-methyl-D-aspartate receptor." Neuron **7**(4): 605-613.
Connors, B. W., B. R. Ransom, D. M. Kunis and M. J. Gutnick (1982). "Activity-dependent K+ accumulation in the developing rat optic nerve." Science **216**(4552): 1341-1343.
Conrad, M. and H. Sato (2012). "The oxidative stress-inducible cystine/glutamate antiporter, system xc−: cystine supplier and beyond." Amino acids **42**(1): 231-246.
Contreras, J. E., H. A. Sánchez, E. A. Eugenín, D. Speidel, M. Theis, K. Willecke, F. F. Bukauskas, M. V. L. Bennett and J. C. Sáez (2002). "Metabolic inhibition induces opening of unapposed connexin 43 gap junction hemichannels and reduces gap junctional

communication in cortical astrocytes in culture." Proceedings of the National Academy of Sciences **99**(1): 495-500.
Coons, A. H., H. J. Creech and R. N. Jones (1941). "Immunological Properties of an Antibody Containing a Fluorescent Group." Experimental Biology and Medicine **47**(2): 200-202.
Crespo, D., D. D. O'Leary and W. M. Cowan (1985). "Changes in the numbers of optic nerve fibers during late prenatal and postnatal development in the albino rat." Brain Res **351**(1): 129-134.
Cui, Y., L. Zhang, K. Utsunomiya, H. Yanase, A. Mitani and K. Kataoka (1999). "Ischemia-induced glutamate release in the dentate gyrus. A microdialysis study in the gerbil." Neurosci Lett **271**(3): 191-194.
Cull-Candy, S., S. Brickley and M. Farrant (2001). "NMDA receptor subunits: diversity, development and disease." Current opinion in neurobiology **11**(3): 327-335.
Dale, N., S. Hatz, F. Tian and E. Llaudet (2005). "Listening to the brain: microelectrode biosensors for neurochemicals." Trends in Biotechnology **23**(8): 420-428.
Dale, N., S. Hatz, F. Tian and E. Llaudet (2005). "Listening to the brain: microelectrode biosensors for neurochemicals." Trends Biotechnol **23**(8): 420-428.
Dale, N., T. Pearson and B. G. Frenguelli (2000). "Direct measurement of adenosine release during hypoxia in the CA1 region of the rat hippocampal slice." J Physiol **1**: 143-155.
Danbolt, N. C. (2001). "Glutamate uptake." Progress in Neurobiology **65**(1): 1-105.
Dantzer, R., R. M. Bluthe, S. Laye, J. L. Bret-Dibat, P. Parnet and K. W. Kelley (1998). "Cytokines and sickness behavior." Ann N Y Acad Sci **840**: 586-590.
David, G., J. N. Barrett and E. F. Barrett (1993). "Activation of internodal potassium conductance in rat myelinated axons." The Journal of Physiology **472**: 177-202.
David, J. C., K. A. Yamada, M. R. Bagwe and M. P. Goldberg (1996). "AMPA receptor activation is rapidly toxic to cortical astrocytes when desensitization is blocked." J Neurosci **16**(1): 200-209.
Davidson, J. O., C. R. Green, B. Nicholson, F. Louise, S. J. O'Carroll, M. Fraser, L. Bennet and A. Jan Gunn (2012). "Connexin hemichannel blockade improves outcomes in a model of fetal ischemia." Annals of neurology **71**(1): 121-132.
Davies, C. A., S. A. Loddick, R. P. Stroemer, J. Hunt and N. J. Rothwell (1998). "An integrated analysis of the progression of cell responses induced by permanent focal middle cerebral artery occlusion in the rat." Exp Neurol **154**(1): 199-212.
Dawson, L. A., S. Djali, C. Gonzales, M. A. Vinegra and M. M. Zaleska (2000). "Characterization of transient focal ischemia-induced increases in extracellular glutamate and aspartate in spontaneously hypertensive rats." Brain Res Bull **53**(6): 767-776.
Dawson, M. R., A. Polito, J. M. Levine and R. Reynolds (2003). "NG2-expressing glial progenitor cells: an abundant and widespread population of cycling cells in the adult rat CNS." Mol Cell Neurosci **24**(2): 476-488.
Dawson, M. R. L., A. Polito, J. M. Levine and R. Reynolds (2003). "NG2-expressing glial progenitor cells: an abundant and widespread population of cycling cells in the adult rat CNS." Molecular and Cellular Neuroscience **24**(2): 476-488.
De Biase, L. M., A. Nishiyama and D. E. Bergles (2010). "Excitability and synaptic communication within the oligodendrocyte lineage." J Neurosci **30**(10): 3600-3611.
Dean, J. M., M. Fraser, A. N. Shelling, L. Bennet, S. George, S. Shaikh, A. Scheepens and A. J. Gunn (2005). "Ontogeny of AMPA and NMDA receptor gene expression in the developing sheep white matter and cerebral cortex." Molecular Brain Research **139**(2): 242-250.
Debanne, D., E. Campanac, A. Bialowas, E. Carlier and G. Alcaraz (2011). "Axon physiology." Physiol Rev **91**(2): 555-602.
Demerens, C., B. Stankoff, M. Logak, P. Anglade, B. Allinquant, F. Couraud, B. Zalc and C. Lubetzki (1996). "Induction of myelination in the central nervous system by electrical activity." Proceedings of the National Academy of Sciences of the United States of America **93**(18): 9887-9892.

Deng, W., P. A. Rosenberg, J. J. Volpe and F. E. Jensen (2003). "Calcium-permeable AMPA/kainate receptors mediate toxicity and preconditioning by oxygen-glucose deprivation in oligodendrocyte precursors." Proceedings of the National Academy of Sciences **100**(11): 6801-6806.
Deng, W., H. Wang, P. A. Rosenberg, J. J. Volpe and F. E. Jensen (2004). "Role of metabotropic glutamate receptors in oligodendrocyte excitotoxicity and oxidative stress." Proceedings of the National Academy of Sciences of the United States of America **101**(20): 7751-7756.
DeSilva, T. M., A. Y. Kabakov, P. E. Goldhoff, J. J. Volpe and P. A. Rosenberg (2009). "Regulation of Glutamate Transport in Developing Rat Oligodendrocytes." The Journal of neuroscience : the official journal of the Society for Neuroscience **29**(24): 7898-7908.
DeSilva, T. M., A. Y. Kabakov, P. E. Goldhoff, J. J. Volpe and P. A. Rosenberg (2009). "Regulation of glutamate transport in developing rat oligodendrocytes." J Neurosci **29**(24): 7898-7908.
Desilva, T. M., H. C. Kinney, N. S. Borenstein, F. L. Trachtenberg, N. Irwin, J. J. Volpe and P. A. Rosenberg (2007). "The glutamate transporter EAAT2 is transiently expressed in developing human cerebral white matter." J Comp Neurol **501**(6): 879-890.
Dewar, D., S. M. Underhill and M. P. Goldberg (2003). "Oligodendrocytes and ischemic brain injury." Journal of Cerebral Blood Flow & Metabolism **23**(3): 263-274.
Dingledine, R., K. Borges, D. Bowie and S. F. Traynelis (1999). "The glutamate receptor ion channels." Pharmacological reviews **51**(1): 7-62.
Dirnagl, U., C. Iadecola and M. A. Moskowitz (1999). "Pathobiology of ischaemic stroke: an integrated view." Trends in neurosciences **22**(9): 391-397.
Disorders, T. N. I. o. N. and S. r.-P. S. S. Group (1995). "Tissue Plasminogen Activator for Acute Ischemic Stroke." New England Journal of Medicine **333**(24): 1581-1588.
Domercq, M., E. Etxebarria, A. Perez-Samartin and C. Matute (2005). "Excitotoxic oligodendrocyte death and axonal damage induced by glutamate transporter inhibition." Glia **52**(1): 36-46.
Domercq, M., A. Perez-Samartin, D. Aparicio, E. Alberdi, O. Pampliega and C. Matute (2010). "P2X7 receptors mediate ischemic damage to oligodendrocytes." Glia **58**(6): 730-740.
Domercq, M., M. V. Sánchez-Gómez, P. Areso and C. Matute (1999). "Expression of glutamate transporters in rat optic nerve oligodendrocytes." European Journal of Neuroscience **11**(7): 2226-2236.
Domercq, M., M. V. Sánchez-Gómez, C. Sherwin, E. Etxebarria, R. Fern and C. Matute (2007). "System x_c[−] and Glutamate Transporter Inhibition Mediates Microglial Toxicity to Oligodendrocytes." The Journal of Immunology **178**(10): 6549-6556.
Dong, C. J. and W. A. Hare (2005). "Contribution to ischemic injury of rat optic nerves by intracellular sodium overload." Doc Ophthalmol **110**(1): 15-23.
Dong, X.-x., Y. Wang and Z.-h. Qin (2009). "Molecular mechanisms of excitotoxicity and their relevance to pathogenesis of neurodegenerative diseases." Acta Pharmacologica Sinica **30**(4): 379-387.
Doyle, K. P., R. P. Simon and M. P. Stenzel-Poore (2008). "Mechanisms of ischemic brain damage." Neuropharmacology **55**(3): 310-318.
Drance, S. M. and D. R. Anderson (1995). Optic Nerve in Glaucoma, Kugler Publications.
Emery, B. (2010). "Regulation of Oligodendrocyte Differentiation and Myelination." Science **330**(6005): 779-782.
Eng, D. L. and J. D. Kocsis (1987). "Activity-dependent changes in extracellular potassium and excitability in turtle olfactory nerve." Journal of Neurophysiology **57**(3): 740-754.
Engl, E. and D. Attwell (2015). "Non‐signalling energy use in the brain." The Journal of Physiology **593**(16): 3417-3429.
Erlanger, J. and H. S. Gasser (1937). Electrical signs of nervous activity, University of Pennsylvania Press.

Etxeberria, A., K. C. Hokanson, D. Q. Dao, S. R. Mayoral, F. Mei, S. A. Redmond, E. M. Ullian and J. R. Chan (2016). "Dynamic Modulation of Myelination in Response to Visual Stimuli Alters Optic Nerve Conduction Velocity." J Neurosci **36**(26): 6937-6948.
Fannon, J., W. Tarmier and D. Fulton (2015). "Neuronal activity and AMPA-type glutamate receptor activation regulates the morphological development of oligodendrocyte precursor cells." Glia **63**(6): 1021-1035.
Feigin, V. L., M. H. Forouzanfar, R. Krishnamurthi, G. A. Mensah, M. Connor, D. A. Bennett, A. E. Moran, R. L. Sacco, L. Anderson, T. Truelsen, M. O'Donnell, N. Venketasubramanian, S. Barker-Collo, C. M. Lawes, W. Wang, Y. Shinohara, E. Witt, M. Ezzati, M. Naghavi and C. Murray (2014). "Global and regional burden of stroke during 1990-2010: findings from the Global Burden of Disease Study 2010." Lancet **383**(9913): 245-254.
Feng, B., H. W. Tse, D. A. Skifter, R. Morley, D. E. Jane and D. T. Monaghan (2004). "Structure-activity analysis of a novel NR2C/NR2D-preferring NMDA receptor antagonist: 1-(phenanthrene-2-carbonyl) piperazine-2,3-dicarboxylic acid." Br J Pharmacol **141**(3): 508-516.
Fern, R. (1998). "Intracellular Calcium and Cell Death during Ischemia in Neonatal Rat White Matter Astrocytes In Situ." The Journal of Neuroscience **18**(18): 7232-7243.
Fern, R. (2011). "Sources of extracellular glutamate in developing white matter." Malta Medical Journal **23**(3).
Fern, R. (2015). "Ischemic tolerance in pre-myelinated white matter: the role of astrocyte glycogen in brain pathology." Journal of Cerebral Blood Flow & Metabolism **35**(6): 951-958.
Fern, R. and T. Moller (2000). "Rapid ischemic cell death in immature oligodendrocytes: a fatal glutamate release feedback loop." J Neurosci **20**(1): 34-42.
Fern, R., B. R. Ransom and S. G. Waxman (1995). "Voltage-gated calcium channels in CNS white matter: role in anoxic injury." J Neurophysiol **74**(1): 369-377.
Fern, R., B. R. Ransom and S. G. Waxman (1995). "Voltage-gated calcium channels in CNS white matter: role in anoxic injury." Journal of neurophysiology **74**: 369-369.
Fern, R. F., C. Matute and P. K. Stys (2014). "White matter injury: Ischemic and nonischemic." Glia **62**(11): 1780-1789.
Filley, C. (2012). The behavioral neurology of white matter, Oxford University Press.
Filley, C. M. (1998). "The behavioral neurology of cerebral white matter." Neurology **50**(6): 1535-1540.
Fitsiori, A., D. Nguyen, A. Karentzos, J. Delavelle and M. I. Vargas (2011). "The corpus callosum: white matter or terra incognita." The British Journal of Radiology **84**(997): 5-18.
Fleidervish, I. A., C. Gebhardt, N. Astman, M. J. Gutnick and U. Heinemann (2001). "Enhanced Spontaneous Transmitter Release Is the Earliest Consequence of Neocortical Hypoxia That Can Explain the Disruption of Normal Circuit Function." The Journal of Neuroscience **21**(13): 4600-4608.
Flynn, R. W. V., R. S. M. MacWalter and A. S. F. Doney (2008). "The cost of cerebral ischaemia." Neuropharmacology **55**(3): 250-256.
Follett, P. L., P. A. Rosenberg, J. J. Volpe and F. E. Jensen (2000). "NBQX Attenuates Excitotoxic Injury in Developing White Matter." The Journal of Neuroscience **20**(24): 9235-9241.
Follett, P. L., P. A. Rosenberg, J. J. Volpe and F. E. Jensen (2000). "NBQX attenuates excitotoxic injury in developing white matter." J Neurosci **20**(24): 9235-9241.
Foster, R. E., B. W. Connors and S. G. Waxman (1982). "Rat optic nerve: electrophysiological, pharmacological and anatomical studies during development." Brain Res **255**(3): 371-386.
Foster, R. E., B. W. Connors and S. G. Waxman (1982). "Rat optic nerve: Electrophysiological, pharmacological and anatomical studies during development." Developmental Brain Research **3**(3): 371-386.
Frantseva, M. V., L. Kokarovtseva and J. L. Perez Velazquez (2002). "Ischemia-induced brain damage depends on specific gap-junctional coupling." J Cereb Blood Flow Metab **22**(4): 453-462.

Fremeau Jr, R. T., M. D. Troyer, I. Pahner, G. O. Nygaard, C. H. Tran, R. J. Reimer, E. E. Bellocchio, D. Fortin, J. Storm-Mathisen and R. H. Edwards (2001). "The Expression of Vesicular Glutamate Transporters Defines Two Classes of Excitatory Synapse." Neuron **31**(2): 247-260.
Frenguelli, B. G., E. Llaudet and N. Dale (2003). "High-resolution real-time recording with microelectrode biosensors reveals novel aspects of adenosine release during hypoxia in rat hippocampal slices." Journal of Neurochemistry **86**(6): 1506-1515.
Friede, R. L. and W. H. van Houten (1961). "Relations between post-mortem alterations and glycolytic metabolism in the brain." Experimental neurology **4**(3): 197-204.
Fruhbeis, C., D. Frohlich, W. P. Kuo, J. Amphornrat, S. Thilemann, A. S. Saab, F. Kirchhoff, W. Mobius, S. Goebbels, K. A. Nave, A. Schneider, M. Simons, M. Klugmann, J. Trotter and E. M. Kramer-Albers (2013). "Neurotransmitter-triggered transfer of exosomes mediates oligodendrocyte-neuron communication." PLoS Biol **11**(7): e1001604.
Fu, Y., H. Wang, T. B. Huff, R. Shi and J.-X. Cheng (2007). "Coherent Anti-Stokes Raman Scattering Imaging of Myelin Degradation Reveals a Calcium-Dependent Pathway in Lyso-PtdCho-Induced Demyelination." Journal of neuroscience research **85**(13): 2870-2881.
Fujimoto, S., H. Katsuki, T. Kume, S. Kaneko and A. Akaike (2004). "Mechanisms of oxygen glucose deprivation-induced glutamate release from cerebrocortical slice cultures." Neuroscience Research **50**(2): 179-187.
Funfschilling, U., L. M. Supplie, D. Mahad, S. Boretius, A. S. Saab, J. Edgar, B. G. Brinkmann, C. M. Kassmann, I. D. Tzvetanova, W. Mobius, F. Diaz, D. Meijer, U. Suter, B. Hamprecht, M. W. Sereda, C. T. Moraes, J. Frahm, S. Goebbels and K.-A. Nave (2012). "Glycolytic oligodendrocytes maintain myelin and long-term axonal integrity." Nature **485**(7399): 517-521.
Gaffield, M. A. and W. J. Betz (2006). "Imaging synaptic vesicle exocytosis and endocytosis with FM dyes." Nat Protoc **1**(6): 2916-2921.
Gautier, H. O., K. A. Evans, K. Volbracht, R. James, S. Sitnikov, I. Lundgaard, F. James, C. Lao-Peregrin, R. Reynolds, R. J. Franklin and R. T. Karadottir (2015). "Neuronal activity regulates remyelination via glutamate signalling to oligodendrocyte progenitors." Nat Commun **6**: 8518.
Gautier, H. O. B., K. A. Evans, K. Volbracht, R. James, S. Sitnikov, I. Lundgaard, F. James, C. Lao-Peregrin, R. Reynolds, R. J. M. Franklin and R. T. Karadottir (2015). "Neuronal activity regulates remyelination via glutamate signalling to oligodendrocyte progenitors." Nat Commun **6**.
George, P. M. and G. K. Steinberg (2015). "Novel Stroke Therapeutics: Unraveling Stroke Pathophysiology and Its Impact on Clinical Treatments." Neuron **87**(2): 297-309.
Gibson, A. and P. J. D. Andrews (2013). "Therapeutic hypothermia, still “too cool to be true?”." F1000Prime Reports **5**: 26.
Gido, G., T. Kristian and B. K. Siesjo (1997). "Extracellular potassium in a neocortical core area after transient focal ischemia." Stroke **28**(1): 206-210.
Gill, S. S. and O. M. Pulido (2001). "Glutamate receptors in peripheral tissues: current knowledge, future research, and implications for toxicology." Toxicol Pathol **29**(2): 208-223.
Gill, S. S., O. M. Pulido, R. W. Mueller and P. F. McGuire (1999). "Immunochemical localization of the metabotropic glutamate receptors in the rat heart." Brain Res Bull **48**(2): 143-146.
Globus, M. Y., R. Busto, E. Martinez, I. Valdes and W. D. Dietrich (1990). "Ischemia induces release of glutamate in regions spared from histopathologic damage in the rat." Stroke **21**(11 Suppl): Iii43-46.
Goldberg, M. P. and B. R. Ransom (2003). "New light on white matter." Stroke **34**(2): 330-332.
Gomes, J. and A. M. Wachsman (2013). Types of Strokes. Handbook of Clinical Nutrition and Stroke, Springer**:** 15-31.
Graf, R., E. Kumura, C. Dohmen, G. Rosner and W.-D. Heiss (2001). Pathophysiological Consequences of White Matter Compared to Gray Matter Ischemia. Ischemic Blood Flow in the Brain, Springer**:** 195-201.

Gravel, C., R. Sasseville and R. Hawkes (1990). "Maturation of the corpus callosum of the rat: II. Influence of thyroid hormones on the number and maturation of axons." J Comp Neurol **291**(1): 147-161.
Grewer, C., A. Gameiro, Z. Zhang, Z. Tao, S. Braams and T. Rauen (2008). "Glutamate forward and reverse transport: From molecular mechanism to transporter-mediated release after ischemia." IUBMB life **60**(9): 609-619.
Grewer, C., A. Gameiro, Z. Zhang, Z. Tao, S. Braams and T. Rauen (2008). "Glutamate forward and reverse transport: from molecular mechanism to transporter-mediated release after ischemia." IUBMB Life **60**(9): 609-619.
Gudz, T. I., H. Komuro and W. B. Macklin (2006). "Glutamate Stimulates Oligodendrocyte Progenitor Migration Mediated via an α_v Integrin/Myelin Proteolipid Protein Complex." The Journal of Neuroscience **26**(9): 2458-2466.
Gyllensten, L. and T. Malmfors (1963). "Myelinization of the optic nerve and its dependence on visual function--a quantitative investigation in mice." J Embryol Exp Morphol **11**: 255-266.
Hackett, M. L., M. Yang, C. S. Anderson, J. A. Horrocks and A. House (2010). "Pharmaceutical interventions for emotionalism after stroke." Cochrane Database Syst Rev(2): Cd003690.
Hamilton, N., P. S. Hubbard and A. M. Butt (2009). "Effects of glutamate receptor activation on NG2‐glia in the rat optic nerve." Journal of anatomy **214**(2): 208-218.
Hamilton, N., S. Vayro, F. Kirchhoff, A. Verkhratsky, J. Robbins, D. C. Gorecki and A. M. Butt (2008). "Mechanisms of ATP- and glutamate-mediated calcium signaling in white matter astrocytes." Glia **56**(7): 734-749.
Hamilton, N., S. Vayro, R. Wigley and A. M. Butt (2010). "Axons and astrocytes release ATP and glutamate to evoke calcium signals in NG2-glia." Glia **58**(1): 66-79.
Hamilton, N. B. and D. Attwell (2010). "Do astrocytes really exocytose neurotransmitters?" Nat Rev Neurosci **11**(4): 227-238.
Hamilton, N. B., K. Kolodziejczyk, E. Kougioumtzidou and D. Attwell (2016). "Proton-gated Ca(2+)-permeable TRP channels damage myelin in conditions mimicking ischaemia." Nature **529**(7587): 523-527.
Hansen, A. J. (1985). "Effect of anoxia on ion distribution in the brain." Physiol Rev **65**(1): 101-148.
Hansen, D. B., N. Garrido-Comas, M. Salter and R. Fern (2015). "HCO3−-independent pH Regulation in Astrocytes in Situ Is Dominated by V-ATPase." Journal of Biological Chemistry **290**(13): 8039-8047.
Hansen, K. B. and S. F. Traynelis (2011). "Structural and mechanistic determinants of a novel site for non-competitive inhibition of GluN2D-containing NMDA receptors." The Journal of neuroscience : the official journal of the Society for Neuroscience **31**(10): 3650-3661.
Harper, A. M. and S. Jennett (1990). Cerebral blood flow and metabolism, Manchester University Press.
Harris, J. J. and D. Attwell (2012). "The Energetics of CNS White Matter." The Journal of Neuroscience **32**(1): 356-371.
Harukuni, I. and A. Bhardwaj (2006). "Mechanisms of brain injury after global cerebral ischemia." Neurol Clin **24**(1): 1-21.
Hayashi, T. (1952). "A physiological study of epileptic seizures following cortical stimulation in animals and its application to human clinics." Jpn J Physiol **3**(1): 46-64.
Hicks, A. and J. Jolkkonen (2009). "Challenges and possibilities of intravascular cell therapy in stroke." Acta Neurobiol Exp (Wars) **69**(1): 1-11.
Hildebrand, C. and S. G. Waxman (1984). "Postnatal differentiation of rat optic nerve fibers: electron microscopic observations on the development of nodes of Ranvier and axoglial relations." J Comp Neurol **224**(1): 25-37.
Ho, P. W., D. C. Reutens, T. G. Phan, P. M. Wright, R. Markus, I. Indra, D. Young and G. A. Donnan (2005). "Is White Matter Involved in Patients Entered into Typical Trials of Neuroprotection?" Stroke **36**(12): 2742-2744.
Hollmann, M. and S. Heinemann (1994). "Cloned glutamate receptors." Annu Rev Neurosci **17**: 31-108.

Hoopmann, P., S. O. Rizzoli and W. J. Betz (2012). "Imaging synaptic vesicle recycling by staining and destaining vesicles with FM dyes." Cold Spring Harb Protoc **2012**(1): 77-83.
Hoyt, K. R., S. R. Arden, E. Aizenman and I. J. Reynolds (1998). "Reverse Na+/Ca2+ exchange contributes to glutamate-induced intracellular Ca2+ concentration increases in cultured rat forebrain neurons." Mol Pharmacol **53**(4): 742-749.
Hummel, F., P. Celnik, P. Giraux, A. Floel, W. H. Wu, C. Gerloff and L. G. Cohen (2005). "Effects of non-invasive cortical stimulation on skilled motor function in chronic stroke." Brain **128**(Pt 3): 490-499.
Huria, T., N. M. Beeraka, B. Al-Ghamdi and R. Fern (2014). "Premyelinated Central Axons Express Neurotoxic NMDA Receptors: Relevance to Early Developing White-Matter Injury." Journal of Cerebral Blood Flow & Metabolism **35**(4): 543-553.
Huria, T., N. M. Beeraka, B. Al-Ghamdi and R. Fern (2015). "Premyelinated central axons express neurotoxic NMDA receptors: relevance to early developing white-matter injury." J Cereb Blood Flow Metab **35**(4): 543-553.
Hynd, M. R., H. L. Scott and P. R. Dodd (2004). "Glutamate-mediated excitotoxicity and neurodegeneration in Alzheimer's disease." Neurochem Int **45**(5): 583-595.
Ishii, A., R. Dutta, G. M. Wark, S. I. Hwang, D. K. Han, B. D. Trapp, S. E. Pfeiffer and R. Bansal (2009). "Human myelin proteome and comparative analysis with mouse myelin." Proc Natl Acad Sci U S A **106**(34): 14605-14610.
Jabaudon, D., M. Scanziani, B. H. Gahwiler and U. Gerber (2000). "Acute decrease in net glutamate uptake during energy deprivation." Proc Natl Acad Sci U S A **97**(10): 5610-5615.
Jackson, V. M., S. J. Trout, K. L. Brain and T. C. Cunnane (2001). "Characterization of action potential-evoked calcium transients in mouse postganglionic sympathetic axon bundles." The Journal of Physiology **537**(Pt 1): 3-16.
Jahn, O., S. Tenzer and H. B. Werner (2009). "Myelin proteomics: molecular anatomy of an insulating sheath." Mol Neurobiol **40**(1): 55-72.
Jin, C., I. Londono, C. Mallard and G. A. Lodygensky (2015). "New means to assess neonatal inflammatory brain injury." J Neuroinflammation **12**: 180.
Jin, C. and J. J. Woodward (2006). "Effects of 8 different NR1 splice variants on the ethanol inhibition of recombinant NMDA receptors." Alcohol Clin Exp Res **30**(4): 673-679.
John, S. A., R. Kondo, S.-Y. Wang, J. I. Goldhaber and J. N. Weiss (1999). "Connexin-43 Hemichannels Opened by Metabolic Inhibition." Journal of Biological Chemistry **274**(1): 236-240.
Johnson, J. W. and P. Ascher (1990). "Voltage-dependent block by intracellular Mg2+ of N-methyl-D-aspartate-activated channels." Biophysical Journal **57**(5): 1085-1090.
Jorgensen, M. B. and N. H. Diemer (1982). "Selective neuron loss after cerebral ischemia in the rat: possible role of transmitter glutamate." Acta Neurol Scand **66**(5): 536-546.
Kampa, B. M., J. Clements, P. Jonas and G. J. Stuart (2004). "Kinetics of Mg(2+) unblock of NMDA receptors: implications for spike-timing dependent synaptic plasticity." The Journal of Physiology **556**(Pt 2): 337-345.
Kanellopoulos, G. K., X. M. Xu, C. Y. Hsu, X. Lu, T. M. Sundt and N. T. Kouchoukos (2000). "White matter injury in spinal cord ischemia protection by AMPA/kainate glutamate receptor antagonism." Stroke **31**(8): 1945-1952.
Kanellopoulos, G. K., X. M. Xu, C. Y. Hsu, X. Lu, T. M. Sundt and N. T. Kouchoukos (2000). "White Matter Injury in Spinal Cord Ischemia: Protection by AMPA/Kainate Glutamate Receptor Antagonism." Stroke **31**(8): 1945-1952.
Karadottir, R., P. Cavelier, L. H. Bergersen and D. Attwell (2005). "NMDA receptors are expressed in oligodendrocytes and activated in ischaemia." Nature **438**(7071): 1162-1166.
Káradóttir, R., P. Cavelier, L. H. Bergersen and D. Attwell (2005). "NMDA receptors are expressed in oligodendrocytes and activated in ischaemia." Nature **438**(7071): 1162-1166.
Katchman, A. N. and N. Hershkowitz (1993). "Early anoxia-induced vesicular glutamate release results from mobilization of calcium from intracellular stores." Journal of Neurophysiology **70**(1): 1-7.

Kawakami, M., M. Sekiguchi, K. Sato, S. Kozaki and M. Takahashi (2001). "Erythropoietin Receptor-mediated Inhibition of Exocytotic Glutamate Release Confers Neuroprotection during Chemical Ischemia." Journal of Biological Chemistry **276**(42): 39469-39475.
Khwaja, O. and J. J. Volpe (2008). "Pathogenesis of cerebral white matter injury of prematurity." Archives of disease in childhood. Fetal and neonatal edition **93**(2): F153-F161.
Kimelberg, H. K. (2005). "Astrocytic swelling in cerebral ischemia as a possible cause of injury and target for therapy." Glia **50**(4): 389-397.
Kimelberg, H. K. (2005). "Astrocytic swelling in cerebral ischemia as a possible cause of injury and target for therapy." Glia **50**(4): 389-397.
Kimelberg, H. K., S. K. Goderie, S. Higman, S. Pang and R. A. Waniewski (1990). "Swelling-induced release of glutamate, aspartate, and taurine from astrocyte cultures." J Neurosci **10**(5): 1583-1591.
Kimura, M., K. Sawada, T. Miyagawa, M. Kuwada, K. Katayama and Y. Nishizawa (1998). "Role of glutamate receptors and voltage-dependent calcium and sodium channels in the extracellular glutamate/aspartate accumulation and subsequent neuronal injury induced by oxygen/glucose deprivation in cultured hippocampal neurons." J Pharmacol Exp Ther **285**(1): 178-185.
Kingham, P. J., M. L. Cuzner and J. M. Pocock (1999). "Apoptotic pathways mobilized in microglia and neurones as a consequence of chromogranin A-induced microglial activation." J Neurochem **73**(2): 538-547.
Kleckner, N. W. and R. Dingledine (1988). "Requirement for glycine in activation of NMDA-receptors expressed in Xenopus oocytes." Science **241**(4867): 835-837.
Koh, J. Y., E. Palmer and C. W. Cotman (1991). "Activation of the metabotropic glutamate receptor attenuates N-methyl-D-aspartate neurotoxicity in cortical cultures." Proceedings of the National Academy of Sciences **88**(21): 9431-9435.
Kole, M. H. and G. J. Stuart (2012). "Signal processing in the axon initial segment." Neuron **73**(2): 235-247.
Kondo, R. P., S. Y. Wang, S. A. John, J. N. Weiss and J. I. Goldhaber (2000). "Metabolic inhibition activates a non-selective current through connexin hemichannels in isolated ventricular myocytes." J Mol Cell Cardiol **32**(10): 1859-1872.
Kuban, K. C. and F. H. Gilles (1985). "Human telencephalic angiogenesis." Ann Neurol **17**(6): 539-548.
Kuban , K. C. K. and A. Leviton (1994). "Cerebral Palsy." New England Journal of Medicine **330**(3): 188-195.
Kukley, M., E. Capetillo-Zarate and D. Dietrich (2007). "Vesicular glutamate release from axons in white matter." Nat Neurosci **10**(3): 311-320.
Kukley, M., E. Capetillo-Zarate and D. Dietrich (2007). "Vesicular glutamate release from axons in white matter." Nature neuroscience **10**(3): 311-320.
Lalo, U., Y. Pankratov, F. Kirchhoff, R. A. North and A. Verkhratsky (2006). "NMDA Receptors Mediate Neuron-to-Glia Signaling in Mouse Cortical Astrocytes." The Journal of Neuroscience **26**(10): 2673-2683.
Lankiewicz, S., C. Marc Luetjens, N. Truc Bui, A. J. Krohn, M. Poppe, G. M. Cole, T. C. Saido and J. H. M. Prehn (2000). "Activation of Calpain I Converts Excitotoxic Neuron Death into a Caspase-independent Cell Death." Journal of Biological Chemistry **275**(22): 17064-17071.
Lee, J.-M., G. J. Zipfel and D. W. Choi (1999). "The changing landscape of ischaemic brain injury mechanisms." Nature **399**(Supplementary): A7-A14.
Lee, S., A. C. Shafe and M. R. Cowie (2011). "UK stroke incidence, mortality and cardiovascular risk management 1999–2008: time-trend analysis from the General Practice Research Database." BMJ open **1**(2): e000269.
Lee, S., A. C. E. Shafe and M. R. Cowie (2011). "UK stroke incidence, mortality and cardiovascular risk management 1999–2008: time-trend analysis from the General Practice Research Database." BMJ Open **1**(2).

Lee, S. Y. and J. H. Kim (2015). "Mechanisms underlying presynaptic Ca2+ transient and vesicular glutamate release at a CNS nerve terminal during in vitro ischaemia." J Physiol **593**(13): 2793-2806.
Lee, Y., B. M. Morrison, Y. Li, S. Lengacher, M. H. Farah, P. N. Hoffman, Y. Liu, A. Tsingalia, L. Jin, P. W. Zhang, L. Pellerin, P. J. Magistretti and J. D. Rothstein (2012). "Oligodendroglia metabolically support axons and contribute to neurodegeneration." Nature **487**(7408): 443-448.
Lerdal, A., L. N. Bakken, E. F. Rasmussen, C. Beiermann, S. Ryen, S. Pynten, A. S. Drefvelin, A. M. Dahl, G. Rognstad, A. Finset, K. A. Lee and H. S. Kim (2011). "Physical impairment, depressive symptoms and pre-stroke fatigue are related to fatigue in the acute phase after stroke." Disabil Rehabil **33**(4): 334-342.
Li, C., L. Xiao, X. Liu, W. Yang, W. Shen, C. Hu, G. Yang and C. He (2013). "A functional role of NMDA receptor in regulating the differentiation of oligodendrocyte precursor cells and remyelination." Glia **61**(5): 732-749.
Li, L., A. A. Velumian, M. Samoilova and M. G. Fehlings (2016). "A Novel Approach for Studying the Physiology and Pathophysiology of Myelinated and Non-Myelinated Axons in the CNS White Matter." PLoS ONE **11**(11): e0165637.
Li, S., Q. Jiang and P. K. Stys (2000). "Important role of reverse Na(+)-Ca(2+) exchange in spinal cord white matter injury at physiological temperature." J Neurophysiol **84**(2): 1116-1119.
Li, S., G. A. Mealing, P. Morley and P. K. Stys (1999). "Novel injury mechanism in anoxia and trauma of spinal cord white matter: glutamate release via reverse Na+-dependent glutamate transport." J Neurosci **19**(14).
Li, S., G. A. Mealing, P. Morley and P. K. Stys (1999). "Novel injury mechanism in anoxia and trauma of spinal cord white matter: glutamate release via reverse Na+-dependent glutamate transport." J Neurosci **19**(14): Rc16.
Li, S. and P. Stys (2001). "Na< sup>+</sup>–K< sup>+</sup>-ATPase inhibition and depolarization induce glutamate release via reverse Na< sup>+</sup>-dependent transport in spinal cord white matter." Neuroscience **107**(4): 675-683.
Li, S. and P. K. Stys (2000). "Mechanisms of Ionotropic Glutamate Receptor-Mediated Excitotoxicity in Isolated Spinal Cord White Matter." The Journal of Neuroscience **20**(3): 1190-1198.
Liberatore, G. T., A. Samson, C. Bladin, W. D. Schleuning and R. L. Medcalf (2003). "Vampire bat salivary plasminogen activator (desmoteplase): a unique fibrinolytic enzyme that does not promote neurodegeneration." Stroke **34**(2): 537-543.
Lipton, S. A. (2004). "Failures and Successes of NMDA Receptor Antagonists: Molecular Basis for the Use of Open-Channel Blockers like Memantine in the Treatment of Acute and Chronic Neurologic Insults." NeuroRx **1**(1): 101-110.
Litsky, M. L., C. M. Hohl, J. H. Lucas and M. S. Jurkowitz (1999). "Inosine and guanosine preserve neuronal and glial cell viability in mouse spinal cord cultures during chemical hypoxia." Brain Research **821**(2): 426-432.
LoPachin, R. M., Jr. and P. K. Stys (1995). "Elemental composition and water content of rat optic nerve myelinated axons and glial cells: effects of in vitro anoxia and reoxygenation." J Neurosci **15**(10): 6735-6746.
Lozovaya, N., S. Gataullina, T. Tsintsadze, V. Tsintsadze, E. Pallesi-Pocachard, M. Minlebaev, N. A. Goriounova, E. Buhler, F. Watrin, S. Shityakov, A. J. Becker, A. Bordey, M. Milh, D. Scavarda, C. Bulteau, G. Dorfmuller, O. Delalande, A. Represa, C. Cardoso, O. Dulac, Y. Ben-Ari and N. Burnashev (2014). "Selective suppression of excessive GluN2C expression rescues early epilepsy in a tuberous sclerosis murine model." Nat Commun **5**: 4563.
Lucas, D. and J. Newhouse (1957). "The toxic effect of sodium L-glutamate on the inner layers of the retina." AMA Archives of ophthalmology **58**(2): 193-201.
Luders, E., P. M. Thompson and A. W. Toga (2010). "The development of the corpus callosum in the healthy human brain." J Neurosci **30**(33): 10985-10990.

Lujan, R., R. Shigemoto and G. Lopez-Bendito (2005). "Glutamate and GABA receptor signalling in the developing brain." Neuroscience **130**(3): 567-580.
Lundgaard, I., A. Luzhynskaya, J. H. Stockley, Z. Wang, K. A. Evans, M. Swire, K. Volbracht, H. O. Gautier, R. J. Franklin and D. Attwell (2013). "Neuregulin and BDNF Induce a Switch to NMDA Receptor-Dependent Myelination by Oligodendrocytes." PLoS biology **11**(12): e1001743.
Lundgaard, I., A. Luzhynskaya, J. H. Stockley, Z. Wang, K. A. Evans, M. Swire, K. Volbracht, H. O. Gautier, R. J. Franklin, D. Attwell and R. T. Karadottir (2013). "Neuregulin and BDNF induce a switch to NMDA receptor-dependent myelination by oligodendrocytes." PLoS Biol **11**(12): e1001743.
Lundgaard, I., A. Luzhynskaya, J. H. Stockley, Z. Wang, K. A. Evans, M. Swire, K. Volbracht, H. O. B. Gautier, R. J. M. Franklin, C. ffrench-Constant, D. Attwell and R. T. Káradóttir (2013). "Neuregulin and BDNF Induce a Switch to NMDA Receptor-Dependent Myelination by Oligodendrocytes." PLoS Biology **11**(12): e1001743.
Lundgaard, I., M. J. Osorio, B. T. Kress, S. Sanggaard and M. Nedergaard (2014). "White matter astrocytes in health and disease." Neuroscience **276**: 161-173.
Macrez, R., P. K. Stys, D. Vivien, S. A. Lipton and F. Docagne (2016). "Mechanisms of glutamate toxicity in multiple sclerosis: biomarker and therapeutic opportunities." Lancet Neurol **15**(10): 1089-1102.
Madl, C., L. Kramer, H. Domanovits, R. H. Woolard, H. Gervais, A. Gendo, E. Eisenhuber, G. Grimm and F. Sterz (2000). "Improved outcome prediction in unconscious cardiac arrest survivors with sensory evoked potentials compared with clinical assessment." Crit Care Med **28**(3): 721-726.
Malarkey, E. B. and V. Parpura (2008). "Mechanisms of glutamate release from astrocytes." Neurochemistry international **52**(1): 142-154.
Malayev, A., T. T. Gibbs and D. H. Farb (2002). "Inhibition of the NMDA response by pregnenolone sulphate reveals subtype selective modulation of NMDA receptors by sulphated steroids." British Journal of Pharmacology **135**(4): 901-909.
Malek, S. A., J. S. Adorante and P. K. Stys (2005). "Differential effects of Na-K-ATPase pump inhibition, chemical anoxia, and glycolytic blockade on membrane potential of rat optic nerve." Brain Res **10**: 1-2.
Mangus, D. B., L. Huang, P. M. Applegate, J. W. Gatling, J. Zhang and R. L. Applegate (2014). "A systematic review of neuroprotective strategies after cardiac arrest: from bench to bedside (Part I – Protection via specific pathways)." Medical Gas Research **4**: 9-9.
Manning, S. M., D. M. Talos, C. Zhou, D. B. Selip, H.-K. Park, C.-J. Park, J. J. Volpe and F. E. Jensen (2008). "NMDA Receptor Blockade with Memantine Attenuates White Matter Injury in a Rat Model of Periventricular Leukomalacia." The Journal of neuroscience : the official journal of the Society for Neuroscience **28**(26): 6670-6678.
Marcoli, M., A. Bonfanti, P. Roccatagliata, G. Chiaramonte, E. Ongini, M. Raiteri and G. Maura (2004). "Glutamate efflux from human cerebrocortical slices during ischemia: vesicular-like mode of glutamate release and sensitivity to A2A adenosine receptor blockade." Neuropharmacology **47**(6): 884-891.
Marcoli, M., A. Bonfanti, P. Roccatagliata, G. Chiaramonte, E. Ongini, M. Raiteri and G. Maura (2004). "Glutamate efflux from human cerebrocortical slices during ischemia: vesicular-like mode of glutamate release and sensitivity to A(2A) adenosine receptor blockade." Neuropharmacology **47**(6): 884-891.
Matute, C. (2011). "Glutamate and ATP signalling in white matter pathology." Journal of anatomy **219**(1): 53-64.
Matute, C. (2011). "Glutamate and ATP signalling in white matter pathology." J Anat **219**(1): 53-64.
Matute, C., M. Domercq, A. Pérez-Samartín and B. R. Ransom (2013). "Protecting White Matter From Stroke Injury." Stroke **44**(4): 1204-1211.
Matute, C. and B. R. Ransom (2012). "Roles of white matter in central nervous system pathophysiologies." ASN NEURO **4**(2): e00079.

Matute, C., M. V. Sanchez-Gomez, L. Martinez-Millan and R. Miledi (1997). "Glutamate receptor-mediated toxicity in optic nerve oligodendrocytes." Proc Natl Acad Sci U S A **94**(16): 8830-8835.
Mayer, M. L. and G. L. Westbrook (1987). "Permeation and block of N-methyl-D-aspartic acid receptor channels by divalent cations in mouse cultured central neurones." The Journal of Physiology **394**: 501-527.
McBean, G. J. (2002). "Cerebral cystine uptake: a tale of two transporters." Trends in Pharmacological Sciences **23**(7): 299-302.
McCarran, W. J. and M. P. Goldberg (2007). "White Matter Axon Vulnerability to AMPA/Kainate Receptor-Mediated Ischemic Injury Is Developmentally Regulated." The Journal of Neuroscience **27**(15): 4220-4229.
McCrimmon, R. J., C. M. Ryan and B. M. Frier (2012). "Diabetes and cognitive dysfunction." Lancet **379**(9833): 2291-2299.
Mcdonald, J. W., S. P. Althomsons, K. L. Hyrc, D. W. Choi and M. P. Goldberg (1998). "Oligodendrocytes from forebrain are highly vulnerable to AMPA/kainate receptor-mediated excitotoxicity." Nature medicine **4**(3): 291-297.
McKenzie, I. A., D. Ohayon, H. Li, J. Paes de Faria, B. Emery, K. Tohyama and W. D. Richardson (2014). "Motor skill learning requires active central myelination." Science **346**(6207): 318-322.
McKinnon, R. D., S. Waldron and M. E. Kiel (2005). "PDGF alpha-receptor signal strength controls an RTK rheostat that integrates phosphoinositol 3'-kinase and phospholipase Cgamma pathways during oligodendrocyte maturation." J Neurosci **25**(14): 3499-3508.
Meeks, J. P. and S. Mennerick (2007). "Astrocyte membrane responses and potassium accumulation during neuronal activity." Hippocampus **17**(11): 1100-1108.
Mensch, S., M. Baraban, R. Almeida, T. Czopka, J. Ausborn, A. El Manira and D. A. Lyons (2015). "Synaptic vesicle release regulates myelin sheath number of individual oligodendrocytes in vivo." Nat Neurosci **18**(5): 628-630.
Mi, H. and B. A. Barres (1999). "Purification and characterization of astrocyte precursor cells in the developing rat optic nerve." The Journal of Neuroscience **19**(3): 1049-1061.
Micu, I., Q. Jiang, E. Coderre, A. Ridsdale, L. Zhang, J. Woulfe, X. Yin, B. Trapp, J. McRory and R. Rehak (2006). "NMDA receptors mediate calcium accumulation in myelin during chemical ischaemia." Nature **439**(7079): 988-992.
Micu, I., Q. Jiang, E. Coderre, A. Ridsdale, L. Zhang, J. Woulfe, X. Yin, B. D. Trapp, J. E. McRory, R. Rehak, G. W. Zamponi, W. Wang and P. K. Stys (2006). "NMDA receptors mediate calcium accumulation in myelin during chemical ischaemia." Nature **439**(7079): 988-992.
Micu, I., J. R. Plemel, C. Lachance, J. Proft, A. J. Jansen, K. Cummins, J. van Minnen and P. K. Stys (2016). "The molecular physiology of the axo-myelinic synapse." Exp Neurol **276**: 41-50.
Micu, I., J. R. Plemel, C. Lachance, J. Proft, A. J. Jansen, K. Cummins, J. van Minnen and P. K. Stys (2016). "The molecular physiology of the axo-myelinic synapse." Experimental neurology **276**: 41-50.
Mierzwa, A., S. Shroff and J. Rosenbluth (2010). "Permeability of the Paranodal Junction of Myelinated Nerve Fibers." The Journal of neuroscience : the official journal of the Society for Neuroscience **30**(47): 15962-15968.
Mierzwa, A. J., C. M. Marion, G. M. Sullivan, D. P. McDaniel and R. C. Armstrong (2015). "Components of myelin damage and repair in the progression of white matter pathology after mild traumatic brain injury." J Neuropathol Exp Neurol **74**(3): 218-232.
Miller, R. H. (2002). "Regulation of oligodendrocyte development in the vertebrate CNS." Progress in Neurobiology **67**(6): 451-467.
Mohan, K. M., C. D. Wolfe, A. G. Rudd, P. U. Heuschmann, P. L. Kolominsky-Rabas and A. P. Grieve (2011). "Risk and cumulative risk of stroke recurrence: a systematic review and meta-analysis." Stroke **42**(5): 1489-1494.
Mohr, J., J. C. Grotta, P. A. Wolf, M. A. Moskowitz, M. R. Mayberg and R. Von Kummer (2011). Stroke: pathophysiology, diagnosis, and management, Elsevier Health Sciences.

Montana, V., E. B. Malarkey, C. Verderio, M. Matteoli and V. Parpura (2006). "Vesicular transmitter release from astrocytes." Glia **54**(7): 700-715.
Montana, V., Y. Ni, V. Sunjara, X. Hua and V. Parpura (2004). "Vesicular Glutamate Transporter-Dependent Glutamate Release from Astrocytes." The Journal of Neuroscience **24**(11): 2633-2642.
Moody, D. M., M. A. Bell and V. R. Challa (1988). "The corpus callosum, a unique white-matter tract: anatomic features that may explain sparing in Binswanger disease and resistance to flow of fluid masses." AJNR Am J Neuroradiol **9**(6): 1051-1059.
Morales, P., D. Bustamante, P. Espina-Marchant, T. Neira-Peña, M. A. Gutiérrez-Hernández, C. Allende-Castro and E. Rojas-Mancilla (2011). "Pathophysiology of perinatal asphyxia: can we predict and improve individual outcomes?" The EPMA Journal **2**(2): 211-230.
Mordasini, P., C. Zubler, G. Schroth and J. Gralla (2012). "Thrombectomy for acute ischemic stroke treatment: a review." EJMINT Invited Review **1238000077**: 21.
Moring, J., L. A. Niego, L. M. Ganley, M. W. Trumbore and L. G. Herbette (1994). "Interaction of the NMDA receptor noncompetitive antagonist MK-801 with model and native membranes." Biophys J **67**(6): 2376-2386.
Mosley, C. A., T. M. Acker, K. B. Hansen, P. Mullasseril, K. T. Andersen, P. Le, K. M. Vellano, H. Bräuner-Osborne, D. C. Liotta and S. F. Traynelis (2010). "Quinazolin-4-one derivatives: A novel class of noncompetitive NR2C/D subunit-selective N-methyl-D-aspartate receptor antagonists." Journal of medicinal chemistry **53**(15): 5476-5490.
Moussawi, K., A. Riegel, S. Nair and P. W. Kalivas (2011). "Extracellular Glutamate: Functional Compartments Operate in Different Concentration Ranges." Frontiers in Systems Neuroscience **5**: 94.
Mullasseril, P., K. B. Hansen, K. M. Vance, K. K. Ogden, H. Yuan, N. L. Kurtkaya, R. Santangelo, A. G. Orr, P. Le, K. M. Vellano, D. C. Liotta and S. F. Traynelis (2010). "A subunit-selective potentiator of NR2C- and NR2D-containing NMDA receptors." Nat Commun **1**: 90.
Nagai, T., K. Yamada, M. Yoshimura, K. Ishikawa, Y. Miyamoto, K. Hashimoto, Y. Noda, A. Nitta and T. Nabeshima (2004). "The tissue plasminogen activator-plasmin system participates in the rewarding effect of morphine by regulating dopamine release." Proceedings of the National Academy of Sciences of the United States of America **101**(10): 3650-3655.
Nahum-Levy, R., D. Lipinski, S. Shavit and M. Benveniste (2001). "Desensitization of NMDA receptor channels is modulated by glutamate agonists." Biophysical Journal **80**(5): 2152-2166.
Naleway, J. J., C. M. Fox, D. Robinhold, E. Terpetschnig, N. A. Olson and R. P. Haugland (1994). "Synthesis and use of new fluorogenic precipitating substrates." Tetrahedron letters **35**(46): 8569-8572.
Namura, S., H. Maeno, S. Takami, X. F. Jiang, S. Kamichi, K. Wada and I. Nagata (2002). "Inhibition of glial glutamate transporter GLT-1 augments brain edema after transient focal cerebral ischemia in mice." Neurosci Lett **324**(2): 117-120.
Nave, K.-A. (2010). "Myelination and support of axonal integrity by glia." Nature **468**(7321): 244-252.
Nedergaard, M., T. Takano and A. J. Hansen (2002). "Beyond the role of glutamate as a neurotransmitter." Nat Rev Neurosci **3**(9): 748-755.
Newton, J. and V. Murthy (2006). "Measuring exocytosis in neurons using FM labeling." J Vis Exp(1): 117.
Nicholls, D. G. and S. L. Budd (1998). "Mitochondria and neuronal glutamate excitotoxicity." Biochimica et Biophysica Acta (BBA) - Bioenergetics **1366**(1–2): 97-112.
Nicholls, D. G. and M. W. Ward (2000). "Mitochondrial membrane potential and neuronal glutamate excitotoxicity: mortality and millivolts." Trends in Neurosciences **23**(4): 166-174.
Nielsen, N., K. Sunde, J. Hovdenes, R. R. Riker, S. Rubertsson, P. Stammet, F. Nilsson and H. Friberg (2011). "Adverse events and their relation to mortality in out-of-hospital cardiac arrest patients treated with therapeutic hypothermia." Crit Care Med **39**(1): 57-64.

Nikolaeva, M. A., B. Mukherjee and P. K. Stys (2005). "Na⁺-Dependent Sources of Intra-Axonal Ca²⁺ Release in Rat Optic Nerve during In Vitro Chemical Ischemia." The Journal of Neuroscience **25**(43): 9960-9967.
Nishiyama, A., A. Chang and B. D. Trapp (1999). "NG2+ glial cells: a novel glial cell population in the adult brain." J Neuropathol Exp Neurol **58**(11): 1113-1124.
Nishizaki, T., R. Yamauchi, M. Tanimoto and Y. Okada (1988). "Effects of temperature on the oxygen consumption in thin slices from different brain regions." Neurosci Lett **86**(3): 301-305.
Nishizawa, Y. (2001). "Glutamate release and neuronal damage in ischemia." Life Sciences **69**(4): 369-381.
Niswender, C. M. and P. J. Conn (2010). "Metabotropic Glutamate Receptors: Physiology, Pharmacology, and Disease." Annual review of pharmacology and toxicology **50**: 295-322.
Niswender, C. M. and P. J. Conn (2010). "Metabotropic glutamate receptors: physiology, pharmacology, and disease." Annu Rev Pharmacol Toxicol **50**: 295-322.
Nualart-Marti, A., C. Solsona and R. D. Fields (2013). "Gap Junction Communication in Myelinating Glia." Biochimica et biophysica acta **1828**(1): 69-78.
Ogden, K. K. and S. F. Traynelis (2011). "New advances in NMDA receptor pharmacology." Trends Pharmacol Sci **32**(12): 726-733.
Oka, A., M. J. Belliveau, P. A. Rosenberg and J. J. Volpe (1993). "Vulnerability of oligodendroglia to glutamate: pharmacology, mechanisms, and prevention." J Neurosci **13**(4): 1441-1453.
Oldendorf, W. H. (1974). "Lipid solubility and drug penetration of the blood brain barrier." Proc Soc Exp Biol Med **147**(3): 813-815.
Olney, J. W. (1969). "Brain lesions, obesity, and other disturbances in mice treated with monosodium glutamate." Science **164**(3880): 719-721.
Olney, J. W., M. T. Price, L. Samson and J. Labruyere (1986). "The role of specific ions in glutamate neurotoxicity." Neuroscience Letters **65**(1): 65-71.
Olney, J. W., V. Rhee and O. L. Ho (1974). "Kainic acid: a powerful neurotoxic analogue of glutamate." Brain Res **77**(3): 507-512.
Orthmann-Murphy, J. L., C. K. Abrams and S. S. Scherer (2008). "Gap Junctions Couple Astrocytes and Oligodendrocytes." Journal of molecular neuroscience : MN **35**(1): 101-116.
Ouardouz, M., E. Coderre, A. Basak, A. Chen, G. W. Zamponi, S. Hameed, R. Rehak, X. Yin, B. D. Trapp and P. K. Stys (2009). "Glutamate receptors on myelinated spinal cord axons: I. GluR6 kainate receptors." Ann Neurol **65**(2): 151-159.
Ouardouz, M., E. Coderre, G. W. Zamponi, S. Hameed, X. Yin, B. D. Trapp and P. K. Stys (2009). "Glutamate receptors on myelinated spinal cord axons: II. AMPA and GluR5 receptors." Annals of neurology **65**(2): 160-166.
Ouardouz, M., S. Malek, E. Coderre and P. K. Stys (2006). "Complex interplay between glutamate receptors and intracellular Ca2+ stores during ischaemia in rat spinal cord white matter." J Physiol **577**(Pt 1): 191-204.
Ouardouz, M., S. Malek, E. Coderre and P. K. Stys (2006). "Complex interplay between glutamate receptors and intracellular Ca2+ stores during ischaemia in rat spinal cord white matter." The Journal of physiology **577**(1): 191-204.
Ouardouz, M., S. Malek, E. Coderre and P. K. Stys (2006). "Complex interplay between glutamate receptors and intracellular Ca(2+) stores during ischaemia in rat spinal cord white matter." The Journal of Physiology **577**(Pt 1): 191-204.
Ouardouz, M., M. A. Nikolaeva, E. Coderre, G. W. Zamponi, J. E. McRory, B. D. Trapp, X. Yin, W. Wang, J. Woulfe and P. K. Stys (2003). "Depolarization-induced Ca2+ release in ischemic spinal cord white matter involves L-type Ca2+ channel activation of ryanodine receptors." Neuron **40**(1): 53-63.
Ovbiagele, B. and M. N. Nguyen-Huynh (2011). "Stroke Epidemiology: Advancing Our Understanding of Disease Mechanism and Therapy." Neurotherapeutics **8**(3): 319-329.
Oyinbo, C. A. (2011). "Secondary injury mechanisms in traumatic spinal cord injury: a nugget of this multiply cascade." Acta Neurobiol Exp (Wars) **71**(2): 281-299.

Ozawa, S., H. Kamiya and K. Tsuzuki (1998). "Glutamate receptors in the mammalian central nervous system." Progress in Neurobiology **54**(5): 581-618.
Pan, W. and A. J. Kastin (2001). "Changing the chemokine gradient: CINC1 crosses the blood-brain barrier." J Neuroimmunol **115**(1-2): 64-70.
Pantoni, L., J. H. Garcia and J. A. Gutierrez (1996). "Cerebral white matter is highly vulnerable to ischemia." Stroke **27**(9): 1641-1647.
Paoletti, P. and J. Neyton (2007). "NMDA receptor subunits: function and pharmacology." Current Opinion in Pharmacology **7**(1): 39-47.
Papouin, T., L. Ladepeche, J. Ruel, S. Sacchi, M. Labasque, M. Hanini, L. Groc, L. Pollegioni, J. P. Mothet and S. H. Oliet (2012). "Synaptic and extrasynaptic NMDA receptors are gated by different endogenous coagonists." Cell **150**(3): 633-646.
Pardo, B., L. Contreras and J. Satrustegui (2013). "De novo Synthesis of Glial Glutamate and Glutamine in Young Mice Requires Aspartate Provided by the Neuronal Mitochondrial Aspartate-Glutamate Carrier Aralar/AGC1." Front Endocrinol **4**(149): 00149.
Pardridge, W. M. (2001). Brain drug targeting: the future of brain drug development, Cambridge University Press.
Pardridge, W. M. (2005). "The Blood-Brain Barrier: Bottleneck in Brain Drug Development." NeuroRx **2**(1): 3-14.
Parpura, V., T. A. Basarsky, F. Liu, K. Jeftinija, S. Jeftinija and P. G. Haydon (1994). "Glutamate-mediated astrocyte-neuron signalling." Nature **369**(6483): 744-747.
Parsons, C. G., W. Danysz and G. Quack (1998). "Glutamate in CNS disorders as a target for drug development: an update." Drug News Perspect **11**(9): 523-569.
Patneau, D. K., P. W. Wright, C. Winters, M. L. Mayer and V. Gallo (1994). "Glial cells of the oligodendrocyte lineage express both kainate-and AMPA-preferring subtypes of glutamate receptor." Neuron **12**(2): 357-371.
Patton, A. J., P. G. Genever, M. A. Birch, L. J. Suva and T. M. Skerry (1998). "Expression of an N-Methyl-D-Aspartate-Type Receptor by Human and Rat Osteoblasts and Osteoclasts Suggests a Novel Glutamate Signaling Pathway in Bone." Bone **22**(6): 645-649.
Perry, V. H. and J. Teeling (2013). "Microglia and macrophages of the central nervous system: the contribution of microglia priming and systemic inflammation to chronic neurodegeneration." Seminars in Immunopathology **35**(5): 601-612.
Pina-Crespo, J. C., M. Talantova, I. Micu, B. States, H. S. Chen, S. Tu, N. Nakanishi, G. Tong, D. Zhang, S. F. Heinemann, G. W. Zamponi, P. K. Stys and S. A. Lipton (2010). "Excitatory glycine responses of CNS myelin mediated by NR1/NR3 "NMDA" receptor subunits." J Neurosci **30**(34): 11501-11505.
Piña-Crespo, J. C., M. Talantova, I. Micu, B. States, H. S. V. Chen, S. Tu, N. Nakanishi, G. Tong, D. Zhang, S. F. Heinemann, G. W. Zamponi, P. K. Stys and S. A. Lipton (2010). "Excitatory glycine responses of CNS myelin mediated by NR1/NR3 'NMDA' receptor subunits." The Journal of neuroscience : the official journal of the Society for Neuroscience **30**(34): 11501-11505.
Platt, S. R. (2007). "The role of glutamate in central nervous system health and disease--a review." Vet J **173**(2): 278-286.
Polito, A. and R. Reynolds (2005). "NG2-expressing cells as oligodendrocyte progenitors in the normal and demyelinated adult central nervous system." J Anat **207**(6): 707-716.
Prada, I., J. Marchaland, P. Podini, L. Magrassi, R. D'Alessandro, P. Bezzi and J. Meldolesi (2011). "REST/NRSF governs the expression of dense-core vesicle gliosecretion in astrocytes." The Journal of Cell Biology **193**(3): 537-549.
Pu, Y., Q.-F. Li, C.-M. Zeng, J. Gao, J. Qi, D.-X. Luo, S. Mahankali, P. T. Fox and J.-H. Gao (2000). "Increased Detectability of Alpha Brain Glutamate/Glutamine in Neonatal Hypoxic-Ischemic Encephalopathy." American Journal of Neuroradiology **21**(1): 203-212.
Pyle, J. L., E. T. Kavalali, S. Choi and R. W. Tsien (1999). "Visualization of Synaptic Activity in Hippocampal Slices with FM1-43 Enabled by Fluorescence Quenching." Neuron **24**(4): 803-808.
Qian, A. and J. W. Johnson (2002). "Channel gating of NMDA receptors." Physiology & Behavior **77**(4–5): 577-582.

Quarles, R. H., W. B. Macklin and P. Morell (2006). Myelin formation, structure and biochemistry, Elsevier London.
Raff, M. C. (1989). "Glial cell diversification in the rat optic nerve." Science **243**(4897): 1450-1455.
Raley-Susman, K., I. Kass, J. Cottrell, R. Newman, G. Chambers and J. Wang (2001). "Sodium influx blockade and hypoxic damage to CA1 pyramidal neurons in rat hippocampal slices." Journal of Neurophysiology **86**(6): 2715-2726.
Ransom, B. R. and A. M. Brown (2003). "Intracellular Ca2+ Release and Ischemic Axon Injury: The Trojan Horse Is Back." Neuron **40**(1): 2-4.
Ransom, B. R. and R. Fern (1997). "Does astrocytic glycogen benefit axon function and survival in CNS white matter during glucose deprivation?" Glia **21**(1): 134-141.
Ransom, B. R. and S. Goldring (1973). "Ionic determinants of membrane potential of cells presumed to be glia in cerebral cortex of cat." J Neurophysiol **36**(5): 855-868.
Ransom, B. R., W. Walz, P. K. Davis and W. G. Carlini (1992). "Anoxia-induced changes in extracellular K+ and pH in mammalian central white matter." J Cereb Blood Flow Metab **12**(4): 593-602.
Ransom, C. B., B. R. Ransom and H. Sontheimer (2000). "Activity-dependent extracellular K+ accumulation in rat optic nerve: the role of glial and axonal Na+ pumps." J Physiol **522 Pt 3**: 427-442.
Rasband, M. N. and P. Shrager (2000). "Ion channel sequestration in central nervous system axons." The Journal of Physiology **525**(Pt 1): 63-73.
Rawanduzy, A., A. Hansen, T. W. Hansen and M. Nedergaard (1997). "Effective reduction of infarct volume by gap junction blockade in a rodent model of stroke." J Neurosurg **87**(6): 916-920.
Reeves, T. M., A. E. Doperalski and L. L. Phillips (2014). Unmyelinated and Myelinated Axons Exhibit Differential Injury and Treatment Responses Following Traumatic Injury. White Matter Injury in Stroke and CNS Disease. S. Baltan, S. T. Carmichael, C. Matute, G. Xi and J. H. Zhang. New York, NY, Springer New York**:** 321-372.
Rehncrona, S., I. Rosén and B. K. Siesjö (1981). "Brain lactic acidosis and ischemic cell damage: 1. Biochemistry and neurophysiology." Journal of Cerebral Blood Flow & Metabolism **1**(3): 297-311.
Reisberg , B., R. Doody , A. Stöffler , F. Schmitt , S. Ferris and H. J. Möbius (2003). "Memantine in Moderate-to-Severe Alzheimer's Disease." New England Journal of Medicine **348**(14): 1333-1341.
Reissner, K. J. (2014). "The cystine/glutamate antiporter: when too much of a good thing goes bad." The Journal of Clinical Investigation **124**(8): 3279-3281.
Ren, Y., A. Ridsdale, E. Coderre and P. K. Stys (2000). "Calcium imaging in live rat optic nerve myelinated axons in vitro using confocal laser microscopy." Journal of Neuroscience Methods **102**(2): 165-176.
Ren, Y., A. Ridsdale, E. Coderre and P. K. Stys (2000). "Calcium imaging in live rat optic nerve myelinated axons in vitro using confocal laser microscopy." J Neurosci Methods **102**(2): 165-176.
Renigunta, V., G. Schlichthorl and J. Daut (2015). "Much more than a leak: structure and function of K(2)p-channels." Pflugers Arch **467**(5): 867-894.
Reynolds, R., M. Dawson, D. Papadopoulos, A. Polito, I. C. Di Bello, D. Pham-Dinh and J. Levine (2002). "The response of NG2-expressing oligodendrocyte progenitors to demyelination in MOG-EAE and MS." J Neurocytol **31**(6-7): 523-536.
Rha, J. H. and J. L. Saver (2007). "The impact of recanalization on ischemic stroke outcome: a meta-analysis." Stroke **38**(3): 967-973.
Rios, J. C., C. V. Melendez-Vasquez, S. Einheber, M. Lustig, M. Grumet, J. Hemperly, E. Peles and J. L. Salzer (2000). "Contactin-Associated Protein (Caspr) and Contactin Form a Complex That Is Targeted to the Paranodal Junctions during Myelination." The Journal of Neuroscience **20**(22): 8354-8364.
Roettger, V. and P. Lipton (1996). "Mechanism of glutamate release from rat hippocampal slices during in vitro ischemia." Neuroscience **75**(3): 677-685.

Rosenberg, P. (2014). Mechanisms Underlying the Selective Vulnerability of Developing Human White Matter. White Matter Injury in Stroke and CNS Disease. S. Baltan, S. T. Carmichael, C. Matute, G. Xi and J. H. Zhang, Springer New York. **4:** 109-141.
Rosenberg, S. S., E. E. Kelland, E. Tokar, A. R. De La Torre and J. R. Chan (2008). "The geometric and spatial constraints of the microenvironment induce oligodendrocyte differentiation." Proceedings of the National Academy of Sciences of the United States of America **105**(38): 14662-14667.
Rosenbluth, J. (2009). "Multiple functions of the paranodal junction of myelinated nerve fibers." J Neurosci Res **87**(15): 3250-3258.
Rosenmund, C., A. Feltz and G. L. Westbrook (1995). "Calcium-dependent inactivation of synaptic NMDA receptors in hippocampal neurons." J Neurophysiol **73**(1): 427-430.
Rosenzweig, S. and S. T. Carmichael (2013). "Age-dependent exacerbation of white matter stroke outcomes: a role for oxidative damageand inflammatory mediators." Stroke; a journal of cerebral circulation **44**(9): 2579-2586.
Rossi, D. J., J. D. Brady and C. Mohr (2007). "Astrocyte metabolism and signaling during brain ischemia." Nat Neurosci **10**(11): 1377-1386.
Rossi, D. J., T. Oshima and D. Attwell (2000). "Glutamate release in severe brain ischaemia is mainly by reversed uptake." Nature **403**(6767): 316-321.
Roth, L. J. and C. F. Barlow (1961). "Drugs in the Brain." Autoradiography and radioassay techniques permit analysis of penetration by labeled drugs **134**(3471): 22-31.
Rothstein, J. D., M. Dykes-Hoberg, C. A. Pardo, L. A. Bristol, L. Jin, R. W. Kuncl, Y. Kanai, M. A. Hediger, Y. Wang and J. P. Schielke (1996). "Knockout of glutamate transporters reveals a major role for astroglial transport in excitotoxicity and clearance of glutamate." Neuron **16**(3): 675-686.
Rutledge, E. M. and H. K. Kimelberg (1996). "Release of [3H]-D-aspartate from primary astrocyte cultures in response to raised external potassium." J Neurosci **16**(24): 7803-7811.
Saab, A. S., I. D. Tzvetavona, A. Trevisiol, S. Baltan, P. Dibaj, K. Kusch, W. Mobius, B. Goetze, H. M. Jahn, W. Huang, H. Steffens, E. D. Schomburg, A. Perez-Samartin, F. Perez-Cerda, D. Bakhtiari, C. Matute, S. Lowel, C. Griesinger, J. Hirrlinger, F. Kirchhoff and K. A. Nave (2016). "Oligodendroglial NMDA Receptors Regulate Glucose Import and Axonal Energy Metabolism." Neuron **91**(1): 119-132.
Salter, M. G. and R. Fern (2005). "NMDA receptors are expressed in developing oligodendrocyte processes and mediate injury." Nature **438**(7071): 1167-1171.
Salter, M. G. and R. Fern (2005). "NMDA receptors are expressed in developing oligodendrocyte processes and mediate injury." Nature **438**(7071): 1167-1171.
Salter, M. G. and R. Fern (2008). "The mechanisms of acute ischemic injury in the cell processes of developing white matter astrocytes." Journal of Cerebral Blood Flow & Metabolism **28**(3): 588-601.
Salter, M. G. and R. Fern (2008). "The mechanisms of acute ischemic injury in the cell processes of developing white matter astrocytes." J Cereb Blood Flow Metab **28**(3): 588-601.
Sasaki, T., N. Matsuki and Y. Ikegaya (2011). "Action-potential modulation during axonal conduction." Science **331**(6017): 599-601.
Sasaki, Y. F., T. Rothe, L. S. Premkumar, S. Das, J. Cui, M. V. Talantova, H.-K. Wong, X. Gong, S. F. Chan and D. Zhang (2002). "Characterization and comparison of the NR3A subunit of the NMDA receptor in recombinant systems and primary cortical neurons." Journal of neurophysiology **87**(4): 2052-2063.
Scarborough, P., P. Bhatnagar, K. K. Wickramasinghe, S. Allender, C. Foster and M. Rayner (2011). "The economic burden of ill health due to diet, physical inactivity, smoking, alcohol and obesity in the UK: an update to 2006–07 NHS costs." Journal of Public Health **33**(4): 527-535.
Schäbitz, W.-R., F. Li and M. Fisher (2000). "The N-Methyl-d-Aspartate Antagonist CNS 1102 Protects Cerebral Gray and White Matter From Ischemic Injury Following Temporary Focal Ischemia in Rats." Stroke **31**(7): 1709-1714.

Schermelleh, L., R. Heintzmann and H. Leonhardt (2010). "A guide to super-resolution fluorescence microscopy." J Cell Biol **190**(2): 165-175.
Scholz, J., M. C. Klein, T. E. J. Behrens and H. Johansen-Berg (2009). "Training induces changes in white-matter architecture." Nat Neurosci **12**(11): 1370-1371.
Schousboe, A., L. K. Bak and H. S. Waagepetersen (2013). "Astrocytic Control of Biosynthesis and Turnover of the Neurotransmitters Glutamate and GABA." Frontiers in Endocrinology **4**: 102.
Schousboe, A., S. Scafidi, L. K. Bak, H. S. Waagepetersen and M. C. McKenna (2014). "Glutamate Metabolism in the Brain Focusing on Astrocytes." Advances in neurobiology **11**: 13-30.
Schwaller, B. (2010). "Cytosolic Ca(2+) Buffers." Cold Spring Harbor Perspectives in Biology **2**(11): a004051.
Sefton, A. J., G. M. Horsburgh and K. Lam (1985). "The development of the optic nerve in rodents." Aust N Z J Ophthalmol **13**(2): 135-145.
Seki, Y., P. J. Feustel, R. W. Keller, Jr., B. I. Tranmer and H. K. Kimelberg (1999). "Inhibition of ischemia-induced glutamate release in rat striatum by dihydrokinate and an anion channel blocker." Stroke **30**(2): 433-440.
Shank, R. P., G. S. Bennett, S. O. Freytag and G. L. Campbell (1985). "Pyruvate carboxylase: an astrocyte-specific enzyme implicated in the replenishment of amino acid neurotransmitter pools." Brain Res **329**(1-2): 364-367.
Shankaran , S., A. Pappas , S. A. McDonald , B. R. Vohr , S. R. Hintz , K. Yolton , K. E. Gustafson , T. M. Leach , C. Green , R. Bara , C. M. P. Huitema , R. A. Ehrenkranz , J. E. Tyson , A. Das , J. Hammond , M. Peralta-Carcelen , P. W. Evans , R. J. Heyne , D. E. Wilson-Costello , Y. E. Vaucher , C. R. Bauer , A. M. Dusick , I. Adams-Chapman , R. F. Goldstein , R. Guillet , L.-A. Papile and R. D. Higgins (2012). "Childhood Outcomes after Hypothermia for Neonatal Encephalopathy." New England Journal of Medicine **366**(22): 2085-2092.
Shannon, C., M. Salter and R. Fern (2007). "GFP imaging of live astrocytes: regional differences in the effects of ischaemia upon astrocytes." Journal of anatomy **210**(6): 684-692.
Shen, Y., X. B. Liu, D. E. Pleasure and W. Deng (2012). "Axon-glia synapses are highly vulnerable to white matter injury in the developing brain." J Neurosci Res **90**(1): 105-121.
Shepherd, G. M. G. and M. Raastad (2003). "Axonal varicosity distributions along parallel fibers: a new angle on a cerebellar circuit." The Cerebellum **2**(2): 110-113.
Sherwin, C. and R. Fern (2005). "Acute lipopolysaccharide-mediated injury in neonatal white matter glia: role of TNF-alpha, IL-1beta, and calcium." J Immunol **175**(1): 155-161.
Shigeri, Y., R. P. Seal and K. Shimamoto (2004). "Molecular pharmacology of glutamate transporters, EAATs and VGLUTs." Brain Research Reviews **45**(3): 250-265.
Shrager, P. and S. D. Novakovic (1995). "Control of myelination, axonal growth, and synapse formation in spinal cord explants by ion channels and electrical activity." Brain Res Dev Brain Res **88**(1): 68-78.
Small, R. K., P. Riddle and M. Noble (1987). "Evidence for migration of oligodendrocyte-type-2 astrocyte progenitor cells into the developing rat optic nerve." Nature **328**(6126): 155-157.
Smith, K. J. (1994). "Conduction properties of central demyelinated and remyelinated axons, and their relation to symptom production in demyelinating disorders." Eye (Lond) **8 (Pt 2)**: 224-237.
Somjen, G. G. (1979). "Extracellular potassium in the mammalian central nervous system." Annu Rev Physiol **41**: 159-177.
Somjen, G. G. (2002). "Ion regulation in the brain: implications for pathophysiology." Neuroscientist **8**(3): 254-267.
Song, M., A. Woodbury and S. P. Yu (2014). White Matter Injury and Potential Treatment in Ischemic Stroke. White Matter Injury in Stroke and CNS Disease. S. Baltan, S. T. Carmichael, C. Matute, G. Xi and J. H. Zhang. New York, NY, Springer New York**:** 39-52.

Soria, F. N., A. Pérez-Samartín, A. Martin, K. B. Gona, J. Llop, B. Szczupak, J. C. Chara, C. Matute and M. Domercq (2014). "Extrasynaptic glutamate release through cystine/glutamate antiporter contributes to ischemic damage." The Journal of Clinical Investigation **124**(8): 3645-3655.
Sozmen, E. G., J. D. Hinman and S. T. Carmichael (2012). "Models That Matter: White Matter Stroke Models." Neurotherapeutics **9**(2): 349-358.
Spitzer, S., K. Volbracht, I. Lundgaard and R. T. Karadottir (2016). "Glutamate signalling: A multifaceted modulator of oligodendrocyte lineage cells in health and disease." Neuropharmacology **110**(Pt B): 574-585.
Stallcup, W. B. (2002). "The NG2 proteoglycan: past insights and future prospects." Journal of neurocytology **31**(6-7): 423 ppl=-435.
Stankowski, J. N. and R. Gupta (2011). "Therapeutic Targets for Neuroprotection in Acute Ischemic Stroke: Lost in Translation?" Antioxidants & Redox Signaling **14**(10): 1841-1851.
Stegmüller, J., H. Werner, K.-A. Nave and J. Trotter (2003). "The Proteoglycan NG2 Is Complexed with α-Amino-3-hydroxy-5-methyl-4-isoxazolepropionic Acid (AMPA) Receptors by the PDZ Glutamate Receptor Interaction Protein (GRIP) in Glial Progenitor Cells IMPLICATIONS FOR GLIAL-NEURONAL SIGNALING." Journal of Biological Chemistry **278**(6): 3590-3598.
Streit, W. J. (2000). "Microglial response to brain injury: a brief synopsis." Toxicol Pathol **28**(1): 28-30.
Strub, R. L. (2003). "Vascular Dementia." The Ochsner Journal **5**(1): 40-43.
Stuart, G., N. Spruston, B. Sakmann and M. Häusser (1997). "Action potential initiation and backpropagation in neurons of the mammalian CNS." Trends in Neurosciences **20**(3): 125-131.
Sturrock, R. R. (1980). "Myelination of the mouse corpus callosum." Neuropathol Appl Neurobiol **6**(6): 415-420.
Stys, P. K. (1998). "Anoxic and ischemic injury of myelinated axons in CNS white matter: from mechanistic concepts to therapeutics." Journal of Cerebral Blood Flow & Metabolism **18**(1): 2-25.
Stys, P. K. (1998). "Anoxic and ischemic injury of myelinated axons in CNS white matter: from mechanistic concepts to therapeutics." J Cereb Blood Flow Metab **18**(1): 2-25.
Stys, P. K. (2005). "General mechanisms of axonal damage and its prevention." Journal of the Neurological Sciences **233**(1–2): 3-13.
Stys, P. K. (2005). "General mechanisms of axonal damage and its prevention." J Neurol Sci **233**(1-2): 3-13.
Stys, P. K. (2011). "The axo-myelinic synapse." Trends Neurosci **34**(8): 393-400.
Stys, P. K., E. Lehning, A. J. Saubermann and R. M. LoPachin, Jr. (1997). "Intracellular concentrations of major ions in rat myelinated axons and glia: calculations based on electron probe X-ray microanalyses." J Neurochem **68**(5): 1920-1928.
Stys, P. K. and S. A. Lipton (2007). "White matter NMDA receptors: an unexpected new therapeutic target?" Trends in Pharmacological Sciences **28**(11): 561-566.
Stys, P. K. and S. A. Lipton (2007). "White matter NMDA receptors: an unexpected new therapeutic target?" Trends Pharmacol Sci **28**(11): 561-566.
Stys, P. K., B. R. Ransom and S. G. Waxman (1990). "Effects of polyvalent cations and dihydropyridine calcium channel blockers on recovery of CNS white matter from anoxia." Neurosci Lett **115**(2-3): 293-299.
Stys, P. K., B. R. Ransom and S. G. Waxman (1991). "Compound action potential of nerve recorded by suction electrode: a theoretical and experimental analysis." Brain Res **546**(1): 18-32.
Stys, P. K., B. R. Ransom, S. G. Waxman and P. K. Davis (1990). "Role of extracellular calcium in anoxic injury of mammalian central white matter." Proc Natl Acad Sci U S A **87**(11): 4212-4216.
Stys, P. K., S. G. Waxman and B. R. Ransom (1992). "Effects of Temperature on Evoked Electrical Activity and Anoxic Injury in CNS White Matter." Journal of Cerebral Blood Flow & Metabolism **12**(6): 977-986.

Stys, P. K., S. G. Waxman and B. R. Ransom (1992). "Ionic mechanisms of anoxic injury in mammalian CNS white matter: role of Na+ channels and Na(+)-Ca2+ exchanger." J Neurosci **12**(2): 430-439.
Su, G., D. B. Kintner, M. Flagella, G. E. Shull and D. Sun (2002). "Astrocytes from Na+-K+-Cl− cotransporter-null mice exhibit absence of swelling and decrease in EAA release." American Journal of Physiology-Cell Physiology **282**(5): C1147-C1160.
Su, G., D. B. Kintner and D. Sun (2002). "Contribution of Na(+)-K(+)-Cl(-) cotransporter to high-[K(+)](o)- induced swelling and EAA release in astrocytes." Am J Physiol Cell Physiol **282**(5): C1136-1146.
Sugimoto, Y., M. Taniguchi, T. Yagi, Y. Akagi, Y. Nojyo and N. Tamamaki (2001). "Guidance of glial precursor cell migration by secreted cues in the developing optic nerve." Development **128**(17): 3321-3330.
Sun, H.-s. and Z.-p. Feng (2013). "Neuroprotective role of ATP-sensitive potassium channels in cerebral ischemia." Acta Pharmacologica Sinica **34**(1): 24-32.
Sydenham, E., I. Roberts and P. Alderson (2009). "Hypothermia for traumatic head injury." Cochrane Database Syst Rev(1): Cd001048.
Szatkowski, M. and D. Attwell (1994). "Triggering and execution of neuronal death in brain ischaemia: two phases of glutamate release by different mechanisms." Trends in Neurosciences **17**(9): 359-365.
Szatkowski, M., B. Barbour and D. Attwell (1990). "Non-vesicular release of glutamate from glial cells by reversed electrogenic glutamate uptake." Nature **348**(6300): 443-446.
Szydlowska, K. and M. Tymianski (2010). "Calcium, ischemia and excitotoxicity." Cell Calcium **47**(2): 122-129.
Takahashi, S., M. Shibata and Y. Fukuuchi (1997). "Effects of increased extracellular potassium on influx of sodium ions in cultured rat astroglia and neurons." Brain Res Dev Brain Res **104**(1-2): 111-117.
Takizawa, S., K. Matsushima, H. Fujita, K. Nanri, S. Ogawa and Y. Shinohara (1995). "A selective N-type calcium channel antagonist reduces extracellular glutamate release and infarct volume in focal cerebral ischemia." J Cereb Blood Flow Metab **15**(4): 611-618.
Tekkok, S. B. and M. P. Goldberg (2001). "Ampa/kainate receptor activation mediates hypoxic oligodendrocyte death and axonal injury in cerebral white matter." J Neurosci **21**(12): 4237-4248.
Tekkök, S. B. and M. P. Goldberg (2001). "AMPA/Kainate Receptor Activation Mediates Hypoxic Oligodendrocyte Death and Axonal Injury in Cerebral White Matter." The Journal of Neuroscience **21**(12): 4237-4248.
Tekkok, S. B. and B. R. Ransom (2004). "Anoxia effects on CNS function and survival: regional differences." Neurochem Res **29**(11): 2163-2169.
Tekkok, S. B., Z. Ye and B. R. Ransom (2007). "Excitotoxic mechanisms of ischemic injury in myelinated white matter." J Cereb Blood Flow Metab **27**(9): 1540-1552.
Tekkök, S. B., Z. Ye and B. R. Ransom (2007). "Excitotoxic Mechanisms of Ischemic Injury in Myelinated White Matter." Journal of Cerebral Blood Flow & Metabolism **27**(9): 1540-1552.
Temple, S. and M. C. Raff (1986). "Clonal analysis of oligodendrocyte development in culture: evidence for a developmental clock that counts cell divisions." Cell **44**(5): 773-779.
Thomas, R., M. G. Salter, S. Wilke, A. Husen, N. Allcock, M. Nivison, A. N. Nnoli and R. Fern (2004). "Acute ischemic injury of astrocytes is mediated by Na-K-Cl cotransport and not Ca2+ influx at a key point in white matter development." J Neuropathol Exp Neurol **63**(8): 856-871.
Thuret, S., L. D. F. Moon and F. H. Gage (2006). "Therapeutic interventions after spinal cord injury." Nat Rev Neurosci **7**(8): 628-643.
Tian, F., A. V. Gourine, R. T. R. Huckstepp and N. Dale (2009). "A microelectrode biosensor for real time monitoring of l-glutamate release." Analytica Chimica Acta **645**(1–2): 86-91.
Tong, G., D. Shepherd and C. E. Jahr (1995). "Synaptic desensitization of NMDA receptors by calcineurin." Science **267**(5203): 1510.

Traynelis, S. F. and S. G. Cull-Candy (1990). "Proton inhibition of N-methyl-D-aspartate receptors in cerebellar neurons." Nature **345**(6273): 347-350.
Traynelis, S. F., L. P. Wollmuth, C. J. McBain, F. S. Menniti, K. M. Vance, K. K. Ogden, K. B. Hansen, H. Yuan, S. J. Myers and R. Dingledine (2010). "Glutamate receptor ion channels: structure, regulation, and function." Pharmacol Rev **62**(3): 405-496.
Trexler, E. B., M. V. Bennett, T. A. Bargiello and V. K. Verselis (1996). "Voltage gating and permeation in a gap junction hemichannel." Proceedings of the National Academy of Sciences of the United States of America **93**(12): 5836-5841.
Tripathi, R. B., L. E. Rivers, K. M. Young, F. Jamen and W. D. Richardson (2010). "NG2 Glia Generate New Oligodendrocytes But Few Astrocytes in a Murine Experimental Autoimmune Encephalomyelitis Model of Demyelinating Disease." The Journal of Neuroscience **30**(48): 16383-16390.
Trotman, M., P. Vermehren, C. L. Gibson and R. Fern (2015). "The dichotomy of memantine treatment for ischemic stroke: dose-dependent protective and detrimental effects." J Cereb Blood Flow Metab **35**(2): 230-239.
Valentino, M., C. Zammit, G. Di Giovanni, M. Pierucci and R. Muscat (2011). "Two-photon microscopy-sequential imaging studies in vivo." Malta Medical Journal **23**(03).
van der Worp, H. B., E. S. Sena, G. A. Donnan, D. W. Howells and M. R. Macleod (2007). "Hypothermia in animal models of acute ischaemic stroke: a systematic review and meta-analysis." Brain **130**(Pt 12): 3063-3074.
van Velthoven, C. T., A. Kavelaars, F. van Bel and C. J. Heijnen (2010). "Nasal administration of stem cells: a promising novel route to treat neonatal ischemic brain damage." Pediatr Res **68**(5): 419-422.
Vaughn, J. E. (1969). "An electron microscopic analysis of gliogenesis in rat optic nerves." Z Zellforsch Mikrosk Anat **94**(3): 293-324.
Velumian, A. and M. Samoilova (2014). White Matter: Basic Principles of Axonal Organization and Function. White Matter Injury in Stroke and CNS Disease. S. Baltan, S. T. Carmichael, C. Matute, G. Xi and J. H. Zhang. New York, NY, Springer New York**:** 3-38.
Velumian, A. and M. Samoilova (2014). White Matter: Basic Principles of Axonal Organization and Function. White Matter Injury in Stroke and CNS Disease. S. Baltan, S. T. Carmichael, C. Matute, G. Xi and J. H. Zhang, Springer New York. **4:** 3-38.
Verbny, Y., C. L. Zhang and S. Y. Chiu (2002). "Coupling of calcium homeostasis to axonal sodium in axons of mouse optic nerve." J Neurophysiol **88**(2): 802-816.
Verkhratsky, A. and A. Butt (2007). Introduction to Glia. Glial Neurobiology, John Wiley & Sons, Ltd**:** 1-12.
Verkhratsky, A. and C. Steinhauser (2000). "Ion channels in glial cells." Brain Res Brain Res Rev **32**(2-3): 380-412.
Verstreken, P., T. Ohyama and H. J. Bellen (2008). "FM 1-43 labeling of synaptic vesicle pools at the Drosophila neuromuscular junction." Methods Mol Biol **440**: 349-369.
Vezzani, A., R. Serafini, M. A. Stasi, S. Caccia, I. Conti, R. V. Tridico and R. Samanin (1989). "Kinetics of MK-801 and its effect on quinolinic acid-induced seizures and neurotoxicity in rats." J Pharmacol Exp Ther **249**(1): 278-283.
Volpe, J. J. (2001). "Neurobiology of periventricular leukomalacia in the premature infant." Pediatric research **50**(5): 553-562.
Volpe, J. J. (2008). Neurology of the Newborn, Elsevier Health Sciences.
Volterra, A. and J. Meldolesi (2005). "Astrocytes, from brain glue to communication elements: the revolution continues." Nature Reviews Neuroscience **6**(8): 626-640.
Volterra, A. and J. Meldolesi (2005). "Astrocytes, from brain glue to communication elements: the revolution continues." Nat Rev Neurosci **6**(8): 626-640.
Vyklicky, V., M. Korinek, T. Smejkalova, A. Balik, B. Krausova, M. Kaniakova, K. Lichnerova, J. Cerny, J. Krusek and I. Dittert (2014). "Structure, function, and pharmacology of NMDA receptor channels." Physiological Research **63**: S191.
Wahl, F., T. P. Obrenovitch, A. M. Hardy, M. Plotkine, R. Boulu and L. Symon (1994). "Extracellular glutamate during focal cerebral ischaemia in rats: time course and calcium dependency." J Neurochem **63**(3): 1003-1011.

Wakana, S., H. Jiang, L. M. Nagae-Poetscher, P. C. van Zijl and S. Mori (2004). "Fiber tract-based atlas of human white matter anatomy." Radiology **230**(1): 77-87.
Wake, H., P. R. Lee and R. D. Fields (2011). "Control of Local Protein Synthesis and Initial Events in Myelination by Action Potentials." Science (New York, N.Y.) **333**(6049): 1647-1651.
Wake, H., P. R. Lee and R. D. Fields (2011). "Control of local protein synthesis and initial events in myelination by action potentials." Science **333**(6049): 1647-1651.
Wake, H., F. C. Ortiz, D. H. Woo, P. R. Lee, M. C. Angulo and R. D. Fields (2015). "Nonsynaptic junctions on myelinating glia promote preferential myelination of electrically active axons." Nat Commun **6**: 7844.
Walker, E. J. and G. A. Rosenberg (2010). "Divergent role for MMP-2 in myelin breakdown and oligodendrocyte death following transient global ischemia." J Neurosci Res **88**(4): 764-773.
Wang, C., D. C. Popescu, C. Wu, J. Zhu, W. Macklin and Y. Wang (2010). "In situ fluorescence imaging of myelination." J Histochem Cytochem **58**(7): 611-621.
Wang, C., W. F. Pralong, M. F. Schulz, G. Rougon, J. M. Aubry, S. Pagliusi, A. Robert and J. Z. Kiss (1996). "Functional N-methyl-D-aspartate receptors in O-2A glial precursor cells: a critical role in regulating polysialic acid-neural cell adhesion molecule expression and cell migration." J Cell Biol **135**(6 Pt 1): 1565-1581.
Wang, S. and K. M. Young (2014). "White matter plasticity in adulthood." Neuroscience **276**: 148-160.
Wang, S. S.-H., J. R. Shultz, M. J. Burish, K. H. Harrison, P. R. Hof, L. C. Towns, M. W. Wagers and K. D. Wyatt (2008). "Functional Trade-Offs in White Matter Axonal Scaling." The Journal of Neuroscience **28**(15): 4047-4056.
Wang, Y., G. Liu, D. Hong, F. Chen, X. Ji and G. Cao (2016). "White matter injury in ischemic stroke." Progress in Neurobiology **141**: 45-60.
Wang, Y., G. Liu, D. Hong, F. Chen, X. Ji and G. Cao (2016). "White matter injury in ischemic stroke." Prog Neurobiol **141**: 45-60.
Wang, Y. and Z. H. Qin (2010). "Molecular and cellular mechanisms of excitotoxic neuronal death." Apoptosis **15**(11): 1382-1402.
Waxman, S. G., J. A. Black, J. D. Kocsis and J. M. Ritchie (1989). "Low density of sodium channels supports action potential conduction in axons of neonatal rat optic nerve." Proceedings of the National Academy of Sciences of the United States of America **86**(4): 1406-1410.
Waxman, S. G., M. J. Craner and J. A. Black (2004). "Na+ channel expression along axons in multiple sclerosis and its models." Trends Pharmacol Sci **25**(11): 584-591.
Waxman, S. G. and J. D. Kocsis (1995). The axon: structure, function, and pathophysiology, Oxford University Press, USA.
Waxman, S. G. and T. J. Sims (1984). "Specificity in central myelination: evidence for local regulation of myelin thickness." Brain Res **292**(1): 179-185.
Weaver, C. E., P. Marek, M. Park-Chung, S. W. Tam and D. H. Farb (1997). "Neuroprotective activity of a new class of steroidal inhibitors of the N-methyl-D-aspartate receptor." Proceedings of the National Academy of Sciences **94**(19): 10450-10454.
Wender, R., A. M. Brown, R. Fern, R. A. Swanson, K. Farrell and B. R. Ransom (2000). "Astrocytic glycogen influences axon function and survival during glucose deprivation in central white matter." J Neurosci **20**(18): 6804-6810.
Westbrook, G. L. and M. L. Mayer (1987). "Micromolar concentrations of Zn2+ antagonize NMDA and GABA responses of hippocampal neurons."
Westenbroek, R. E., N. L. Anderson and M. R. Byers (2004). "Altered localization of Cav1.2 (L-type) calcium channels in nerve fibers, Schwann cells, odontoblasts, and fibroblasts of tooth pulp after tooth injury." J Neurosci Res **75**(3): 371-383.
Westergaard, N., J. Drejer, A. Schousboe and U. Sonnewald (1996). "Evaluation of the importance of transamination versus deamination in astrocytic metabolism of [U‐13C] glutamate." Glia **17**(2): 160-168.

Wilke, S., R. Thomas, N. Allcock and R. Fern (2004). "Mechanism of acute ischemic injury of oligodendroglia in early myelinating white matter: the importance of astrocyte injury and glutamate release." J Neuropathol Exp Neurol **63**(8): 872-881.
Winterer, J., P. K. Stanton and W. Muller (2006). "Direct monitoring of vesicular release and uptake in brain slices by multiphoton excitation of the styryl FM 1-43." Biotechniques **40**(3): 343-351.
Wright, S. H. (2004). "Generation of resting membrane potential." Advances in Physiology Education **28**(4): 139-142.
Writing Group, M., V. L. Roger, A. S. Go, D. M. Lloyd-Jones, E. J. Benjamin, J. D. Berry, W. B. Borden, D. M. Bravata, S. Dai, E. S. Ford, C. S. Fox, H. J. Fullerton, C. Gillespie, S. M. Hailpern, J. A. Heit, V. J. Howard, B. M. Kissela, S. J. Kittner, D. T. Lackland, J. H. Lichtman, L. D. Lisabeth, D. M. Makuc, G. M. Marcus, A. Marelli, D. B. Matchar, C. S. Moy, D. Mozaffarian, M. E. Mussolino, G. Nichol, N. P. Paynter, E. Z. Soliman, P. D. Sorlie, N. Sotoodehnia, T. N. Turan, S. S. Virani, N. D. Wong, D. Woo and M. B. Turner (2012). "Heart Disease and Stroke Statistics—2012 Update: A Report From the American Heart Association." Circulation **125**(1): e2-e220.
Wyatt, C. N. and K. J. Buckler (2004). "The effect of mitochondrial inhibitors on membrane currents in isolated neonatal rat carotid body type I cells." J Physiol **556**(Pt 1): 175-191.
Xu, G. Y., M. G. Hughes, Z. Ye, C. E. Hulsebosch and D. J. McAdoo (2004). "Concentrations of glutamate released following spinal cord injury kill oligodendrocytes in the spinal cord." Exp Neurol **187**(2): 329-336.
Yaguchi, T. and T. Nishizaki (2010). "Extracellular high K+ stimulates vesicular glutamate release from astrocytes by activating voltage-dependent calcium channels." J Cell Physiol **225**(2): 512-518.
Yam, P. S., L. T. Dunn, D. I. Graham, D. Dewar and J. McCulloch (2000). "NMDA Receptor Blockade Fails to Alter Axonal Injury in Focal Cerebral Ischemia." Journal of Cerebral Blood Flow & Metabolism **20**(5): 772-779.
Yang, B., Q. Ren, M. Ma, Q.-X. Chen and K. Hashimoto (2016). "Antidepressant Effects of (+)-MK-801 and (-)-MK-801 in the Social Defeat Stress Model." International Journal of Neuropsychopharmacology **19**(12): pyw080.
Yang, X., M. A. Hamner, A. M. Brown, R. D. Evans, Z.-C. Ye, S. Chen and B. R. Ransom (2014). "Novel hypoglycemic injury mechanism: N-methyl-D-aspartate receptor–mediated white matter damage." Annals of neurology **75**(4): 492-507.
Yang, X., M. A. Hamner, A. M. Brown, R. D. Evans, Z. C. Ye, S. Chen and B. R. Ransom (2014). "Novel hypoglycemic injury mechanism: N-methyl-D-aspartate receptor-mediated white matter damage." Ann Neurol **75**(4): 492-507.
Ye, Z. C., M. S. Wyeth, S. Baltan-Tekkok and B. R. Ransom (2003). "Functional hemichannels in astrocytes: a novel mechanism of glutamate release." J Neurosci **23**(9): 3588-3596.
Yi, J.-H. and A. S. Hazell (2006). "Excitotoxic mechanisms and the role of astrocytic glutamate transporters in traumatic brain injury." Neurochemistry International **48**(5): 394-403.
Yuan, X., A. M. Eisen, C. J. McBain and V. Gallo (1998). "A role for glutamate and its receptors in the regulation of oligodendrocyte development in cerebellar tissue slices." Development **125**(15): 2901-2914.
Zatorre, R. J., R. D. Fields and H. Johansen-Berg (2012). "Plasticity in gray and white: neuroimaging changes in brain structure during learning." Nat Neurosci **15**(4): 528-536.
Zawadzka, M., L. E. Rivers, S. P. Fancy, C. Zhao, R. Tripathi, F. Jamen, K. Young, A. Goncharevich, H. Pohl, M. Rizzi, D. H. Rowitch, N. Kessaris, U. Suter, W. D. Richardson and R. J. Franklin (2010). "CNS-resident glial progenitor/stem cells produce Schwann cells as well as oligodendrocytes during repair of CNS demyelination." Cell Stem Cell **6**(6): 578-590.
Zerangue, N. and M. P. Kavanaugh (1996). "Flux coupling in a neuronal glutamate transporter." Nature **383**(6601): 634-637.

Zhang, C.-L., J. A. Wilson, J. Williams and S. Y. Chiu (2006). "Action Potentials Induce Uniform Calcium Influx in Mammalian Myelinated Optic Nerves." Journal of Neurophysiology **96**(2): 695-709.
Zhang, K. and T. J. Sejnowski (2000). "A universal scaling law between gray matter and white matter of cerebral cortex." Proceedings of the National Academy of Sciences **97**(10): 5621-5626.
Zhang, S.-C. (2001). "Defining glial cells during CNS development." Nature Reviews Neuroscience **2**(11): 840-843.
Zhang, S.-C. (2001). "Defining glial cells during CNS development." Nat Rev Neurosci **2**(11): 840-843.
Zhao, H., G. K. Steinberg and R. M. Sapolsky (2007). "General versus specific actions of mild-moderate hypothermia in attenuating cerebral ischemic damage." J Cereb Blood Flow Metab **27**(12): 1879-1894.
Ziskin, J. L., A. Nishiyama, M. Rubio, M. Fukaya and D. E. Bergles (2007). "Vesicular release of glutamate from unmyelinated axons in white matter." Nature neuroscience **10**(3): 321-330.
Ziskin, J. L., A. Nishiyama, M. Rubio, M. Fukaya and D. E. Bergles (2007). "Vesicular release of glutamate from unmyelinated axons in white matter." Nat Neurosci **10**(3): 321-330.
Zukin, R. S. and M. V. Bennett (1995). "Alternatively spliced isoforms of the NMDARI receptor subunit." Trends Neurosci **18**(7): 306-313.